PADAMOT

Palaeohydrogeological Data Analysis and Model Testing

Fifth Framework Programme

Interpretative Modelling of Palaeohydrogeological Data: Final Report

PADAMOT Project – EU FP5 Contract No FIKW-CT2001-20129

Technical Report WP4

February 2005

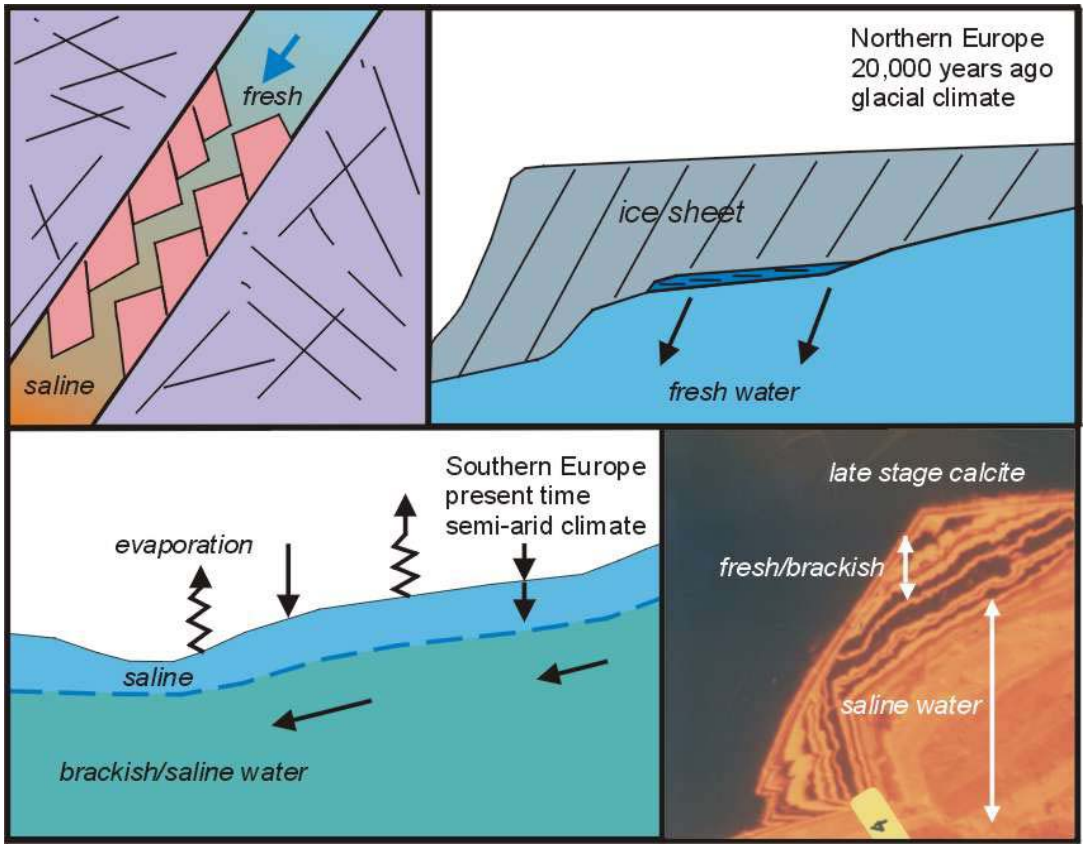

nirex enresa SKB BGS British Geological Survey NATURAL ENVIRONMENT RESEARCH COUNCIL INTELLISCI

Univerzita Karlova v Praze

TERRALOGICA AB

UNIVERSIDADE DA CORUÑA Ciemat

PADAMOT PROJECT

TECHNICAL REPORT WP4

Interpretative Modelling of Palaeohydrogeological Data: Final Report

A Bath[1], L Lomba[3], J Delgado[5], D Noy[6], B Buil[5], J Eugenio[7], V Frydrych[4], M Havlík[4], R Juncosa[3], J. Krásný[4], J Mls[4], M Polák, C Ruiz[3], T de Torres[7], A Cortés[2], F Recreo[3] and J Šilar[4]

Editors

A Cortés Ruiz[2] and A Bath[1]

[1] Intellisci Ltd, Loughborough, UK

[2] ENRESA, Madrid, Spain

[3] CIEMAT, Dept. Impacto Ambiental de la Energia, Madrid, Spain

[4] Univerzita Karlova v Praze, Ústav Hydrogeologie, Inženýrské Geologie a Užité Geofyziky, Praha, Czech Republic

[5] Universidad de la Coruña, Escuela Técnica Superior de Ingenieros de Caminos, Canales y Puertos, A Coruña, Spain

[6] British Geological Survey, Keyworth, Nottingham, UK

[7] Universidad Politecnica de Madrid, Escuela Tecnica Superior de Ingenieros de Minas, Madrid, Spain

Bibliographical reference

CORTÉS RUIZ, A. AND BATH, A. (EDITORS). 2005. Interpretative Modelling of Palaeohydrogeological Data: Final Report. *PADAMOT Project Technical Report* WP4. 135pp.

Harwell UK Nirex Limited 2005

Foreword

PADAMOT, 'Palaeohydrogeological Data Analysis and Model Testing', is a project within the European Union's 5th Framework RTD programme in nuclear fission safety (Contract Number FIKW-CT-2001-00129). It aims to improve the understanding of past groundwater conditions that supports assessments of future long-term safety of repositories for radioactive wastes. The project began in December 2001 with duration of 36 months. The consortium of organisations involved in the PADAMOT project comprises:

United Kingdom Nirex Limited (UK)

Svensk Kärnbränslehantering AB (Sweden)

Terralogica AB (Sweden)

Empresa Nacional de Residuos Radioactivos S.A. (Spain)

Centro de Investigaciones Energéticas, Medioambientales y Tecnológicas (Spain)

Intellisci Ltd (UK)

British Geological Survey (UK)

Charles University (Czech Republic)

University of Edinburgh (UK)

Universidad Politecnica de Madrid - School of Mines (Spain)

Safety assessments of proposed repositories for the long-term storage or disposal of radioactive wastes must take into account scenarios for environmental change over the long period of time during which the waste will be a hazard, typically up to one million years into the future. The scientific consensus in a number of countries is that disposing of long-lived and/or higher activity radioactive wastes and spent nuclear fuel deep underground in a 'geological repository' is the preferred option for long-term radioactive waste management. The reasons for preferring this option are that the host rock for a deep repository should provide stable conditions for performance of the engineered barrier system and that the rock mass separating a repository from the surface environment is a further barrier to radionuclide migration.

During the last two million years (the Quaternary Period), global climate has fluctuated between extremes of ice ages and warmer conditions than at present. Over various intervals in the past, large areas of northern Europe were covered by ice sheets and experienced extensive permafrost, whilst southern Europe was sometimes more pluvial (wetter). Consequently, the present-day climate is not representative of the climate that has existed for much of the Quaternary. This natural pattern of climatic fluctuation is expected to continue into the future, albeit modified by the impacts of anthropogenic greenhouse gas emissions. Variations in climate and in other environmental factors may affect future movements and compositions of groundwaters in the vicinity of a repository and thus affect the mobility of radionuclides and the rate of their migration back to the surface. It could be argued, therefore, that present-day groundwater conditions may not be an adequate basis for assessing long-term repository safety. However, if it can be demonstrated that, despite significant environmental change at the surface, groundwater flows and compositions at depth remain stable or change in a way that does not impact significantly on safety, then confidence in repository concepts for disposal will be increased.

PADAMOT has sought to address the following questions. How can such groundwater stability be assessed, with respect to climate-driven environmental change? In particular, what evidence is there that a deep geological repository will eliminate or reduce the effects of extreme changes in environmental conditions in the long term? In seeking to answer these questions, PADAMOT

has investigated geosphere systems at various European sites, using analytical methods and numerical modelling.

PADAMOT comprises five work packages (WPs) with the following tasks:

WP1. Convening a preliminary workshop of PA specialists, PADAMOT researchers and other geoscientists on the use of palaeohydrogeology in PA.

WP2. Making palaeohydrogeological data measurements on mineral samples and groundwaters from sites in Spain, Czech Republic, Sweden and UK, using high resolution and high precision analytical methods, e.g. ion probe and laser ablation.

WP3. Constructing a relational database and a public domain website to store data from EQUIP and PADAMOT, accessible to project partners and to external researchers via the internet.

WP4. Developing numerical models to test palaeohydrogeological information interpreted from proxy geochemical, mineralogical and isotopic data, based on understanding of the processes that link the proxy data with climate-driven groundwater phenomena.

WP5. Synthesising project outcomes and disseminating an improved approach to the use of palaeohydrogeological information in the description of FEPs and hydrogeological scenarios for PA.

There are final reports from each of the five WPs plus a Summary report:

Technical Report WP1.	The Long-Term Stability of Groundwater Conditions at Repository Sites: Proceedings of the PADAMOT Workshop, Brussels 2002.
Technical Report WP2.	Application of Mineralogical, Petrological and Geochemical Tools for Evaluating the Palaeohydrogeological Evolution of the PADAMOT Study Sites.
Technical Report WP3.	Design and Compilation of Database: Final Report.
Technical Report WP4.	Interpretative Modelling of Palaeohydrogeological Data: Final Report.
Technical Report WP5.	Dissemination and Use of Palaeohydrogeological Results for Safety Assessment.
Summary Report.	PADAMOT: Palaeohydrogeological Data Analysis and Model Testing – Overview.

Further Information

Further information on the PADAMOT programme can be obtained from the project website www.bgs.ac.uk/padamot

Abstract

The objective of Work Package (WP) 4 of the PADAMOT project has been to test and improve our understanding of palaeohydrogeological information obtained from 'proxy' data (geochemical, mineralogical, isotopic, etc) by using numerical interpretative models. The potential value of palaeohydrogeology in Performance Assessment (PA) is in understanding better the time-varying changes of the groundwater flux and flow direction, chemical environment, and other scenarios that are related to climate or other external environmental changes. Proxy data are interpreted using expert judgement and quantitative modelling to extract information that is relevant to PA. Interpretative models have been developed with particular focus on the processes that are relevant to data that has been acquired in WP2 from the sites in Spain (Los Ratones), UK (Sellafield) and Czech Republic (Melechov). Essentially, the interpretative models for process-understanding can be calibrated using palaeohydrological information and thus provide interfaces between palaeohydrogeological information and FEPs (features, events and processes) for scenario development in PA.

For Los Ratones, the objective has been to investigate the ways that climate changes might be propagated into groundwater recharge and thence into changes in groundwater compositions and ultimately into the geochemical and mineralogical proxies. This has involved the integration of models for surface water mass balance, groundwater flow and reactive transport of solutes. The methodology allows different climatic and hydrological proxies to be interfaced with a palaeohydrogeological model which supports the construction and calibration of a groundwater model for PA with boundary conditions appropriate for future changing climate. This has been achieved in the model for Los Ratones by using the VISUAL-BALAN code to estimate time-dependent changes of recharge rate constrained by palaeoclimate information from measurements of microfaunal, pollen, isotopic and organic geochemical proxies. The evolution of groundwater compositions and secondary minerals for different boundary conditions has then been simulated with the CORE^{2D} code.

For Sellafield, the objective has been to mimic the geochemical reactions that might have accounted for precipitation of late-stage calcites in fractured rock groundwater systems and to understand the significance of variations of Fe and Mn contents of secondary calcite with respect to past redox conditions in groundwater systems. Equilibrium modelling has been carried out with the PHREEQC2 code for a range of batch mixing and reaction conditions and this has been supplemented by some coupled transport and reaction modelling with the PRECIP code. The conceptual geochemical models are not unique and involve assumptions about the reactions, water mixing and pre-existing solid phases that control dissolved Fe and Mn, and about how Fe and Mn are distributed between calcite and water.

For Melechov, the objective is to understand groundwater conditions in the western part of the granite massif, using the results of a hydrogeological survey with numerical modelling of the spatial distribution of hydraulic potential, groundwater flows and travel times. This is the initial stage in the development of a site investigation methodology that is appropriate for fractured granitic rocks in the terrain and climate of the Bohemian massif. The MODFLOW code was used to construct a two-dimensional spatial model of groundwater flow. Knowledge of the hydrogeological properties from borehole testing is limited to the shallow part of the system, so modelling has tested the sensitivity of flows and travel times at greater depths to uncertainties in hydrogeological properties and infiltration.

Modelling in WP4 has made progress towards the integration of independent models of biosphere/climate, groundwater and geochemistry. Integration requires information to be transferred between the various models, e.g. recharge data from the biosphere model to the groundwater model, water flux data from the groundwater model to the geochemical model.

Data for palaeoclimate, geochemical, isotopic and mineralogical proxies are needed to calibrate the models. Integration also involves expert judgement and understanding of uncertainties especially with respect to temporal and spatial variability. The possibilities and realities of integration with PA groups, especially with regard to the identification and quantification of FEPs and scenarios, are considered in the report for WP5.

Acknowledgements

Richard Metcalfe (Quintessa K.K., Japan) carried out an independent review of this report, as a result of which further improvements have been made.

The support and involvement of Henning von Maravic and Michel Raynal of EC-DG Research is gratefully acknowledged. The work described in this report was carried out as Work Package 4 of the PADAMOT project in the European Union's 5th Framework Programme of RTD in Nuclear Fission Safety, Contract No. FIKW-CT-2001-00129. It was also supported by funds from UK Nirex Limited and ENRESA.

Contents

1 Introduction and Objectives of WP4

Adrian Bath, Intellisci, UK

The general objective in the context of PADAMOT has been to quantify the indicators and processes that trace the hydrogeological and geochemical evolution of groundwater systems due to climatic and surface environmental changes. The approach taken in WP4 has been to test and improve our understanding of palaeohydrogeological information obtained from 'proxy' data (geochemical, mineralogical, isotopic, etc) that have been studied in WP2 by using numerical interpretative models. Interpretative models have investigated the processes that link proxy data with groundwater phenomena that might be driven by past changes of climate or other environmental characteristics, i.e. the 'cause-effect' relationship.

Four types of interpretative models have been developed with particular focus on the processes that are relevant to data that has been acquired in WP2 from the sites in Spain (Los Ratones), UK (Sellafield) and Czech Republic (Melechov).

For Los Ratones, the specific objective in WP4 has been to investigate the ways that climate changes might be propagated into changes to groundwater recharge and other boundary conditions for the groundwater flow model, and thence into changes in groundwater compositions and ultimately into the geochemical and mineralogical proxies. This has involved the integration of models for surface water mass balance, groundwater flow, and reactive transport of solutes. Surface water balance is an important variable for this location because of its semi-arid climate. Modelling of surface water balance has been constrained by the input of information from palaeoclimatic and palaeohydrological indicators that have been measured in WP2. From the analysis of palaeoclimatic indicators it was possible to derive a number of climate types which were then used to compute a water mass balance model with the VISUAL-BALAN code. Each climate type was considered representative of a given time period. Linking consecutive time periods, it was possible to obtain the time-dependent recharge function used for groundwater flow and reactive transport modelling. Groundwater flow and reactive transport were modelled together in the CORE^{2D} code to give two-dimensional distributions of groundwater compositions and of secondary mineral products, for the limiting scenarios of maximum and minimum recharge to the groundwater system.

For Sellafield, the specific objective in WP4 has been to construct a geochemical model that quantifies the processes that account for the deposition and composition of secondary calcites in fractured rock groundwater systems such as that at Sellafield. The hypothesis that has been investigated is that the formation of late stage secondary calcite is stimulated by the hydrodynamic mixing of groundwaters with different compositions in deep fractured rock systems such as Sellafield and Äspö where variable groundwater salinities are found. Mineralogical descriptions and chemical and isotopic analyses of secondary calcites at Sellafield and Äspö have been made in WP2 and this geochemical modelling establishes the theoretical basis for the process and conditions of formation. Coupled flow and reactive transport modelling of hydrodynamic mixing between groundwaters with different compositions was carried out with the PRECIP and CORE^{2D} codes, showing how fluctuating flow conditions would produce growth-zoned calcite, similar to that observed in WP2. This modelling study also provided a base for comparing the two reactive mass transport codes and showed that they give similar results.

A second stage of geochemical modelling for Sellafield has studied the relationship between redox conditions and the Fe and Mn contents of secondary calcite. This has addressed the need

to establish a quantitative theoretical basis for interpreting the significance for palaeo-redox conditions of variations of Fe and Mn in calcite growth zones that have been measured in WP2. Equilibrium modelling has been carried out with the PHREEQCI code (version 2.8) for a range of batch mixing and reaction conditions and this has been supplemented by some coupled transport and reaction modelling with the PRECIP code.

Some modelling was also carried out to simulate the geochemical processes that control secondary calcite deposition in shallow fresh groundwater systems where coherent flows from recharge to discharge are evident. In this type of groundwater system, which is typical of the uppermost parts of fractured rock groundwater systems, water-rock weathering reactions rather than mixing of groundwaters account for calcite precipitation. The results of this modelling are summarised in an appendix to this report.

For Melechov, the specific objective in WP4 has been to achieve a basic understanding of groundwater conditions in the western part of the granite massif, using the results of a hydrogeological survey with numerical modelling of the spatial distribution of hydraulic potential, groundwater flows and travel times. The MODFLOW code was used to construct a two-dimensional spatial model of groundwater flow. Knowledge of the hydrogeological properties from borehole testing is limited to the shallow part of the system, so hydrogeological modelling has served to illustrate the assumptions that are necessary in extrapolating the model to greater depths and to longer flow paths and travel times that have palaeohydrogeological significance.

2 Interpretative Modelling Methods and Tools

Adrian Bath, Jordi Delgado Martín, Luis Lomba Falcón, David Noy, Fernando Recreo Jiménez

2.1 GEOCHEMICAL EQUILIBRIUM MODELLING: PHREEQC

The widely-used PHREEQC program from the US Geological Survey is based on an ion-association aqueous model and on equilibrium chemistry of aqueous solutions interacting with minerals, gases, solid solutions, exchangers, and sorption surfaces. It performs a wide variety of low-temperature aqueous geochemical calculations. Its main capabilities of relevance for present applications are (i) mixing of waters with speciation and saturation-index calculations, (ii) batch-reaction and mass transfer calculations of reversible and irreversible reactions involving aqueous, solid and gas phases, and (iii) one-dimensional advective mass transport. PHREEQCI v2.8 (Parkhurst and Appelo, 1999) was used with the PHREEQC rev2.3 thermodynamic database. This expansion of the code includes capabilities to simulate dispersion and diffusion in 1D-transport calculations including matrix exchange in a dual porosity medium, to model kinetic reactions, and to model the formation or dissolution of binary solid solutions, plus some improved flexibility in the input and output of data.

In batch-reaction calculations, PHREEQC is oriented toward system equilibrium so that all of the moles of each element are distributed among the aqueous phase, pure phases, solid solutions, gas phase, exchange sites, and surface sites to attain system equilibrium. The pe is calculated initially by a mass balance on hydrogen and oxygen. Distribution of redox elements among their valence states can be based on a specified pe or any redox couple for which data are available.

The framework for numerically efficient 1D advective transport modelling coupled iteratively with reversible and irreversible chemical reactions is provided by PHREEQC's capability to define multiple solutions and multiple assemblages combined with the capability to determine the stable phase assemblage. The input to PHREEQC is completely free format and is based on chemical symbolism. Balanced equations, written in chemical symbols, are used to define aqueous species, exchange species, surface-complexation species, solid solutions, and pure phases.

2.2 FLOW AND REACTION MODELLING: PRECIP AND CORE-2D

2.2.1 PRECIP: 1D flow and reactive transport code (BGS)

The general conceptual approach of the reactive transport code PRECIP is of a one dimensional flow path along which flow is Darcian and on which precipitation and dissolution reactions can take place amongst a number of components. The flow field is defined by either fixed head values at each end of the path or by a specified flow rate along it. The chemical reactions are described by kinetic rate laws and the aqueous components are transported by advection and dispersion. As the chemical reactions proceed, the masses of precipitates change at each point on the path with consequent changes in the porosity. These porosity changes may be related to changes of permeability by a user defined function, thereby affecting the flow field. The reactions may be dependent upon a user specified temperature variation along the flow path and optional aqueous phase speciation and solution-mineral equilibria may also be included. The transport and reaction equations are fully coupled and solved simultaneously.

The mathematical development of the model starts with equations for the description of the precipitation and dissolution of minerals as kinetic processes. A second set of equations describing the transport of multiple reacting aqueous species is then developed. Finally, a form of the groundwater flow equation which explicitly takes account of the changing of porosity with time is added. These three mathematical components form a complete description of the coupled system and can be solved using spatial discretization based on simple central finite differences. Numerical integration over time of the resulting system of coupled non-linear ordinary differential equations is achieved using Gear's method. A detailed description of the code, together with input data specifications and verification examples, are found in Noy (1998). Thermodynamic data have been selected, appropriately for the reactions being modelled, from the EQ3NR/EQ6 database version data0.com.V8.R6.

2.2.2 CORE^{2D}: Flow and reactive transport Code (ENRESA-UDC)

CORE^{2D} is a finite element code which solves for groundwater flow, heat transport and multi-component reactive solute transport under the following conditions:

1. 2-D confined or unconfined, saturated or unsaturated, steady or transient groundwater flow with general boundary conditions (Dirichlet, Neuman and Cauchy)
2. Transient heat transport considering conduction, convection and heat dispersion processes.
3. Chemical processes occurring at the equilibrium or kinetically controlled, including homogeneous and heterogeneous reactions
4. Radioactive decay

CORE^{2D} is based on the sequential iteration approach (SIA) to solve the coupled hydrological transport processes and hydrogeochemical reactions. In this approach the transport and chemical equilibrium equations are considered as two different subsystems. These subsystems are solved separately in a sequential manner following an iterative procedure. At any given iteration, the chemical sink/source term is assumed known (or taken equal to the value at the previous iteration) for the purpose of solving the transport equations. This renders the differential equations linear which allows the use of fast numerical methods for solving the linear system of equations. After solving the transport equations, the set of chemical equations is solved on a node-basis. Solution of these non linear equations is carried out using Newton-Raphson iterative procedures. After convergence, the chemical source term is updated. The whole iterative process (transport + chemistry) is repeated until overall convergence is attained. The finite element method is used for spatial discretization, while implicit, explicit and general finite difference schemes are used for time discretization. CORE^{2D} can cope with heterogeneous systems having irregular internal and external boundaries. The code can handle heterogeneous and anisotropic media in: (1) two-dimensional horizontal planes for confined or unconfined flow, (2) two-dimensional vertical planes and (3) three-dimensional problems having axial symmetry for confined aquifers and variably saturated porous media.

Both steady-state and transient flow regimes can be simulated. Prescribed head and water flux as well as mixed boundary conditions are included. Both point and areal fluid sources can be specified. In addition, free drainage boundary condition (unit gradient type) is allowed for variably saturated flow. Solute transport processes included in the code are: advection, molecular diffusion and mechanical dispersion. Solute transport boundary conditions include: (1) specified solute mass fluxes, (2) specified solute concentrations and (3) solute sources associated with fluid sources.

Heat transport is solved at each time step. Computed temperatures are used for updating equilibrium constants and the constants for calculating activity coefficients.

The input of aqueous species, minerals, gases, and adsorbed/exchanged species only requires specifying their names. Thermodynamic data and stoichiometric coefficients of the reactions are read directly from a database modified from the EQ3NR/EQ6 software package (data0.com.V7.R22a; Wolery, 1992). The thermodynamic database of CORE^{2D} has a different structure to that of EQ3/EQ6, but identical thermodynamic data (log K's) and associated reactions, etc (Samper et al., 2000). For the purpose of PADAMOT, the database was supplemented with a new equilibrium constant for the solubility of the ideal stoichiometric ankerite $Ca(Fe_{0.5}Mg_{0.5})(CO_3)_2$, based on data by Langmuir (1997) and the reaction:

$$\text{Ankerite} + 2H^+ = Ca^{2+} + \tfrac{1}{2}\, Fe^{2+} + \tfrac{1}{2}\, Mg^{2+} + 2\, HCO_3^-$$

2.3 HYDROLOGICAL BALANCE MODELLING: VISUAL-BALAN

VISUAL BALAN is code designed to compute hydrological water mass balances. Typically, it is employed within the soil (edaphic) zone, the non-saturated zone and the aquifer.

Water transferences among these reservoirs are summarized in Figure 3.1. Precipitation plus irrigation (*P*) are split into interception (*In*), runoff (E_s) and infiltration (*I*). A given amount of the total water might be affected by evapotranspiration (ETR) while a part of the remaining water contributes to soil water reserve and to the in transit recharge or effective rain (P_e).

Within the unsaturated zone, water can flow laterally towards the surface as hypodermic flux (Q_h) or contribute to the aquifer via vertical movement as recharge (Q_p). Finally, the underground discharge (Q_s) represents the natural water exit towards streams and rivers.

In order to make the mass balance, it is necessary to consider an aggregated model where the properties of the three groundwater reservoirs are assumed to be homogenous throughout the entire catchment. Thus, the representativity of the water balance will depend on the degree of homogeneity of the catchment and its size.

The water balance is based on the application of the mass conservation law within a given region of known volume and boundary conditions. In the time frame considered, the change in the amount of water stored in the aquifer is related to the differences between the total water input and output.

The basic equation for water balance in the soil is usually integrated between two given times t_i and t_f $(\Delta t = t_f - t_i)$:

$$P + D - IN - E_S - ETR - P_e = \Delta\theta \tag{1}$$

where P, D, IN, E_S, ETR, P_e and $\Delta\theta$ represent precipitation, irrigation, interception, runoff, real evapotranspiration, in transit recharge (which is identical to recharge when lateral flow through the unsaturated zone does not occur) and change in moisture content, respectively.

Because water balances are performed on a surface basis, the unknowns in equation (1) are expressed as volume per unit surface area or equivalent water height (i.e. mm). Strictly speaking, the water balance equation should incorporate an explicit term accounting for infiltration (I). Then:

$$I - \left(ETR + P_e\right) = \Delta\theta \tag{2}$$

where

$$P + D - IN - E_S = I \tag{3}$$

One of the key points of a successful water mass balance model is the computation of ETR, which is, in turn, related to a model to compute the potential evapotranspiration, ETP. Thus, both

ETP and ETR are mutually related and connected with the moisture conditions prevailing in the soil.

Because the earlier water mass balance models were developed for humid regions, their applicability to arid or semi-arid regions cannot be taken for granted. They are most successful if the region in question has a well developed soil layer, the moisture content is higher and, therefore, when ETR and ETP have similar values.

An additional point to take into account is the preferential movement of water through macropores. It is a well known fact that there might be recharge even in the case of soil water deficiency (Rushton and Ward, 1979). In order to account for that, there are a number of available empirical formulations. The simplest one considers that it is directly proportional to the amount of precipitation beyond a given threshold.

The major part of the components participating in the water mass balance (I, E_s, ETR, P_e) depend on soil's moisture content on a non-linear way. Thus, the exact resolution of equation (1) would require the implementation of numerical iterative procedures. However, for common applications it is enough to consider sufficiently small time increments, Δt, and constraints so that the moisture content of the soil does not exceed given values (wilting point and full saturation).

In the application for PADAMOT, the water mass balances have been computed with VISUAL-BALAN following four consecutive stages:

First stage (A): Definition of the geographical situation of the studied area; properties of soil, non saturated zone and aquifer; climatic information from the available weather stations (one single time series).

Second stage (B): Preliminary evaluation of ETP, which is needed whether the Thornthwaite, Turc, Makkink, Blanney-Criddle or Penman models are selected. Then, a number of climatic parameters are given (theoretical daily sunny hours; monthly heat index for Thornthwaite's method; ratio between the monthly averaged maximum time of insolation and the corresponding yearly averaged value according to Blanney-Criddle's method; global radiation according to Makkink's method; and extraterrestrial radiation and altitude anemometer correction following Penman's method).

Third stage (C): Here the hydrometeorology balance is done. For each single day the code performs a series of sequential calculations. Firstly, and only when irrigation is considered, it computes the amount of water applied to the soil. Then, the ETP is computed according to one of the four methods originally implemented in the code. After that, VISUAL BALAN computes the interception and the amount of flow through preferential channels which is the followed by the calculation of runoff, ETR and outflow. Once the water soil balance is completed, the water balance in the non-saturated zone is performed, computing first the hypodermic flow and the aquifer recharge. Finally, the change in piezometer levels is accounted.

Fourth stage (D): The results for each considered catchment (main and secondary) are provided by the code, including: daily, monthly and yearly values; results of the sensitivity analyses; cumulative and averaged values; computed and measured water levels; computed and measured water flux; recharge and/or leakage functions; and results related to automatic calibrations.

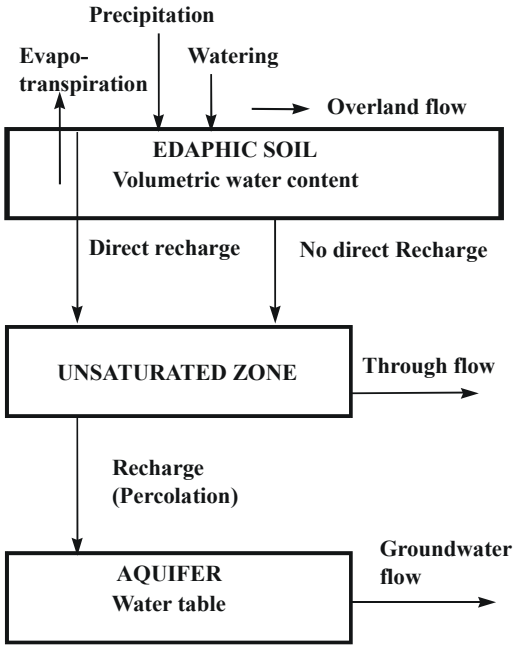

Figure 2.1. Summary of the major components of the hydrologic cycle considered by VISUAL-BALAN.

2.4 GROUNDWATER TRAVEL TIME MODELLING: MODFLOW

The Ground Water Vistas (GWV) modelling package by J. and D. Rumbaugh, Environmental Simulation, Inc. was used (Rumbaugh and Rumbaugh, 1998). The flow solver MODFLOW (McDonald and Harbaugh, 1988), which is a part of the GWV package, was used for groundwater flow and groundwater travel time modelling.

The well known MODFLOW solver uses the finite difference method for solving the equation governing flow:

$$\frac{\partial}{\partial x}\left(k_{xx}\frac{\partial h}{\partial x}\right)+\frac{\partial}{\partial y}\left(k_{yy}\frac{\partial h}{\partial y}\right)+\frac{\partial}{\partial z}\left(k_{zz}\frac{\partial h}{\partial z}\right)-W=S_s\frac{\partial h}{\partial t} \qquad [1]$$

where k_{xx}, k_{yy} and k_{zz}… hydraulic conductivity along x, y and z axis, parallel with main tensors of permeability (L/t),

h … piezometric head (L),

W … infiltration and evapotranspiration (1/t),

S_s … specific value of material storativity (1/L),

t … time (T)

Equation [1] describes three dimensional groundwater flows in a heterogeneous and anisotropic environment. This equation, together with boundary and initial conditions, represents a numerical expression of transient groundwater movement.

3 Integrated Palaeoclimate, Palaeohydrological and Scenario Modelling – Case Study: Los Ratones

Jordi Delgado Martín, Luis Lomba Falcón, Belen Buil, Fernando Recreo Jiménez, Trinidad de Torres Perezhidalgo and Ricardo Juncosa Rivera

3.1 DESCRIPTION OF APPROACH AND METHODOLOGY

The specific aim of this task is to identify indicators and processes that can be used to trace the evolution of the groundwater system due to fluctuations associated with environmental and climatic changes. This basic knowledge will support the development of conceptual models for surface water mass balances and groundwater flow and reactive transport models. Because PADAMOT is an integrated project, it is important to link geochemical data (i.e. the palaeoindicators identified in WP2 of PADAMOT), to reconstruct palaeoclimate scenarios and to model their effects in order to constrain the impact of the evolving climate conditions on the groundwater system.

The case study presented in this section was based on these goals. A short summary of the methodology that was developed is given next. A more detailed description is in Appendix A.

In order to conduct our studies, we selected two separate areas. The first area is located in SE Spain (close to the city of Granada), where a series of world-class continental sedimentary sequences allow the study and reconstruction of a nearly complete time-series record accounting for climate oscillations dating back as early as 2 million years. The second area corresponds to an old uranium mine (Los Ratones mine, Cáceres), located about 500 km WNW from Granada and developed in a fractured granitic batholith. The area where the mine is located was studied in detail (geophysical surveys, local and regional hydrogeology, hydrochemistry, petrophysics, geochemistry, mineralogy, etc) in association with a land restoration/reclamation and research program conducted by ENRESA.

Because Los Ratones mine does not have direct evidence of climate change (or, at least, easily interpretable palaeoclimatic indicators), it was decided to obtain such a data from a neighbouring zone and to transfer it to Los Ratones assuming that the most relevant effect of climate change over the groundwater regime in a fractured massif was the modification of recharge. Thus, the sedimentary sequences of SE Spain (Padul and Cúllar-Baza) were used with a twofold purpose: 1) to improve the knowledge on past climate conditions in southern Europe and 2) to derive a time-dependent recharge function amenable for use at Los Ratones. This transfer function is based on computation of several models for water mass balance that take into account the best available knowledge derived from selected palaeoindicators.

The transfer of palaeoclimatic conditions between two separated areas like the ones considered in our study might be found controversial. However, the validity of the working hypothesis of climatic equivalence is based on similarity of the present-day climatic conditions in both areas, assuming that this situation could have also prevailed in the past.

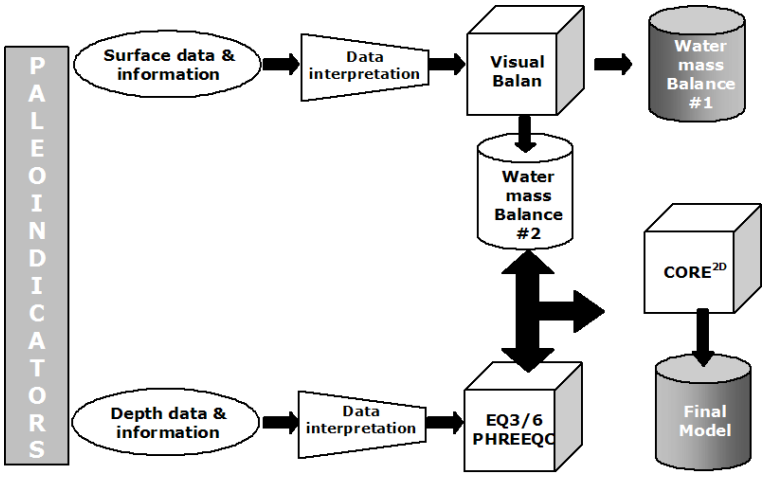

Figure 3.1. Summary of the methodology used to compute the effects of changing the climatic conditions on the groundwater system of Los Ratones.

Modelling was accomplished in a series of steps which are summarized in Figure 3.1. Thus, from the analysis of palaeoclimatic indicators it was possible to derive a number of climate types which were then used to compute a water mass balance model with the code VISUAL-BALAN. Each climate type was considered representative of a given time period. Linking consecutive time periods, it was possible to obtain the time-dependent recharge function used for reactive transport modelling. Recharge is assumed to be constant for each time period considered representative of a climate type and is a stepwise (discontinuous) function.

Several palaeoclimatic indicators were analyzed in our study: ostracods and other fossil environmental monitors, ostracod-shell stable isotope ratios ($\delta^{13}C$, $\delta^{18}O$), major and trace element composition (Mg, Ca, Sr), a large number of biomarkers and pollen content. Among all of them, the pollen content was selected for our work although a considerable effort was devoted to trying to derive usable information from the other palaeoindicators. Further work is needed in order to improve the soundness of the palaeoclimatic reconstruction.

3.2 INTRODUCTION TO THE SITE MODEL

To meet the objective of PADAMOT, simultaneous modelling of surface and groundwater processes cannot be carried out with the same computer code. This is the reason why a part of the modelling task was performed with VISUAL-BALAN (surface water system) and part with $CORE^{2D}$ (groundwaters). The conceptual link between the two codes is the recharge value which is provided by the first code and is an input function for the second code.

Thus, it was necessary to develop three different tasks before computing a comprehensive simulation of the behaviour of the groundwater system with respect to climate oscillations. The main tasks are: 1) computation of a hydrologic (surface) model; 2) computation of a groundwater flow model; and 3) computation of a reactive transport model of increasing complexity: a) transport of conservative species; b) transport of species affected by radioactive decay; c) multicomponent fully reactive system.

The hydrologic model is aimed at obtaining recharge values associated with specific bioclimatic conditions that, in turn, are associated with given time periods. Recharge originates from the mass balance of water infiltrating through the soil layer and, therefore, this layer has been included in the VISUAL-BALAN modelling.

The flow model at Los Ratones area is constructed from pre-existing information and additional inputs coming from PADAMOT's WP2. All this information contributes to a "geognostic"

model which comprises detailed studies on the petrology and geochemistry of the granite, mineralogy (fracture infill, rock assemblages, etc), hydrochemistry, regional and local groundwater hydrodynamics, and the identification and definition of relevant geochemical processes. This allowed the setting of reasonable initial and boundary conditions whose validity was later checked through sensitivity analyses.

The groundwater flow model considers the mass transfers of water in the aquifer. In brief, it can be separated in to vertical (associated with surface recharge) and horizontal water movements, the latter due to hydraulic gradients resulting from the given boundary conditions and/or regional groundwater flows.

The reactive transport model includes a number of homogeneous and heterogeneous chemical reactions, which will be described later.

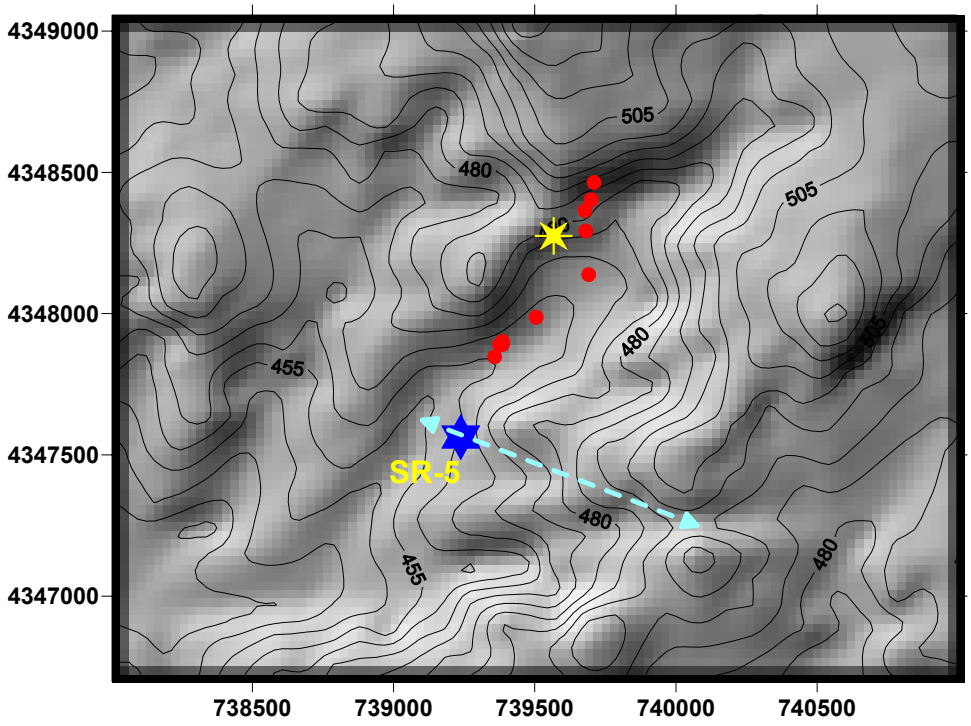

Figure 3.2. Shaded relief and contour map of the Los Ratones area (UTM coordinates) and location of the SR-5 borehole (blue star). The red dots correspond to the location of other boreholes. The yellow star is the location of the main (vertical) shaft of the old Los Ratones uranium mine. The dashed line represents the orientation of the vertical section selected for modelling.

Los Ratones area was selected on the basis of detailed information existing at the start of the project. It must be stressed that modelling the old uranium mine was not among the aims of the project and that the drifts and shafts associated with the mine openings should not be taken into account in a model that, starting at present, covers a period of 1 million years in the past. Thus, it was decided to focus on the volume around a borehole (SR-5), a short distance from the main mine workings and representing the hydrochemical conditions prevailing in the granite massif without being influenced by the mine. SR-5 is located in a small catchment (~10.1 Km^2) defined around a small stream named Arroyo Maderos. The reactive transport model refers to this small catchment (local model) and the corresponding boundary conditions are affected by the watershed divides, the creek as discharge zone and the regional groundwater flow.

A 2D vertical section, starting at the watershed divide and ending at the Arroyo Maderos creek passing through SR-5, was selected (Figures 3.2 and 3.3). According to Martínez-Landa et al. (1999a,b), the flow lines close to the SR-5 borehole have a preferential E-W orientation discharging at the creek.

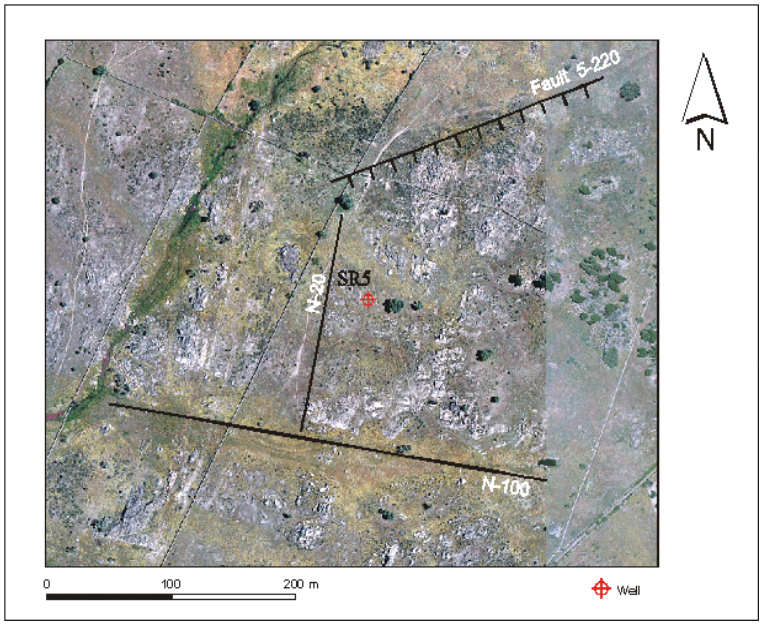

Figure 3.3. Orthophotomap showing the vicinity of the SR-5 borehole. Three minor faults are indicated (5-220, N-20 and N-100). The green band running NE-SW at the left side of the picture is the Arroyo Maderos creek. Note that topography is nearly flat.

Figure 3.4 shows a generalised vertical profile of the different hydrodynamic domains used in the model, which are based on the work by Martínez Landa et al. (1999).

The VISUAL-BALAN water mass balance model is concerned with the loam/soil layer (Figure 3.5) while the CORE^{2D} groundwater model is concerned with the different hydrodynamic units described earlier.

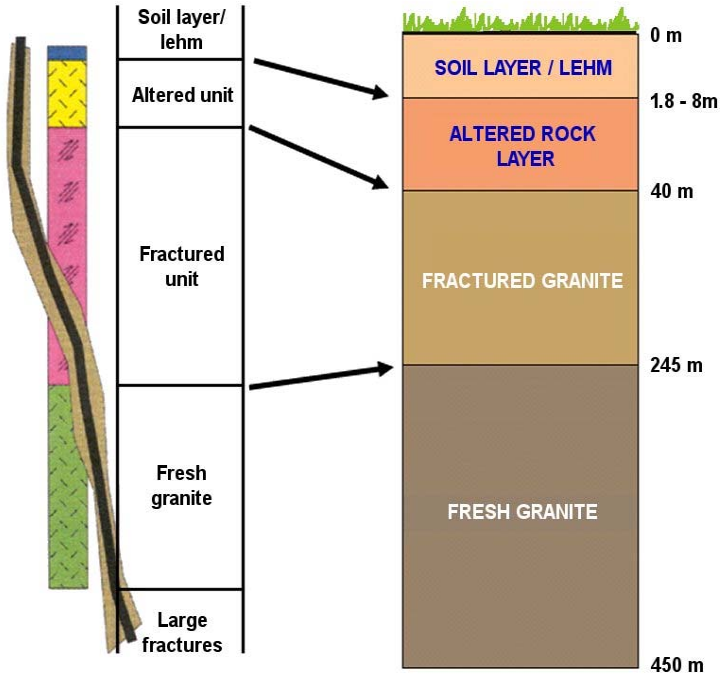

Figure 3.4. Schematic cartoon illustrating a generalised flow model and hydrodynamic units used in the modelling (soil/loam layer, fractured granite, fresh granite and fault zone). Thicknesses of corresponding units are approximate (modified from Martinez Landa et al., 1999).

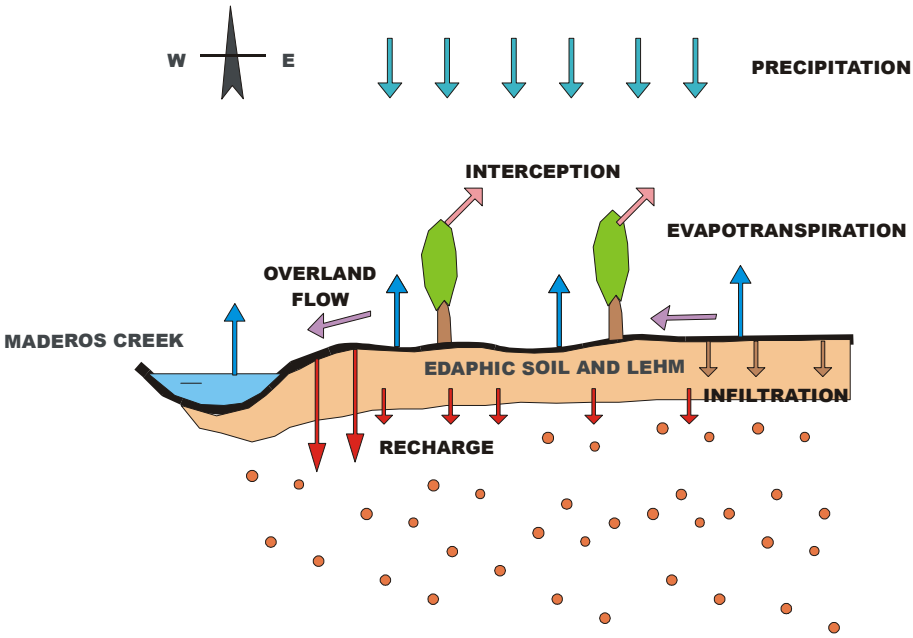

Figure 3.5. Idealized hydrologic water mass balance model used to compute recharge coming from the soil layer and loam.

A number of working hypotheses about hydrology and hydrogeology have been assumed in the reactive transport model:

- Palaeoclimatic information originated in the SE Spain (Padul peat bog) has been used to set up a model for the climatic dependence of recharge in the Arroyo Maderos catchment.
- The precipitation regime is homogeneous throughout the modelled domain both in terms of time and space because the Arroyo Maderos catchment is small (~10.1 km^2). Accordingly, for given time periods, recharge will be constant.
- The soil/loam layer has spatially and temporally constant and homogeneous hydrodynamic properties.
- Recharge takes place homogeneously along the upper boundary of the modelled domain.
- Groundwater movement will be constrained by the boundary conditions prevailing at the fractured granite zone.
- In the fresh granite zone, groundwater movement will be dominated by regional-scale gradients. Thus, in addition to the selected chemical species and minerals, the multicomponent reactive transport model will be affected by the flow regime resulting from the interaction among the distinct hydrodynamic domains.
- The corresponding hydrodynamic properties (k, f, S_S, etc.) for each spatial domain do not change with time.
- The hydraulically-active fractures at present have also controlled the hydrogeology of the area in the past.
- For the timeframe considered in modelling, the topography of the area has remained unchanged.
- Mine shafts and drifts are not considered in the model.

3.3 PALAEORECHARGE CALCULATIONS

Water budget modelling provides an estimate of the current balance between total aquifer withdrawals and discharge, aquifer recharge, and changes in aquifer storage. However, a number of factors - hydrogeological, hydrological and climatological, control groundwater occurrence and movement. The precise assessment of recharge and discharge is rather difficult, as no techniques are currently available for direct measurements. Hence, the methods employed for groundwater resource estimation are all indirect. Groundwater resources, being dynamic and replenishable, are generally estimated based on the component of annual recharge.

The aggregate nature of the water budget masks the differences between inflows to and outflows from individual aquifer zones. Much of the infiltration may only recharge shallow aquifers; recharge to deeper zones depends on local vertical hydraulic gradients and aquifer material properties.

For quantification of groundwater resources proper understanding of the behaviour and characteristics of the aquifers is essential. An aquifer has two main functions: a) to transmit water and b) to store it. Groundwater resources in unconfined aquifers can be described in terms of saturated conditions (i.e. the amount of groundwater available in the permeable portion of the aquifer below the zone of water level fluctuation) or unsaturated conditions (i.e. the amount of groundwater available in the zone of water level fluctuation).

The methodologies adopted for computing groundwater resources, are generally based on the hydrological budget techniques. The hydrologic equation for groundwater regime is a specialized form of water balance equation that requires quantification of various terms for inflow to and outflow from a groundwater reservoir, as well as of changes in storage. A few of these are directly measurable, some may be determined by differences between measured volumes or rates of flow of surface water and some require indirect methods of estimation.

Recharge can be estimated using a water-balance model. Simulated inputs and outputs of water from the soil root zone (i.e. precipitation, irrigation, surface runoff, evaporation and recharge) are monitored in a water-balance model using a bookkeeping-like procedure. The size of the soil root zone is defined on the basis of the root depth and the available water capacity. The available water capacity is the relative portion of the soil volume occupied by water held at tension values between the wilting point and total porosity. The available water content of the soil is computed iteratively starting from an assumed initial condition. Actual evaporation is estimated as a fraction of the potential evapotranspiration dependent on the relative available water content of the root zone. Recharge is simulated to occur whenever root-zone water exceeds the field capacity.

Surface evapotranspiration may be assessed by any of various meteorological methods, such as the Thornthwaite equation or using pan evaporation measurements with appropriate adjustments. Differences in evaporation characteristics of particular land covers can be recognized with the use of an evaporation factor, applied to the reference surface potential evaporation. Runoff can be estimated using a simple rainfall-runoff model such as the Horton model. Infiltration is computed as a function of the hydrodynamic parameters of the soil.

In typical hydrologic assessments, to allow the spatial diversity of climate and surface characteristics to be represented, the region of interest is usually divided into smaller spatial units for which characteristics can be assumed uniform. The simulation done for each sub-division requires a comprehensive time series of climate information. Thus, a multi-year weather time series is usually necessary to capture the effects of interannual rainfall variability. With sufficient point data in the region, incomplete records can be improved (synthetic series) in order to get a complete time series.

Hydrologic models are usually based on a general assumption of climatic seasonality. However, the large time frame considered by PADAMOT (i.e. 1 million years) makes it necessary to consider the impacts of long-term climate change (temperature, rainfall, evapotranspiration,…) on the regional hydrologic system and on groundwater recharge.

In order to estimate the palaeorecharge values associated with the timeframe of PADAMOT, a new methodology was developed based on the water budget principle. The starting point for the methodology was the actual information from weather stations in the two studied regions: Padul and Ratones/Alcuéscar. Among the available weather stations we have selected those two with the most complete and reliable time series which cover a period of 41 and 50 years respectively. In order to cope with the missing values found in the time series of Alcuéscar, we have applied a criterion by which those months without data were filled in with the corresponding weighted mean values of the same month from Padul. In other cases, when monthly averaged values for a given year were not available, missing values were obtained by considering the mean of the values for the same month from the complete time series. In order to test this assumption, changes introduced by this procedure in the mean annual precipitation were checked by confirming that the effect is negligible.

Based on the historic time-series data, we can observe that the weather stations of Padul and Alcuéscar (close to Ratones) share similar seasonal precipitation regimes and mean annual temperature. This is not the case, however, for the corresponding mean annual precipitation values. Nonetheless, both places have a comparable climate (Csa of the Köppen classification). Thus, if we take as a reference the mean annual precipitation of the two sites, it is possible to approximate the precipitation observed in each one of them by applying scale factors related to these mean values. For the sake of modelling we have assumed that the observed present day climatic similarity can be extrapolated to the past and, therefore, the mean annual precipitation correction is appropriate within the longer timeframe. Although of minor importance, a similar approach has been employed to correct temperatures between the two studied sites.

In contrast with typical hydrological studies, we have estimated the mean annual precipitation for Los Ratones in the past 120 ky from the palaeoclimatic series of Padul by scaling based on the ratio between the present-day mean annual rainfall values from the two sites. Moreover, in order to compute groundwater recharge at Los Ratones, we have built the time evolution of precipitation for each time period associated with constant climatic conditions. From these data, precipitation at Los Ratones was computed by scaling the time series, taking into account the ratio between the present-day mean annual rainfall and the corresponding estimated mean annual precipitation for each time period. For instance, if the mean annual precipitation from 0 to 5400 years has been estimated to be 1000 mm and our present day mean annual rainfall in the past 50 years (i.e. the time covered by the available meteorological data) is 600 mm, we have constructed a hypothetical time series with seasonal fluctuations by multiplying daily precipitation values by 1000/600. By doing that, the observed seasonality is preserved but precipitation is scaled to the long-term average. An analogous procedure has been used to correct temperatures. However the change in temperature by as much as 1 to 2 ºC will not affect significantly the water budget.

It is noted that we should not consider that the mean annual recharge will change in proportion to the ratios between the mean annual precipitation. In fact, the infiltration capacity of a soil layer depends on several parameters including time, soil properties (grain size, moisture content, porosity, etc), topography, etc.

The Padul site provides a continuous record of palaeoclimatic information. Taking the pollen content of several stratigraphic sections through the Padul peat bog as the principal indicator, it has been possible to identify a continuous series of climate stages from 500 ky BP up to present time. Each climate stage is characterized by the ombrothermal conditions constrained by the corresponding vegetation cover.

3.4 LOCAL HYDROGEOLOGICAL MODEL

According to the local hydrogeological model developed by Martínez Landa et al. (1999), groundwater in the vertical section that we have selected for modelling flows from a local watershed divide located at the east of the modelled domain towards the west. Within this domain, the Arroyo Maderos acts as a local discharge zone. As pointed out earlier, the hydrodynamic behaviour of the granitic massif determines the individualization of two flow domains of different scale and residence time: a) a shallow unconfined zone with relatively fast water movement associated with the moderately altered and fractured granite rock; b) a deep zone, made of fresh rock with scarce fractures. Each one of the two domains can be identified with shallow and deep aquifer systems. The flow of the latter one is constrained by regional hydraulic gradients extending far away from our modelled domain. A top layer including the soil zone and heavily weathered granite (loam) has been considered in connection with the shallow aquifer.

Information is not available concerning the 3D distribution of the thicknesses of the upper two layers (soil/loam layer and fractured zone). There is evidence that each one of the two layers may reach thicknesses of up to 46 and 205 m, respectively. Taking this into account and measuring from the surface, we have assumed constant thicknesses for both of them (45 and 225 m, respectively).

Apart from these major hydraulic systems, discrete fracture zones may play a significant role and we have considered the existence of the outcropping fault 5-220, that has been observed to crosscut the SR5 borehole at a depth of about 200m below the surface. This fault zone has enhanced permeability and porosity and distorts the flow lines, having a significant impact on the solute mass budget in the reactive transport modelling.

The reference timeframe considered for PADAMOT extends 1 million years from the present into the past. However, the responses of the key features relating flow and transport to the effect of climate change can be tested with shorter time periods. Therefore, we have considered two time-slices that, ending at the present time, cover 120 and 320 ky in the past. It is worth noting that extending the modelling timeframe does not constitute a technical handicap although it must be acknowledged that a single run with the longest timeframe (320 ky) and with the most complete reactive transport system may take more than 4 days using a PC computer (Pentium 4, 1800 MHz with 2 Gb RAM).

The model has focused on the effect of varying recharge conditions within the 120 ky initially considered. In order to proceed with the calculations we designed a finite element mesh made of 420 triangular elements and 242 nodes. Using the nomenclature of CORE^{2D} (Samper et al., 2000) we have defined four hydrodynamic material zones (Figure 3.6) whose properties are given in Table 3.1.

The domain represents a two-layer unconfined saturated aquifer under a transient regime. In order to satisfy the Courant number constraint, the selected time step was 1 year.

According to Martínez Landa et al (1999a,b) a mixed (Cauchy) boundary condition has been assigned to the node representing the Arroyo Maderos. The corresponding leakage coefficient, α, is 10^{-5} m^2/s while the reference head, H is 450 m. On the right edge of the model there are two types of boundary condition. A no-flow condition (which is consistent with the watershed divide character of this side of the model) has been associated with the nodes pertaining to the altered granite zone while for the nodes pertaining to the fresh rock (including that of the interface with altered rock) a constant head (Dirichlet condition) of 460 m was set up. Similarly, on the opposite edge (left end) the nodes associated to the fresh rock a constant water head of 450 m was given.

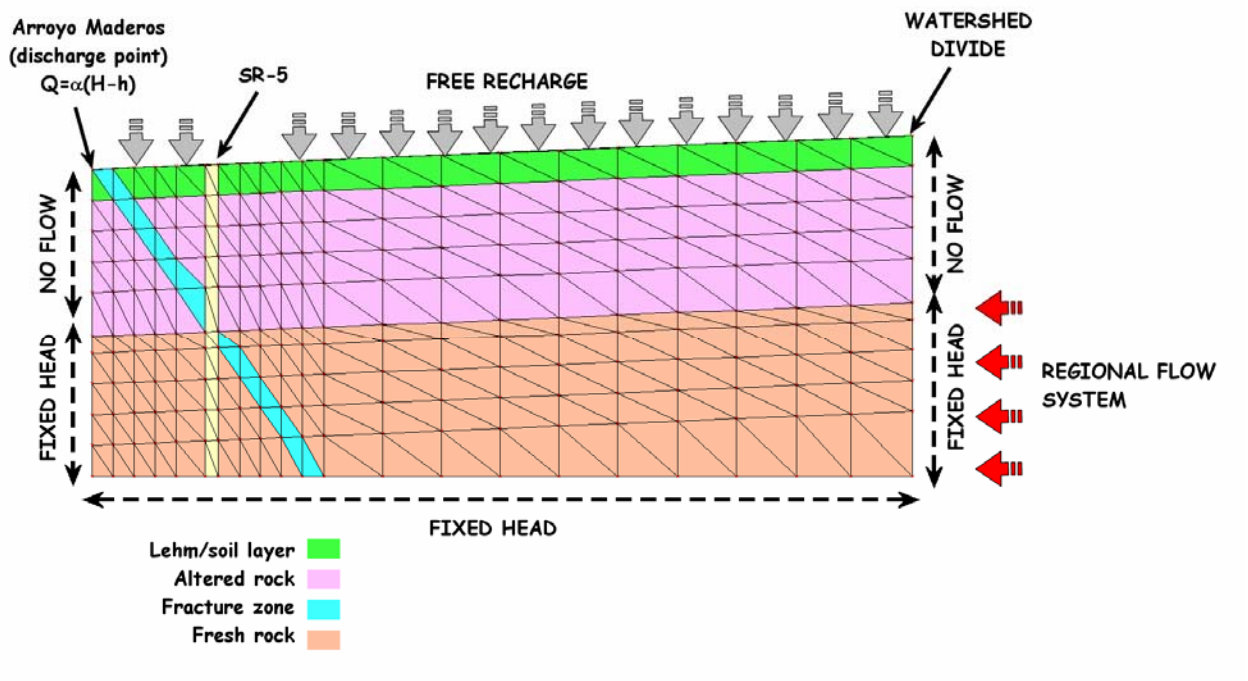

Figure 3.6. Finite element mesh and associated boundary conditions used in the modelling.

A time-dependent function for recharge has been assigned to the each one of the surface nodes. It has to be stressed that, as we mentioned before, the time-dependent recharge function represents the lower recharge estimates based on the palaeoclimate reconstruction.

Table 3.1. Summary of the hydrodynamic parameters corresponding to the different zones used in the modelling. K_{xx} and K_{yy} are the components of the hydraulic conductivity tensor and 'angle' is their angle with respect to horizontal.

Layer	K_{xx} (m/s)	K_{yy} (m/s)	angle	S_s (m^{-1})	ϕ
Soil/loam layer	10^{-5}	10^{-5}	0	$2.5x10^{-6}$	0.25
Altered rock layer	$2x10^{-8}$	$2x10^{-8}$	0	$5x10^{-6}$	0.20
Fresh rock	$2x10^{-10}$	$2x10^{-10}$	0	$5x10^{-8}$	0.01
Fracture zone	$4x10^{-5}$	$4x10^{-5}$	0	$2.5x10^{-6}$	0.25

Figure 3.7 represents the time evolution of the water flux discharging at the node simulating Arroyo Maderos during the past 320 ky. In the same figure there is a representation of the time-dependent mean recharge function. As expected, water recharge directly influences the amount of water discharging through the creek. It is worth noting that steady state (in the terms of flux) is achieved within one year after the change in recharge. This is related to the upper, high permeability zones (10^{-5} to $2x10^{-8}$ m/s for soil/loam layer, altered granite and fracture zone). The deeper lower permeability zone ($2x10^{-10}$ m/s) is less affected by recharge variations but attainment of steady state here may take longer times. Another factor is the small size of the catchment area modelled, 1200 m; the relatively low discharge values must be understood in that context.

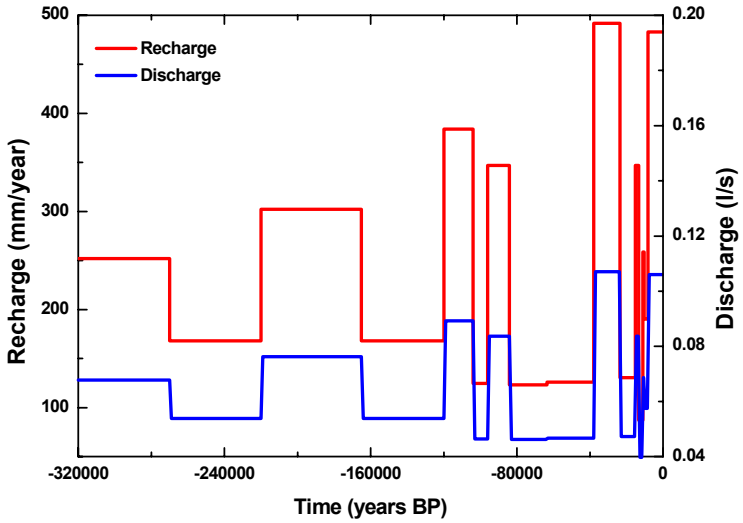

Figure 3.7. Time dependent evolution of recharge (minimum estimates) and associated discharge via the Arroyo Maderos creek.

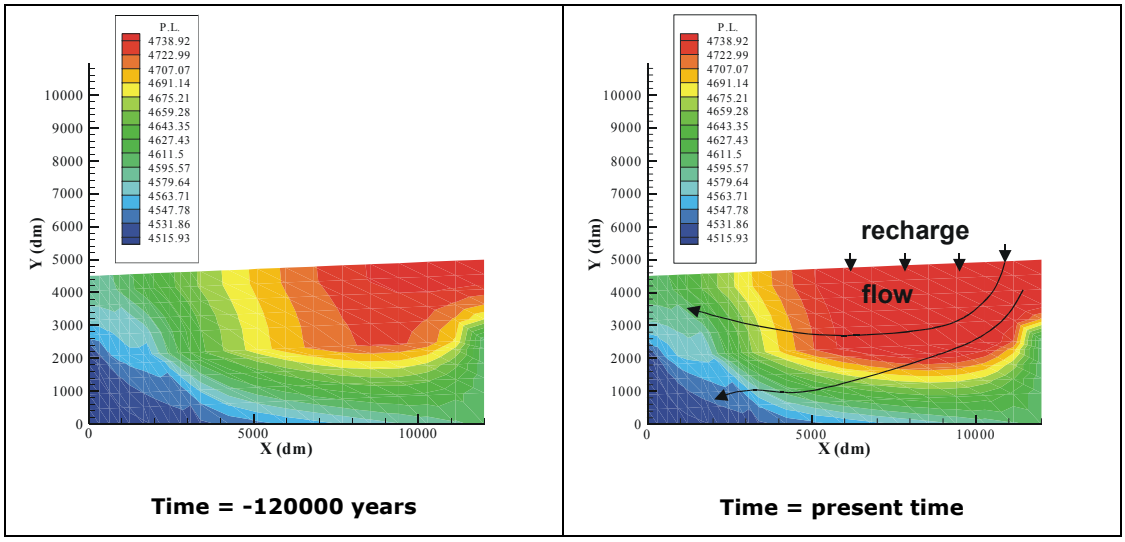

Figure 3.8. Spatial distribution of the piezometric levels within the modelled domain at times -120 ky (left) and present (right). The arrows on the right figure suggest the associated flow lines.

Figure 3.8 represents the spatial distribution of the piezometric levels in the past (-120 ky) and at present time. It is interesting to observe that the recharge-related water flow overprints the regional water flow system prevailing in the zones of fresh granite. We can see that flow occurs from surface to depth, with a substantial horizontal component. Finally, as expected, the fault acts as a preferential water conduit.

Additional results related to the sensitivity analyses are given in later sections.

3.5 CONSERVATIVE TRANSPORT MODEL ± RADIOACTIVE DECAY

The flow model provides the hydrodynamic base for the transport models (conservative and reactive). In the case of transport of conservative chemical species we have considered it of greater interest to test the behaviour of a component experiencing radioactive decay, ^{36}Cl. Thus, it is possible to compare the different concentrations arriving at the Arroyo Maderos discharge point as a result of varying climatic conditions and/or decay.

The simple conceptual model considers the existence of a radioactive source delivering an infinite and continuous supply of ^{36}Cl to the groundwaters. This source (a proxy for a failed repository) has been located at the lower boundary of the modelled domain, close to the watershed divide (X=1113.8 m; Figure 3.9). The node associated with that point has been assigned arbitrarily a constant Cl molality of 3.65 – note that this concentration has no relationship with the actual observed Cl concentration at Los Ratones (see below).

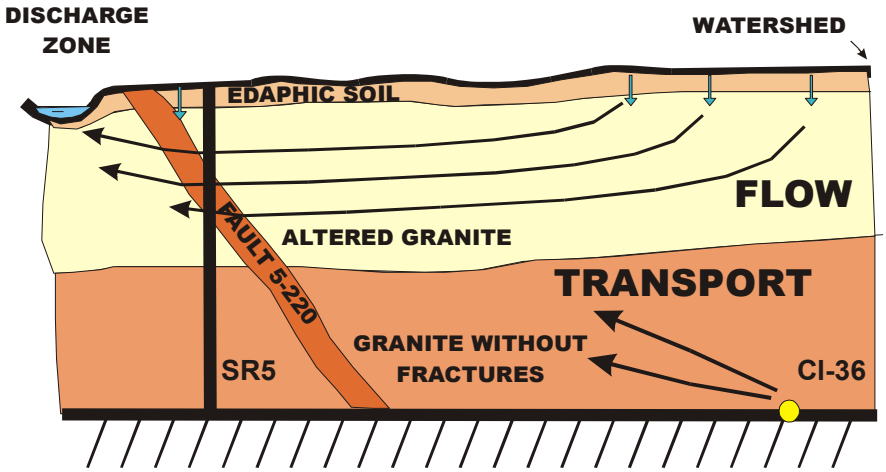

Figure 3.9. Simplified conceptual model for the ^{36}Cl transport model.

The diffusion coefficient for chloride has been set as $2x10^{-9}$ m^2/s while values of longitudinal and transverse dispersivities are both equal to 800 m. These values satisfy the Peclet number constraint ($P_e \leq 2$) for numerical stability.

Figure 3.10 represents the time evolution of chloride concentration at the discharge node for the timeframe of 120 ky. Conservative transport with and without radioactive decay are both shown in the plot. If a lower concentration for the initial point source of ^{36}Cl were to be modelled, the absolute heights of the peaks at the discharge point would be lowered. In addition, the smooth rises or falls around each peak would be affected because these parts of the curve are governed by diffusion.

It is interesting to observe that there exists a direct coupling between changes in recharge and chloride concentration although, in contrast to that observed in the flow model, the shape of the breakthrough curves are modified according to the diffusivity of chloride. This means that, when considering transport without radioactive decay, the steady state is achieved after longer periods of time than in the case of water flux. In the case of transport plus radioactive decay, steady state is not achieved because the decay constant of ^{36}Cl (301 ky) is greater than the timeframe for modelling. It can be seen that the modelling shows that external effects like those associated with climatic fluctuations can affect the discharging concentration of the contaminating nuclide in a very significant way which is counter to the simple concept of radionuclide decay reducing dose consistently over time: consider the peaks at ca. -95,000 and -38,000 years.

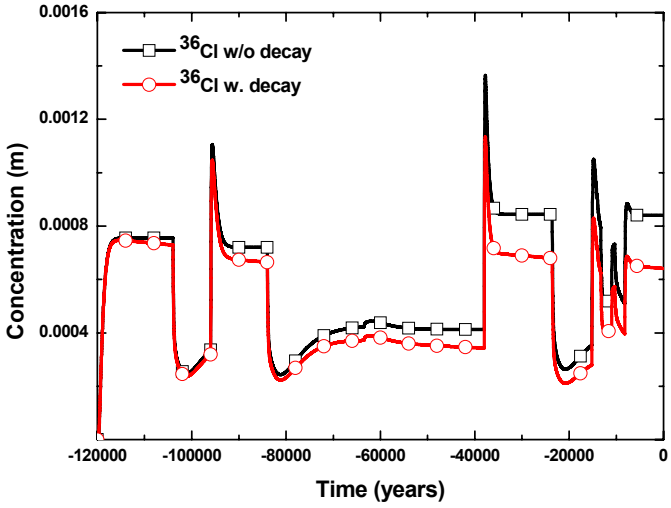

Figure 3.10. Time-dependent evolution of the concentration of ^{36}Cl discharging at the Arroyo Maderos. Note that each curve corresponds to cases considering or not radioactive decay (circles and squares, respectively).

On the other hand, high recharge values correlate with low Cl concentrations, a fact that should be expected because of the higher volume of water discharging under these conditions.

The effect of radioactive decay is to lower the total chloride concentrations attained as a function of time although the profile of the breakthrough curve is comparable to that of the other case.

Further details concerning the results of different sensitivity analyses are given in the following sections.

3.6 REACTIVE TRANSPORT MODELLING

Thirteen chemical components (or primary species) are used to define the chemistry of groundwaters and rocks of the modelled domain: H_2O, H^+, e^-, Na, K, Ca, Mg, Fe, Cl, HCO_3, SO_4, PO_4 and SiO_2. Fifty-eight additional aqueous (secondary) species were considered in the speciation model. Modelling was carried out for a constant temperature of 25°C (though the average temperature of the Los Ratones system is 15°C – the resulting error is insignificant relative to other uncertainties). Aqueous species were selected on the basis of which were expected to be the most abundant within the expected limits of pH, T and redox.

Eight mineral phases were considered relevant for the system: quartz, calcite, siderite, ankerite, dolomite, hydroxyapatite, goethite and pyrite. Ankerite is a solid solution mineral that has been identified to be present in the vein fillings of Los Ratones. Its composition has been assumed to be equal to that of the pure Ca-Fe 1:1 stoichiometric carbonate, and the corresponding equilibrium constant (log K_{eq} = +2.4876) is given by Langmuir (1997).

Kinetically-controlled feldspar dissolution/precipitation reactions might also be significant over the modelled timescale. However it cannot be assumed that feldspars, though present, have always been available for reaction because alteration minerals (microcrystalline quartz, kaolinite, gibbsite, etc) may protect it. If this is the case, the effective reactive surface area is undetermined and variable. This concept is supported by the observation that fresh feldspar surfaces are not seen in the Los Ratones system. The issue then is: is it better or not to include kinetics in the modelling? Including kinetics would benefit the model in terms of

comprehensiveness, complexity and illustration of the magnitude of different processes, but would be very uncertain. The present modelling, though simplified, is sufficient for present purposes, i.e. to demonstrate that it is plausible that climatic change could affect the groundwater system down to the expected depth of a future HLW repository. However this has not yet been supported by field data for the Los Ratones case. Further work, both field studies at appropriate sites and new, more constrained modelling, should start from that provisional finding.

Some of the selected mineral phases of the system are assumed to be present at the beginning of modelling (Table 3.2) while some others are the products of mass transfer. Whatever the case, the total amount of reactive minerals changes as a function of time in response to water movement.

There is no information on the amounts of minerals present in the system in the past. However, there is a wide database on the chemical characteristics and mineral distribution of the present-day Los Ratones System. Based on that, we have assumed initial volume fractions for some minerals but it must be emphasized that they are educated guesses. In fact, there is little uncertainty in the mineral abundances of the granite rock but a much lower definition in vein-filling minerals.

The chemical compositions of the groundwater and recharge water used in the modelling are given in Table 3.3. As in the case of mineral phases, there is no available information on the chemical characteristics of groundwaters in the past. However, the exhaustive hydrochemical survey conducted at Los Ratones at the end of 1990's and beginning of the 2000's provides a clear picture of the present day groundwater features. Thus, in the vicinity of the SR-5 borehole (a site considered representative of the undisturbed nature of the granite massif) significant changes are observed as a function of depth that must be related to different residence times and reactive histories of the recharge waters (Figure 3.11).

Table 3.2. Minerals, associated volume fractions and identification of water types present initially in the different material zones considered in the modelling of Los Ratones system. Other minerals were assumed to be non-reactive.

Layer	Water Type	Quartz	Calcite	Dolomite	Hydroxy-apatite	Goethite	Ankerite	Pyrite
Soil/loam layer	IW-1	0.1	0.0	0.0	0.05	0.05	0.0	0.0
Altered rock layer	IW-2	0.25	0.1	0.0	0.005	0.0	0.0	0.0003
Fresh rock	IW-3	0.25	0.1	0.0	0.005	0.0	0.0	0.0003
Fault zone	IW-2/IW/3	0.25	0.1	0.0	0.2	0.0	0.1	0.005

Any decision concerning the selection of waters for modelling could be questioned. Making the composition of BW-2 (deep groundwater) equal to that of the deepest groundwaters in borehole SR-5 might be reasonable considering the long residence times (several tens of thousands of years) of water in the deep system, i.e. reflecting a composition constrained by water/rock interactions operating through long periods of time.

Table 3.3. Chemical composition of the different waters used to model Los Ratones system. All the concentrations are reported as log molality values except pH and Eh (in volts). Data from Gómez (2002).

Water Type	IW-1	IW-2	IW-3	BW-1	BW-2
pH	7.2	7.5	7.9	7.1	7.9
Eh	0.003	-0.167	-0.226	0.799	-0.226
Na	-2.807	-2.793	-2.353	-2.807	-2.353
K	-4.048	-4.101	-4.249	-4.048	-4.249
Ca	-3.489	-3.373	-3.745	-3.489	-3.745
Mg	-4.488	-3.357	-3.686	-4.488	-3.686
Fe	-6.975	-6.145	-5.370	-20.0	-5.370
Cl	-3.550	-3.550	-3.319	-3.550	-3.319
HCO_3	-5.561	-2.022	-1.733	-4.120	-1.733
SO_4	-4.478	-4.177	-1.893	-4.478	-1.893
PO_4	-4.215	-20.0	-5.678	-20.0	-5.678
SiO_2	-3.317	-4.000	-3.987	-3.317	-3.987
Balance (%)	+2.6	-1.2	-2.7	+5.9	-2.7

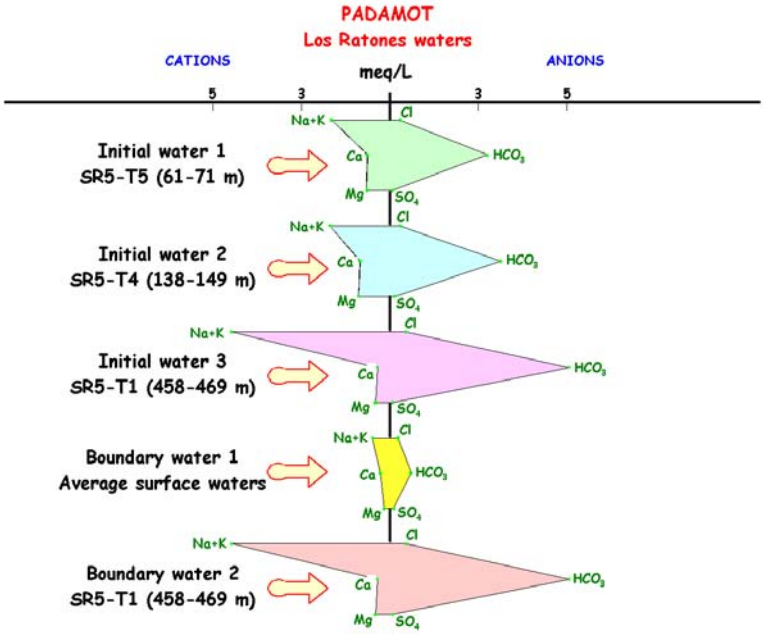

Figure 3.11. Stiff plots illustrating the major ion chemical characteristics of the waters used in the modelling. Note that initial water #3 and boundary water #2 have the same chemical composition.

For modelling, we have assigned chemical compositions for groundwaters in the different material zones of the domain. Accordingly, we have defined three types of initial waters (IW-1, IW-2 and IW-3) and two boundary waters (BW-1 and BW-2). IW-1 corresponds to the present day measured concentrations found in the SR-5 borehole within a depth interval of 61-71 m while IW-2 and IW-3 are associated with depth intervals of 138-149 and 458-469 m respectively. BW-1 represents the average composition of small creeks and other surface waters. The chemical composition of BW-2 is identical to that of initial water #3, i.e. deep groundwater belonging to the regional flow system. On the other hand, the boundary water #1 (BW-1, recharge water) has a composition equal to that of water in the upper layer (soil/loam layer) although the bicarbonate content and redox value have been fixed by equilibrium with the atmospheric partial pressures of CO_2 (P_{CO2}= 0.00032 bar) and O_2 (P_{O2}=0.205 bar) (Figure 3.12).

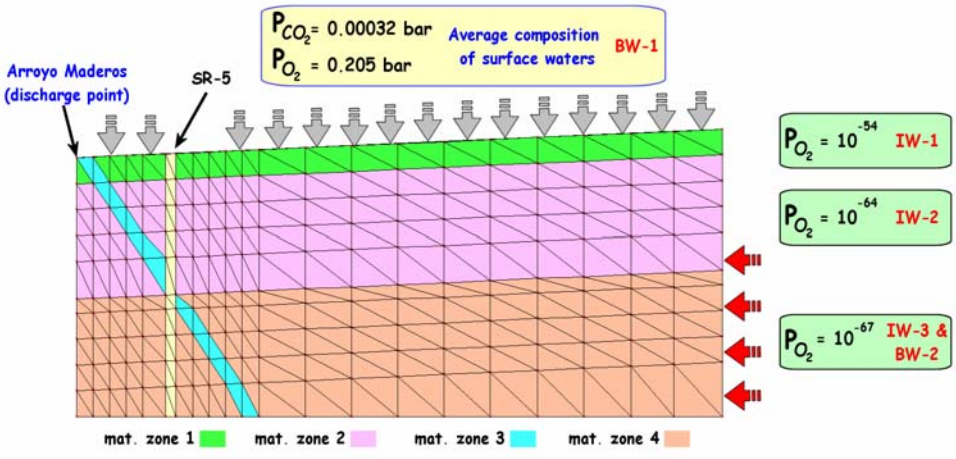

Figure 3.12. Assignment of water types and corresponding initial chemical conditions related to redox and total carbonate content.

At the present time, soil cover in the area is scarce (see the aerial photograph shown in Figure 3.3). It could be suggested that present-day depleted soil cover is not representative of the modelled timeframe and that, for some periods, recharge water might have had lower (more reducing) redox and higher P_{CO2}. However several lines of evidence suggest that soil cover might have been depleted throughout the period. For instance, the flat topography suggests that if a thick soil cover were developed in the past it should remain on site today, at least in part. The average major ion chemistry of river waters (BW-1) in the area has similar ion ratios to those in the waters of the upper (altered granite, IW-1) and intermediate (fractured granite, IW-2) layers. On the other hand, measured redox (Eh) is ~0.0 volts for IW-1 and becomes more reducing with depth (-0.17 v for IW-2 and -0.23 v for IW-3). Hence, water in the upper zone keeps an oxidising fingerprint that might not be compatible with a reducing soil solution. River waters have an average pH of 7.1 while IW-1, IW-2 and IW-3 have values of 7.2, 7.5 and 7.9 respectively. Thus, the acidic fingerprint typical of many soil solutions is not observed in the upper layer of the system. In summary, the simplest assumption of boundary conditions being temporally invariant has been adopted for this preliminary modelling.

In a detailed study by Gómez (2002), a number of geochemical processes have been invoked to account for the variable hydrochemistry found at Los Ratones system. They include:

- Dissolution of carbonates (ankerite-calcite) in presence of CO_2 ($CaCO_3 + CO_{2(g)} + H_2O \Leftrightarrow Ca^{2+} + 2HCO_3^-$)
- Oxidation of sulfide minerals and precipitation of Fe^{3+} oxyhydroxides
- Dissolution/precipitation of apatite
- Alteration of albite to kaolinite and smectite
- Cation exchange reactions:

$$\tfrac{1}{2}\, Ca^{2+} + NaX \Leftrightarrow \tfrac{1}{2}\, CaX_2 + Na^+$$

$$\tfrac{1}{2}\, Mg^{2+} + NaX \Leftrightarrow \tfrac{1}{2}\, MgX_2 + Na^+$$

$$\tfrac{1}{2}\, Fe^{2+} + NaX \Leftrightarrow \tfrac{1}{2}\, FeX_2 + Na^+$$

In order to perform a rigorous reactive transport analysis, the time-dependent rate of mineral dissolution/precipitation should be taken into account. However, there is no available information at present regarding reactive surface areas. Therefore, for the purpose of PADAMOT we did not consider the kinetics of dissolution/precipitation reactions involving silicate minerals other than quartz and for the rest we assumed an equilibrium constraint. Likewise, there are not enough data related to ion exchange reactions (i.e. cation exchange capacities, mineral abundances, selectivity coefficients) to justify the inclusion of such a process in the modelling.

Modelling was carried out in a series of consecutive steps of increasing complexity. The final runs included all the components, water types, minerals and aqueous species described earlier. In order to fulfil the Peclet and Courant number criteria for the grid, a run covering 120 ky requires ~60,000 time steps, a number that, in terms of computing effort, has to be multiplied by the number of nodes and the number of iterations needed to solve the flow, transport and geochemical equations. To give an idea about the modelling times, a model with the more complex geochemical system over a timeframe of 320 ky took about four days of intensive, exclusive, computation in a PC computer (Pentium 4, 1800 MHz with 2 Gb RAM).

The most significant results of the reactive transport modelling are outlined next.

Figure 3.13 represents the spatial distribution of Na, K, and Mg at two given times representative of low and high recharge values. In all of them the effect of changing recharge on the concentration of these species is evident.

The fault zone acts as a major water conduit so that below that zone, a body of relatively stagnant water is preserved. This water body makes it possible to describe the relative differences found between the two recharge situations. Thus, it is interesting to observe in Table 3.3 that the aqueous concentrations of Na and Mg in the initial water of the deep aquifer are smaller than these corresponding to the recharge waters. The opposite happens to K. Hence, low recharge values determine a lower degree of replacement of the waters initially present in the aquifers. Alternating high and low recharge values result in a sequence of site-dependent low and high concentrations of Na, K and Mg accordingly to the distinct chemical characteristics of the two boundary waters. The same pattern prevails for chloride and is also present in other non-conservative species.

Figure 3.14 illustrates the spatial distributions of the aqueous concentrations of Ca, total inorganic carbon and pH. In this case, all the species are related not only via dilution and mixing, but are also involved in chemical reactions related to the dissolution and precipitation of different carbonate minerals. It is interesting to observe that, from the soil layer downwards, low recharge values are associated with slightly more basic waters than when recharge is higher. This is due not only to the infiltration characteristics of groundwaters but to the reactivity of the geological system.

The modelled mineral patterns and parageneses are broadly consistent with those observed in the field or in the boreholes. In addition the model predicts that, due to changes in recharge, the rate of precipitation of some minerals may change, i.e. giving rise to banded mineral growth patterns like the ones observed in some fracture fillings from borehole SR5.

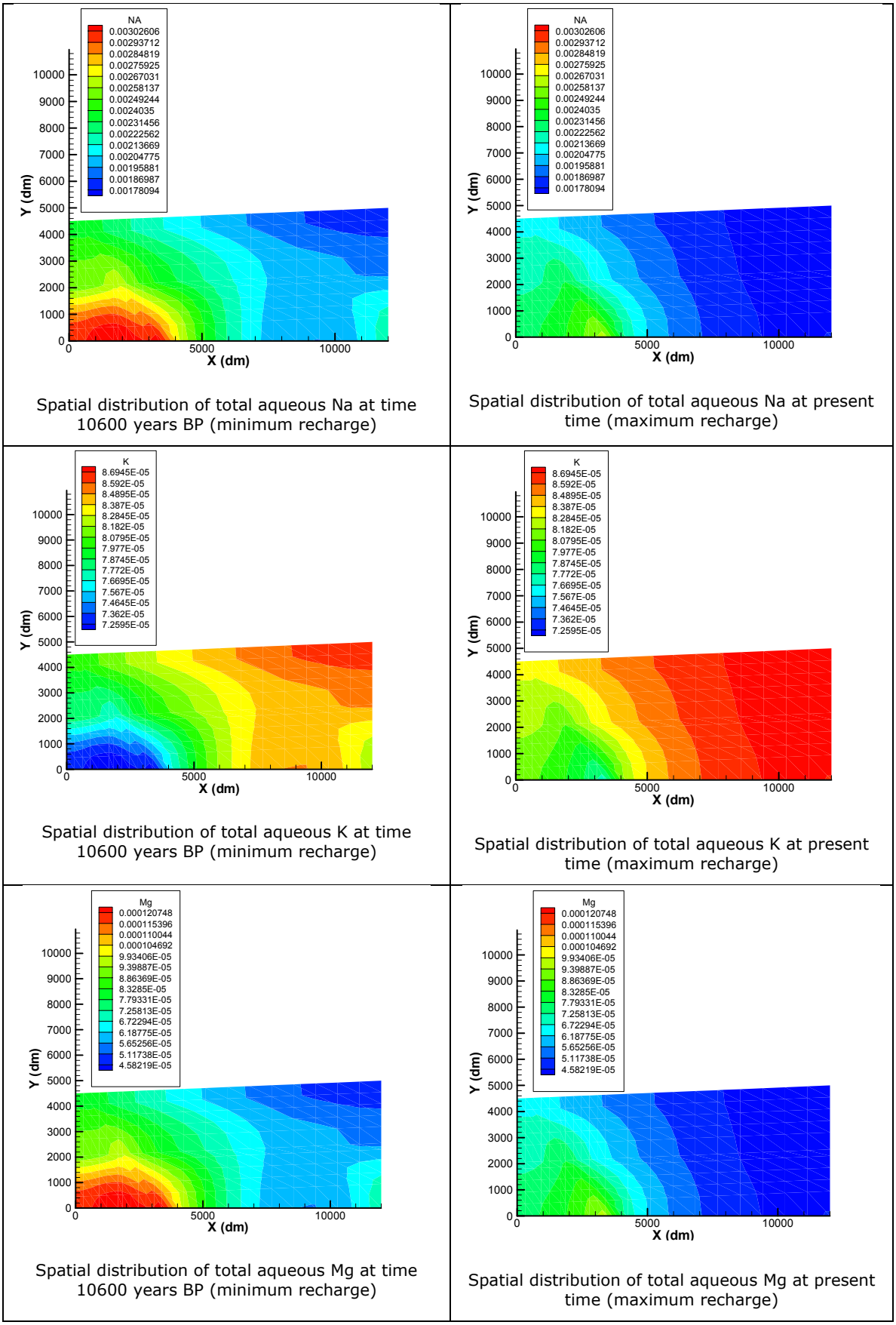

Spatial distribution of total aqueous Na at time 10600 years BP (minimum recharge)

Spatial distribution of total aqueous Na at present time (maximum recharge)

Spatial distribution of total aqueous K at time 10600 years BP (minimum recharge)

Spatial distribution of total aqueous K at present time (maximum recharge)

Spatial distribution of total aqueous Mg at time 10600 years BP (minimum recharge)

Spatial distribution of total aqueous Mg at present time (maximum recharge)

Figure 3.13. Spatial distribution of Na, K and Mg at two times representing minimum and maximum recharge (left and right, respectively)

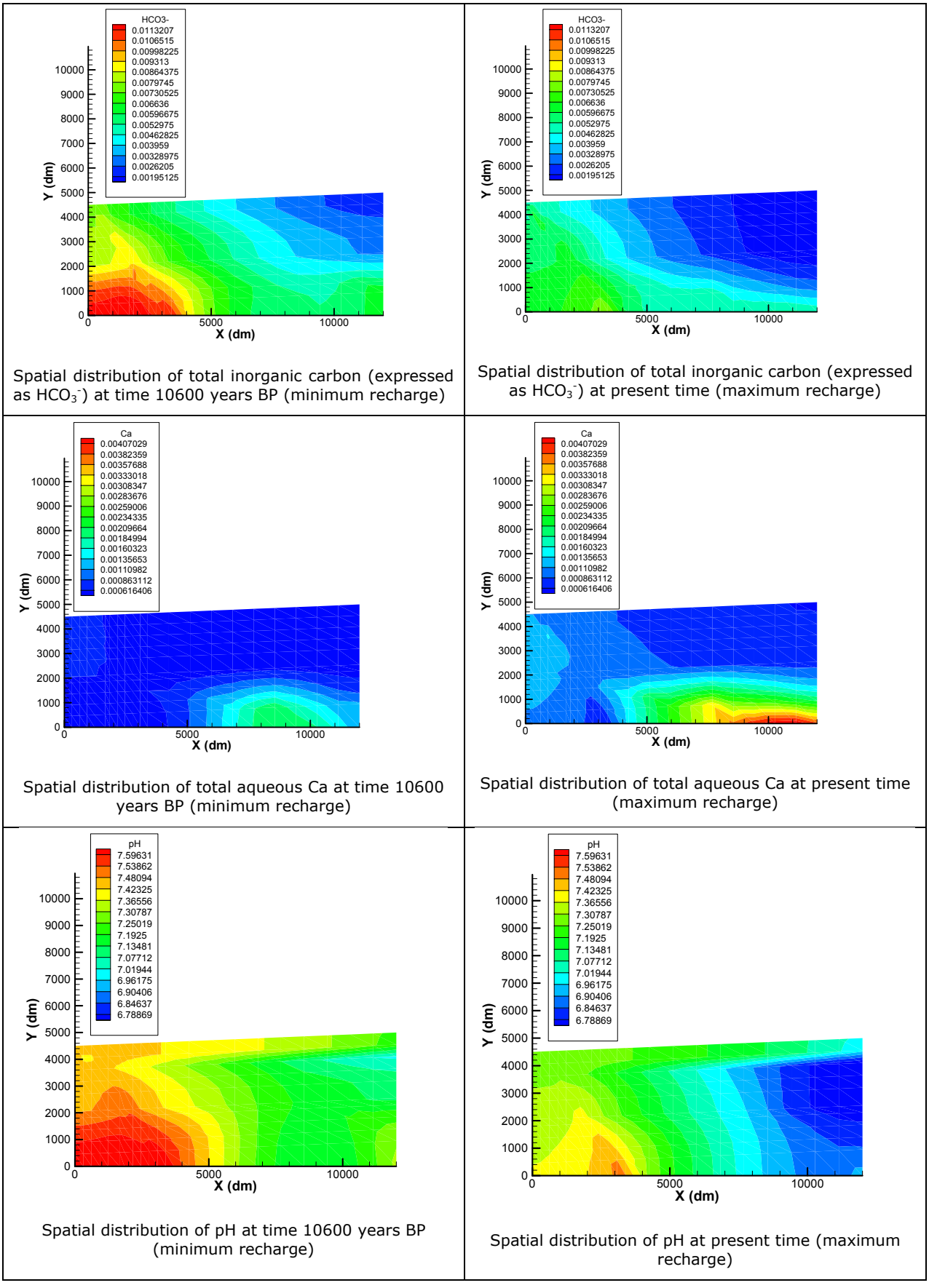

Spatial distribution of total inorganic carbon (expressed as HCO_3^-) at time 10600 years BP (minimum recharge)

Spatial distribution of total inorganic carbon (expressed as HCO_3^-) at present time (maximum recharge)

Spatial distribution of total aqueous Ca at time 10600 years BP (minimum recharge)

Spatial distribution of total aqueous Ca at present time (maximum recharge)

Spatial distribution of pH at time 10600 years BP (minimum recharge)

Spatial distribution of pH at present time (maximum recharge)

Figure 3.14. Spatial distribution of Ca, total inorganic carbon (as HCO_3) and pH at two times representing minimum and maximum recharge (left and right, respectively)

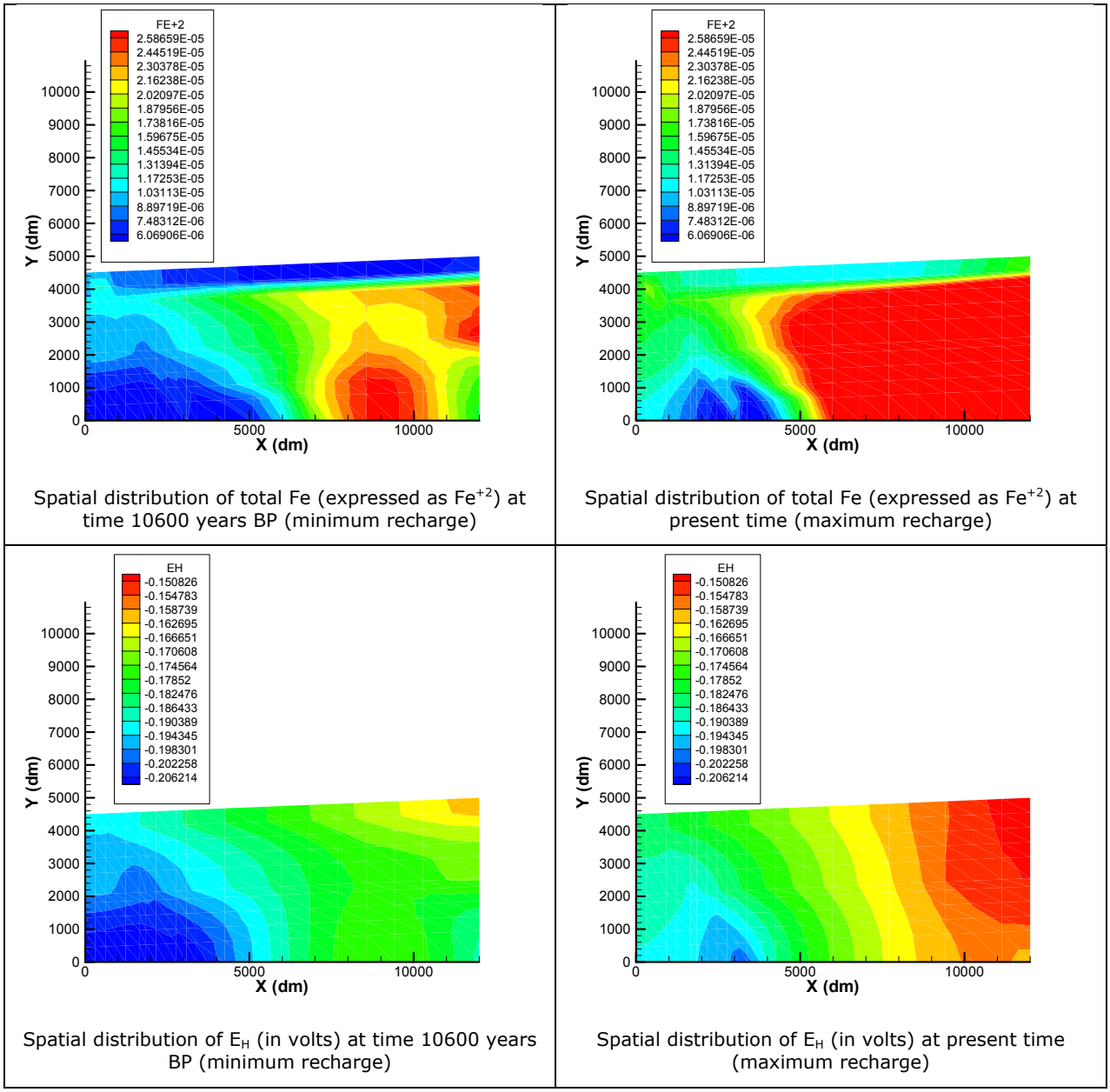

Figure 3.15. Spatial distribution of the total dissolved iron content and redox at two times representing minimum and maximum recharge (left and right, respectively).

Figure 3.15 shows the spatial distribution of iron and redox potential (Eh) associated with the reference stages of low and high recharge values. It is interesting to observe the complex pattern of iron distribution when recharge is low and the apparent regularity for high values of recharge. In both cases, there is a significant stratification associated with the upper layer where a significant amount of goethite constrains the amount of Fe in solution. On the other hand, the redox pattern in both cases is clearly negative under all circumstances although it clearly evolves toward slightly more oxidizing values when recharge values are high. This is a clear effect of the influence of relatively oxidizing recharge waters and the relative dominance of the shallow aquifer.

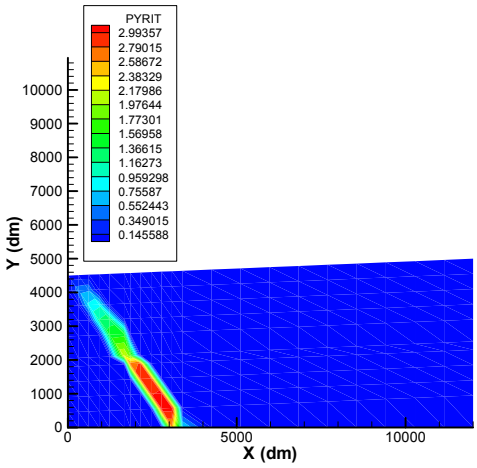

Spatial distribution of precipitated/dissolved pyrite at time 10600 years BP (minimum recharge)

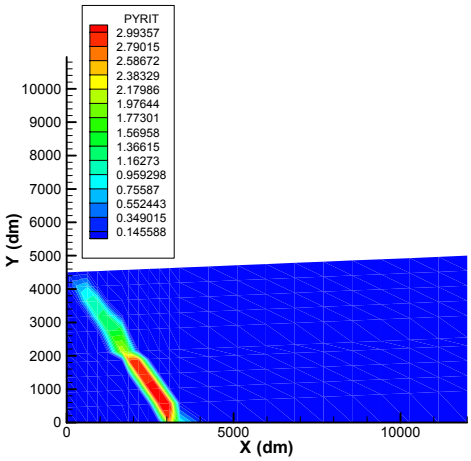

Spatial distribution of total precipitated/dissolved pyrite at present time (maximum recharge)

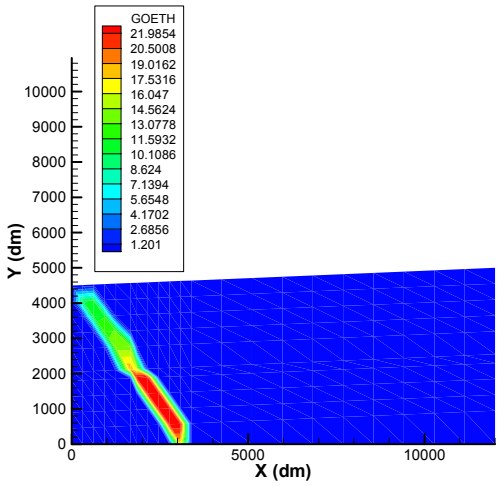

Spatial distribution of precipitated/dissolved goethite at time 10600 years BP (minimum recharge)

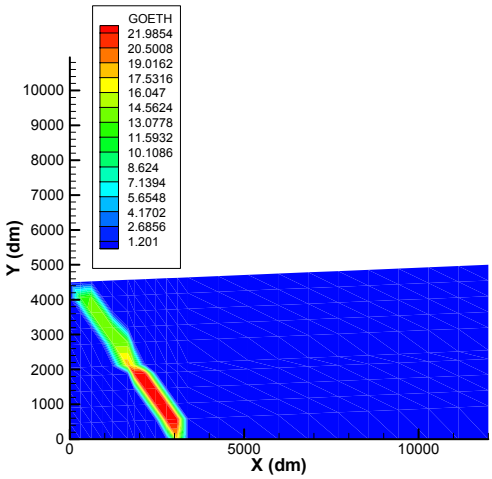

Spatial distribution of precipitated/dissolved goethite at present time (maximum recharge)

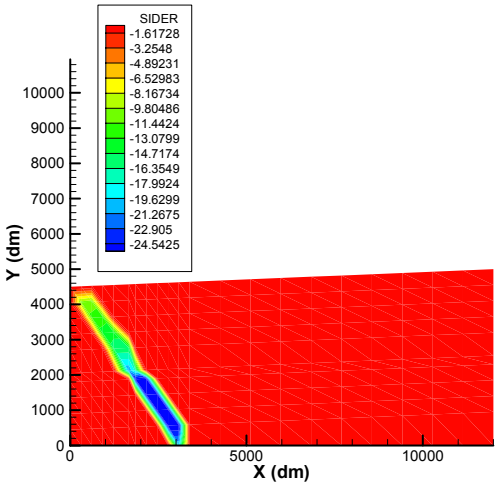

Spatial distribution of precipitated/dissolved ankerite at time 10600 years BP (minimum recharge).

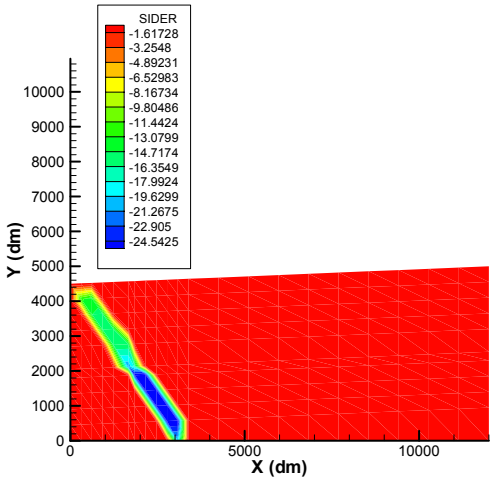

Spatial distribution of precipitated/dissolved ankerite at present time (maximum recharge)

Figure 3.16. Spatial distribution of cumulative mass of mineral dissolved (negative values) and precipitated (positive values) at two times representing minimum and maximum recharge (left and right, respectively): pyrite, goethite and ankerite.

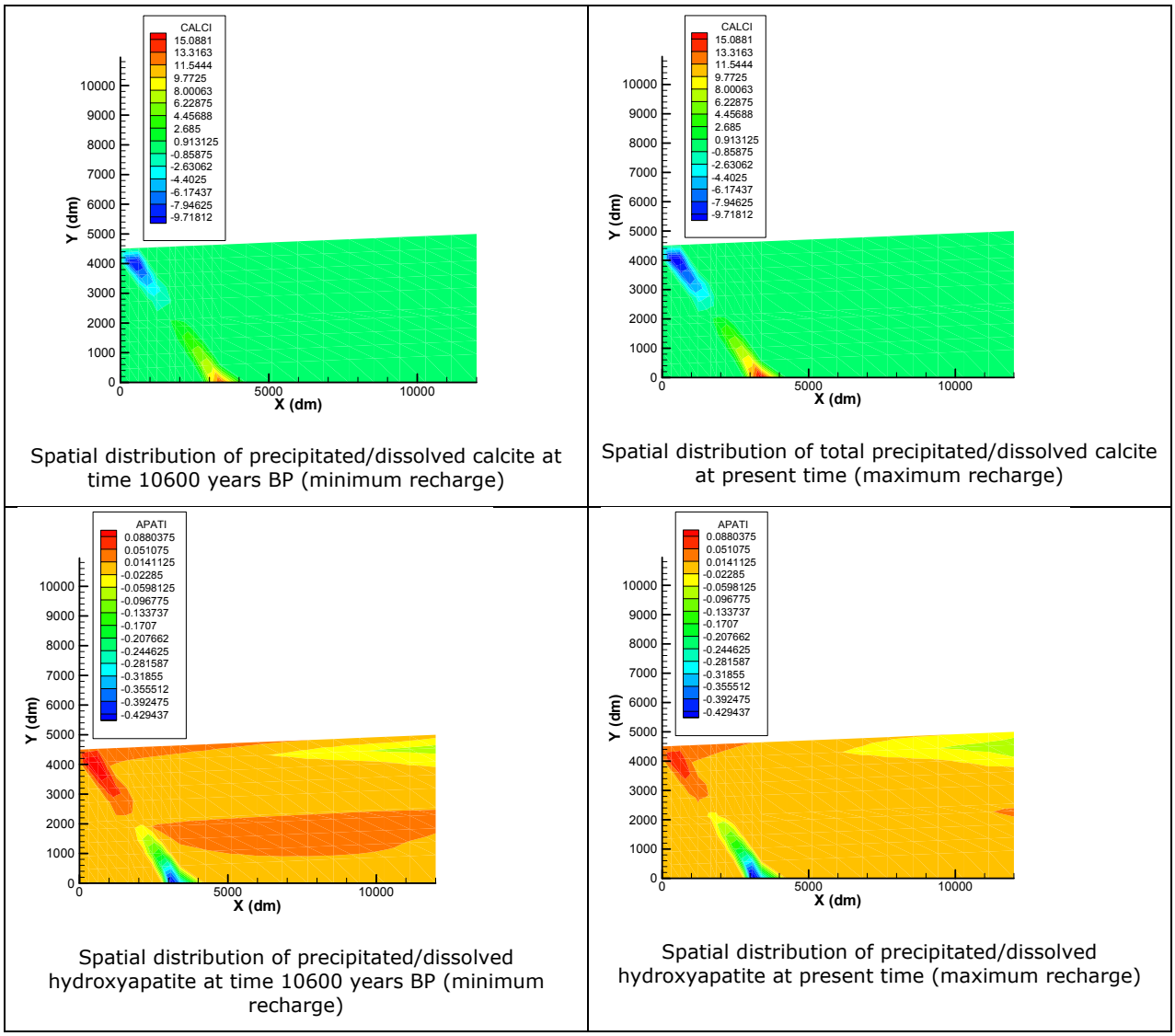

Figure 3.17. Spatial distribution of cumulative mass of mineral dissolved (negative values) and precipitated (positive values) at two times representing minimum and maximum recharge (left and right, respectively): calcite and hydroxyapatite.

Figures 3.16 and 3.17 show the cumulative masses of different minerals dissolved and/or precipitated in the modelled domain. It is interesting to observe that, with the exception of quartz (which is not illustrated here) and to lesser extent hydroxyapatite, the major part of the dissolution/precipitation processes occur within the realm of the fault zone. In the case of quartz, the interface between the shallow aquifer and the deep aquifer concentrates most of the SiO_2 mass transfer, with enhanced precipitation during the low recharge periods and net dissolution when recharge is high. This is related to the maintenance of quartz equilibrium for different proportions of the initial waters IW-1 to IW-3, which have varying initial concentrations of SiO_2. It is worth noting that the precipitation of quartz along the fault zone is constant through time, though at different rates.

In the case of hydroxyapatite, dissolution/precipitation is concentrated in the fault zone. Its behaviour is the opposite to that of calcite: while calcite tends to precipitate at the deepest points, hydroxyapatite tends to dissolve. Conversely, calcite dissolves close to the surface while hydroxyapatite precipitates. This is consistent with the patterns observed in the field.

The switch between low and high recharge apparently induces a slight displacement of the equilibrium interface of both minerals (no dissolution and/or precipitation). Hence, the interface

moves upwards when recharge rises which determine that along this zone there is a chance for alternating precipitation of both minerals as well as the development of eventual corrosion textures.

In the case of pyrite, goethite and ankerite, the behaviour is similar irrespective of the recharge regime. Thus, pyrite and goethite tend to precipitate in the fault zone, with preference for the deepest layers. However, ankerite tends to dissolve throughout the fault but with lesser emphasis on the shallowest layers.

The time-dependent evolution of the parameters previously described on a spatial basis provides new insights on the behaviour of the Los Ratones system when affected by varying groundwater recharge conditions. For the sake of brevity we will show some results related to the 120,000 years model runs.

Four different nodes were selected in order to analyze the trends. They are located along the line representing the SR-5 borehole. Three of the nodes belong to one of the material zones described earlier. The fourth node is associated with the discharge point (i.e. Arroyo Maderos). Each node has been identified in the figures as deep aquifer (fresh rock layer), shallow aquifer (altered rock layer) and near surface (soil/loam layer).

The general trend of conservative species has been shown in the previous section. Hence, we will concentrate on describing the major features arising from the non-conservative species.

Figure 3.18 displays a series of plots related to the evolution of selected solutes and geochemical parameters. In each one of them it is possible to observe the geochemical response of the distinct parts of the groundwater system (i.e. deep vs. shallow aquifer) as a function of recharge. Thus, in terms of pH the response at different layers of the system is nearly instantaneous (at the scale of several years) although there is a delayed response of the deep aquifer when compared to the upper layer and shallow zone (observe the progressive smoothness of the peaks). A similar thing happens to redox. It is interesting to note that, although the recharge water is strictly oxidizing (in equilibrium with atmospheric O_2) its oxidizing capacity is overwhelmed by the buffer capacity of the rock. Hence, the net value of Eh is always negative and we can observe some stratification in the Eh values associated with progressively less deep zones. This tendency might be obscured by the enhanced flow in the fault zone, which is able to raise deep reducing waters towards the surface.

The comparable evolution of total inorganic carbon (TIC), Ca, pH and phosphate is shown in Figure 3.18. Calcite and hydroxyapatite compete for the calcium in solution so that there is a certain incompatibility between these two minerals. It worth noting that the concentration of TIC dominates those of Ca and PO_4, while Ca is higher than PO_4. Thus, changes in the dissolution/precipitation tendency of calcite (triggered by the time-dependent composition of groundwaters) determine variations in the total concentration of Ca which, in turn, affect the behaviour of hydroxyapatite. Although the relative variation of Ca in solution due to varying recharge is small, because the mass action constraint for hydroxyapatite equilibrium requires low Ca concentrations, wider changes in Ca translate into enhanced dissolution/precipitation of the phosphate mineral. The iron and sulphate concentrations are governed by similar effects.

Figure 3.19 shows the dissolution/precipitation behaviour of selected minerals. It is interesting to observe that in most of the plots there are significant modifications in the slopes of the curves. Because the representation is related to time, a change in slope can be understood as a change in the rate of dissolution/precipitation. Thus, changes in the aquifer recharge translate into changes in the rate of mass transfer among solutes and rock. Another interesting feature is that the dissolution/precipitation of mineral phases is a process associated with given areas so that, for the same time, the dissolution of a mineral might be occurring at some given point while precipitation happens elsewhere.

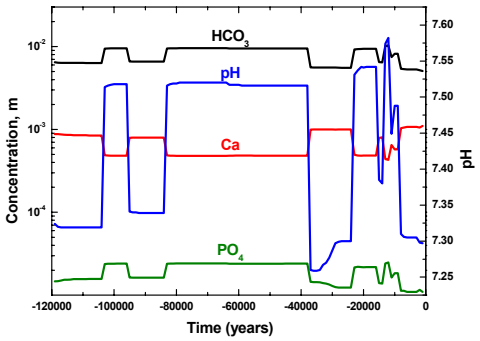

Time evolution of pH and the aqueous concentrations of of Ca, HCO_3 and PO_4 associated with node 11 (discharge point)

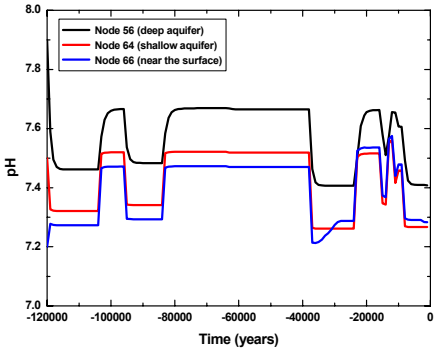

Modelled evolution of pH at three different nodes located along the SR-5 borehole

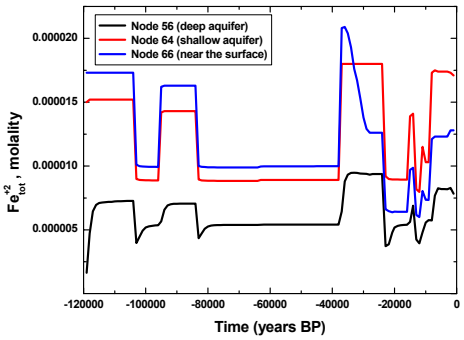

Time evolution of the aqueous concentration of total iron at the nodes associated with the different material zones found along the SR-5 borehole

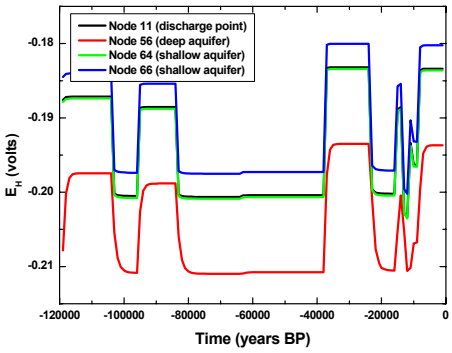

Modelled evolution of Eh at the nodes associated with the different material zones found along the SR-5 borehole

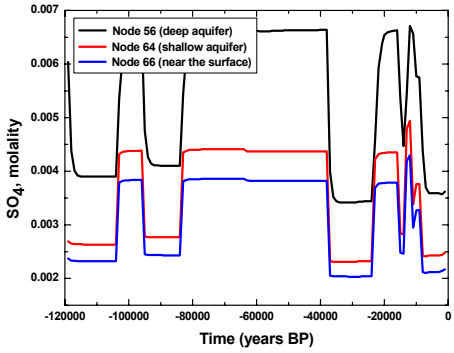

Time evolution of the aqueous concentration of total sulfur at the nodes associated with the different material zones found along the SR-5 borehole

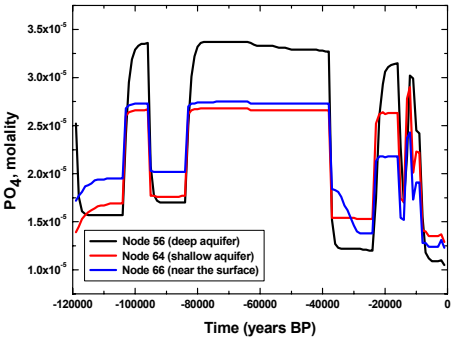

Time evolution of the aqueous concentration of aqueous phosphate at the nodes associated with the different material zones found along the SR-5 borehole

Figure 3.18. Time-dependent evolution of selected aqueous concentrations and geochemical parameters associated with nodes located along the SR-5 borehole and at the discharge point of the system.

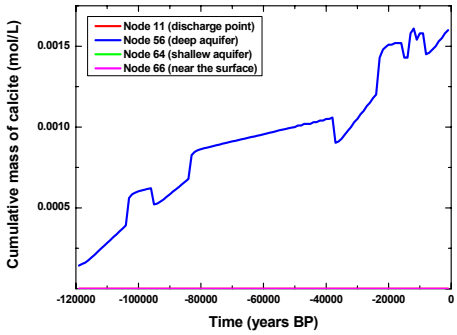

Cumulative mass of calcite precipitated as a function of time at the nodes associated with the different material zones found along the SR-5 borehole. Note the change in the slope disclosing a modification in the rate of calcite precipitation

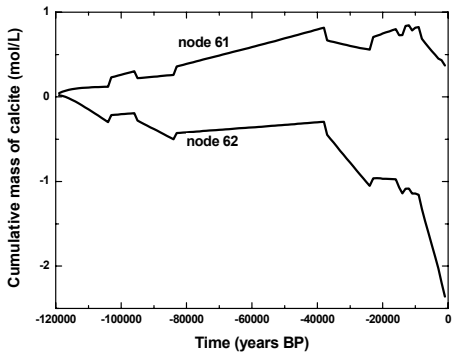

Cumulative mass of calcite precipitated as a function of time at two nodes associated with the fault zone. Note that, while at some points may we have precipitation, at the same time dissolution may take place in the close vicinity

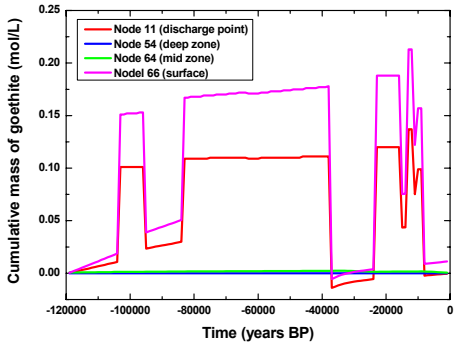

Cumulative mass of goethite precipitated as a function of time at the nodes associated with the different material zones found along the SR-5 borehole

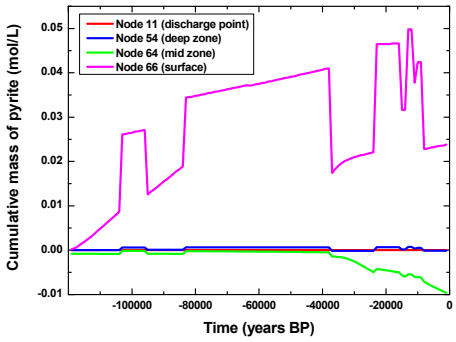

Cumulative mass of pyrite precipitated as a function of time at the nodes associated with the different material zones found along the SR-5 borehole

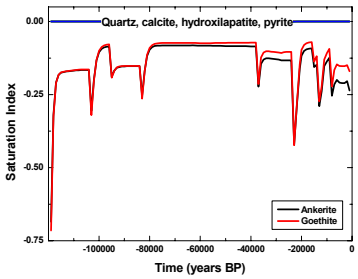

Saturation indices of selected minerals associated with node 56 (deep aquifer) as a function of time. Note the effect of varying recharge on the absolute value of the SI

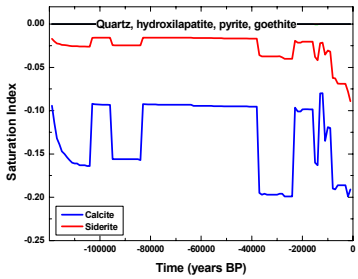

Saturation indices of selected minerals associated with node 64 (shallow aquifer) as a function of time. Note the effect of varying recharge on the absolute value of the SI

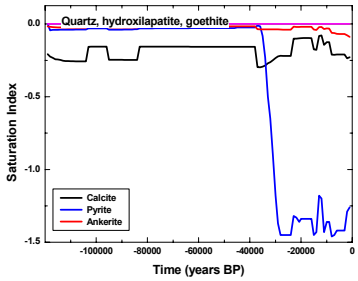

Saturation indices of selected minerals associated with node 66 (near the surface) as a function of time. Note the significant drop of the SI of pyrite at -30000 years

Figure 3.19. Time-dependent evolution of mass transfer among aqueous solution and mineral phases and corresponding saturation indices. Data are shown for selected nodes located along the SR-5 borehole and at the discharge point of the system.

Finally, Figure 3.19 also shows the saturation indices of selected minerals at given nodes. It is interesting to observe that the change in recharge triggers fluctuations in the saturation indices of these minerals not present in the system so that their eventual precipitation might depend on the relative proximity to equilibrium at given times

3.7 SENSITIVITY ANALYSES

A number of sensitivity analyses have been performed in order to test the influence of different parameters on the results obtained. The most significant conclusions drawn from them are outlined next.

3.7.1 Palaeorecharge calculations

Several elements of the hydrological cycle and parameters related to the water budget and derived recharge have been observed. They include forest/grass interception, evapotranspiration, parameters associated with the soil layer and the influence of soil preferential pathways associated with cracks and macropores. This is based on the fact that during a rainfall event, water interception initially determines the amount of water reaching the top soil layer. From that point, the properties of the soil constrain the infiltration ratios and surface runoff.

In our sensitivity analysis we have observed that water interception is the most critical parameter affecting groundwater recharge.

3.7.2 Local flow and transport model

The flow model has been studied taking into account uncertainties in the following parameters: a) permeability; b) porosity; c) leakage coefficient at the discharge point; d) amount of recharge and e) regional flow boundary conditions.

Permeability constrains the shape of piezometric levels once steady state is achieved. Thus, their slope increases as permeability decreases. On the other hand, the specific storage coefficient and porosity will affect the system's behaviour under a transient regime. Because the effective porosity value is significantly larger than the storage coefficient, the effective porosity will affect the water level distribution until it reaches steady state.

The leakage coefficient, L, affects the piezometric levels computed at any given time. Low values of L imply higher slope in the levels attending to the fact the discharge flux towards the Arroyo Maderos creek is higher than if it were smaller. Similarly, changes in recharge affect, at any given time, the spatial distribution of piezometric levels.

Finally, changes in the boundary condition associated with the regional flow system have the greater influence on the behaviour of the groundwater system. Thus, changes in the water head at the right end of the domain (fresh/altered rock interface) directly translates into changes in the amount of water discharging to the creek. However peak water discharges correlate positively with higher recharges while minimum discharges are associated with lower recharge periods.

Although boundary conditions and net recharge are dominant in the solute transport behaviour of conservative and reactive components, the values of several hydrodynamic parameters also play an interesting role. However, among the different effects considered, results are more sensitive to the flow boundary conditions.

Figure 3.20 illustrates the effect of fixing a constant head of 500 m at the interface between the fresh and altered rock, at the right boundary of the modelled domain. That imposes a greater hydraulic gradient between the two edges of the system, which significantly affects the distribution of piezometric levels as can be observed by comparing Figures 3.8 and 3.20a. For these conditions, the deep groundwater system exerts a greater impact over the shallow aquifer. The influence of the flow system over solute transport is also clarified by Figure 3.20b,

representing a conservative species (chloride) affected (or not) by radioactive decay. In contrast to what happened before (Figure 3.10), there is an antithetic response to recharge: higher chloride concentrations are found whenever recharge is lower and the opposite.

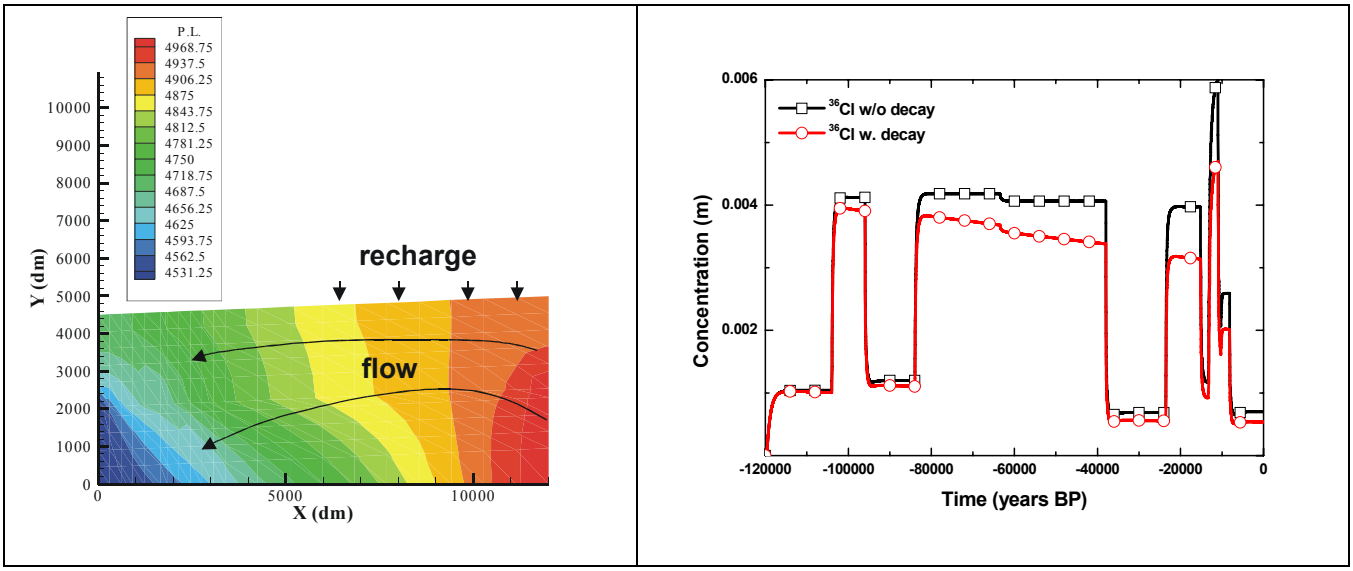

Figure 3.20. On the left (a), spatial distribution of piezometric levels considering a higher hydraulic gradient between the left and right modelled boundaries. Arrows indicate recharge from surface and flow lines. On the right (b), time dependent chloride concentration leaving out the system through the discharge point. Compare with Figures 3.8 and 3.10.

3.7.3 Reactive transport model

The sensitivity analyses of the reactive transport model have considered a series of hydrodynamic and transport parameters that have varying degrees of influence on the results obtained. Among the parameters analyzed we can mention a) dispersivities (longitudinal and traverse); b) flow boundary conditions; c) absolute recharge values; d) diffusion coefficient.

As in the previous case, the greater influence is exerted by the selection of flow boundary conditions with lesser influence of dispersivity and diffusivity on the final results.

On the other hand, the selection of chemical components and reactive phases has a large influence on the final results. Modelling was carried out in a series of consecutive steps of increasing complexity. The final runs included all the components, water types, minerals and aqueous species described earlier, thus providing some degree of sensitivity analysis, though processes like ion exchange and kinetics of dissolution/precipitation reactions were not considered. Ion exchange is considered to be of minor importance, except perhaps in the uppermost part of the system. Kinetically-controlled reactions have not been considered because the small time steps required are impractical with present computing power. Because of the uncertainties related to amount, distribution and identification of mineral phases in the past as well as the corresponding reactive surface areas, a sensitivity analysis does not provide additional constraints on the validity of the reactive transport model.

3.8 CONCLUSIONS AND RECOMMENDATIONS TO R&D GROUPS AND PA GROUPS

The selection of Los Ratones for this modelling exercise was based on the availability of data from prior hydrochemical characterization and from potential climate-constraining mineralogical

observations in WP2 of PADAMOT that would provide valuable constraints to the modelling. Within the realm of a granite massif the questions are:

- Which are the geochemical/mineralogical indicators that trace the climate evolution in the past?
- Can these proxy indicators be dated?
- Is it possible to make a time sequence based on such indicators?

It has not been possible to clearly identify climatic indicators for the Ratones system. Hence no 'real' data were available to compare with the model. However, at least the character and distribution of minerals arising from forward modelling of the system are consistent with what has been observed in the field.

In future applications of this approach, it would be necessary to define better the objective of modelling with respect to site characterization. The modelling methodology developed under this section will need to successfully integrate:

(a) Data and information interpreted from palaeoindicators in order to deduce how climate has evolved to the points in time being considered. This means a detailed reconstruction of *in situ* climate conditions experienced up to each point in time that is being analysed.

(b) Information recorded from meteorological stations in areas that can be used as analogues of the site and groundwater system to be modelled in which palaeoindicators constrain the evolution of conditions. The model allows palaeorecharge of the groundwater system to be quantitatively evaluated.

(c) Geological and hydrogeological properties of the site to be assessed, considering the groundwater system either as effectively at steady-state for the purpose of assessment or in a transient state, and

(d) Hydrogeochemical and mineralogical characteristics of the site that can provide valuable information about long-term reactive transport and hydrogeochemical evolution in the past.

This integration allows us to understand the climatic and hydrogeologic performance of the repository site in the past by constructing palaeoclimate-hydrogeochemical 'scenarios' at various time slices, taking into consideration:

- Climate conditions at each time slice,
- Hydrogeochemical and mineralogical signatures at the same time slices and at repository depth, and
- Evolutionary trends of deep hydrogeochemical conditions in relation to climate changes.

Performance Assessments for deep repositories have to project conditions into future time frames. So the value of this approach based on "the past as the key of the future" depends on the degree of our understanding of how future climate and hydrogeological conditions might compare with past conditions. Thus, in addition to the above mentioned methodological steps (a) to (d), it is necessary to take into account a further step:

(e) Forecasts of local and regional climate conditions during the time periods when those poorly-retarded long-lived radionuclides that could migrate from the waste repository and return to the biosphere might pose a radiological hazard.

The EU BIOCLIM Project has proposed a methodology to address this issue of long-term climate change, through the use of climate models and a scheme for investigating the impacts of climate and environmental change in Performance Assessment. One question that remains open is that the methodology considered in BIOCLIM, and the complimentary approaches suggested here, have not yet fully investigated the potential impact of environmental change due to present

and future human actions, both in respect of climate change and e.g. soil use, agricultural strategy, etc.

The PADAMOT modelling methodology now has to be implemented in a twofold manner:

1) Calibrating or validating reactive transport models to be used for actual deep repository PA;
2) Applying validated reactive transport models for future changing climate conditions, taking as initial boundary conditions the current hydrogeochemical conditions at repository depth.

At the end of this process, PA groups should be able to obtain quantitative information relating to:

- Recharge of the groundwater system;
- Hydrogeochemical behaviour-reactive transport.
- Discharge from the geosphere to the biosphere system.

This information can be used to better constrain, and to improve confidence in, the overall PA calculations of transfer indexes, doses and radiotoxicity values.

4 Geochemical Modelling of Secondary Calcite Formation and Its Composition in Deep Saline Groundwaters – Case Study: Sellafield

Adrian Bath and David Noy

This section describes the work carried out for WP4 of PADAMOT by UK partners Intellisci and British Geological Survey (BGS). The work comprised the simulation of hydrogeochemical processes that are involved in the precipitation of late-stage secondary calcite. Simulations were carried out using batch-reaction modelling with the geochemical speciation and equilibrium computer program PHREEQC2 (Parkhurst and Appelo, 1999) and fully-coupled flow, transport and reaction modelling with the BGS program PRECIP (Noy, 1998) and the Universidade da Coruña program CORE^{2D} (Samper et al., 2000).

The overall purpose of doing the simulations was to mimic the geochemical reactions that might have accounted for precipitation of late-stage calcites and to study the ways that variations in the contents of the redox-sensitive trace elements Fe and Mn in the calcites are related to variations in Fe and Mn in co-existing groundwaters and thus to the redox conditions. The insights gained from this modelling should provide understanding that improves confidence in the interpretations of data acquired in WP2 of PADAMOT. Work was carried out in several stages between early-2002 and end-2004.

4.1 BACKGROUND AND OBJECTIVES

Late-stage secondary calcite as an indicator of palaeohydrogeology has been studied in PADAMOT and the preceding EQUIP project (Bath et al., 2000; Bath et al., in preparation). It has been found that various properties of secondary calcite – the distribution and paragenesis, morphology, compositional variations and isotopic compositions – are indicative of groundwater conditions when the calcite was deposited in the past. Calcite precipitates when various parameters in the chemical composition of groundwater change and affect the speciation and equilibrium so that calcite becomes oversaturated or undersaturated. In shallow 'immature' groundwaters, this may happen as primary minerals are altered in weathering reactions and Ca^{2+} ions are released into solution and/or as pH changes due to alteration reactions or the gain/loss of CO_2. In deep 'mature' groundwaters, mixing of waters of different compositions may be a more important cause of calcite precipitation. For example, mixing of waters with different salinities may result in calcite precipitation or dissolution, even though the component waters are at equilibrium. The amounts and properties of secondary calcite thus formed would be potentially useful as palaeohydrogeological indicators.

In the first stage of this project, geochemical modelling has been carried out to investigate the reactions that might account for secondary calcite to be precipitated in both shallow and deep groundwaters. Modelling of a shallow groundwater system is described in the full report of work for WP4 by the UK partners (see Appendix B). Only the modelling of a deep groundwater system is described here, focusing on the specific example from the UK study site at Sellafield where it is believed that precipitation of calcite has occurred when fresh groundwater has flowed to depth and mixed with saline groundwater.

Groundwater compositions change with depth at Sellafield with a sharp increase in salinity occurring at about 300-350 m depth in the centre of the investigated site, where shallow circulating fresh water interfaces with deeper saline groundwater in a 'Saline Transition Zone'

(Figure 4.1; Richards and Bath, 1997; Bath et al., 2005). It is hypothesised that dispersion and mixing of waters with differing compositions has caused the precipitation of the late stage secondary calcite at Sellafield that has been the subject of detailed studies in WP2 of PADAMOT. This modelling is a test of that hypothesis and sets out to establish a quantitative basis for interpreting the measured properties of the calcite in terms of co-existing hydrochemical conditions. Although the model is set up with data that are specific to Sellafield, the general concept of mixing between groundwaters with different salinities is typical of other sites and the model and approach have generic applicability.

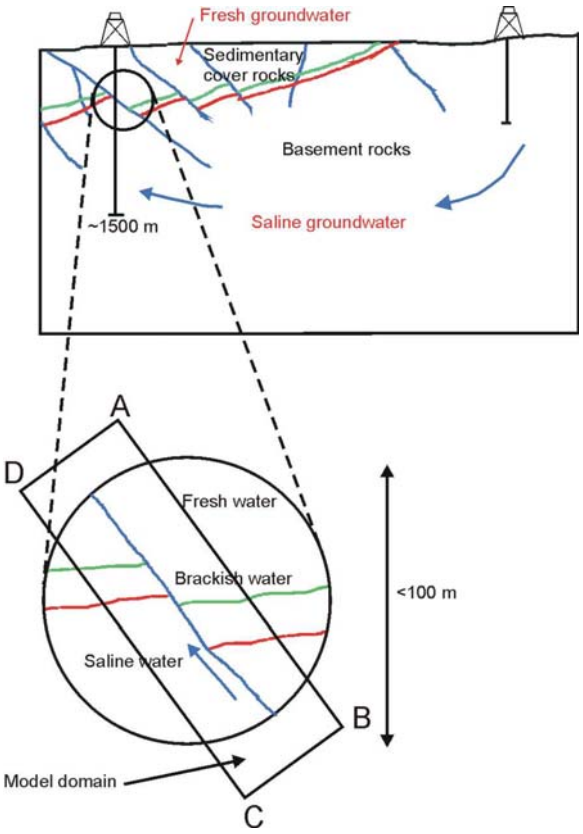

Figure 4.1. An illustration of the mixing between fresh-brackish and saline groundwaters at Sellafield which is believed to be the cause of secondary calcite formation. Sedimentary cover rocks contain fresh-brackish water and basement rocks contain saline water. Waters with different compositions mix by dispersion during groundwater movement which occurs mainly through a network of fractures.

Growth zones in secondary calcites have been detected by cathodoluminescence (CL) and by microprobe analyses in WP2 of PADAMOT. CL is promoted by Mn content and is quenched by Fe content, and its intensity is therefore indicative of Mn and Fe contents and, potentially, of palaeohydrogeological variations in redox conditions. A qualitative relationship between CL and redox fluctuations has been used in various studies (e.g. Fraser et al., 1989; Horbury and Adams, 1989; Lee and Harwood, 1989) and was proposed by Metcalfe and Moore (1997) in a contribution to the EQUIP project.

In the second part of this project, geochemical modelling has been carried out to investigate quantitatively the factors that control Fe and Mn concentrations in groundwaters. These factors are primarily the ambient redox conditions and the identity of the mineral phases containing Fe and Mn. The aim of this modelling is to obtain a more rigourous understanding of the significance of CL zoning and Fe and Mn contents of secondary calcite with respect to past redox conditions in groundwater systems. The approach described here has assumed that Fe:Mn ratios in secondary calcites are the same as Fe:Mn ratios in co-existing groundwater at the time of precipitation. It is proposed that a sound basis for palaeohydrogeological interpretation of

redox conditions is a dual approach of geochemical modelling of Fe and Mn, as developed here, and empirical correlation with other redox indicators in solid phases or fluid inclusions.

4.2 SECONDARY CALCITE GROWTH IN DEEP GROUNDWATERS

4.2.1 Modelling approach and data

Precipitation of secondary calcite has been modelled in a 1D simulation with the PRECIP code. Some of these simulations were replicated using the CORE^{2D} code as a basis for comparing performance and capabilities of the two codes. Then CORE^{2D} was used to model repeated cycles of mixing and reaction as simulations of the development of successive growth zones in calcite. The second stage of geochemical modelling involved using PHREEQC2 and PRECIP to investigate the evolution of water compositions with respect to redox, Fe and Mn thus to evaluate the redox significance of Mn and Fe variations that are indicated by cathodoluminescence and microprobe analyses of the trace element compositions of calcite growth zones.

PRECIP calculates the transport of reactive solutes along a flowpath and allows precipitation and dissolution of the rock matrix to be incorporated using kinetic rate laws, rather than the more common equilibrium formulation (Noy, 1998). This feature can be of particular importance when considering silicate reactions at low temperatures. PRECIP also incorporates the interaction between porosity changes and the groundwater flow, so that, for example, a zone of rapid precipitation may generate flows that tend to push the solutes away from it.

Hydrochemical data representing fresh and saline groundwaters were selected as reference waters from a large data set from earlier Nirex investigations at Sellafield (Nirex, 1997; Bath et al., 2004). Data were selected for depths of 357 and 543 m in Borehole 2 and are shown in Table 4.1. Measured pH data for these water samples are not reliable because contamination by alkaline drilling fluids caused quite large uncertainties in inferred in situ values, so pH was fixed at 7 in both cases and it was assumed that both waters are equilibrated with calcite. This is a reasonable assumption because the groundwaters will have evolved to equilibrium at shallow depths, probably soon after recharge.

Table 4.1. Anion and cation concentrations in Sellafield groundwaters selected for modelling. The fresh water composition is from test DET3 from Borehole 2 (357 m depth) and the saline water data are from test DET10 in Borehole 2 (543 m depth).

Reference water	A: Fresh water	B: Saline water
TDS (mg/l)	259	23060
Assumed pH (see text)	(7)	(7)
Na (mg/l)	86.6	8000
K (mg/l)	5.49	102
Ca (mg/l)	11.7	685
Mg (mg/l)	4.3	82.3
Cl (mg/l)	10	13000
SO_4 (mg/l)	16.7	1060
Alk (mg/l as HCO_3)	229	85.9
SiO_2 (mg/l)	7.4	4.4

The geometrical concept of the simulation is a 1D fracture that traverses a zone of groundwater mixing (Figure 4.2). One or both of the reference groundwaters flows along the fracture, with

possibilities for dispersive mixing within the fracture and diffusive exchange with the adjacent matrix ('dual porosity' type of system). The model runs are shown in Figures 4.3 to 4.7.

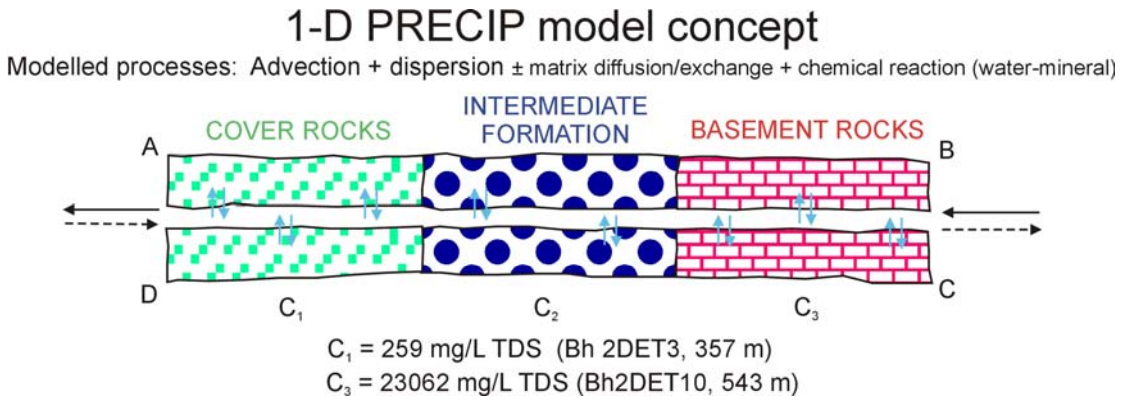

Figure 4.2. Processes and parameters for the PRECIP model of advection-diffusion-reaction in a fracture with an interface between fresh-brackish and saline groundwaters. ABCD refer to the location of this geometrical model in Figure 4.1.

4.2.2 Role of matrix diffusion

The first stage of modelling was to add the process of solute exchange by diffusion between flowing water in the fracture and stationary water in the adjacent rock matrix. These two types of water may have different compositions and thus matrix diffusion is a process that might contribute to calcite precipitation. Figure 4.3 shows calcite precipitating within a fracture as solutes diffuse from saline pore water in the matrix into flowing fresh water. This is a simple simulation of a change of groundwater conditions (e.g. a palaeohydrogeological change of the external boundary conditions that control flow) whereby fresh water invades a part of the system previously occupied by saline water and the composition of matrix pore water changes more slowly than the composition of fracture water. The model shows that the relative amount of deposited calcite decreases with distance along the fracture.

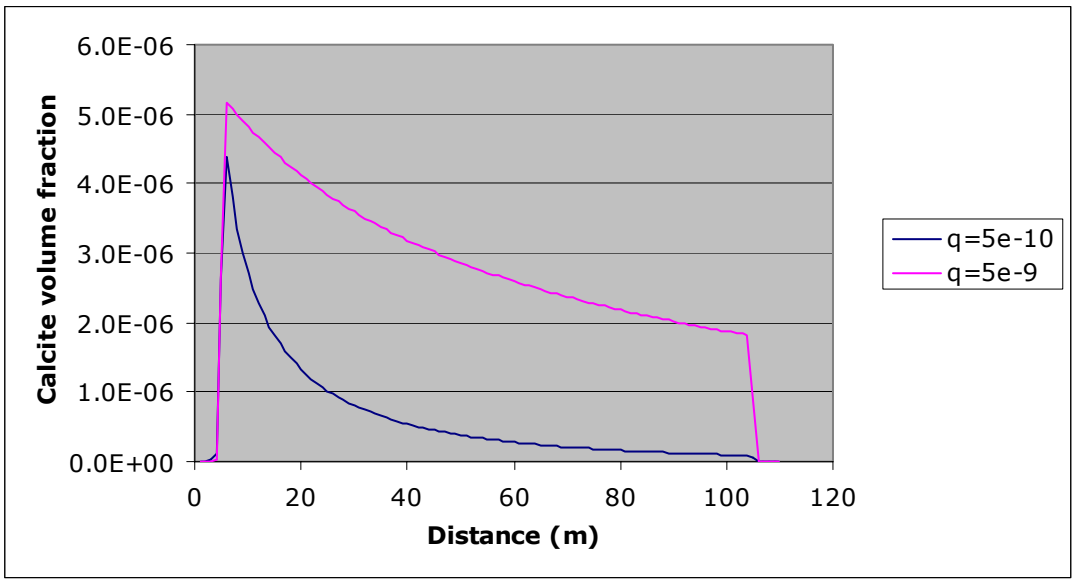

Figure 4.3. Amount and location of calcite precipitated in the fracture as reference water A (fresh) flows from left (0 m) to right (120 m) and reference water B (saline) diffuses in from the matrix. High fluxes through the fracture (q = $5x10^{-10}$ and $5x10^{-9}$ m^3/s) have been used to compress the pattern of calcite precipitation over the 120 m path length.

4.2.3 Calcite precipitation in a fracture

The next stage of modelling was to simulate calcite precipitation in a fracture initially containing fresh and saline waters with a sharp interface. This represents an episode when saline water is displaced by fresh water (or vice versa), displacing the fresh-saline transition downwards. Palaeohydrogeological episodes where this might occur are injection of glacial melt water into deep saline groundwater or of pluvial meteoric water into saline groundwater under arid climate conditions. In the simplest 'diffusion only' case, calcite precipitates predominantly on the fresh side of the interface due to diffusion of solutes from saline water (Figure 4.4). When water also moves by advection along the fracture, solute mixing occurs by dispersion with the result that calcite precipitates along the fracture in the direction of water flow (Figures 4.5 and 4.6).

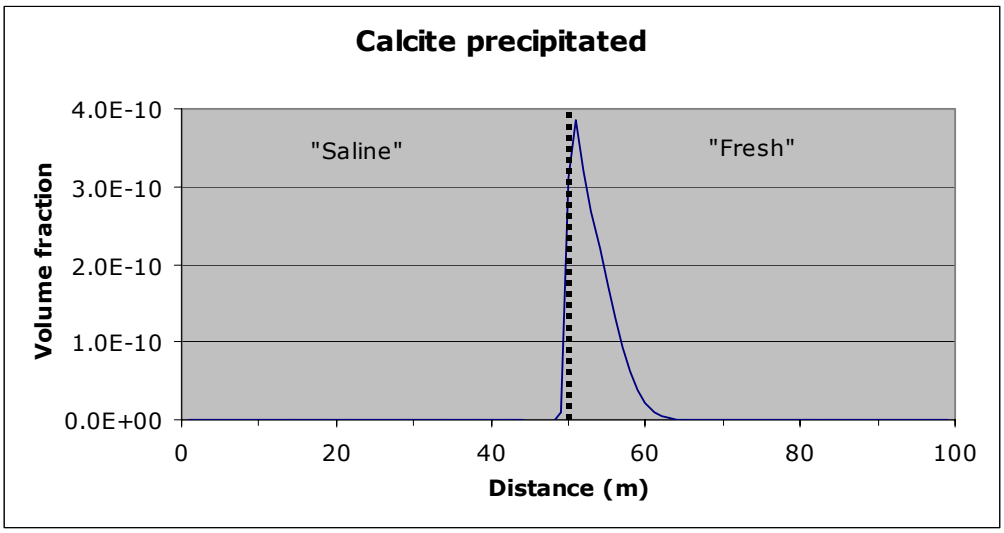

Figure 4.4. Amount of precipitated calcite in a fracture containing static water in which there is a sharp interface at 50 m between reference water A (fresh, on the right) and reference water B (saline, on the left). Calcite precipitates on the fresh water side as in-diffusion from saline water occurs and the saturation index rises above zero (t = 100 years).

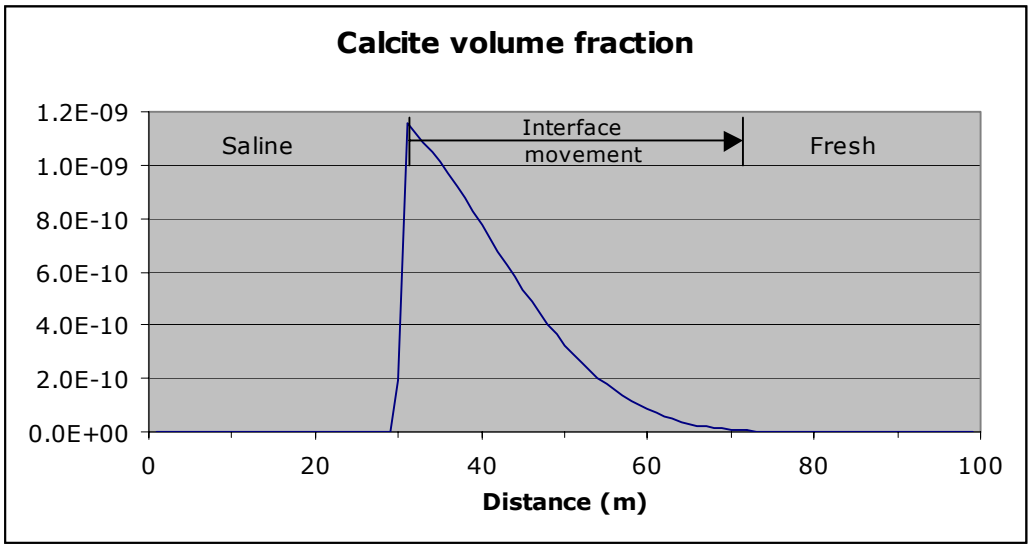

Figure 4.5. Amount of precipitated calcite in a fracture containing water in which there is a moving interface between reference water A (fresh, on the right) and reference water B (saline, on the left). The rate of movement of the interface, or velocity of water in the fracture, is of saline water intruding the fresh water zone at a rate of 40 m in $2x10^8$ secs (6.3 years). In addition, there is diffusive exchange ($D_e = 3x10^{-10}$ m^2/s) between fracture water and matrix water, the matrix water compositions initially having an interface as in fracture water.

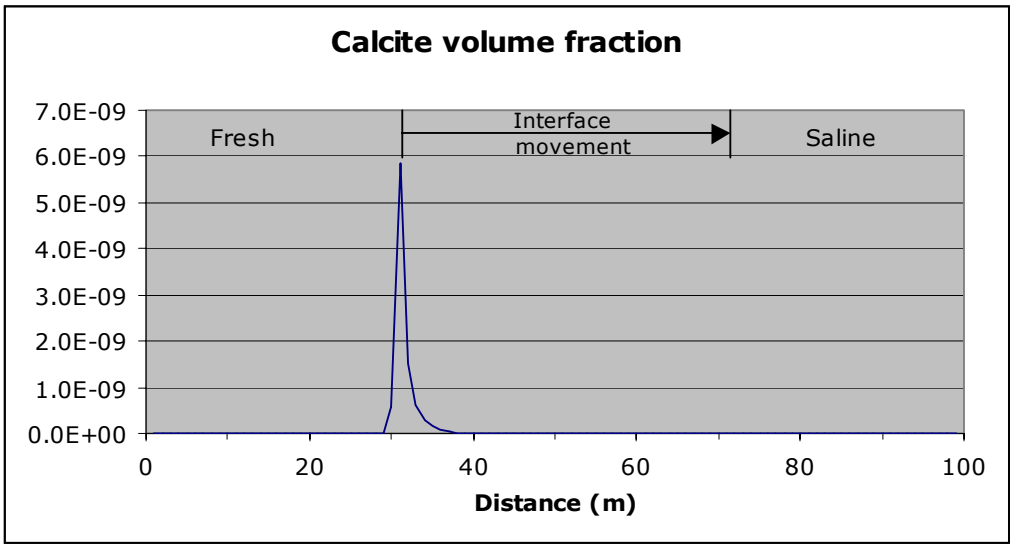

Figure 4.6. Amount of precipitated calcite in a fracture containing water in which there is a moving interface between reference water A (fresh, on the left) and reference water B (saline, on the right). The rate of movement of the interface, or velocity of water in the fracture, is of fresh water intruding saline water at a rate of 40 m in $2x10^8$ secs (6.3 years). In addition, there is diffusive exchange (D_e = $3x10^{-10}$ m^2/s) between fracture water and matrix water, the matrix water compositions initially having an interface as in fracture water.

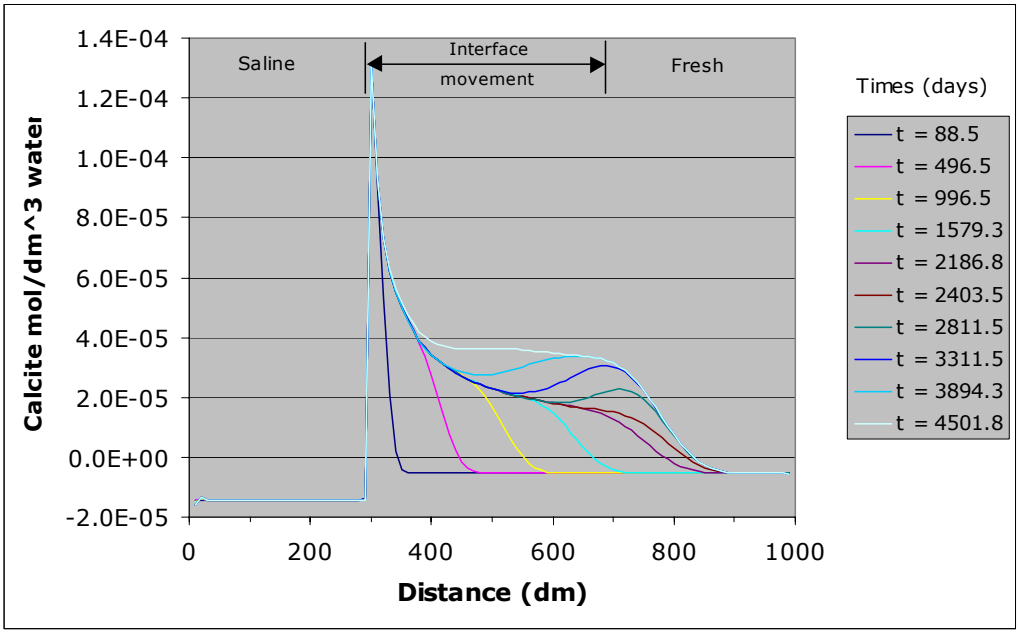

Figure 4.7. Amounts of precipitated calcite (in moles per litre of water) in a fracture containing reference water A (fresh, on the right) and reference water B (saline, on the left) with a sharp interface between them initially, and in which the position of the interface moves 400 m into the fresh water zone and then moves back to its original position, over a period of 12 years. Simulated with CORE^{2D} without matrix exchange.

CORE^{2D} was then used to model a number of oscillations of the interface between fresh and saline waters, simulating the production of discrete growth zones of calcite. Figure 4.7 shows the cumulative growth of calcite in two growth zones, corresponding to the advance and retreat respectively of a saline water front. The amounts of calcite at the end of the advance phase and

at the end of the following retreat phase are illustrated in Figure 4.8. Additional growth zones accumulate as the number of hydrochemical oscillations increases.

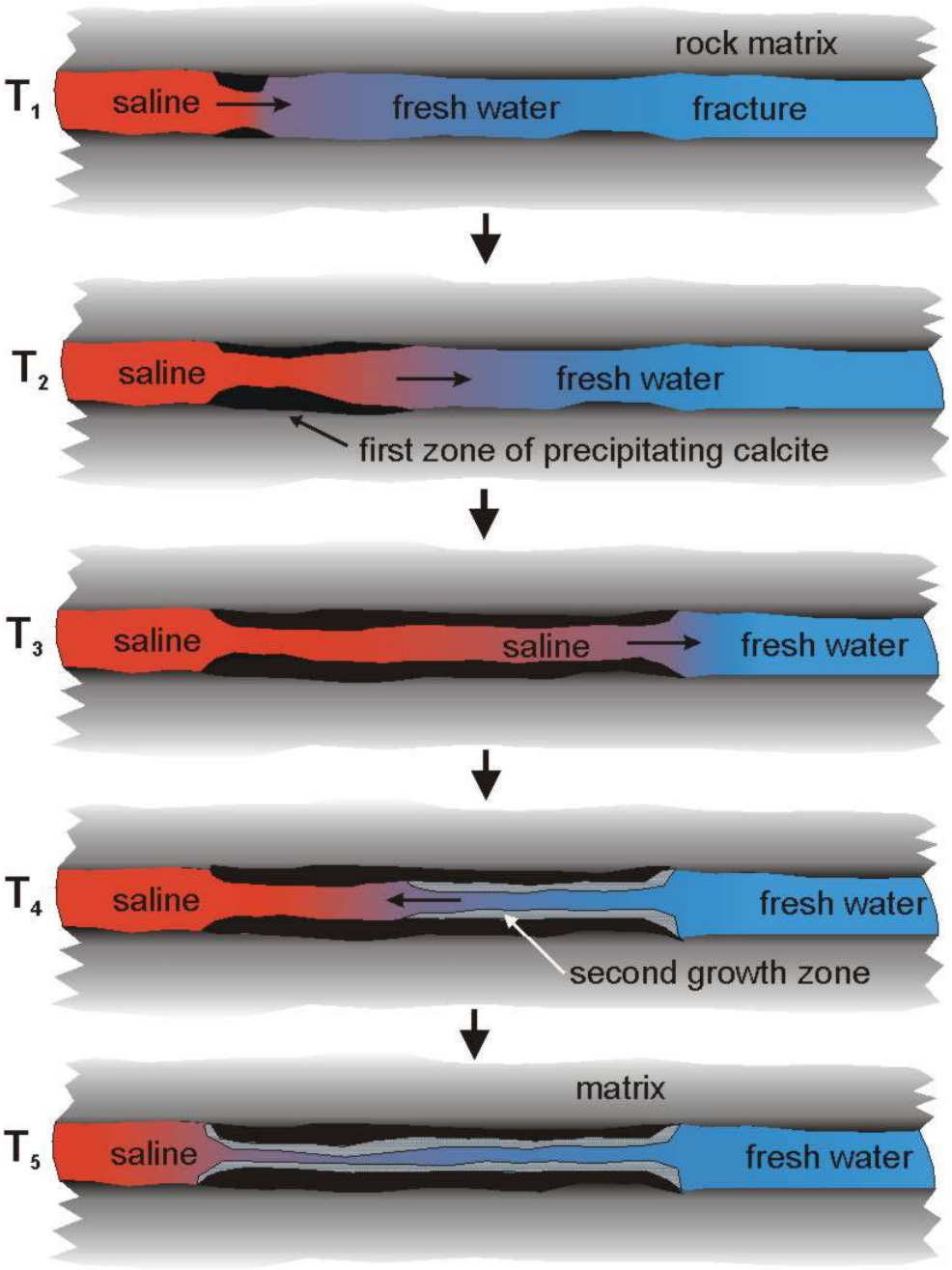

Figure 4.8. Sketch of the amounts of accumulated calcite in the first growth zone, at the end of the saline advance phase, and in the second growth zone, at the end of the saline retreat phase, of a single cycle of hydrochemical oscillation, as modelled in Figure 4.7.

4.2.4 Summary of modelling of calcite growth

The insights gained from modelling hydrochemical processes when mixing occurs in a fresh-saline groundwater transition are summarised as:

- The model is able to simulate the precipitation of secondary calcite as a result of advective-dispersive-diffusive mixing between fresh and saline groundwaters in porous matrices ('diagenetic cementation') and in fractures ('fracture calcite').

- Although it has not been explicitly modelled, calcite dissolution could also be simulated under certain conditions of advective-dispersive-diffusive mixing or by geochemical conditions such as rising P_{CO2} or sulphide mineral oxidation.
- The amounts and distribution of precipitated calcite in a fracture depend on whether fresh water is advancing into saline water or vice versa, and also on the degree of diffusive exchange with matrix pore water solutes.
- A possible mechanism has been confirmed for the growth of zoned calcites when a groundwater system has temporally-varying water compositions due to the hydrodynamic effects of changes at external boundaries.
- This growth zoning may also be a palaeohydrogeological archive of other changes in hydrochemical conditions. The next stage of modelling simulates the distribution of Fe and Mn into secondary calcite and thus illustrates a mechanism that explains variations of cathodoluminescence between growth zones.

4.3 PAST REDOX FROM Fe AND Mn IN SECONDARY CALCITE

4.3.1 Modelling approach and data

Interpretation of Fe and Mn contents of secondary calcite in terms of redox conditions at the time of calcite growth is based on a number of assumptions about the trace element geochemistry of the calcite-water system. The background and scientific justification for these assumptions are discussed in the following paragraphs.

The first assumption is that when two trace cations such as Fe and Mn substitute into calcite, the ratio of the two cations in calcite will be very similar to the ratio in solution. This is based on the similarity of the nature of Fe and Mn solid solutions in calcite and the low abundances of Fe and Mn relative to Ca, so that the free energies of the solid solutions will be close to that of pure calcite and the activity coefficients of Fe and Mn in the crystal lattice will be very similar.

Various experimental and theoretical studies of trace element distributions between calcite and solution have been carried out. Experimental studies tend to evaluate empirical distribution coefficients, K'_d, e.g. Rimstidt et al. (1998) suggested values of about 97 for K'_d of Fe in $CaCO_3$ and 52 for K'_d of Mn in $CaCO_3$ which suggest that the Fe/Mn ratio in calcite is about 1.86 times the molar Fe/Mn ratio in solution. Theoretical studies have considered whether stoichiometric saturation is an appropriate basis for modelling the equilibrium relationship between mineral and solution. Glynn and Reardon (1990) suggest that, if stoichiometric saturation equilibrium occurs, then Fe and Mn distributions should fractionate between solution and calcite. However experimental evidence indicates that stoichiometric saturation, though it is valid for dissolution, is not an appropriate model for normal precipitation of trace elements into a solid solution (Glynn et al., 1990; Astilleras et al., 2003; Lafon, 1978). One of the reasons for this is that precipitation kinetics are faster than dissolution kinetics with less chance of conditions for reversibility and thus re-equilibration, at the mineral-solution interface. If however re-equilibration should take place, i.e. effectively a dissolution-precipitation process, then the distribution of minor elements such as Fe and Mn would be adjusted according to stoichiometric saturation.

The second assumption concerns the solid phases that control Fe and Mn in the component groundwaters prior to mixing and also during the mixing and consequent precipitation of secondary calcite. There are two alternative models for the evolution of dissolved Fe and Mn in the component groundwaters and the mixed water. One model assumes that Fe and Mn in the component waters are controlled by equilibrium with Fe- and Mn-phases and that the Fe and Mn concentrations of the mixed water are linear combinations of these concentrations. An alternative model is that Fe and/or Mn concentrations in the mixed water are re-equilibrated with

one or more secondary phases, typically pyrite, siderite and rhodochrosite. For example, it is apparent that secondary pyrite has precipitated in at least some growth zones of secondary calcite in Sellafield samples, and therefore it is possible that the co-existing Fe concentration in the mixture and thus in secondary calcite is conditioned by equilibrium with pyrite. In a palaeohydrogeological study of a shallow aquifer using CL in secondary calcite, Barnaby and Rimstidt (1989) assumed that aqueous Fe and Mn were controlled by MnO_2 and amorphous ferric oxyhydroxide and then back-calculated the free energies of formation (ΔG^o_f) of the two phases so that Mn and Fe contents from CL indicated consistent redox conditions (Eh).

The modelling approach used here is to construct geochemical models that calculate Fe and Mn concentrations in component waters and in the mixed groundwater from which secondary calcite precipitates, using the programs PHREEQC and PRECIP. The modelling uses the same component water compositions from the Sellafield data set as were used in the first part of this project (Table 4.1). Prior to the model simulation of mixing, each of the component groundwaters is conditioned to calcite equilibrium and is also equilibrated with Fe- and Mn-containing phases to fix the Fe and Mn concentrations (Tables 4.2 and 4.3). In a few model runs, the pH of the fresh water component is fixed by the model so that mixing with a fresh water component with unusually low (to pH 6) or unusually high (to 8.5) pH is investigated.

In summary, these model results show that Fe concentrations in equilibrium with Fe-oxyhydroxide (Fe-ox) are insensitive to pH whereas Mn concentrations in equilibrium with $MnCO_3$ are more sensitive to pH (decreasing as pH increases). Overall, Fe/Mn increases in these conditions as pH increases, but it remains <1. Fe concentrations in equilibrium with Fe-oxyhydroxide decrease as pe increases, i.e. as redox becomes more oxidising. In these simulations, redox is dependent upon both Fe- and Mn phases with which solution is equilibrated: the general order of oxidising potential is MnO_2 > Fe-oxyhydroxide (more oxidising at lower pH) >$FeCO_3$, Fe concentrations are highest in equilibrium with $FeCO_3$, in which conditions redox is reducing, and in this case Fe/Mn>1.

Table 4.2. Conditioning of fresh water component: Results of PHREEQC modelling of equilibration of reference water A (Table 4.1) with various mineral phases; the pH has also been fixed at values between 6 and 8.5 in some model runs (Eh in mV = pe x 59.1).

Equilibrium phases	pe	pH	Fe (M)	Mn (M)	Fe/Mn
Calcite, Fe-ox, MnO_2	+8.74	7.59	2.7e-8	1.6e-6	0.016
Calcite, $FeCO_3$, $MnCO_3$	-3.21	7.60	3.3e-6	2.3e-6	1.47
Calcite, Fe-ox, $MnCO_3$	+1.72	7.60	5.6e-7	2.3e-6	0.25
Calcite, Fe-ox, $MnCO_3$	+6.7	6	7.6e-7	6.9e-5	0.01
Calcite, Fe-ox, $MnCO_3$	+5.1	6.5	6.2e-7	2.1e-5	0.03
Calcite, Fe-ox, $MnCO_3$	+3.5	7	5.8e-7	7.0e-6	0.08
Calcite, Fe-ox, $MnCO_3$	+2.0	7.5	5.6e-7	2.7e-6	0.21
Calcite, Fe-ox, $MnCO_3$	+0.6	8	5.6e-7	1.3e-6	0.45
Calcite, Fe-ox, $MnCO_3$	+0.8	8.5	5.6e-7	8.1e-7	0.70

Conditioning of the saline water component in equilibrium with calcite, $FeCO_3$ or pyrite, and $MnCO_3$ gives the range of hydrochemical conditions shown in Table 3. The Fe concentration in equilibrium with pyrite is significantly lower than that with $FeCO_3$ so that the Fe/Mn is also lower at <0.01, though pe is similar for $FeCO_3$ and pyrite redox controls. Comparison of model results in Tables 2 and 3 shows that Fe and Mn concentrations in equilibrium with $FeCO_3$ and

$MnCO_3$ are dependent on pH (i.e. higher at lower pH), although Fe/Mn remains fairly constant at 1.43.

Table 4.3 Conditioning of saline water component: Results of PHREEQC modelling of equilibration of reference water B (Table 4.1) with various mineral phases.

Equilibrium phases	pe	pH	Fe (M)	Mn (M)	Fe/Mn
Calcite, $FeCO_3$, $MnCO_3$	-3.04	7.27	7.4e-5	5.2e-5	1.43
Calcite, pyrite, $MnCO_3$	-3.10	7.27	2.2e-7	5.2e-5	0.0042

4.3.2 Geochemical modelling of Fe, Mn and redox

As discussed above, two different approaches were used with regard to re-equilibration of mixed water with a solid phase. In model runs with PRECIP, the Fe and Mn concentrations in the resulting mixtures are not subject to further control except for precipitation of selected minerals. Thus Fe and Mn in the mixed waters are simply linear mixtures of the concentrations in the component waters. In many of the batch mixing-reactions model runs with PHREEQC, the mixed groundwater is re-equilibrated with one or more Fe- and Mn-containing minerals, allowing both dissolution and precipitation in some runs and precipitation-only in other runs.

It is expected that pe and concentrations of Fe and Mn in a mixed groundwater will vary continuously as the mixing proportions between the component waters change. PHREEQC modelling of batch-mixing and reaction has provided some insight into the parameters in mixed waters near to each end of the mixing spectrum (i.e. at ratios of 2:8, 8:2 and 1:1). Reactions during continuous dispersive mixing have also been modelled with PRECIP and PHREEQC in 'transport mode' mode. Graphical outputs from those model runs illustrate continuous variations of pe, Fe and Mn corresponding to the zoned growth of calcite that was modelled in the first part of this project.

A large number of model simulations of mixing between these fresh and saline component waters have been carried out, using PHREEQC (in either batch mixing + reaction mode or transport + reaction mode) and PRECIP. The model conditions and constraints in each case are shown in Tables 4.4 and 4.5.

Table 4.4 Model conditions and results for simulations of mixing between fresh and saline waters using PHREEQC in batch mixing and reaction mode ('B').

		Equilibrating phases			Mixed groundwater composition			
Model run	Model Program	Fresh component	Saline component	Mixed groundwater[1]	pe	Fe (M)	Mn (M)	Fe/Mn
3c	PHREEQC/B	Fe-ox+$MnCO_3$	$FeCO_3$+$MnCO_3$	1:1 no equilibrating calcite or Fe & Mn phases	+0.4	3.7e-5	2.7e-5	1.37
3d&3e	PHREEQC/B	Fe-ox+$MnCO_3$	$FeCO_3$+$MnCO_3$	8:2 & 2:8 no equilibrating Fe & Mn phases	+1.3 & +0.4	1.5e-5 & 5.9e-5	1.2e-5 & 4.2e-5	1.28 &1.42
3h	PHREEQC/B	Fe-ox+MnO_2	Pyrite+$MnCO_3$	8:2 Feox(P)	+3.8	6.6e-8	1.2e-5	0.0056
3i	PHREEQC/B	Fe-ox+MnO_2	Pyrite+$MnCO_3$	2:8 Pyrite(P)	+2.7	1.8e-7	4.2e-5	0.0044
3a	PHREEQC/B	$FeCO_3$+$MnCO_3$	$FeCO_3$+$MnCO_3$	1:1 $FeCO_3$(P&D)+$MnCO_3$(P&D)	-2.9	3.7e-5	2.4e-5	1.53
3b	PHREEQC/B	Fe-ox+$MnCO_3$	$FeCO_3$+$MnCO_3$	1:1 $FeCO_3$(P&D)+$MnCO_3$(P&D)	+1.0	3.7e-5	2.4e-5	1.53
3f&3g	PHREEQC/B	Fe-ox+MnO_2	$FeCO_3$+$MnCO_3$	8:2 & 2:8 Fe-ox(P&D)	+1.5 & +1.2	1.5e-5 & 5.9e-5	1.2e-5 & 4.2e-5	1.28 & 1.42
3j&3k	PHREEQC/B	Fe-ox+MnO_2	Pyrite+$MnCO_3$	8:2 & 2:8 Pyrite(P&D)+/-Fe-ox(P)	-3.1 & -3.0	6.7e-8 & 1.8e-7	1.2e-5 & 4.2e-5	0.0058 & 0.0044
3l	PHREEQC/B	Fe-ox+MnO_2	Pyrite+$MnCO_3$	2:8 Pyrite(P&D)+$FeCO_3$(P&D)	-2.8	5.8e-5	4.2e-5	1.40
6a	PHREEQC/B	Fe-ox+$MnCO_3$	Pyrite+$MnCO_3$	8:2 Fe-ox(P&D)+Pyrite(P&D)	-4.2	2e-3	1.2e-5	165
6b	PHREEQC/B	Fe-ox+$MnCO_3$	Pyrite+$MnCO_3$	2:8 $FeCO_3$(P&D)+Pyrite(P&D)	-2.8	5.9e-5	4.2e-5	1.4
6c-6h	PHREEQC/B	Fe-ox+$MnCO_3$ (fixed pH 6 to 8.5)	Pyrite+$MnCO_3$	8:2 Feox(P&D)+Pyrite(P&D)	-3.4 to -4.2	1.9e-2 to 1.7e-3	6.5e-5 to 1.1e-5	293 to 155
6i	PHREEQC/B	Fe-ox+$MnCO_3$ (fixed pH 7.5)	Pyrite+$MnCO_3$	8:2 $FeCO_3$(P&D)+Pyrite(P&D)	-2.9	1.7e-5	1.2e-5	1.42
6j-6o	PHREEQC/B	Fe-ox+$MnCO_3$ (fixed pH 6 to 8.5)	Pyrite+$MnCO_3$	2:8 $FeCO_3$(P&D)+Pyrite(P&D)	-2.1 to -2.9	9e-5 to 5.8e-5	5.5e-5 to 4.2e-5	1.63 to 1.38

Notes:[1] P = precipitating, D = dissolving; calcite equilibrates in all model runs; ratio, e.g. 2:8, is proportions of fresh and saline component waters in batch mixing PHREEQC model

Table 4.5 Model conditions and results for simulations of mixing between fresh and saline waters using PRECIP and PHREEQC in transport, mixing and reaction mode ('T').

		Equilibrating phases			Mixed groundwater at end of transport simulation			
Model run	Model Program	Fresh component	Saline component	Mixed groundwater[1]	pe	Fe (M)	Mn (M)	Fe/Mn
4b 14c.obs	PRECIP	Fe-ox+$MnCO_3$	$FeCO_3$+$MnCO_3$	no equilibrating Fe & Mn phases	-2.8			1.03
4a 14.obs	PRECIP	Fe-ox+$MnCO_3$	$FeCO_3$+$MnCO_3$	$FeCO_3$(P)+$MnCO_3$(P)	-2.8	1.7e-4	1.6e-4	1.03
4c 16c.obs	PRECIP	Fe-ox+$MnCO_3$	Pyrite+$MnCO_3$	$MnCO_3$(P)	-3.2	1e-5	1.6e-4	0.06
7a det3-10.rt2	PHREEQC/T	Fe-ox+$MnCO_3$	$FeCO_3$+$MnCO_3$	$FeCO_3$(P)+$MnCO_3$(P)	-2.8			1.00
7b&7c det3-10.rt4&6	PHREEQC/T	Fe-ox+$MnCO_3$ (pH 8 & 6)	$FeCO_3$+$MnCO_3$	$FeCO_3$(P)+$MnCO_3$(P)	-2.8			1.00
7d det3-10.rt8	PHREEQC/T	Fe-ox+$MnCO_3$	Pyrite+$MnCO_3$	Pyrite(P)+$MnCO_3$(P)	-3.2	3e-6	1.8e-4	0.02
7e det3-10.rt9	PHREEQC/T	Fe-ox+$MnCO_3$	Pyrite+$MnCO_3$	Pyrite(P)	-3.2	3e-6	1.8e-4	0.02
7f det3-10.rt10	PHREEQC/T	Fe-ox+$MnCO_3$	Pyrite+Feox+$MnCO_3$	Pyrite(P)+$MnCO_3$(P)	-5.1	1.1e-3	1.8e-4	6.2
7g det3-10.rt11	PHREEQC/T	Fe-ox+$MnCO_3$	Pyrite+Feox+$MnCO_3$	Pyrite(P)	-5.1	1.1e-3	1.8e-4	6.2
7h det3-10.rt12	PHREEQC/T	Fe-ox+$MnCO_3$	Pyrite+$MnCO_3$	Pyrite(P&D)	-3.2	3e-6	1.8e-4	0.016

Notes:[1] P = precipitating, D = dissolving; calcite is allowed to precipitate in all model runs.

The following paragraphs summarise the possible interpretations of low to high Fe/Mn ratios that are indicated by the modelling results in Tables 4 and 5.

Very low Fe/Mn (0.006-0.004)

Either (a) or (b):

(a) Oxidising water (pe = +2 to +4) from mixing of a fresh water with redox buffered by Fe-ox + MnO_2 with a saline water with redox buffered by pyrite. The mixed water does not re-equilibrate by dissolution, so redox is dominated by the fresh water component. Fe is very low ($\sim 10^{-7}$M) due to precipitation of Fe-ox or pyrite. Mn is also low ($\sim 10^{-5}$M).

(b) Reducing water (pe = ca. -3) from the re-equilibration of the mixed groundwater described in (a) above with pyrite which is allowed to dissolve in the model. Fe is very low, as in (a), because of very low Fe ($\sim 10^{-7}$M) in the oxidising fresh water component and re-equilibration of the mixture with pyrite.

Moderately low Fe/Mn (0.01-0.06)

Reducing waters (pe = -3.2) from mixing of moderately oxidising fresh water (Fe-ox equilibrated) with reducing saline water (pyrite equilibrated). Fe is quite low (10^{-6} to 10^{-5}M) due to equilibration with pyrite in the saline component and, in some model runs, also in the mixed water. Mn is higher ($\sim 10^{-4}$M) and is equilibrated with $MnCO_3$.

Fe/Mn close to unity (1.0 – 1.6)

Either (a), (b) or (c):

(a) Oxidising water (pe = 0 to +1.5) from intermediate mixing of a fresh water with redox buffered by Fe-ox with a saline water with redox buffered by siderite $FeCO_3$. The mixed water may or may not re-equilibrate with $FeCO_3$. Pyrite is not involved as a reactant mineral. Fe is moderately high at 1.5 x 10^{-5}M, whilst Mn is quite low at 1-4 x 10^{-5}M.

(b) Reducing water (pe = -2.8 to -2.9) in a mixture that is dominated by a saline water with redox buffered by siderite $FeCO_3$. Fe is high at 3 x 10^{-5} to 2 x 10^{-4}M. Mn is between 2 x 10^{-5} and 2 x 10^{-4}M, in equilibrium with $MnCO_3$.

(c) Reducing water (pe = -2.1 to -2.9) in a mixture of a fresh water with a saline water with redox buffered by pyrite. The mixture re-equilibrates by dissolution reaction with pyrite. Fe is moderately high at 1-9 x 10^{-5}M.

Moderately high Fe/Mn (~6)

Strongly reducing water (pe = -5) from mixing of an oxidising fresh water with a saline water buffered by equilibrium with both pyrite and Fe-ox. The mixed water is allowed to equilibrate with pyrite by precipitation only; dissolution reaction is not allowed in this model. Fe is very high at $\sim 10^{-3}$M due to the saline component's equilibration with pyrite and Fe-ox. Mn is around 2 x 10^{-4}M due to equilibration of both components with $MnCO_3$.

Very high Fe/Mn (150-300)

Reducing water (pe = -3.4 to -4.2) in a mixture that is dominated by a fresh water component that is equilibrated with Fe-ox, plus a minor proportion of a saline water component that is equilibrated with pyrite. The mixed water is re-equilibrated with both Fe-ox and pyrite by dissolution reaction. Fe is very high at 2 x 10^{-2} to 2 x 10^{-3}M due to dual equilibrium with Fe-ox and pyrite. Mn is 1-7 x 10^{-5}M due to equilibration with $MnCO_3$ in both component waters.

4.4 SUMMARY OF Fe/Mn IN CALCITE AS A REDOX INDICATOR

The interpretation and models used here have involved many simplifications and assumptions which place constraints and caveats on the validity of this approach. The basic interpretative model assumes that secondary calcite is precipitated as a result of ongoing slow dispersive mixing of groundwaters with different compositions, e.g. typified by a fresh water and a saline water. These component waters are already 'mature', i.e. they are at equilibrium with calcite and dissolved Fe and Mn are in equilibrium with corresponding oxide or carbonate phases or, for Fe, with pyrite. Two alternative geochemical conditions for the mixed groundwater are considered: either that secondary calcite forms without any re-equilibration of the mixed groundwater with Fe and Mn phases, or that the mixed groundwater re-equilibrates with co-existing Fe and Mn phases at the same time as precipitating calcite. A further basic premise is that Fe/Mn ratios in secondary calcites are identical (or at least very similar) to those in the source groundwaters.

A simple assertion for interpreting measured Fe/Mn in calcite might be that low ratios correspond to oxidising conditions whilst high ratios correspond to reducing conditions. Geochemical modelling has shown that the interpretation of redox from variations of Fe/Mn in secondary calcite is not that simple and that Fe/Mn ratios should be considered in the context of geochemical and mineralogical conditions.

Oxidising palaeo-redox conditions could be indicated by very low Fe/Mn (<0.01) or by Fe/Mn close to unity (1.0 – 1.6). The caveat on the former interpretation is that the very low ratio is preserved if the mixed groundwater re-equilibrates with available pyrite and then becomes reducing. Two caveats apply to the latter interpretation. The first is that a similar Fe/Mn ratio (i.e. ~1) can occur in reducing conditions in a mixed groundwater dominated by a component water that is equilibrated with siderite, $FeCO_3$. The second is that the same Fe/Mn ratio can arise if both saline component and mixture equilibrate with available pyrite. It is clear from these caveats that the possibility of reaction of a component water and/or the resulting mixed groundwater with co-existing pyrite or siderite is an important consideration. This requires knowledge of co-existing mineral paragenesis at a microscopic scale and the exercise of expert judgement in identifying the most likely water-mineral reactions.

Reducing palaeo-redox conditions could be indicated, in addition to those conditions described in the caveats in the previous paragraph, by moderately low Fe/Mn (0.01-0.06) or by moderately high (~6) and very high (150-300) Fe/Mn ratios. The latter two conditions, with high to very high Fe/Mn, arise in groundwaters where precursor components or the mixed water equilibrate with both pyrite and Fe-oxyhydroxide. This seems an unlikely condition in which both Fe^{II} and Fe^{III} minerals co-exist and react, but it is not impossible and may be sensible in groundwaters hosted by rocks with both pyrite and hematite in the mineral assemblage. The first condition, where low Fe/Mn corresponds with reducing conditions, applies where the mixed water has substantial proportions of both the oxidising fresh component (very low Fe) and the reducing pyrite-equilibrated saline component (Fe not so low but not high either). In such a mixture of comparable proportions, the pe of the saline component is sufficient to dominate the pe of the mixture whereas the Fe concentration is quite low.

4.5 CONCLUSIONS AND RECOMMENDATIONS TO R&D GROUPS AND PA GROUPS

The work described in Section 4 and in Appendix B has simulated processes that were possibly involved in the formation of secondary calcites that have been sampled and analysed in Work Package 2. Deep and shallow groundwaters in typical fractured hard rock environments have been modelled. The relationships between geochemical and hydrogeological environments are implicit in the approach to modelling, especially where coupled transport-reaction models have been used. In addition to the general geochemistry of calcite growth, specific modelling has

been carried out to study with the theory behind the interpretation of the Fe and Mn contents of secondary calcites as 'palaeo-redox' indicators. The outcomes from this are summarised in the following:

- It is a plausible hypothesis that secondary calcite in deep groundwater environments has formed due to mixing of groundwaters with varying compositions, typically showing up as varying salinities. Other factors that might also play a part are temperature fluctuation and re-mobilisation or pre-existing carbonate mineralisation. Geochemical models for the formation of calcite (and other secondary minerals) are non-unique and therefore precipitation and dissolution conditions each occupy wide ranges of parameter space.
- Growth of secondary calcite in distinct microscopic zones may be caused by hydrodynamic fluctuations in water movements and compositions plus the influence of matrix storage and exchange. The growth zones therefore are an archive of information about the ambient geochemical conditions when they were deposited. Geochemical modelling provides the framework in which the palaeohydrogeological significance of geochemical and isotopic data can be interpreted.
- A more rigourous theoretical basis for interpreting Fe and Mn contents of calcite, and thus also of cathodoluminescence has been established. The conceptual geochemical models are not unique and involve assumptions about the reactions, water mixing and pre-existing solid phases that control dissolved Fe and Mn, and about how Fe and Mn are distributed between calcite and water. The same approach could be used in principle to assess the significance of other redox- and pH-sensitive trace elements (such as Ce and U), but in reality the thermodynamic base for their calcite-solution distribution is inadequately understood.
- It is an oversimplifying interpretation to assert that low Fe/Mn corresponds always to oxidising conditions and that high Fe/Mn corresponds invariably to reducing conditions. Fe/Mn ratios and cathodoluminescence activity should be considered in the context of co-existing geochemical and mineralogical conditions. Very low Fe/Mn (<0.01) is indeed typical of a mixed groundwater between oxidising component waters, but the low Fe/Mn will have been preserved if the mixed groundwater then re-equilibrates with pyrite and becomes reducing. Moderate Fe/Mn (~1) is typical of perhaps the most usual geochemical system for deep mixed reducing groundwaters in which both saline component and mixed waters have equilibrated with pyrite. A similar condition evolves if siderite instead of pyrite is the redox buffer. High or very high (~6 up to ~300) Fe/Mn ratios may be unusual because they are characteristic of reducing groundwaters in which equilibration with both Fe-oxyhydroxide and pyrite has played a prominent role.

From these outcomes, some recommendations can be passed on to researchers and planners for site investigations:

- It is evident from quantitative modelling as well as from qualitative conceptual models of these geochemical and mineral systems that data and interpretations have substantial uncertainties and non-uniqueness. The implications need to be considered in planning research and site investigations.
- Modelling also makes it clear that robust interpretations are made possible by integration of diverse geochemical and mineralogical data. This means that a comprehensive range of sampling and analytical techniques need to be deployed to obtain distributions and paragenesis, solid solution compositions and growth zoning at microscopic scale, stable isotopic ratios, ages, trace element contents, fluid inclusion compositions, etc for secondary minerals.
- Coupled flow-transport-reaction modelling and geochemical mass budget calculations are valuable for relating geochemical changes to possible palaeohydrogeological flow conditions.

- Conceptual geochemical models for secondary calcite in shallow and deep groundwater systems are distinct, with the former involving open-system weathering in which CO2 and other direct impacts of climate have important roles. Deep groundwaters involve groundwater mixing and closed system evolution so that the mass budgets for C and H+ may limit carbonates and other secondary minerals. It would be valuable in site investigations and in generic research to look more closely at the locations of these two parts of the overall groundwater system. The similarity with the biosphere-geosphere interface needs to be investigated.

The main concerns of PA teams in the context of palaeohydrogeology are with time-varying changes of the groundwater flux and flow direction, chemical environment, and other scenarios that are related to climate or other external environmental changes. The significance of modelling has to be coupled with that of the geochemical and mineralogical measurements at a particular site:

- Palaeohydrogeology provide essential support to the development of scenarios and to consideration of the range of plausible scenarios related to climate and environmental changes. Modelling of the geochemical and hydrogeological processes, especially when coupled together, indicates the potential importance of step changes and thresholds to change in chemical and hydrodynamic properties of a system that are significant to PA. Equally, the 'asymmetry' of past and future conditions has to be considered so that palaeohydrogeology does not necessarily define the limitations of scenarios.
- Scientific uncertainties and alternative conceptual models and interpretations are inherent in the application of palaeohydrogeology to supporting scenario developments for PA. Modelling provides a theoretical framework for understanding the scale of these uncertainties. This understanding is particularly important with respect to the interpretative models that are involved in converting proxy data to geochemical and hydrogeological properties of a system and relating these to climatic and environmental variations over time.

5 Shallow Groundwater Evolution – Case Study: Melechov

Václav Frydrych, Michal Havlík, Jiří Mls, Jiri Krásný, Michal Polák and Jan Šilar

The Melechov granite massif in the vicinity of Ledeč, Sázavou, Světlá and Sázavou has been chosen for work by the Czech partners in the PADAMOT project. In order to achieve a basic understanding of the groundwater flow conditions in the western part of this granite massif, a hydrogeological survey has been carried out, followed by numerical modelling of the hydrogeological situation.

Groundwater Vistas modelling software was used to construct a spatial model of groundwater flow (McDonald and Harbaugh, 1988; Rumbaugh and Rumbaugh, 1998). The main objective of the groundwater flow simulation was the determination of the spatial hydraulic potential distribution, flow velocities and travel times.

5.1 DESCRIPTION OF APPROACH

The Melechov granite massif is situated in the central part of Czech Republic (Figure 5.1), 5 to 20 km north of Humpolec and 15 to 20 km west of Havlíčkův Brod. The studied area has an extent of 90 km^2 and covers the western part of the Melechov granite massif and the surrounding mantle of Moldanubic rocks.

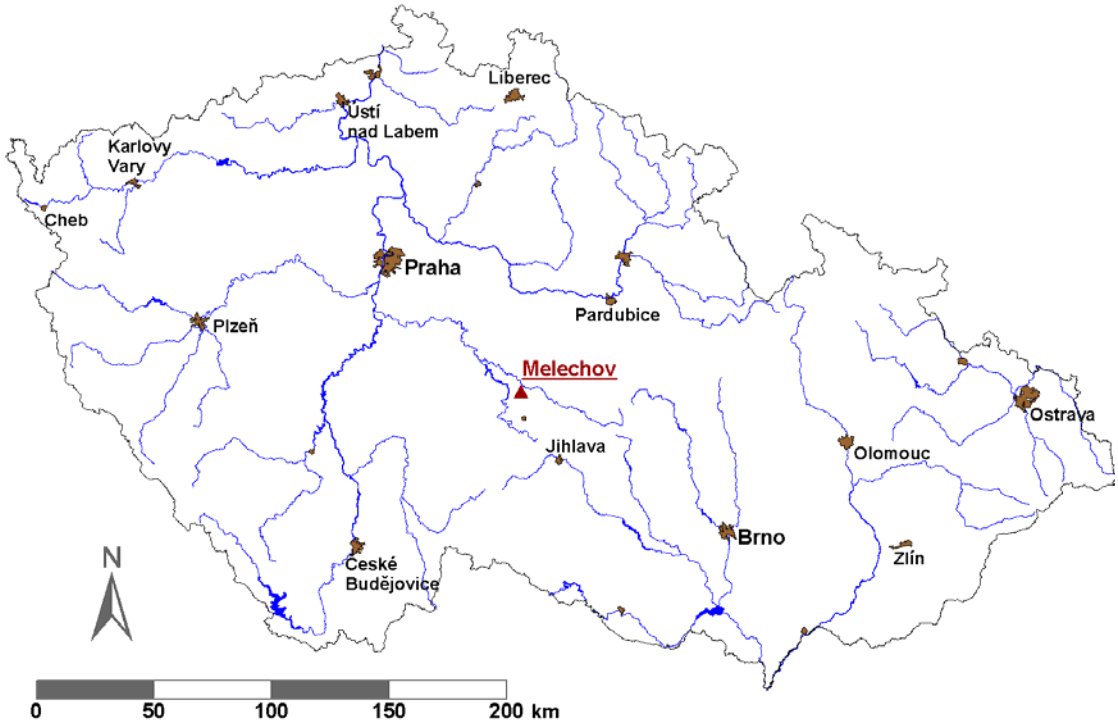

Figure 5.1. Location of the Melechov massif, shown on an outline map of the Czech Republic.

The approximate limits of the study area constitute the Sázava river to the north, Pstružný stream to the east, Želivka river and Švihov reservoir to the west and the line of villages Kejžlice, Kaliště and Hojanovice to the south.

Annual precipitation in the study area ranges from 650 to 700 mm per year. The altitude of the uplands formed by the Melechov granite massif vary from 350 to 710 m above sea level (m.a.s.l.). The highest part of the massif is formed by Melechov hill (708.9 m.a.s.l.) after which the massif was named. A fairly dense river network covers the Melechov massif. Most of the surface water drains into the Sázava river, whilst in the western part of the massif it drains into the Želivka river (Švihov water reservoir).

The Melechov massif belongs to the Moldanubic zone of the Bohemian massif and is formed by several petrographic types of Variscan-aged granite, which is surrounded by metamorphic rocks (mostly paragneiss) in the western part (Figure 5.2). Granites of the massif are relatively homogeneous and can be differentiated only on the basis of structure, texture and chemical composition.

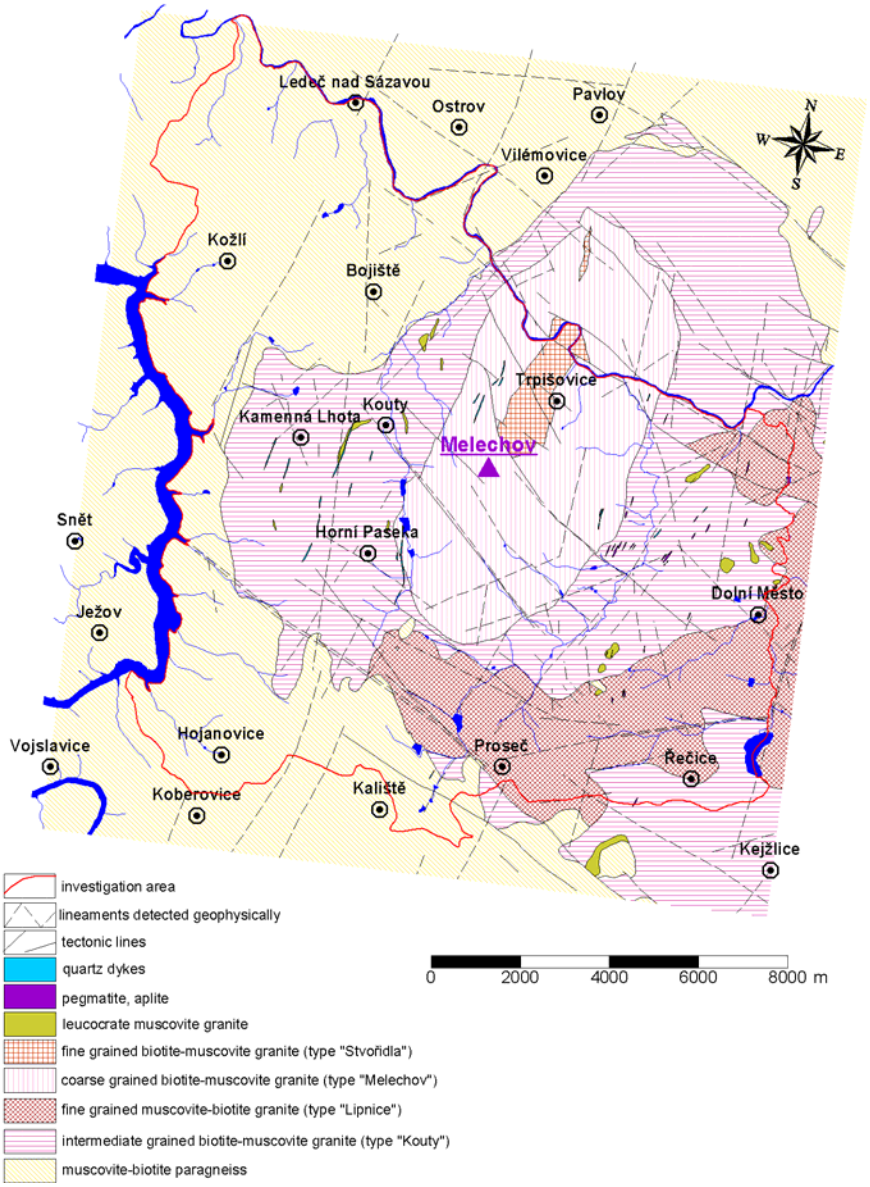

Figure 5.2. Geology of the area of interest.

The deep structure of the massif is known only from geophysical investigations. According to gravimetry measurements and modelling (Šrámek and Sedlák, 2001), the Melechov granite constitutes a subvertical cylindrical body reaching depths of more than 12 km. The granitic body generally plunges at 25-30° dip towards NE.

There are two main fracture systems at Melechov: an older fracture system oriented NNE-SSW inclined towards the centre of the massif, and a younger subvertical system oriented WNW-ESE (Mlčoch 1994, Mlčoch et al. 2000). There is an especially good relationship of geological boundaries and the courses of rivers with the orientation of the younger fracture system in part of the massif.

According to hydrogeological classification, the study area belongs to a hydrogeological massif. Groundwater flow is mostly related to fracture porosity, which is dependent on fracture occurrence and connectivity of single fractures. Only in the uppermost part of the massif (the weathered mantle) can mixed porosity be found. The thickness of this mixed porosity zone can reach a maximum depth of 30 m, depending on the intensity of erosion, topographic position, etc.

Values of hydraulic conductivity determined by pumping tests vary from 4.26×10^{-5} m/s to 1.18×10^{-6} m/s (Rukavičková 2001). These values represent only the shallow part of the massif (maximum depth 30 m); deeper values are not known because of the absence of deep boreholes. The magnitude of hydraulic conductivity is related to the thickness of weathering, topographic position and of course on fracture occurrence, and does not depend on geology.

5.2 APPLICATION TO MELECHOV GROUNDWATERS

The model mesh was composed of 276 rows and 230 columns with a uniform cell length of 50 m. The total model size represents an area of 158 km^2, of which approximately 92 km^2 is actually simulated. Inactive cells were set in the residual area (the greyed area in Figure 5.4). In areal view, the model contains 37,162 active and 26,318 inactive cells.

In vertical cross section, the model was divided into 14 layers (Figure 5.3). The first layer had uniform thickness of 50 m and the next 5 layers uniform thickness of 100 m. Average thickness of the 8 remaining layers varied from 75 m in layer 7 to 250 m in last layer 14. The total number of active cells in the vertical section is 520,268.

Recharge

Average annual precipitation in the vicinity of the Melechov massif varies from 650 to 700 mm/year. The proportion of precipitation infiltrating was estimated at 20%. So the initial value of recharge rate was set to 4.3×10^{-9} m/s.

Hydraulic conductivity

As described above, five hydrogeological units were identified, based on geology. These comprised the four granite types (Melechov, Kouty, Lipnice, Stvořidla) and the surrounding paragneiss. Initial values of their hydraulic conductivities in the uppermost model layer vary according to granite type as shown in Table 5.1; the spatial distribution of the granite types is shown in Figure 5.4. As indicated by equation [1], hydraulic conductivity was assumed to decrease with depth. Hydraulic conductivities of deeper model layers are discussed further below.

Boundary conditions

Boundary conditions were described above. The spatial distribution of these is shown in Figure 5.4.

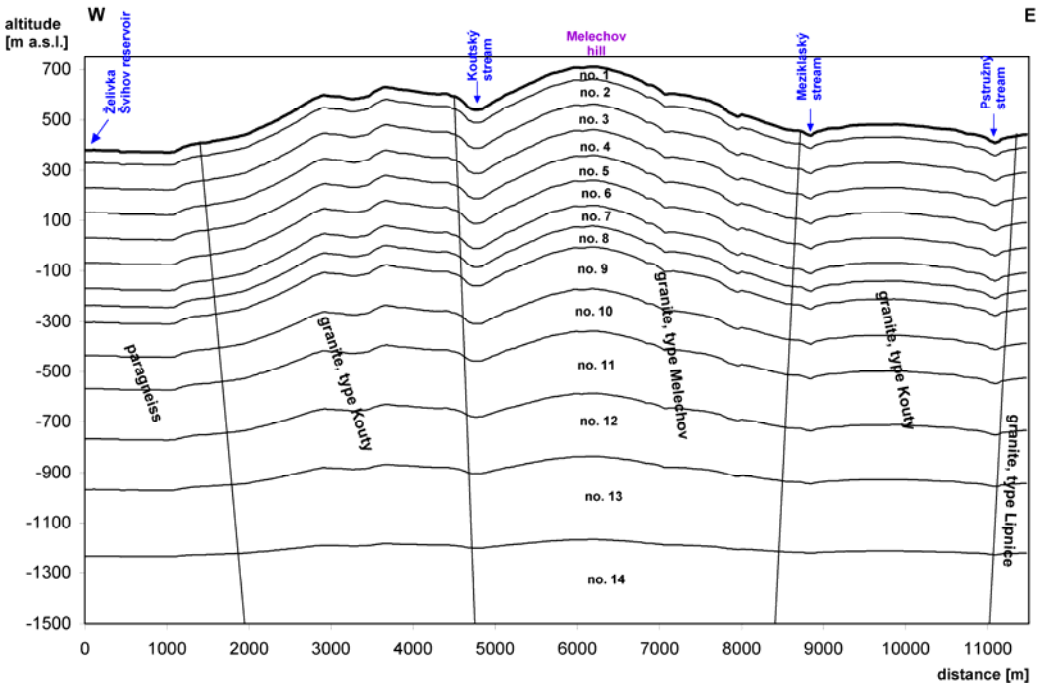

Figure 5.3. W-E cross-section showing model layers.

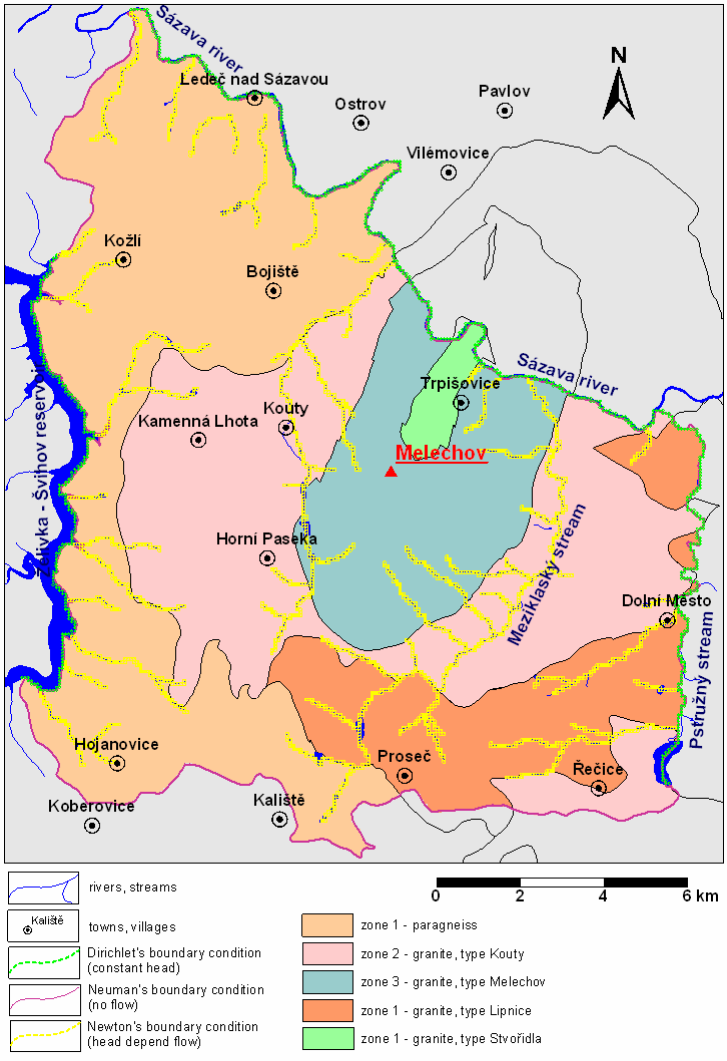

Figure 5.4. Model parameters and boundary condition distribution.

5.3 INTERPRETATION OF GROUNDWATER EVOLUTION

The main objectives of model calibration are to achieve a simulation that replicates the natural conditions in the study area. So calibration consists of the minimization of differences between model results and known hydraulic pressure values by an initial adjustment of hydrogeological parameters.

In this case, only recharge rate and hydraulic conductivity were adjusted for model calibration. Model accuracy was compared with water table levels at selected wells and at springs with significant flow rates. Together with these values, the accuracy of flow rates in rivers was checked.

The model calibration results and resulting hydrogeological parameters are described and commented on below.

Hydraulic conductivity

Hydraulic conductivities of all hydrogeological units were adjusted for model calibration. The resulting values of hydraulic conductivities in the shallow part of the Melechov massif are approximately 10x lower than values determined from pumping tests. The reason for these differences is in the thickness of the shallow model layer which is 50 m, whilst pumping tests have characterized only the part of this to depths of 30 m maximum. Values of hydraulic conductivity at greater depths were assumed according to equation [1] in Appendix C. During model calibration, better model results were achieved using a value of 400 m for coefficient C instead of the original value of 500 m. Table 5.1 shows the final values of hydraulic conductivities and their spatial distribution.

Table 5.1. Distribution of hydraulic conductivities

layer no.	average depth [m]	paragneiss	granite, type kouty [m·s^{-1}]	granite, type melechov [m·s^{-1}]	granite, type lipnice [m·s^{-1}]	granite, type stvořidla [m·s^{-1}]
1	25	2.70E-06	4.30E-06	3.90E-06	3.70E-06	3.60E-06
2	100	1.75E-06	2.79E-06	2.53E-06	2.40E-06	2.34E-06
3	200	9.86E-07	1.57E-06	1.42E-06	1.35E-06	1.31E-06
4	300	5.54E-07	8.83E-07	8.01E-07	7.60E-07	7.39E-07
5	400	3.12E-07	4.97E-07	4.50E-07	4.27E-07	4.16E-07
6	500	1.75E-07	2.79E-07	2.53E-07	2.40E-07	2.34E-07
7	590	9.04E-08	1.44E-07	1.31E-07	1.24E-07	1.21E-07
8	710	4.53E-08	7.22E-08	6.55E-08	6.21E-08	6.04E-08
9	820	2.41E-08	3.83E-08	3.48E-08	3.30E-08	3.21E-08
10	940	1.21E-08	1.92E-08	1.74E-08	1.65E-08	1.61E-08
11	1050	6.40E-09	1.02E-08	9.25E-09	8.77E-09	8.54E-09
12	1170	3.21E-09	5.11E-09	4.64E-09	4.40E-09	4.28E-09
13	1280	1.70E-09	2.71E-09	2.46E-09	2.33E-09	2.27E-09
14	1400	8.54E-10	1.36E-09	1.23E-09	1.17E-09	1.14E-09

Recharge

An initial value of recharge rate of 4.3×10^{-9} m/s was used in the model. During model calibration, this value was changed to 5.4×10^{-9} m/s. This represents 25% of the total average

annual precipitation. The slightly higher value is reasonable taking into account the sandy character of the weathered granite layer.

5.4 INTERPRETATION OF RESULTS

5.4.1 Hydraulic head distribution

Some of the model results are included as an example in Figure 5.5 to 5.9, showing the spatial distribution of hydraulic heads and directions of water flow in selected layers and cross-sections.

The model results show that the Sázava river and Švihov reservoir have a significant drainage function. The drainage function of other watercourses is significant mainly in low-lying flat parts of the massif; for example, the drainage function of the Meziklaský stream is significant. In contrast, drainage of watercourses situated in incised upland areas is reduced. Owing to surface topography, the main hydraulic gradient of shallow groundwater is towards the lower part of massif where is drained. This is the case for watercourses situated at the west and north-west part of the Melechov massif. With increasing depth, the drainage function of watercourses decreases and the importance of the topography of the regional watershed formed by the Melechov massif increases.

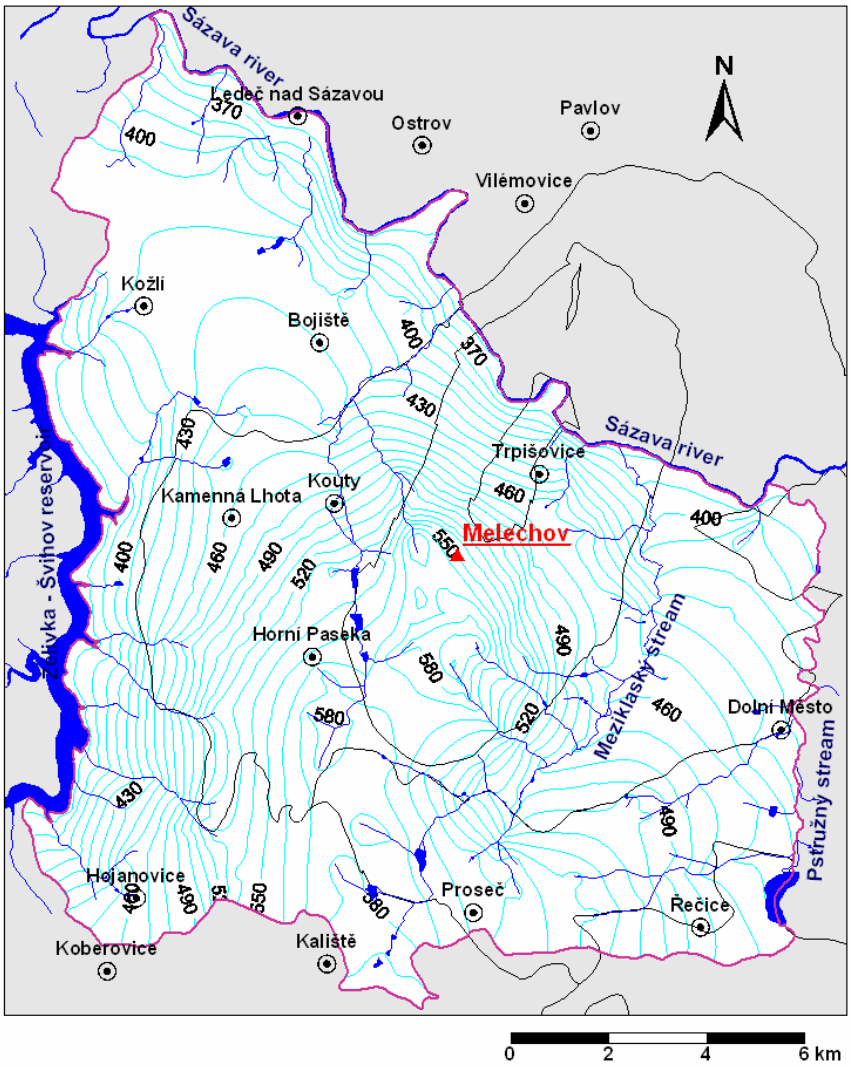

Figure 5.5. Hydraulic head contours in the uppermost model layer.

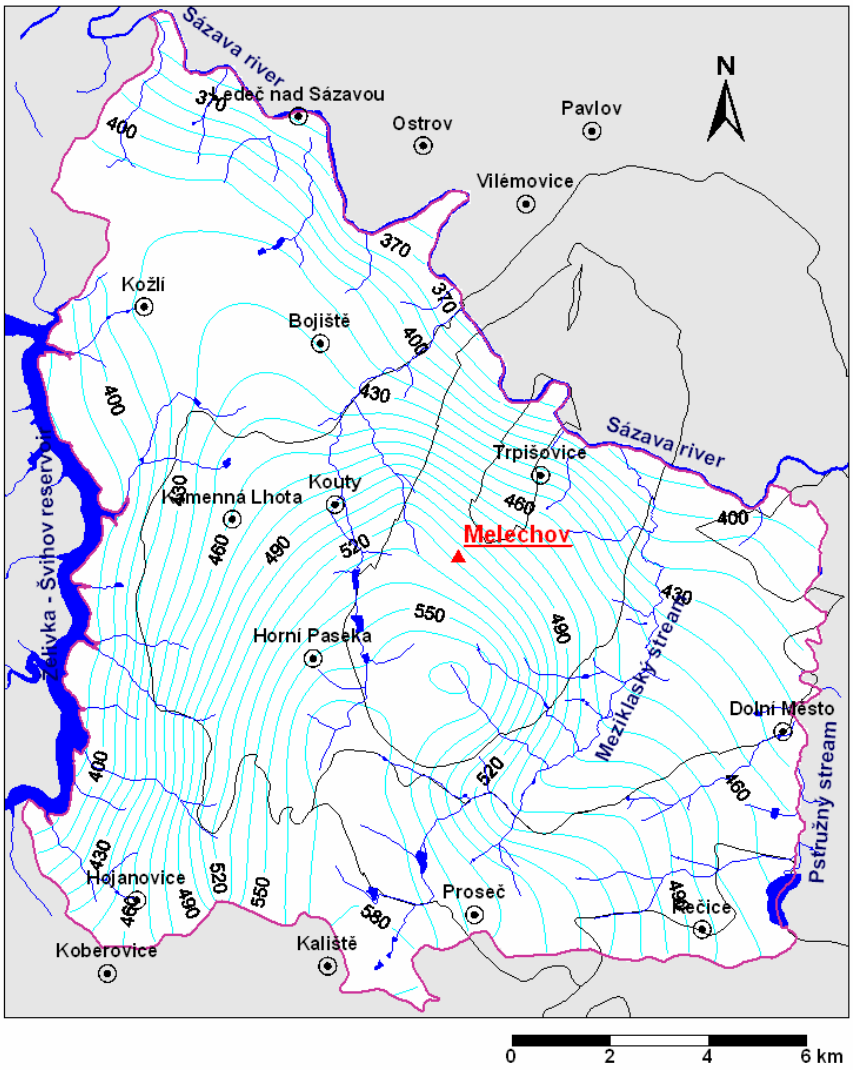

Figure 5.6. Hydraulic head contours in the fourth model layer.

5.4.2 Flow velocities and travel times

A specific simplification was necessary to simulate flow velocities and travel times. The limitation of the software required that fracture flow had to be replaced by porous medium flow. This simplification is acceptable because of the extent of the modelled area, the limited degree of investigation of the massif and the objectives of the model. The magnitude of error caused by this simplification depends on the density of fracturing, its depth dependence, sediment filling, connections between fractures, etc. Because of the limited extent of investigation of the massif, knowledge about these fracture characteristics is at a low level.

Computations of flow velocities and travel times were performed for three cases which include different densities of fracturing. In the model, changes in the densities of fracturing have been simulated by means of changes in values for vertical hydraulic conductivity and porosity. Resulting flow velocities and travel times for various fracturing densities in the Melechov massif are shown in Table 5.2. The extreme values of fracturing (low and high in Table 5.2) represent 10-20% changes against the average values of vertical hydraulic conductivity and porosity.

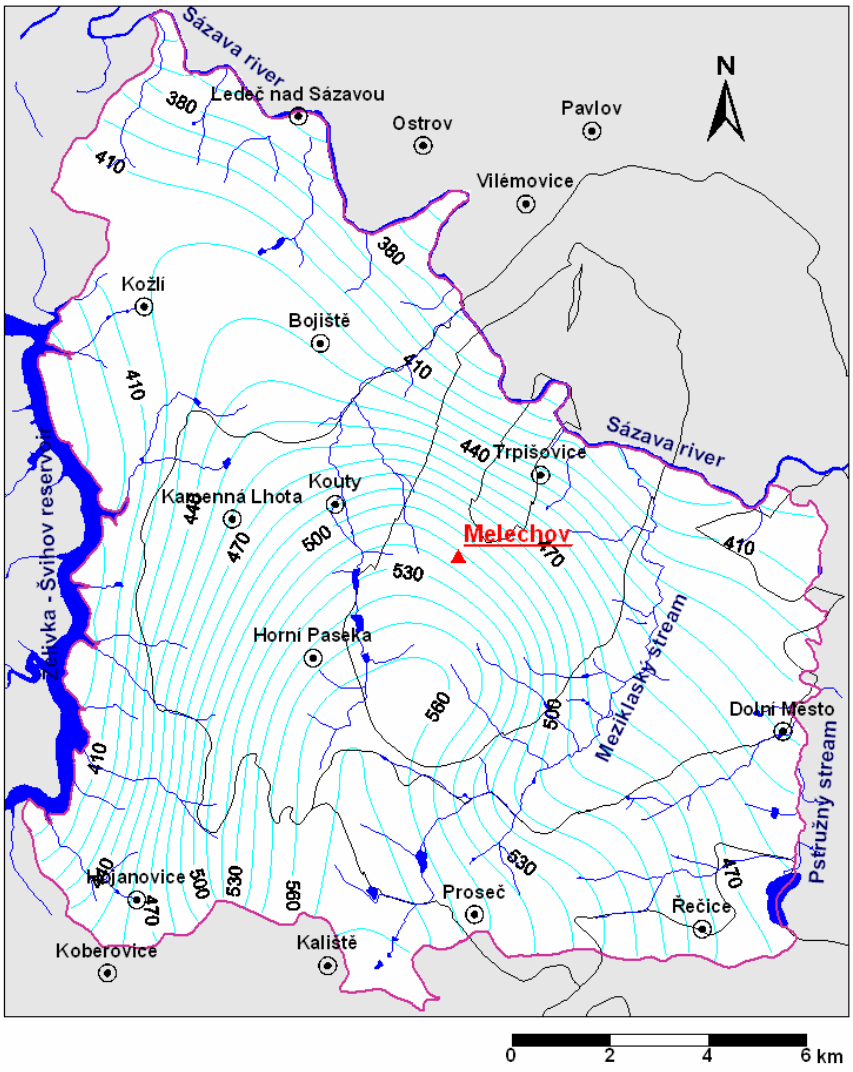

Figure 5.7. Hydraulic head contours in the tenth model layer.

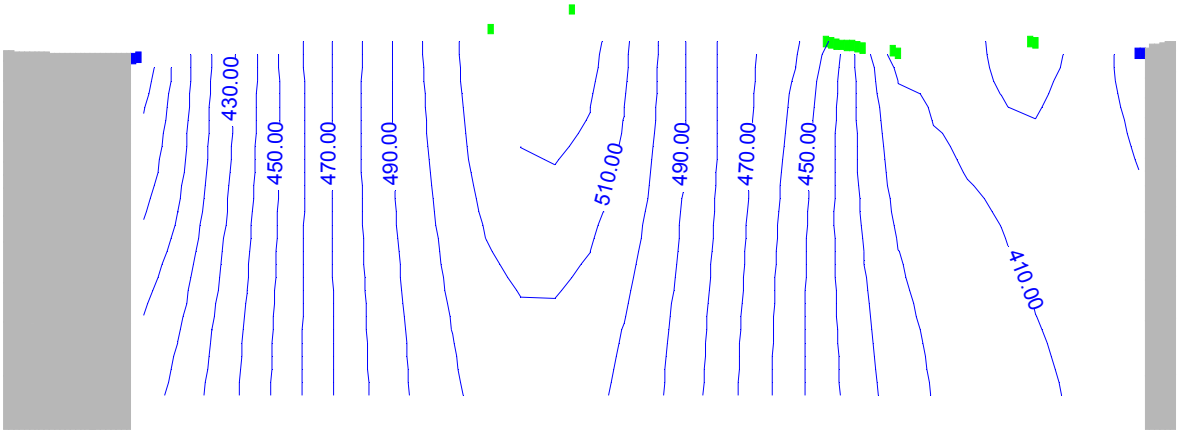

Figure 5.8. Hydraulic head contours in W-E cross section.

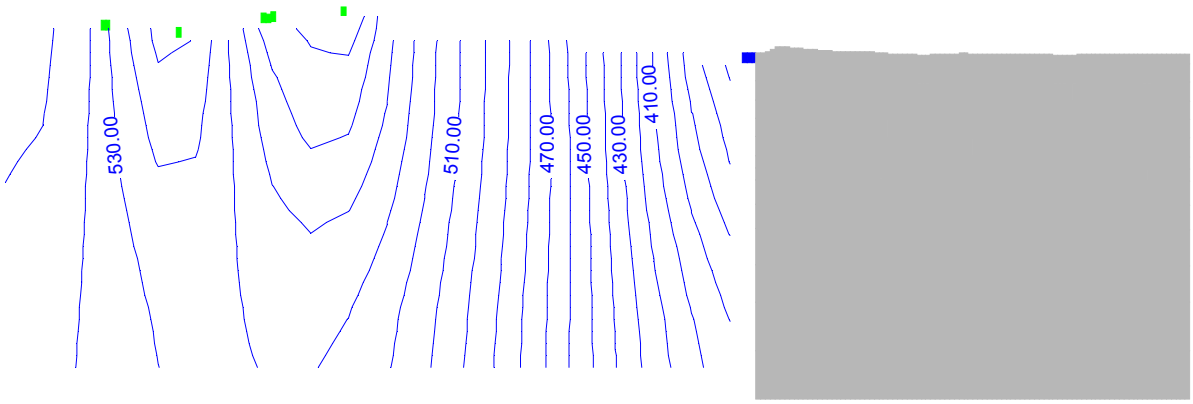

Figure 5.9. Hydraulic head contours in N-S cross section.

Table 5.2. Flow velocities and travel times

depth level [m]	Average flow velocity [m·s^{-1}]			Travel time for distance of 1000 m [year]		
	low fracturing	average fracturing	high fracturing	low fracturing	average fracturing	high fracturing
0 – 100	2.40E-06	3.00E-06	3.60E-06	13	10	9
100 – 200	4.24E-07	5.30E-07	6.36E-07	75	60	50
200 – 500	5.44E-08	6.80E-08	8.16E-08	580	470	390
500 – 1000	4.64E-09	5.80E-09	6.96E-09	6800	5500	4600
1000 – 1800	3.28E-10	4.10E-10	4.92E-10	97000	77500	65000

5.5 CONCLUSIONS AND RECOMMENDATIONS TO R&D GROUPS AND PA GROUPS

This modelling study is the preliminary stage of developing an understanding of the present-day hydrogeology and palaeohydrogeology of the Melechov granitic massif. Calibration of the model is severely constrained by the absence of deep boreholes and data only from the shallow borehole at Melechov. Topography of the massif has about 350 metres contrast from the high point at Melechov to the hydrological boundaries of the surface catchment that are partly defined by rivers. Important questions about present-day hydrogeology at the outset of modelling are:

- The effect of uncertainties in the hydrogeological properties of the deep granites on groundwater flow paths through the massif;
- The sensitivity of flow paths and travel times to infiltration;
- Travel times to discharge points in relation to depth at various points in the massif.

Palaeohydrogeology is a subsidiary objective of modelling at this preliminary stage, but some aspects of palaeohydrogeology raise similar questions to those above that concern the impact of uncertainties on the present-day groundwater model, for example:

- Changes of the groundwater flow paths and travel times at times in the past when infiltration might have been higher or lower than at present;
- Effects of changes in the properties of the upper weathered mantle on infiltration and groundwater flow at greater depths;

- Impacts of permafrost episodes when ground was partly or pervasively frozen and therefore inhibited infiltration;
- Effects of climate changes on the locations and hydrology of the boundaries of the shallow and deep groundwater systems.

Conclusions from this initial stage of modelling are summarised as, and include some recommendations for future research objectives:

- The depth and properties of the weathered mantle, thought to be about 30 metres deep, are important with respect to the lateral diversion of shallow groundwater which also affects the infiltration flux to deeper flow paths;
- It is necessary to investigate the relationship of hydraulic conductivity variation with the depth of the weathered mantle as identified in investigations of drillcore;
- The relationship between granite type and hydrogeological properties has been assumed for this modelling study but needs to be investigated further;
- The model has been calibrated against recharge rate by adjusting the hydraulic conductivities to obtain the best fit to the position of the water table that is known from wells and spring outflow elevations;
- Groundwater flow mainly towards the NE and W boundaries is indicated by the calibrated model, as expected from topographic considerations, but the magnitudes and directions of groundwater fluxes in the deep model layers have large uncertainties due to the assumptions about depth-dependence of hydraulic properties and about infiltration below the weathered mantle;
- Travel times and flow velocities have been calculated on the basis of the porous medium model and are, for example, in the order of 5000 years per 1000 metres flow path in the depth interval between 500-1000 m, assuming a porosity value corresponding to 'average' fracturing, but these estimates are strongly dependent on many factors including the porosity and hydraulic gradient/direction at that depth.

For making recommendations for preliminary PA scoping, the basic understanding of this system has to be developed further by additional modelling, calibration with borehole data and by comparison with other studied granites. Palaeohydrogeology needs to be developed further by establishing a series of past hydrological regimes based on known climate history, and then developing conceptual models for the palaeohydrogeological conditions that might have been associated with those regimes. An important constraint on palaeohydrogeology is the topography of the massif and the influence this has on the boundary conditions.

6 Summary and Implications for Palaeohydrogeological Interpretations of Geochemical Data

6.1 ABOUT SPECIFIC OBJECTIVES

Work Package (WP) 4 has had the objective of developing and applying interpretative models that are tools for:

(a) Understanding the processes that link the geochemical measurements made in WP2 and databased in WP3 with the evolution of past groundwater conditions, and

(b) Estimating parameters that are required for PA groundwater models, such as limits on boundary conditions, travel times, redox and salinity fluctuations.

Essentially, the interpretative models for process-understanding should be able to be calibrated using palaeohydrological information and provide an interface between a database of palaeohydrogeological information and FEPs for scenario development in PA.

The background to the objective for WP4 is that geochemical and mineralogical measurements in WP2 provide data that are 'proxies' for palaeohydrogeological information. Proxy data have to be interpreted using expert judgement and quantitative modelling to extract information that is relevant to FEPs and PA. The ways that these interpretations are carried out, and the extent and significance of uncertainties, are not easily apparent to PA groups. Consequently, palaeohydrogeological information has tended to be discounted when FEPs are being screened for the development of scenarios in PA. The methods developed here should help PA groups to identify and screen scenarios and to constrain them with quantitative information, for example with respect to:

- Recharge to the groundwater system in relation to future changing climate conditions,
- Hydrogeochemical behaviour and reactive transport at repository depth, for example with respect to salinity and stability of redox conditions,
- Locations and fluxes of groundwater discharge from the geosphere to the biosphere.

6.2 ABOUT METHODOLOGY

To meet the objectives of WP4, interpretative tools have been developed to quantify interpretations or proxies as much as possible. The interpretative models also help to clarify the uncertainties. An important part of the methodology in WP4 has been the use of coupled models that have recently become available to examine spatial and temporal variability of processes that control palaeohydrogeological proxies. The two coupled reactive transport models that have been used, CORE^{2D} and PRECIP, simulate geochemical changes coupled with groundwater flow in 2- and 1-dimensions respectively. They have been used to investigate the variations of geochemical parameters and the growth of proxies so that proxy data can be used to calibrate the models which could then be applied to the evolution of a site for future changing climate conditions.

Another aspect of the methodology has been aimed at developing a way of interfacing different climatic and hydrological proxies with a palaeohydrogeological model as support for the construction and calibration of a groundwater model with boundary conditions appropriate for future changing climate. This has been achieved in the model for Los Ratones by using the

VISUAL-BALAN code to estimate time-dependent changes of recharge rate. These estimations have been constrained by palaeoclimate information from measurements of microfaunal, pollen, isotopic and organic geochemical proxies in WP2. In general, the integration of models in this way should make the conceptual assumptions and uncertainties more explicit and the range of plausible palaeohydrogeological conditions better understood.

The modelling approach to understanding the hydrodynamics of the Melechov site is the initial stage in the development of a site investigation methodology that is appropriate for fractured granitic rocks in the terrain and climate of the Bohemian massif. The type of palaeohydrogeological information that will inform FEPs for this area are the proxies that contain evidence of climatic influences on recharge rate, distribution of flow between shallow and deep flow paths, and the locations of discharge at the peripheral hydrological boundaries and at intermediate topographic features. Future investigations would integrate further hydrogeological modelling for varying boundary conditions and additional geochemical studies of the palaeohydrogeological proxies that have been developed in WP2. Present experience at Melechov suggests that those proxies will only be applicable at greater depth than so far investigated.

The last part of the methodology developed in WP4 has involved forward modelling of geochemical proxies for redox during growth of secondary calcite. It has been carried out to provide a firm basis for interpreting palaeoredox proxies measured in WP2. In this case, the conceptual assumptions regarding the groundwater mixing process and the mineral controls on Fe and Mn concentrations in solutions have been made fully explicit in the model. This quantifies the uncertainties in relating the geochemical proxies to redox and also describes the science that underpins expert judgement.

6.3 ABOUT DATA NEEDS

Data that are involved in the modelling and interpretation of palaeohydrogeological information from geochemical proxies comprise several categories:

- 'Reconnaissance' of the distributions and characters of potential geochemical and mineralogical proxies, e.g. weathering profiles, secondary minerals, fluid inclusions, isotopic compositions, redox-sensitive trace elements and minerals.
- Scope of potential palaeoclimate impacts on time-varying conditions at the surface boundary of the groundwater system, e.g. likely typical and/or extreme impacts on recharge, water table, river-groundwater interaction, hydraulic gradients.
- Hypothetical FEPs that describe the extent to which shallow palaeoclimate impacts might be propagated to depth, i.e. conceptual models of possible deep perturbations of geochemistry and hydrogeology.
- Calibration parameters for process models, e.g. kinetics of precipitation and distribution of primary and secondary minerals with respect to groundwater flow rates and reactive surface areas, mineral assemblages, pH- and redox-controlling reactions, chemical compositions of possible end-member groundwaters.
- Chronological data for ages of proxies, i.e. isotopic ages and other independent age data that will allow the palaeohydrological interpretations to be tied in with palaeoclimate records.

It is characteristic of the types of geochemical and mineralogical measurements in PADAMOT that they provide an incomplete and discontinuous archive of timewise variations or in some cases represent single episodes of uncertain duration. Data density and the extent of gaps in the record, and an understanding of their significance need to be considered. A palaeohydrogeological interpretation should evaluate the probability of identifying and understanding the significance of episodes that might have removed or altered geochemical

proxies, for example by dissolution or by redox-sensitive alteration reactions. The continuity of mineral growth zoning and of other proxies that are relevant to specific environments has to be considered in this context.

It should be recognised in planning data collection to test hypothetical palaeohydrogeological models that multiple lines of evidence are desirable to build confidence in interpretations. Consistency between independent data with respect to palaeohydrogeological parameters can in principle be tested in several groups:

- Water origins: chemical isotopic compositions of present-day mixed groundwaters, isotopic compositions of secondary minerals, compositions of fluid inclusions.
- Water salinities: salinities of present-day mixed groundwaters, fluid inclusions, morphologies of secondary calcite growth zones, evaporitic secondary minerals, fresh water alteration minerals.
- Palaeoredox of groundwater system: minerals assemblage including redox-sensitive and redox-buffering minerals, mineral associations in calcite growth zones, trace element contents of secondary minerals, e.g. Fe, Mn, Ce, stable carbon isotopic ratios in calcite.

6.4 ABOUT CODES AND NUMERICAL TOOLS

WP4 has deployed a range of computer codes as tools for calculating various physical and chemical conditions of the groundwater systems of interest. Notable success has been demonstrated in the integration of groundwater flow, solute transport and geochemical simulations with CORE^{2D} and PRECIP.

An integration of hydrological calculations and palaeoclimate data for the upper boundary conditions of groundwaters in semi-arid conditions has been demonstrated with VISUAL-BALAN. The more widely-available generic codes MODFLOW and PHREEQC, for groundwater flow and geochemical reaction respectively, have been shown to be valuable for calculating 'snapshots' of the groundwater and geochemical properties of a system to test outcomes for particular assumptions of relevant properties, boundary conditions and other constraints.

The value of further developments and integration of numerical tools is, arguably, limited by the acquisition of palaeohydrogeological proxies that can test spatial and temporal variability with increasing resolution and reliability. The capabilities of CORE^{2D} and PRECIP to simulate transient systems (in 2D and 1D respectively) have been demonstrated in WP4, but the validity of their simulations is limited by calibration data.

Some interesting developments in palaeohydrogeological modelling are happening outside PADAMOT, most notably in SKB's site investigation project in Sweden. The 3D groundwater flow and solute transport codes CONNECTFLOW and DarcyTools have been used to simulate the evolution of groundwater chemical and isotopic compositions up to the present-day, testing assumed hydrogeological properties and initial/boundary conditions. Geochemical reactions and equilibria are not included in these models, so essentially salinity and stable isotope composition are simulated and are the principal calibrations.

6.5 ABOUT INTEGRATION OF WORKGROUPS (BIOSPHERE, HYDROGEOLOGY, GEOCHEMISTRY, MODELLING, PA)

Modelling in WP4 has made progress towards the integration of independent models of biosphere/climate, groundwater and geochemistry. Palaeoclimate, geochemical, isotopic and mineralogical proxies have been used to calibrate the models. Integration has been achieved by identifying what information needs to be transferred between the various models, e.g. recharge

data from the biosphere model to the groundwater model, water flux data from the groundwater model to the geochemical model. Acquisition of proxy information, interpretation by expert judgement and modelling and understanding of uncertainties especially with respect to temporal variability are then the focus of integration between the different workgroups.

Integration will also be facilitated by having realistic modelling ambitions that recognise the differing spatial and temporal resolutions. Biosphere modelling with respect to palaeoclimate has much greater temporal resolution than is appropriate for temporal changes of boundary conditions for groundwater models. Spatial resolution in groundwater flow and solute transport models is, currently, more refined than that in transport and reaction modelling.

The possibilities and realities of integration with PA groups, especially with regard to the identification and quantification of FEPs and scenarios, is considered in the report for Work Package 5.

6.6 ABOUT NEXT STEPS

Both the EQUIP and PADAMOT projects have focused on geochemical and mineralogical proxies for palaeohydrogeology. It could be argued that these programmes of research have exhausted the potential of such proxies to provide useful information and have identified the limitations of the various methodologies and modelling tools. However WP2 has shown that further progress in characterising proxies and interpreting palaeohydrogeological information is possible with state-of-the-art analytical techniques.

There can be no doubt that future developments in analytical tools will bring about additional improvements in the resolution and sensitivity of mineralogical, geochemical and isotopic analyses and in the reliable quantification of these types of information. Interpretative modelling will need to develop further the approaches that have been demonstrated in WP4 so that the significance of 'proxy' data for palaeohydrogeology and specifically for information that is useful for scenario development can be realised and calibrated.

Advances in modelling capabilities and computing power will enable proxy data to be better used for palaeohydrogeology. The integration of climate-driven hydrological modelling with reactive mass-transport modelling of groundwaters, via changes of time-dependent boundary conditions, is one of the areas developed in WP4 which offers the possibility of directly linking scenarios for groundwater conditions down to repository depth with climate scenarios in PA. This approach to evolutionary coupled modelling over long timescales matches the advances in PA codes which take into account temporally variable boundary conditions.

Finally, a comment is appropriate about the future direction of field-based research in support of the use of palaeohydrogeological proxies at potential repository sites. In this project, proxy data and models have been investigated using samples and data from past site investigations that were readily available in each of the partner countries. A logical next step would be a research study that targets investigations on locations that are scientifically-selected to be representative of specific 'worst case' palaeohydrogeological impacts or evolutions.

7 References

Agüero, A., Lomba, L. and Pinedo, P., 2003. Current description of Spanish Regions of interest for the BIOCLIM EU project. CIEMAT/DIAE/551/55160/02/03.

AITEMIN: Ortuño, F., Floría. E., Carretero G. and Suso, J., 2001. Hidrogeología de Mina Ratones.

Astilleros, J.M., Pina, C.M., Fernández-Díaz, L. and Putnis, A., 2003. Supersaturation functions in binary solid solution-aqueous solution systems. Geochim. Cosmochim. Acta., 67/9, 1601-1608

Barnaby, R.J. and Rimstidt, J.D., 1989. Redox conditions of calcite cementation interpreted from Mn and Fe contents of authigenic calcites. Geol. Soc. Of Amer. Bulletin, 101/6, 795-804

Bath, A., Milodowski, A., Ruotsalainen, P., Tullborg, E.-L., Cortés Ruiz, A. and Aranyossy, J.-F., 2000. Evidence from Mineralogy and Geochemistry for the Evolution of Groundwater Systems During the Quaternary for Use In Radioactive Waste Repository Assessment (EQUIP Project). Final Report, Contract No FI4W-CT96-0031. Euratom/EC DG Research Report EUR 19613EN. European Commission, Luxembourg. 157pp.

Bath, A., Richards, H., Metcalfe, R., McCartney, R., Degnan, P. and Littleboy, A., 2005. Geochemical Indicators of Deep Groundwater Movements at Sellafield, UK. Journal of Geochemical Exploration, Spec. Vol. 'Geochemical Aspects of Radioactive Waste Disposal' (guest eds. J-B Peyaud, T de Putter and I McKinley).

Bath, A., Milodowski, A., Tullborg, E-L., Kärki, A., Ruotsalainen, P., Shepherd, T., Cortés Ruiz, A. and Aranyossy, J-F. (in preparation) Palaeohydrogeological information from secondary calcite in fractured rocks at European sites.

Carpenter, A.B. and Oglesby, T.W., 1976. A model for the formation of luminescently zoned calcite cements and its implications. Geol. Soc. Am. Abstracts with Programs.

Emery, D. and Marshall, J.D., 1989. Zoned calcite cements: has analysis outpaced interpretation? Sedimentary Geology, 65/3-4, 205-210

Florschütz, F., Menéndez Amor, J, and Wijmstra, T.A., 1971. Palinology of a thick Quaternary succession in southern Spain. Palaeogeography, Palaeoclimatology, Palaeoecology 10, 233-264.

Fraser, D.G., Feltham D. and Whiteman, M., 1989. High-resolution scanning proton microprobe studies of micron-scale trace element zoning in a secondary dolomite: implications for studies of redox behaviour in dolomites. Sedimentary Geology, 65/3-4, 223-232

Glynn, P.D. and Reardon, E.J., 1990. Solid-solution aqueous-solution equilibria: thermodynamic theory and representation. Amer. J. Sci., 290, 164-201

Glynn, P.D., Reardon, E.J., Plummer, L.N. and Busenberg, E., 1990. Reaction paths and equilibrium end-points in solid-solution aqueous-solution systems. Geochim. Cosmochim. Acta., 54, 267-282

Gómez, P., 2002. Impacto de la Mina Ratones (Albalá, Cáceres) sobre las aguas superficiales y subterráneas: Modelización hidrogeoquímica. ENRESA Technical Publication #06/2002; 303 pp.

Horbury, A.D. and Adams, A.E., 1989. Meteoric phreatic diagenesis in cyclic late Dinantian carbonates, northwest England. Sedimentary Geology, 65/3-4, 319-344

Juncosa, R. and Delgado, J., 2003a. Modelo hidrológico: cálculo de la recarga (Padul y Mina Ratones). E.T.S.I. de Caminos, Canales y Puertos de la Universidad de La Coruña. La Coruña.

Juncosa, R. and Delgado, J., 2003b. Modelo de flujo subterráneo. E.T.S.I. de Caminos, Canales y Puertos de la Universidad de La Coruña. La Coruña.

Juncosa, R. and Delgado, J., 2004. Modelo de Transporte Reactivo multicomponente. E.T.S.I. de Caminos, Canales y Puertos de la Universidad de La Coruña. La Coruña.

Lafon, G.M., 1978. Discussion of "Equilibrium criteria for two-component solids reacting with fixed composition in an aqueous phase-example: the magnesian calcites". Amer. J. Sci., 274, 1455-1468

Langmuir, D.M., 1997. Aqueous Environmental Geochemistry. Prentice Hall, 600 pp.

Lee, M.R. and Harwood, G.M., 1989. Dolomite calcitization and cement zonation relation to uplift of the Raisby Formation (Zechstein carbonate), northeast England. Sedimentary Geology, 65/3-4, 285-305

Lomba, L., 2002. Bioclimatic characterization of the central Spain area, Padul and Cúllar-Baza (Granada) zones. CIEMAT/DIAE/551/55160/10/02. Madrid.

Lomba, L. and Recreo, F., 2002. Condiciones ombrotérmicas y ambientales de las principales especies vegetales de la Península Ibérica. CIEMAT/DIAE/551/ 55120/07/02. Madrid.

Lomba, L. and Recreo, F., 2002. Paleoclimatic reconstruction of Padul and Cúllar-Baza basin. Palaeodata for Toledo area. CIEMAT/DIAE/551/55160/11/02.

Lomba, L., Recreo, F. and Ruiz, C., 2002. Preliminary identification of meteorological stations as potential climate analogues. BIOCLIM Project. WP3 Task TA 4/12 B.

Lomba, L., Ruiz, C. and F. Recreo, F., 2002. Identificación Preliminar de Estaciones Meteorológicas como potenciales Análogos Climáticos. CIEMAT/DIAE/551/55160/14/02.

Lomba, L., Recreo, F. and Ruiz, C., 2003. Preliminary Identification of Meteorological Stations as Potential Warm Climate Analogues. BIOCLIM Project WP3 TA4/12B and WP4 TA 5/10 Tasks. CIEMAT/DIAE/551/55160/03/03.

Lomba, L., Ruiz, C., Recreo, F., 2003. Breve descripción bioclimática de la Cuenca del Duero. CIEMAT/DIAE/551/55120/05/03

Lomba, L. and Ruiz, C., 2003. Proyecto PADAMOT. Evaluación de la Recarga en el pasado en el entorno de la Mina Ratones (10^4 ka BP). CIEMAT/DIAE/551/55170/06/03.

Lomba, L., Ruiz Rivas, C. y Recreo, F., 2003. Proyecto AGP ENRESA 2003-Arcilla. Actividad: Escenarios de Evolución Ambiental. CIEMAT/DIAE/55120/07/03.

Lomba, L. and Recreo, F., 2004. Proyecto PADAMOT. Modelo Paleoclimático de la zona de Padul (Granada) desde el Pleistoceno Medio hasta el Eemiense deducido del registro polínico. Condiciones ambientales y ombrotérmicas regionales. CIEMAT/DIAE/54650/2/04.

Lomba, L., Ruiz, C. and Recreo, F., 2004. Evaluación de la recarga en el entorno de la Mina Ratones Ratones entre el Pleistoceno Medio y el interglacial Eemiense (500-100 ka BP). PADAMOT Project. CIEMAT/DIAE/54650/01/04.

Martínez-Landa, L, Ortuño, F. and Bitzer, K, 1999a. Modelo Hidrogeológico regional de Ratones. Informe final 10-UPC-IF-01. Departamento de Ingeniería del terreno y Cartografía. Universidad Politécnica de Cataluña. 63 pp.

Martínez-Landa, L, Vives, L, and Marcuello, A, 1999b. Modelo Hidrogeológico local de Ratones. Informe final 10-UPC-IF-02. Departamento de Ingeniería del terreno y Cartografía. Universidad Politécnica de Cataluña. 73 pp.

McDonald, M.G. and Harbaugh, A.W., 1988. A Modular Three-Dimensional Finite-Difference Ground-Water Flow Model, Techniques of Water-Resources Investigations of the U.S. Geological Survey Book 6, Ch. A1: 576 p.

Metcalfe, R. and Moore, Y.A., 1997. The possible geochemical and mineralogical consequences of Quaternary climate change: A theoretical scoping study. Technical Report WE/97/25C. Fluid Processes Group, British Geological Survey, Keyworth.

Mlčoch, B., 1994. Zpráva o detailním geologickém mapování 1:10,000 lokality Dolní Město. MS ČGÚ. Praha.

Mlčoch, B. et al., 2000. Vysvětlivky k aktualizované účelové geologické mapě melechovského masívu 1:10 000

Mlčoch, B. et al., 2000. Aktualizovaná účelová geologická mapa melechovského masivu v měřítku 1: 10 000. SÚRAO. Praha.

Noy, D.J., 1998. User Guide to PRECIP. a Program for Coupled Flow and Reactive Solute Transport. Brit. Geol. Surv. Tech. Rep. WE/98/13. British Geological Survey, Keyworth, UK.

Parkhurst, D.L. and Appelo, C.A.J., 1999. User's guide to PHREEQC (version 2) – a computer program for speciation, batch-reaction, one-dimensional transport, and inverse geochemical calculations. Water-Resources Investigations Report 99-4259. U.S. Geological Survey, Denver

Pons, A. and Reille, M., 1988. The Holocene and Upper Pleistocene pollen record from Padul (Granada, Spain): A new study. Palaeogeography, Palaeoclimatology, Palaeoecology, 66: 243-263.

Recreo, F. and Ruiz, C., 1997. Consideración del Cambio Medioambiental en la Evaluación de la Seguridad. Escenarios Climáticos a largo plazo en la Península Ibérica. ENRESA, Publicación Técnica Número 01/97.

Recreo, F., Lomba, L. and Ruiz, C. 2005. Potential climatic and landscape evolution of central Spain (Toledo area) over the next 200,000 years. BIOCLIM Project, TA 5/10: Broad narrative descriptions of biosphere system changes in climate Transitions. CIEMAT/DIAE/551/55160/01/03.

Recreo, F., Lomba L. and Ruiz C. 2002. Broad narrative descriptions of biosphere system changes in climate transitions. Participación CIEMAT-ENRESA-ETSIMM en el Proyecto BIOCLIM, Deliverable D4. (TA5/10).

Recreo, F. and Lomba, L. Quaternary Climate Stages for South of Spain. BIOCLIM Project. Deliverable D2. Task 3-13.

Richards, H.G. and Bath, A.H., 1997. The Hydrochemistry of Sellafield: 1997 Update. Nirex Report SA/97/089. UK Nirex Ltd.

Rimstidt, J.D., Balog, A. and Webb, J., 1998. Distribution of trace elements between carbonate minerals and aqueous solutions. Geochim. Cosmochim. Acta, 62/11, 1851-1863

Rumbaugh J.O. and Rumbaugh D.B., 1998. Guide to Using Groundwater Vistas, Version 2, Environmental Simulations, Inc. Herndon, Virginia

Rukavičková, L., 2001. Účelová hydrogeologická mapa melechovského masivu (zpráva o hydrogeologickém výzkumu). ČGÚ, Praha. MS SÚRAO. Praha

Samper, J., Huguet, Ll., Ares., J., and García., M., 1999. Manual del usuario del programa VISUAL BALAN V. 1.0. Código interactivo para la realización de balances hidrológicos y la estimación de la recarga. Publicación Técnica ENRESA 05/99. 132 pp.

Samper, J., Juncosa, R., Delgado, J. and Montenegro L, 2000. CORE^{2D}. A code for non-isothermal water flow and reactive solute transport. Users manual versión 2. E.T.S. ingenieros de

Caminos, Canales y Puertos. Universidad de La Coruña. Publicación Técnica ENRESA 06/2000. 132 pp.

Šrámek, J. and Sedlák, K., 2001. Regionální sv.-jz. tíhový profil na lokalitě melechovský masiv. Geofyzika Brno a ČGÚ Praha

Wolery, T.J., 1992. EQ3/6, a software package for geochemical modeling of aqueous systems. Report No. URCL-MA-110662 PT III, Lawrence Livermore National Laboratory, USA

APPENDICES

Appendix A: Methodological Approach for Palaeohydrogeological Characterisation. Spanish Case

Appendix B: Secondary Calcite in a Shallow Recharge-to-Discharge Fresh Groundwater System

Appendix C: Mathematical Modelling of Groundwater Flow in Fractured Rocks at Melechov Massif

Appendix A: Methodological Approach for Palaeohydrogeological Characterisation: Spanish Case

Luis Lomba Falcón, Fernando Recreo Jiménez, Trinidad de Torres Perezhidalgo, Ricardo Juncosa Rivera

A1 Introduction

The recent consideration of the long-term climatic change for Deep Geological Repository Performance Assessment expounds new methodological problems because there is still not a consolidated and well-established approach in this respect.

The natural evolution of climate due to astronomical variations of the Earth orbit induces temperature and pluviometric oscillations and, therefore, originates evident changes in the vegetation of a region along the time.

It is possible to observe this evolution by analysing suitable fossil records such as those from peat bogs, among others, in order to study the vegetable evolution and, therefore, the climate evolution. The climate evolution will also have an influence in the relief, in the ecosystems and both in the surface hydrology and in shallow aquifer conditions, as well as, eventually, in the deep aquifer. So, the presence of certain vegetable associations in a pollen sequence indicates the climatic and environmental conditions for each different time period that can be distinguished for this record and then, the climatic evolution.

Therefore, it will be necessary to calculate or to evaluate the potential water recharges on the repository system in future time besides advancing the ecosystem vegetal associations to which the radionuclides will return.

According to Ruiz Zapata (2000) the pollinic content of sediments is a good palaeoclimatic indicator as well as a very useful tool in the reconstruction of the vegetable landscape and their evolution. The vegetable associations recorded in a pollen sequence allows at least to deduce the ombrothermic variations for a certain region along the time, to reconstruct the succession of their climatic conditions and to assign the different climatic classes in function of such conditions. Compared to other available palaeoindicators, the pollen has the advantage to offer information not only of the temperature, but also of the precipitation, because the distribution of vegetables responds to seasonal variations, to the annual conditions and to the humidity balances (Prentice et al., 1992). Besides, it could be used in order to refine the palaeoclimatic reconstructions in addition to another type of indicators (Guiot et al., 1993; Cheddadi et al., 1997).

The palaeoclimatic reconstruction of the Iberian Peninsula is difficult because it is an authentic vegetable landscape mosaic, due to its geographical situation, the varied relief and the recent climatic evolution (Ruiz Zapata et al., 1999). The different studies carried out in the Padul peat bog (Granada province) have been a starting point for the Quaternary palaeoclimatic knowledge of the southern zone of the Iberian Peninsula and a referent key too in order to reconstruct the palaeoenvironment of the Mediterranean continental region in general. So, the existent pollen diagrams cover an important lack of data of this zone from the Middle Pleistocene, for which not many records are available (Martín Arroyo, 1998). The more highlighted palynological analyses are these from Menéndez Amor and Florschütz (1962, 1964), from Florschütz, Menéndez Amor and Wijmstra (1971) and from Pons and Reille (1988), in chronological order.

The palaeoclimatic reconstruction from pollen records carried out has given values for the ombrothermic parameters and the results were assigned as Köppen climate classes (UE BIOCLIM project methodology) and as Rivas-Martínez bioclimatic levels (DGR PA ENRESA 2000 and 2003 methodology). That is the basis to evaluate the precipitation and temperature evolution for the recorded time. In this context the climate class concept help us to obtain the ombrothermic diagram for the average year corresponding to that climate class, so that it is easier to deduce the hydrometeorological parameters required for the recharge calculations. In spite of the remaining uncertainties it could be assumed that the Padul peat bog pollen record is climatically representative of the mean regional characteristics, because all the Mediterranean bioclimatic levels defined by Rivas-Martínez are near to this area.

In order to characterise the palaeo-water recharge for the Los Ratones area for the whole defined period, the Florschütz, Menéndez Amor and Wijmstra (1971) pollen diagrams were used for the palaeoclimatic characterisation and the ombrothermic reconstruction between *ca.* 500 ky BP and *ca.* 104 ky BP, and those from Pons and Reille (1988) for the period from *ca.* 104 ky BP. The palaeo-water recharge was calculated with the VISUAL-BALAN code (Samper et al., 1999), adapted by Juncosa and Delgado (UDC, 2003). The ombrothermic values and the type of vegetal cover for each time interval defined are input data for this code, therefore is very important to make a good palaeoclimatic reconstruction. Padul and Los Ratones site currently belong to the same Köppen climate class, and during past Quaternary geological evolution it could be assumed similar palaeoclimatic and palaeoenvironmental conditions. In addition, the recent datations carried out by Torres et al. (2003) has been important for help us to correlate the studied records.

A2 Synthetic Description of the Studied Records

The first referenced palynological studies about Padul peat bog are from Menéndez Amor and Florschütz who, in the year 1962, characterised the upper 20m of a 50m borehole. Later, in 1964, they completed the analysis of the whole borehole and published fourteen ^{14}C datations carried out in the University of Groningen, for between 4980±60 years BP and >54000 years BP, this last measurement about 12m of depth.

Later on, in 1971, Florschütz, Menéndez Amor and Wijmstra published the pollen analysis results of the upper 70m of a new 101m borehole named 'Padul IVa' (Figure A1). The first 24m, specified as 'Padul IV', formerly correlated by Florschütz et al. with the Tenagi Philippon (Macedonie) pollen sequence, were correlated later on by Pons and Reille (1988) with the sequences from two new boreholes, 'Padul 2' and 'Padul 3', both drilled very close to the previous one, and which reach sediment levels dated from *ca.*104 ky BP. There is a good pollen correlation between the upper 50m of 'Padul IVa' borehole and the whole first referenced borehole. According to Pons and Reille, whose studies are supported with twenty one ^{14}C datations from 63500 years BP, 'Padul 2' and 'Padul 3' boreholes, with a length of 15m and 8m respectively, correlate with 'Padul IV'. Pons and Reille boreholes, although drilled in near but separated sites, overlap each other by few meters. Torres et al. (2004) established a new palaeoenvironmental evolution for the last million years of southern part of the Iberian Peninsula studying both the Guadix Baza basin and the Padul peat bog, carrying out organic and isotopic geochemical studies.

Florschütz, Menéndez Amor and Wijmstra (1971) and Pons and Reille (1988) pollen diagrams are the analysed records to palaeoclimatically characterise the Padul area in the PADAMOT Project, the first one between *ca.* 500 ky BP and *ca.* 104 ky BP, and the second one from *ca.* 104 ky BP. More specifically, only the 'Padul IVa' the sequence between 20m and 70m has been fully analysed because the 'Padul IV' sequence is chronologically equivalent to Pons and Reille

pollen diagram, that is more rich and varied in general than 'Padul IVa', and was already studied for the BIOCLIM Project.

These authors consider the variety of vegetation present in the Padul peat bog proximity, due to several elements such as the mountainous relief and the different pluviometric and thermometric conditions it causes, as a possibility for that these characteristics could affected the pollen records. By the way, for this region they deduce a predominant open steppe type vegetation during glacial times, a more oceanic and humid vegetation of *Quercus-Pinus* with Ericaceae forest for interglacial stages, while interstadial episodes were dominated by dry forests of different character.

A2.1 FLORSCHÜTZ, MENÉNDEZ AMOR AND WIJMSTRA (1971) DIAGRAM

In order to represent the pollen changes with time they chose several entire sums of pollen as calculation basis of different, complementary percentages: the arboreal pollen, the arboreal pollen and the steppe pollen (*Artemisia*, Chenopodiaceae and *Ephedra*), and the arboreal pollen together with the herbaceous species but excluding Cyperaceae and aquatic species. These authors established several zones according to the vegetal associations and their own characteristics, mainly in function of the fluctuations of *Pinus* and *Quercus* for the arboreal pollen curve as well as those of *Artemisia*-Chenopodiaceae and Ericaceae for the non arboreal pollen (Figure A1).

The upper part of the sequence, known as 'Padul IV', has been correlated by Pons and Reille with 'Padul 2' and 'Padul 3' boreholes and ages until the Eemian interglacial episode have been assigned (Figure A2). In summary, they propose a palynological zonation with a great unity named GI, that includes several vegetation zones (R, S, T, U, V, X, Y) inserted between two zones, Q and Z, that correspond to the Eemian and to the Holocene respectively, in which the arboreal pollen percentage is high and the arboreal composition is varied, with *Abies*, *Fagus* and *Alnus*. The GI unity has high non arboreal pollen percentages, with a general prevalence of Chenopodiaceae and *Artemisia* with *Ephedra* and other species. The open steppe vegetation zones, with the assigned ages by the authors, are R1, R3 and T (Early Glacial), V2 (Lower Pleniglacial), X4 (Interpleniglacial), X6 and X8 (Upper Pleniglacial) and, finally, Y3 (Late Glacial) zones. As for the Holocene or Z zone in the diagram, it has open forest of *Quercus ilex* character. They have been ombrothermically characterised according to the corresponding climate class diagrams.

The Q zone, that has very specific characteristics and corresponds to the Eemian interglacial episode, is a clear reference zone with the most humid conditions for the whole-analysed record. In the bottom of this zone *Quercus pubescens* and/or *robur* and *Calluna* are present as well as *Ilex aquifolium* and *Acer*. In the middle of the zone, Ericaceae are more important, and the presence of *Armeria* and *Plantago* suggest that *Quercus pubescens* is an open type forest for this subzone. Finally, in the top of Q zone there are *Abies* and *Fagus* together with *Quercus pubescens*.

The 24-70m section is also divided in several vegetation zones, but the vegetal fluctuations inside every zone are not considered by Florschütz et al., so that they carried out only a general outline of vegetal evolution. For this section the distinguished zones are denominated such as G, at the bottom, to N, belonging K, L, M and N zones to the great GII unity, that is below the Q zone, according the authors. In the G zone the non-arboreal pollen percentages are high, with a notable amount of *Artemisia* and Chenopodiaceae as well as the presence of *Ephedra*, being Pinus the most important specie within the scarce arboreal pollen. The H level is characterised by an increment of arboreal pollen, up to 60%, mainly due to the great rise of *Pinus*, but the marked presence of steppe species such as *Ephedra, Artemisia* and Chenopodiaceae indicates an open vegetation with *Pinus*, quite similar in general to I zone, which is representative of steppe

landscape, with high percentages of *Artemisia* and Chenopodiaceae. Quite palynologically different from this last episode is the J zone, also with high amount of arboreal pollen, even 60-70%, but relatively low *Artemisia* and Chenopodiaceae percentages. According to Florschütz et al., *Abies, Tsuga*, *Quercus pubescens*, *Ilex*, *Juglans*, *Cistus*, *Fraxinus ornus* and *Vitis* are confirmed. It is to say that the vegetable characteristics are similar to an open warm and humid forest, ratified by the presence of *Erica*. The authors assigned this zone to the Holstein interglacial period, basically. The long K zone is quite uniform in general and presents steppe-like vegetation conditions, with high percentages of *Artemisia* and Chenopodiaceae, besides *Ephedra*. In the L interval the amount of *Pinus* is high and there is an increase of *Quercus*, and the quantity of *Artemisia* is still notable, in spite of Chenopodiaceae which are decreasing. The general characteristics are such as an open *Pinus* forest within an *Artemisia* steppe. In the M zone the steppe species are less important in the arboreal pollen/non arboreal pollen relation, reaching the *Quercus* curve the maximum value, with *Quercus ilex* as the most important oak tree, but *Quercus pubescens* is present too as well as Ericaceae. Probably there was a quite humid *Quercus* landscape, similar to the current *Quercus ilex* belt defined by Schmid (1956) for the Sierra Nevada range. Finally, the N zone, just below the Q interval, is characterised by important amounts of *Artemisia* and Chenopodiaceae as well as the presence of *Ephedra*, indicating a typical steppe landscape.

A2.2 PONS AND REILLE (1988) DIAGRAM

In their diagram the frequencies are calculated starting from a basic sum including 20 taxa at least, but some aquatic species were excluded. They also established several zones according to the vegetal associations based on the variations of at least two ecologically different species (Figure A2).

This diagram presents a greater variety of species than those currently carried out at that time, and so it is more useful in order to study the palaeoclimatology of Padul for the last glacial cycle. Nevertheless, in the middle part of the last glacial it shows poorly characterised climatic fluctuations, as it is frequent in Europe for that period. There is a change in the sequence toward 15 ky BP that is interpreted as a great expansion of the regional steppe cover, that reflects the beginning of the Oldest Dryas, already referenced several times in the southeast of France. The climatic improvement toward 13 ky BP is more marked in Padul than anywhere in Europe, while those toward 10 ky BP is not clearly reflected. Pons and Reille explain this because of the southern situation and closeness to the Pleniglacial refuge zones, which has consistency enough with marine isotopic records. The Tardiglacial and Holocene vegetation are characterised for the earlier appearance and dominance of *Quercus ilex* southern type forest as well as the early presence of *Quercus suber* and *Olea*, that is the first reaction in relation to a postglacial reforestation in a region with a semiarid climate. The authors explain the Holocene Thermal Optimum, that is reached just before 8 ky BP, as a warm and humid episode, as well as the Holocene climatic fluctuations had not been very intensive.

A3 Chronostratigraphic Assignment of Analysed Records

The starting point we have kept in mind in order to establish the chronostratigraphic correlation and age assignment has been the different datations carried out by the mentioned authors, although the oldest one is only 63.5 ky BP. The more recent datations carried out by Torres et al. (2003) in the new borehole already cited has been important to help us to complete the chronostratigraphic age assignment. (Figure A3). We have correlated these datations with the studied records assuming that they were carried out in a theoretical sequence, because of the boreholes proximity as well as the tectonic and sediment characteristics of the basin, without

important age variations between similar levels of the different drillings. A graph has been made according to these assumptions, reflecting the age versus the depth (Figure A4), which is very useful in order to assume a time age for a lot of non dated levels. So, the available pollen sequences may reach *ca.* 500 ky BP, confirming the vegetable associations significance, that generally is in agreement with the Florschütz et al. assignment, although with still quite shades.

The palaeoclimatic characterisation of Pons and Reille (1988) pollen diagram, from *ca.* 104 ky BP to *ca.* 4450 ky BP was already made for the UE BIOCLIM project (2000-2003), and is reflected in the Table A1, corresponding to deliverable D2 of this project. Although the main bases are the Pons and Reille diagrams for Padul, the Rossignol-Strick and Planchais (1989) studies about the KET 8003 borehole in the Tirreno sea and those from Guiot, Pons, De Beaulieu and Reille (1989) about Les Echets and La Grande Pile records (ENRESA, 1997) have also been taken into account.

The Florschütz, Menéndez Amor and Wijmstra (1971) pollen diagram includes the Holocene, the Upper Pleistocene and an important part of the Middle Pleistocene, from the Mindel glacial stage. The upper 24m of the record, 'Padul IVa', that corresponds to the last glacial cycle in general, is particularly different to the remaining part. So, the *Artemisia* and Chenopodiaceae percentages in the lower 46m of the diagram are generally higher than in the upper part. By the way, between 24m and 70m the variability of the relative proportions of the key vegetal species is less than in the uppermost section. The starting point for the interpretation and for the correlation carried out, was the climate oscillations and variations as reflected in the vegetable associations, following the initial postulates of Florschütz at al. as well as many authors, supported with the chronostratigraphic assignment made. Thereby, in a general sense, in the Mediterranean region there was a predominant herbaceous and/or bush vegetal cover with absence or shortage of trees for cold periods, while in climatic improvement times there was some arboreal elements at the beginning and more or less dense forest later on. *Artemisia* and Chenopodiaceae have a great value for deducing steppe conditions, so that their high quantity corresponds in general with a forest descent (Florschütz et al., 1971). So, most of the authors consider that an open steppe was the predominant landscape, although *Pinus* may be present in the glacial episodes. The interstadial periods were characterised by different types of not very humid or rather dry forests, with *Quercus ilex* being the predominant arboreal species, and finally for the interglacial and temperate interstadial episodes the commonest landscape was the more oceanic and humid forest, with *Quercus* and *Pinus* and Atlantic elements such as Ericaceae and *Ilex aquifolium* (Florschütz et al., 1971).

When the Florschütz et al. diagram is analysed, in spite of it being much less varied than the Pons and Reille sequence, it is possible to establish several climatic responses. Basically, in order to establish a chronological assignment for the vegetal zones defined by Florschütz et al., we have analysed the relative proportions of the different recorded vegetal associations and the arboreal pollen characteristics of these associations, being *Quercus* one of the most significant genus, as well as the steppe *Artemisia* and Chenopodiaceae, mainly, and the other significant vegetal species, like the Ericaceae family.

As an initial reference to compare with, we have considered the defined Q zone of vegetation, assigned by the authors to the Eemian and correlated by Pons and Reille with the P2a and P2b subzones of the 'Padul 2' sequence, which corresponds to the St. Germain Ia, *ca.* 104 ky BP. The Eemian interglacial period is very well defined and is generally accepted like a climate reference episode with palaeoenvironmental specific implications, posterior to the Riss glacial stage, that marks the beginnings of Upper Pleistocene before the Würm glaciation. Florschütz et al. correlated their sequence with the Tenagi Philippon pollen record, in Macedonie, from the Eemian period, although this episode seems to have in Padul some warmer character for the top of the sequence. Taking into account the different available datations and the vegetal associations characteristics, we have proposed an age and a chronostratigraphic assignment for

the analysed record from the lower-middle part of the Middle Pleistocene, *ca.* 500 ky BP, until the end of the Holocene, reaching the oxygen isotopic stage OIS 12. **It** includes the middle-upper part of the Mindel glacial stage, the Mindel-Riss or Holstein interglacial period and the Riss glacial episode, within the Middle Pleistocene, the complete Upper Pleistocene, with the Eemian and the remaining part of the Riss-Würm interglacial and the Würm glacial periods, and finally the Holocene until *ca.* 4.9 ky BP at the top of the sequence. We have basically followed the European Glacial chronology and the Quaternary chronostratigraphy according to Renault-Miskovsky (1992), Torres and Hoyos (unpublished), Cande and Kent (1995), Parés (1995) and Miskovskyand Raugin (2002). So, the Middle Pleistocene period would be embraced between *ca.* 780 ky BP and *ca.* 120 ky BP, including the Cromer or the Gunz-Mindel interstadial time (*ca.* 780-600 ky BP), the Mindel glacial episode (*ca.*600-320 ky BP), the Holstein or the Mindel-Riss interglacial stage (*ca.* 320-270 BP ky BP) and the Riss interglacial (*ca.* 270-120 ky BP). The Upper Pleistocene would embrace the Eemian and the remaining part of the Riss-Würm interglacial episode (*ca.*120-80 ky BP), and the last glacial period, known as Würm (between *ca.* 80 ky BP and *ca.* 10 ky BP). The Figure A5 shows the chronostratigraphic assignment that is being proposed.

A4 Methodology

A4.1 PRECEDENTS

There were significant climate changes in the Iberian Peninsula 3.2 million years ago. These changes gave rise to a decrease in the summer precipitation and a spreading of the Mediterranean climate (Blanco Castro *et al*, 1998). These processes reached their highest intensity 2.3 million years ago, the steppe species becoming relevant, among which the herbaceous (*Artemisia* and Chenopodiaceae) along with a Cupressaceae vegetation and *Ephedra* predominated. A vegetation that reminds the tundra vegetation (Eriaceae, Graminaceae, Cyperaceae, etc.) of the first glaciations in north Europe was also spread out.

The Quaternary climate fluctuations that resulted in from the successive glacial-interglacial phases have shown different effects in the north of Europe from those in the Mediterranean Basin. At Mediterranean latitudes, wetter periods and arid phases have controlled the growing of deciduous and/or perennial forests and the steppe species, respectively.

The Mediterranean pines and the *Juniperus* and *Ephedra* species predominated in the typical steppe vegetation during the driest moments; and during the wetter phases, the Mediterranean forests become significant, being the *Quercus* species the most important ones. Due to the Quaternary glacial processes, many of the established subtropical species disappeared or were adapting themselves to drier conditions, in such a way that specific Mediterranean species were developing. Migrations southern-ward and/or towards lower altitude areas of these Mediterranean or subtropical species have taken place also during colder times, forming refuges where some species could remain preserved under more extreme climates, and new reversed migratory movements could be produced during the milder climate periods.

During the last glacial period (Würm), these processes acquired peak intensity and it was around 18000 years BP when the coldest and driest conditions prevailed. Consequently, when almost all mid-latitude vegetation disappeared, in the Iberian Peninsula there were extensive steppe zones where *Artemisia* and Chenopodiaceae, along with pine species dominated, whereas the leafy ones were located in coastal areas or in low altitudes that have a less extreme climate (Pons and Reille, 1988), and where the refuge areas acquired an important relevance. These refuge areas

influenced in a remarkable way the distribution of forests as the climate smoothed out in the Tardiglacial period.

The last 10000 years, (Holocene), has been characterised by the recovering of the temperate forests in Europe, the climate optimum being reached 5300-8000 years ago, depending on the zones with the *Quercus* genus, mainly deciduous, predominating in the Iberian Peninsula (Blanco Castro *et al*., 1998).

So, the last glaciation is the main decisive element of the structure, composition and dynamics of the current Iberian forests. The bioclimate regions of the Iberian Peninsula have been basically shaped to their current state in the Tardiglacial.

A4.2 MEDITERRANEAN CLIMATE ANALOGUES ACCORDING TO THE VEGETAL ASSOCIATIONS

An extensive interpretation about the general climatic significance of the vegetal associations in the Mediterranean pollen records is very accepted, although some discrepancies exist too. So, is currently admitted that the balance between both relatives *Quercus* and *Artemisia* pollen amounts is very representative, so that high *Quercus* percentages indicate warm and more or less humid conditions depending on the *Quercus* species, with an interglacial character, while glacial phases are reflected by high content of *Artemisia* (Florschütz et al., 1964, 1971; Wijmstra, 1969; Pons and Reille, 1988; Guiot et al., 1989; Burjachs, 1994; Cheddadi and Rossignol-Strick, 1995; Rossignol-Strick and Paterne, 1999; etc.).

In this way, Rossignol-Strick and Paterne (1999) differentiated several types of vegetal associations in the pollen records of different sapropel levels in the Ionic Sea, which reflect distinct Mediterranean climate types. A vegetal association with high amounts of deciduous *Quercus*, more than 30%, and little amounts of *Artemisia*, less than 10%, reflects typical interglacial conditions. Under these conditions a deciduous forest, mainly constrained to oak, in most of the zones between 300m and 1500m of altitude and a little presence of herbaceous, would be developed. At the present time, in the northern boundary zones of the eastern Mediterranean region the deciduous forests is in the middle heights of humid and subhumid altitudinal zones where the annual precipitation is between 600mm and 1200mm (Rossignol-Strick and Paterne, 1999). The other extreme would be represented by a second group, that is characterised by more than 60% of *Artemisia* and less than 15-20% of *Quercus*, and reflects glacial conditions, with semidesertic characteristics marked by steppe species which implies humidity deficit. In this conditions, deciduous forest would be confined to refuge areas in isolated zones of middle elevation (Breug, 1975). At the present time there is a good analogue of semidesertic conditions dominated by *Artemisia* in the Arabic-Syrian desert as well as in the central Asia, within an extensive zone along the 50º north latitude between the desert and the northern hillside bases of mountain ranges (Pamir, Tian-Shan) and the herbaceous steppes of south of Siberia (Walter, 1974).

The climate message of the pollen taxa is mainly expressed in available humidity terms, that is the restricted factor for the Mediterranean region, where the typical temperate climate deciduous trees are eliminated in the low altitudes because the summer drought, not by the high temperatures. The arboreal vegetation is limited in this region because two seasonal conditions, the deciduous temperate-warm and the Mediterranean sclerophyllous (Rossignol-Strick and Paterne, 1999). The extensive periods of winter freeze eliminate the Mediterranean trees as well as the deciduous temperate forests do not tolerate the summer drought. The warm temperate deciduous trees such as deciduous oak (*Quercus robur, Quercus pubescens*) need an annual precipitation above 650mm, without effective drought along more than three months (Glearson and Cronquist, 1964). Inside the Mediterranean environment the temperature is not probably so low for to limit the deciduous forest, alpine elevations excluded, the same as this forest is

satisfactorily adapted to higher temperatures than those present-day in middle and low elevations, such as in the earlier Holocene, when the humidity was most abundant and regular than currently. Only this humidity characteristic successfully competes with the Mediterranean drought tolerant vegetation. Therefore, seasonality is the Mediterranean ecosystems key on an altitude basis. On the contrary, the herbaceous vegetation of sage-brush, with *Artemisia* predominant, can tolerate 200mm of annual precipitation, being currently well represented in the south-west and in the central semideserts of Asia, what demonstrates that it accepts continental conditions with marked seasonal contrasts and very cold winter (Zohary, 1973; Walter, 1974).

A4.3 KÖPPEN CLIMATIC CLASSIFICATION AND RIVAS-MARTÍNEZ BIOCLIMATIC CLASSIFICATION

The basis of the climatic and bioclimatic classification according to Köppen and Rivas-Martínez are briefly described because we have taken into account both methodologies for Padul palaeoclimatic characterisation. These methodologies were followed in UE BIOCLIM project and in DGR PA ENRESA 2000 and 2003, respectively.

Köppen defined the different zones of the Earth in function of the most important climatic elements for the vegetation, because he classified the climate according to the k index that relates the annual precipitation, in cm, with the mean annual temperature. He considers the annual precipitation regime because k is determined as a function of the greatest precipitation period as winter-, summer-, or evenly distributed precipitation regime. Also the different varieties so established take into account the different thermic and pluviometric regimes. Köppen proposes five great climate groups: A, B, C, D and E.

A is the tropical rainy climate, whose average monthly temperature is always above 18ºC, and the annual precipitation is above the annual evaporation. In the B group the annual evaporation surpasses the annual precipitation, therefore there is not water excess. C climates are humid and temperate, and winter and summer seasons are clearly marked; the coldest month temperature is between 18ºC and -3ºC, at least a month being above 10ºC. D group is the boreal climate, whose coldest month temperature is below –3ºC and the hottest month temperature is above 10ºC, that is the north boundary forest growth isotherm. Finally, E climates are those polar and snowy groups.

A, C, D and E types are defined by the average temperatures, while the B type is defined by the balance between evaporation and precipitation. A, C and D groups have temperature and precipitation enough for the forest development. A second letter is used to define different subgroups inside each climate groups, so that twelve great climate class are obtained, and in order to specify more climatic variations a third letter to some above mentioned class was added. Following the Köppen terminology, the main climate classes that have taken place in Padul during the characterised period of time are Csa, Csb, BWk and BSk.

The B type dry climate, are characterised by $k<2$. The BW subtype ($k<1$) is the desert climate, arid, whose annual precipitation is below 200mm, and the BS subtype is the steppe climate, that is present in regions between desert and humid (A, C and D) climate zones. There are two main varieties inside the BS subtype ($1<k<2$), BSh or warm steppe and BSk or cold steppe. The first one has an average annual temperature above 18ºC, and the second one presents an average annual temperature lower than 18ºC. The C type warm temperate climate, has a k index greater than 2 ($k>2$) and a mean temperature of the coldest moth between -3ºC and 18ºC. The Cs subtype, tempered with dry summer, is known such as Mediterranean climate in general. The precipitation of the driest summer month is below 30mm and more than 70% of annual precipitation is recorded in the six coldest months. The Csa variety is rainy temperate with dry and warm summer, and the mean temperature of the hottest month is above 22ºC. Padul area belongs nowadays to this climatic variety, although it is closer to a BSk type zone. In Csb

variety, rainy temperate with dry and warm summer, the mean temperature of the hottest month is below 22 ºC and there are 4 or more months with a mean temperature above 10ºC.

In the Iberian Peninsula two biogeographic regions are distinguished and clearly differentiated the Eurosiberian and the Mediterranean ones. The first one is known as Green and the second one is the Brown. The current limit between both regions is located in the Pirineos and Cantabrica mountain ranges southern slopes, to the north, and between the most continental oceanic and southern Galicia and northern Portugal, to the west (Mesón and Montoya, 1993). In order to separate both regions, the most important climatic factor is the ombroclime because in the Mediterranean area, separately from the mean annual precipitation, a typical period of summer aridity or drought superior to two months always exists, which is absent in the Eurosiberian region. A month is considered as arid when its precipitation, in mm, is numerically inferior to the double of monthly mean temperature, expressed in ºC (P<2T). In order to configure the natural communities of vegetation, the two main climatic elements are precipitation and temperature. Rivas-Martínez (1987) has established a series of bioclimatic units for the Iberian Peninsula in function of those parameters. So, according to the thermo- and ombro-climatic characteristics several bioclimatic levels or vegetation levels have been defined, that is to say, each one of the types or thermoclimatic spaces settled down in function of the latitude or the altitude (Mesón and Montoya, 1993). Inside each bioclimatic level, depending on the amount of precipitation, Rivas-Martínez distinguishes different vegetation types that approximately correspond with the others ombroclimatic units. However, the vegetation levels (Emberger, 1968) depend, besides the climate, on edaphic and orographic conditions as well as on the luminous intensity and duration of the day.

In the Mediterranean biogeographic region of the Iberian Peninsula Rivas-Martínez has defined five out of the six existent bioclimatic levels. The levels are crioromediterranean, oromediterranean, supramediterranean, mesomediterranean and, finally, thermomediterranean, occupying more than three fourth parts of the Iberian surface. The sixth, known as inframediterranean, does not exist in the peninsular territory, being limited to the south-western Morocco. The crioromediterranean level is only present at the highest levels of mountain ranges; the oromediterranean level has an altitude limit that varies depending on the solar exposition, latitude and Atlantic climatic influence, but its lower limit is between 1600m and 2000m of altitude. The supramediterranean bioclimatic level is very extended in the peninsular territory, and its winters are rigorous and long lasting. The most extended bioclimatic level is the mesomediterranean, mainly in the southern middle part, although it reaches enough of northern latitudes as well. The thermomediterranean bioclimatic level occupies more or less the eastern coastal zone. Climatic characteristics of these levels and their representative values (Rivas-Martínez, 1987) are summarised in the Table A1. T is the mean annual temperatures (ºC); m and M are the mean of the minimum and maximum temperature of the coldest month (ºC), respectively; H is the period of months when statistically speaking a freeze is possible (I, January..., XII, December).

Table A1. Representative values of Mediterranean bioclimatic levels.

Bioclimatic Level	T	m	M	It	H
Crioromediterranean	< 4	-7	< 0	< -30	I-XII
Oromediterranean	4-8	-7 to -4	0-2	-30 to 60	I-XII
Supramediterranean	8-13	-4 to -1	2-9	60-210	IX-VI
Mesomediterranean	13-17	-1 to 4	9-14	210-350	X-IV
Thermomediterranean	17-19	4-10	14-18	350-470	XII-II

The annual mean precipitation ranges that define the different ombroclime types in the Mediterranean peninsular region are very variable, from 200mm or less to more than 1600mm. The ombroclime types established by Rivas-Martínez with their value intervals in mm are arid (P<200), semiarid (200-350), dry (350-600), subhumid (600-1000), humid (1000-16000) and hyperhumid (P>1600). The bioclimatic levels can be further subdivided as sublevels or bioclimatic horizons in turn.

The Padul peat bog is included inside the Mediterranean region and is located 20km south of Granada City, in the southern Iberian Peninsula; with an altitude of 720m, it has a Mediterranean climate with continental influence. Although Padul area can be considered in practice as a mesomediterranean bioclimatic level with dry ombroclime characteristics, the remaining bioclimatic level types are very close to it, being represented all of them in a reduced extension. So, there are present from the crioromediterranean, in Sierra Nevada, to the thermomediterranean level in the Izbor valley, close to Padul town.

A4.4 METHODOLOGY

Three main aspects must be considered in order to transform the pollen percentages on vegetation terms (Ruiz Zapata, 2000). These aspects are the identification of the pollen spectra of the current vegetal formations, mainly the most significant species percentages to determine the influence of local or regional vegetal formations in order to explain the presence of non local elements, and to apply multivariate analysis for the purpose of detecting the most representative elements and associations for each spectrum that would be relevant in order to establish the palaeoenvironmental properties as well as the significant events and episodes along the pollen diagram. However we do not have any information about natural current Padul pollen rain and, in addition, the analysed records do not have in general the varied information necessary to carry out this kind of analysis or to apply some of the *ad hoc* codes for this purpose.

In the Padul meteorological station, located at 760m of altitude, with a 50 year (1952-2002 period, INM) record series, the representative climatic values are 16.1ºC of mean annual temperature, being 8.2ºC the mean temperature of the coldest month and 25.5ºC for the hottest month, as well as 409mm of mean annual precipitation. That is to say mesomediterranean and dry characteristics according to Rivas-Martínez classification. On the other hand, in spite of the remaining levels being very close to it, Padul peat bog site belongs to the Csa Köppen climate class at the present time, but with almost steppe characteristics.

In spite of the great vegetal associations diversity in the very near areas, which probably has enough influence in the pollen rain, each genus and species registered in the diagram have been taken into account by the way of the current ombrothermic conditions of the different vegetation series that appear in the different Iberian Peninsula bioclimatic levels. So, the first thing we have taken into account is the typical thermoclime and ombroclime values as well as the bioclimatic characterisation of the series of vegetation following to Rivas-Martínez, likewise the distinct Mediterranean climate analogues according to the vegetal associations.

The starting point, apart from the current well-known climate conditions, has been the inferred conditions from the sample number 1 which has an age of *ca.* 4980 ky BP. Taking into account that both the precipitation and the temperature values are coming down since the Holocene Thermal Optimum *ca.* 6 ky BP (samples 2 to 4, between 0.43m and 1.93m depth for the Florschütz et al. borehole), and comparing them with current ombrothermic values, this sample presents the following percentages: 40% of *Quercus*, 25% of *Pinus*, 2% of Erica, 2% of *Ilex*, 2% of *Ephedra* and about 8% of steppe elements. The ombrothermic significance of this vegetal composition has been taken to be about 17-18ºC of average annual temperature and 500-600mm of average annual precipitation.

In order to establish the precipitation and temperature values for each defined stage, and after considering the ombrothermic conditions for each vegetal genus and species reflected in the pollen diagrams, we have taken into account each vegetal association altogether for each sample in the records. For these purposes a hierarchy of the most representative vegetal elements has been considered, giving values to the humidity or dryness as well as to the warmth or coldness conditions it implies. Furthermore, the available genus or species percentages in representative samples for well-defined and characterised periods, such as the Eemian interglacial episode and others, have been taken into account. For example, Ericaceae implies varied temperature conditions but humid terms in general. So, in order to better estimate the precipitation, the association Ericacea + *Ilex* + *deciduous Quercus* next to the steppe (*Artemisia*, Chenopodiaceae, *Ephedra*) scarcity has been considered as representative of the most humid conditions in the whole analysed record. Less humid conditions would be indicated by Erica + *Quercus* with more steppe percentages than the above-mentioned association. Thereby, and considering the amounts of the different species for each sample, a humidity priority or preference has been established that, in descending order, begins by Ericaceae and continues by *Ilex* and *Quercus.* In this same way, the higher abundance of steppe elements would imply the most arid conditions. It is necessary to emphasise again that the pollen records are not very rich in species, lacking some specific elements, but nevertheless the important species described and cited by the authors have been taken into account. In order to estimate thermal conditions, the more or less thermophyllous elements have been considered as well as the relative abundance of arboreal pollen or steppe elements. Typically thermophyllous elements in the studied records are Oleaceae and some *Quercus* species, although the latter is a genus with quite wide thermal allowance, even temperate (deciduous *Quercus*). It is important to emphasise the marked sclerophyllous character of most of the representative vegetal species that appear in the analysed pollen records, even though some of them are humidity indicators, what reveals typical Mediterranean climatic conditions along the entire characterised period, with a marked dry summer, less humid than the remaining seasons, with independence of the mean annual temperature and precipitation values.

So, the ombrothemic values for each sample have been estimated and the corresponding Köppen climate class as well as the bioclimatic level according Rivas-Martínez, have been defined, taking on the sclerophyllous character of the dominant vegetation in addition to the fact that precipitation and temperature annual regimes are similar to those the present time. In this sense, it is well known that in Padul annual precipitation is mainly recorded between October and May, being therefore much humid the winter season than the summer season, typically dry and warm (second letter ‘s’ in the Köppen climate class ‘C’). To better establish the climate class according to Köppen, a BW type has been considered when the annual precipitation is 200mm or less, and a BS climate class when the annual precipitation value is between 200mm and 400mm. In the same way, BSk implies an annual temperature below 18ºC. Taking on the same proportional differences between the average monthly temperature and the average annual temperature, a climate class of ‘C’ type has been assigned. Therefore, the current Csa Köppen climate class in Padul, which is theoretically defined by a hottest month temperature above 22ºC, would define the conditions for an average annual temperature of 13ºC. On the other hand, the Csb type, where the hottest month temperature is below 22ºC, would define an average annual temperature below 13ºC.

Finally, the assignment of the bioclimatic level according to Rivas-Martínez is direct when the ombrothermic values have been estimated.

The estimated temperature and precipitation values, for the studied interval of time, according to the followed methodology as well as the assigned climatic class and bioclimatic levels are shown in Tables A2 and A3. Figures A6 and A7 illustrate the evolution of the ombrothermic values from *ca.* 500 ky BP at the Padul peat bog area.

A5 General Palaeoclimate Conclusions According to the Pollen Records

Some general conclusions about the palaeo-climate of the southern part of the Iberian Peninsula from *ca.* 500 ky BP could be established according to the task carried out.

According to the studied pollen records, the noteworthy climate differences between the last glacial cycle and the remaining characterised period of time have already been mentioned. So, the steppe species percentages in the diagrams for time periods previous to the Eemian interglacial period are higher than in the last glacial cycle, as well as the variability of the relative amounts of the key vegetal species is lesser than in this last glacial cycle.

These general characteristics apparently indicate less intense climatic oscillations before the Eemian, which are clearly reflected by the main vegetal associations during the Middle Pleistocene than during the Upper Pleistocene and the Holocene.

Pinus reaches values above 70% during a part of the Upper Pleistocene, but only overcomes 50% percentages occasionally during the Middle Pleistocene. In general, a contrary tendency could be appreciated in the sense that a great presence of *Pinus* practically corresponds with few *Quercus* amounts in the entire record. This is very clear in the Middle Pleistocene, where maximum values of *Pinus* are coincident with minimum or zero amounts of *Quercus*, possibly reflecting the warmer and occasionally the drier episodes recorded in this time, such as it happens in the central zone of the Iberian Peninsula (Ruiz Zapata, 2000). At this point is necessary to emphasise that there is not possible to distinguish the different *Pinus* species in a pollen record. *Quercus* genus, that generally reflects warm or temperate and more or less humid climate conditions, reaches the higher percentages along the Holocene period, in which the majority of its values are above 50%, even next to 60% occasionally. *Quercus* presence is more notable in the Upper Pleistocene than in the Middle Pleistocene, and its recovery starting from the beginning of the Eemian interglacial, in general, is clearly appreciated in the pollen diagram. At the beginning of the Eemian, *Quercus* reaches 30%, decreasing and oscillating later on, and reaches even a 40% just before the Last Glacial Maximum. During the most arid and colder stages its presence is very scarce or null, but it is notably increased in the interglacial, and even during interstadial, periods although in these last cases not reflecting excessive humidity. For the recorded Middle and Upper Pleistocene, with in general quite arid climatic conditions of Mediterranean type, the more humid episodes are reflected in the pollen diagrams through relatively hygrophyllous species, such as Ericaceae and *Ilex*, and the presence of *Quercus* confirming these situations. That is to say, typical sclerophyllous elements, as in the whole analysed pollen records, indicate a Mediterranean climate, more or less humid or arid, but with a marked dry season independently of the annual amount of precipitation. During the colder episodes open landscapes predominate, where the steppe species development is very important, and with an arboreal impoverishment with a clear domain of herbaceous and bush elements. There is a progressive arboreal recovery during the less severe phases, with more or less sporadic presence of temperate elements, and the interglacial stages are characterised by temperature and precipitation increases, which are reflected by the forest expansion, specially by those temperate and Mediterranean species.

A5.1 SYNTHESIS OF THE OMBROTHERMIC CHARACTERISTICS FROM CA. 500 KY BP

The resulting tendencies for Padul diagrams are basically reinforced by different studies and diverse records (Figure A8). Among them, the temperature global curve from $\delta^{18}O$ analysis

(Shackleton, 1995), and the surface temperature of North Atlantic as well as the western European arboreal pollen (IPCC, 2001).

So, at the Padul area during the recorded Middle Pleistocene (from *ca.*500 ky BP to *ca.* 120 ky BP) the ombrothermic conditions were drier and colder than those were at the present time, with in general more aridity. The predominant Köppen climate class was BSk or temperate or cold steppe, with its specific precipitation and temperature oscillations. A climatic amelioration took clearly place during certain episodes, the predominant climate class then being strictly Mediterranean such as Köppen Csa class mainly. The Csb climate class could be taken as a transitory stage between the above two mentioned before.

The oldest recorded period, that is to say, the advanced Mindel glacial episode, is characterised by precipitation values below 400mm, between 200mm and 350mm approximately, and with temperate or cold temperatures, from 3ºC to occasional maximums of 13ºC, in function of the different climatic pulsations that happen during this phase. The dominant climate conditions were arid and cold in general, the same as during another glacial episodes. In this sense, the Riss I and the Riss II glacial stages would have had an ombrothermic character very similar to the recorded Mindel. In the climate amelioration period known as Holstein interglacial, the temperature and the precipitation probably were such as these at the present time, with a dominant dry ombroclime, according to Rivas-Martínez, between 400mm and almost 550mm of annual precipitation, but with a little more temperate annual temperatures. Finally, inside the Middle Pleistocene the Riss I-Riss II interstadial episode had specific ombrothermic characters too, with a subhumid ombroclime, between 500mm and 800mm as more representative values, a little more humid and temperate than the Holstein phase, and with the Csb Köppen climate class more extended than in the remaining Middle Pleistocene.

The arid and cool climatic trend broke off at the beginning of the Upper Pleistocene that was initiated with the Eemian interglacial period. This period of time is characterised by specific and typical ombrothermic characteristics warmer and more humid than those current conditions. For this episode we have considered a mean annual temperature between 16ºC and 19ºC, and a mean annual precipitation from 650mm to more than 1000mm, subhumid to humid according to Rivas-Martínez. In general, this was the most humid recorded time, in function of the climate significance of the vegetal associations present in the pollen diagrams. After the Eemian, but inside the Riss/Würm interglacial time too, there were oscillating ombrothermic episodes, drier or less humid than during the Eemian. So, we have assumed a mean annual precipitation below 1000mm for the most humid stages (St. Germain Ib, St. Germain Ic and St. Germain II) and an annual temperature a little below than that of the Eemien. There were sporadic drier and colder episodes inside this interglacial time, such as the St. Germain Ia and the Mélisey II, for which we have assumed a thermoclime between 8ºC and 13ºC and a dry or semiarid ombroclime according to Rivas-Martínez. After this time, during the Würm glacial period, the temperature and the precipitation were almost continuously coming down, with some oscillations, until the Final Würm, in which colder temperatures below 4ºC and a minimum annual precipitation probably were reached. For this period the dominant Köppen climate class were either BSk or BWk, mainly. With the Oldest Dryas a slight climatic amelioration began, and the temperature and precipitation were going up during this period as well as inside the Bölling-Alleröd interglacial episode, even reaching 13º to 17ºC and 600mm to 1000mm values, respectively. The Upper Pleistocene finished with a rapid climatic deterioration, known as the Younger Dryas period, as arid and as cold as during the Oldest Dryas episode.

The Holocene time is climatically characterised by a general amelioration, with high temperature and precipitation and, therefore, by a marked forest recovery. The ombrothermic conditions oscillated between 13ºC and 19ºC for temperature and between more than 350mm and 1000mm for precipitation. The best conditions took place during the Holocene Thermal Optimum, with an annual mean temperature of 17ºC to 19ºC and a mean annual precipitation between 600mm and

1000mm. From that time, both the annuals mean temperature and precipitation values have little by little coming down toward the current records.

Tables A1 and A3 as well as Figures A6 and A7 show these ombrothermic characteristics.

A6 Bibliography

Adams, J. (compiler). Europe during the last 150,000 years. Oak Ridge National Laboratory, Oak Ridge,TN37831,USA.http://www.esd.ornl.gov/projects/QEN/NERCEUROPE.HTML.

Allué Andrade, J.L., 1990. Atlas fitoclimático de España. Taxonomías. Ministerio de Agricultura, Pesca y Alimentación. Instituto Nacional de Investigaciones Agrarias. INIA. Madrid.

BIOCLIM Project, 2001. WP1. Consolidation of the Needs of the European Waste Management Agencies and the Regulator of the Consortium. Draft Deliverable D2: Site-specific and palaeoenvironmental data.

BIOCLIM Project, 2002. WP2. Simulation of the future evolution of the biosphere system using the hierarchical strategy. Draft Deliverable D3: Global climatic features over the next million years and recommendation for specific situations to be considered.

Blanco Castro, E. *et al.*, 1998. Los bosques ibéricos. Una interpretación geobotánica. Editorial Planeta, S.A.. Barcelona.

Burjachs, F., 1994: Palynology of the Upper Pleistocene and Holocene of the North-East Iberian Peninsula: Pla de L'Estany (Catalonia). Historical Biology 9 (17-33).

ENRESA, 1993. Síntesis del Medio Ambiente en España durante los dos últimos millones de años. Contrato CEC F12W-CT91-0075. Informe temático.

Florschütz, F., Menéndez Amor, J, Wijmstra, T.A., 1971. Palinology of a thick Quaternary succession in southern Spain. Palaeogeography, Palaeoclimatology, Palaeoecology 10, 233-264.

Garcin, M., 1994. El Oeste de Europa y la Península Ibérica desde hace 120.000 años hasta el presente. Isostasia glaciar, Paleogeografías y Paleotemperaturas. ENRESA, Publicación Técnica Número 05/94.

Goodess, C. M., Palutikof, J. P. and Davies, T. D., 1992. The nature and Causes of Climate Change: Assessing Long-Term Future. Belhaven Press, London.

Guiot, J., Pons, A., Beaulieu, J.-L., Reille, M., 1989. A 140,000 year continental climate reconstruction from two European pollen records. Nature 338 (309-313).

Horowitz, A., 1989. Continuous pollen diagrams from the last 3.5 my. from Israel: vegetation, climate and correlation with the oxygen isotope record. Palaeogeography, Palaeoclimatology, Palaeoecology 72, 1-2 (63-78).

IPCC TAR, 2001. IPCC 2001, Climate Change 2001: The scientific basis. Cambridge University Press. Houghton *et al*. (Eds). http://www.grida.no/climate/ipcc_tarwg1/.

Lomba, L., 2002. Bioclimatic characterization of the central Spain area, Padul and Cúllar-Baza (Granada) zones. CIEMAT/DIAE/551/55160/10/02. Madrid.

Lomba, L. and Recreo, F., 2002. Condiciones ombrotérmicas y ambientales de las principales especies vegetales de la Península Ibérica. CIEMAT/DIAE/55120/07/02. Madrid.

Lomba, L. and Recreo, F., 2004. Proyecto PADAMOT. Modelo Paleoclimático de la zona de Padul (Granada) desde el Pleistoceno Medio hasta el Eemiense deducido del registro polínico. Condiciones ambientales y ombrotérmicas regionales. CIEMAT/DIAE/54650/2/04.

Lomba, L., Ruiz Rivas, C. y Recreo, F., 2003. Actividad: Escenarios de Evolución Ambiental. AGP ENRESA 2003-Arcilla. CIEMAT/DIAE/55120/07/03.

Lomba, L. and Ruiz, C., 2003. Proyecto PADAMOT. Evaluación de la Recarga en el pasado en el entorno de la Mina Ratones (104 ka BP). CIEMAT/DIAE/551/55170/06/03.

Magny, M., Guiot, J. and Schoellammer, P., 2001. Quantitative reconstruction of Younger Dryas to Mid-Holocene Paleoclimates at Le Locle, Swiss Jura, Using Pollen and Lake-Level Data. Quaternary Research 56 (170-180).

Martín Arroyo, T., Ruiz Zapata, M.B. and Pérez-González, A. Paleoambiente en el valle del Río Tajo durante el Pleistoceno Superior: primeros datos polínicos. En Ramil-Rego, P. *et al.*: Biogeografía Pleistocena-Holocena de la Península Ibérica.

Martín Arroyo, T., Ruiz Zapata, M.B., Pérez-González, A., Valdeolmillos, A., Dorado Valiño, M., Benito, G. y Gil García, M.J., 1999. Paleoclima y Paleoambiente durante el Pleistoceno Superior y el Tardiglaciar en la región central peninsular. Avances en el estudio del Cuaternario español. L. Pallí Buxó y C. Roqué Pau (editores). Pp 317-324. ISBN 84-95138-56-5.

Martín Arroyo, T., Ruiz Zapata, M.B., Pérez-González, A., Dorado Valiño, M., Valdeolmillos Rodríguez, A., y Gil García, M.J., 2000. Registro paleoclimático del Pleistoceno Medio en el valle del río Tajo. Geotemas 1(4), (259-262).

Menéndez Amor, J., Florschütz, F., 1964. Results of the preliminary palynological investigation of samples from a 50 m boring in southern Spain. Boletín de la Real Sociedad Española de Historia Natural (Geología) 62 (251-255).

Mesón, M. and Montoya, 1993. Selvicultura Mediterránea. Ediciones Mundi-Prensa. ISBN 84-7114-461-1. Madrid

Pons, A., Reille, M., 1988. The Holocene and Upper Pleistocene pollen record from Padul (Granada, Spain): A new study. Palaeogeography, Palaeoclimatology, Palaeoecology 66 (243-263).

Recreo, F. and Lomba, L. Quaternary Climate Stages for South of Spain. BIOCLIM Project. Deliverable D2. Task 3-13.

Recreo, F., Lomba L. y Ruiz C., 2002. Broad narrative descriptions of biosphere system changes in climate transitions. Participación CIEMAT-ENRESA-ETSIMM en el Proyecto BIOCLIM, Deliverable D4. (TA5/10).

Recreo, F. and Ruiz, C., 1997. Consideración del Cambio Medioambiental en la Evaluación de la Seguridad. Escenarios Climáticos a largo plazo en la Península Ibérica. ENRESA, Publicación Técnica Número 01/97.

Rivas-Martínez, S., 1987. Memoria del Mapa de series de vegetación de España. ICONA. Ministerio de Agricultura, Pesca y Alimentación. Madrid.

Rossignol-Strick, M. and Planchais, N., 1989. Climate patterns revealed by pollen and oxygen isotope records of a Tyrrhenian sea core. Nature, 342 (6248), 413-416.

Rossignol-Strick, M. and Paterne, M., 1999. A synthetic pollen record of the eastern Mediterranean sapropels of the last 1 Ma: implications for the time-scale and formation of sapropels. Marine Geology 153 (221-237)

Rudloff, W., 1981. World-Climates, Wissenschftliche Verlagsgesellschaft mbH. Stuttgart.

Ruiz Zapata, M.B., Gil García, M.J., Dorado Valiño, M., Valdeolmillos Rodríguez, A., 1997. Vegetación y paleoambientes en el Sistema Central español. Cuaternario Ibérico, 97: 248-260.

Ruiz Zapata, M.B., 2000. Evolución del ambiente y del clima a través de la Palinología. XIII Simposio de la Asociación de Palinólogos en Lengua Española (A.P.L.E.). Libro de textos completos, pp 35-58. Universidad Politécnica de Cartagena.

Ruiz Zapata, M.B., Pérez-González, A., Dorado Valiño, M., Valdeolmillos Rodríguez, A., de Bustamante Gutiérrez, I. y Gil García, M.J., 2000. Caracterización climática de las etapas áridas del Pleistoceno Superior en la Región Central Peninsular. Geotemas 1(4), (273-278).

Torres, T. *et al.*, 2003. Evolución paleoambiental de la mitad sur de la Península Ibérica. Aplicación a la evaluación del comportamiento de los repositorios de residuos radiactivos. Publicación Técnica de ENRESA 04/2003.

Torres, T. and Pérez González, A., 2003. Cambio climático: nuevas aportaciones en la caracterización paleoambiental de la Península Ibérica. V^{as} Jornadas de I+D de ENRESA, Tarragona. Resúmenes de ponencias. En 'Publicación Técnica de ENRESA 06/2003'.

Torres, T., Ortiz, J.E, Llamas, F.J. and García-Martínez, M.J., 2003. Evolución paleoclimática del sur de la Península Ibérica a partir del registro de la cuenca de Guadix-Baza: un modelo paleoclimático perimediterráneo. V^{as} Jornadas de I+D de ENRESA, Tarragona. Sinopsis de pósteres. En 'Publicación Técnica de ENRESA 07/2003'.

Torres, T. *et al.*, 2004. Pleistocene palaeoenvironmental evolution of southern Iberian Peninsula (in press). PADAMOT project.

Walter, H., 1994. Vegetation of the Earth and Ecological Systems of the Geo-biosphere. Third edition. Springer-Verlag. Berlin, Heidelberg, New York, Tokyo.

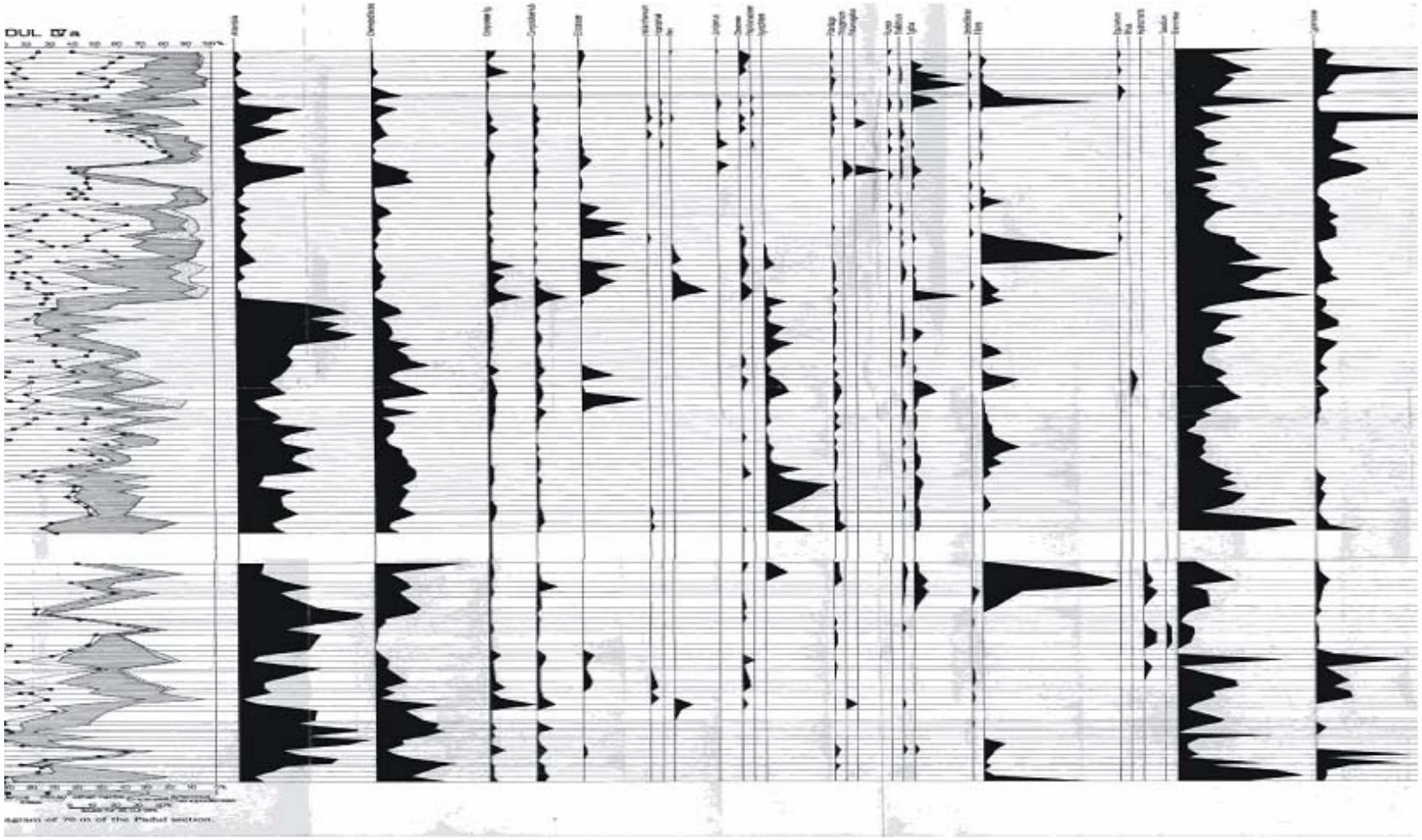

Figure A1. Original pollen diagram from Florschütz, Menéndez Amor and Wijmstra (1971).

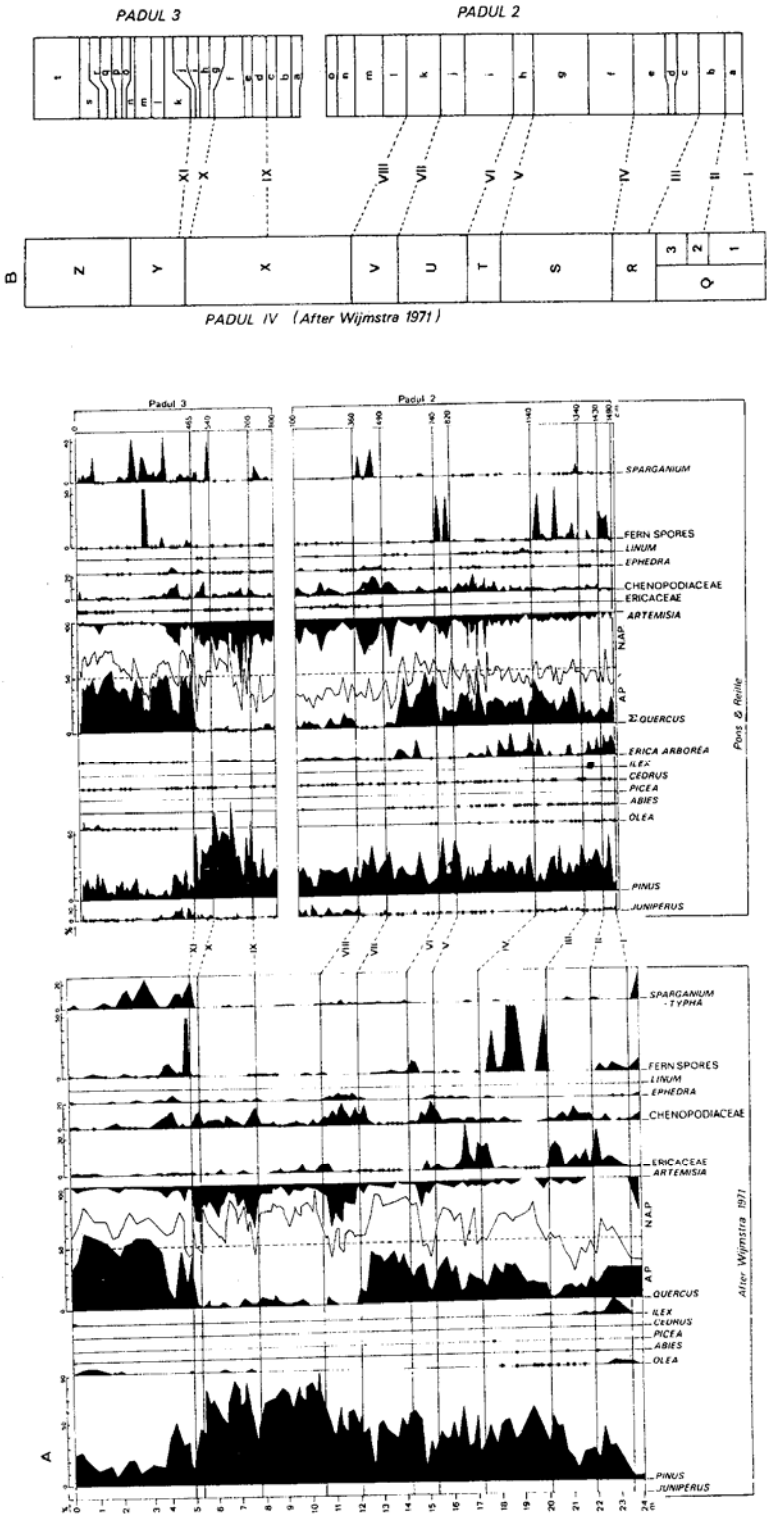

Figure A2. Correlation carried out by Pons and Reille between 'Padul 2', 'Padul 3' and 'Padul IV' pollen records.

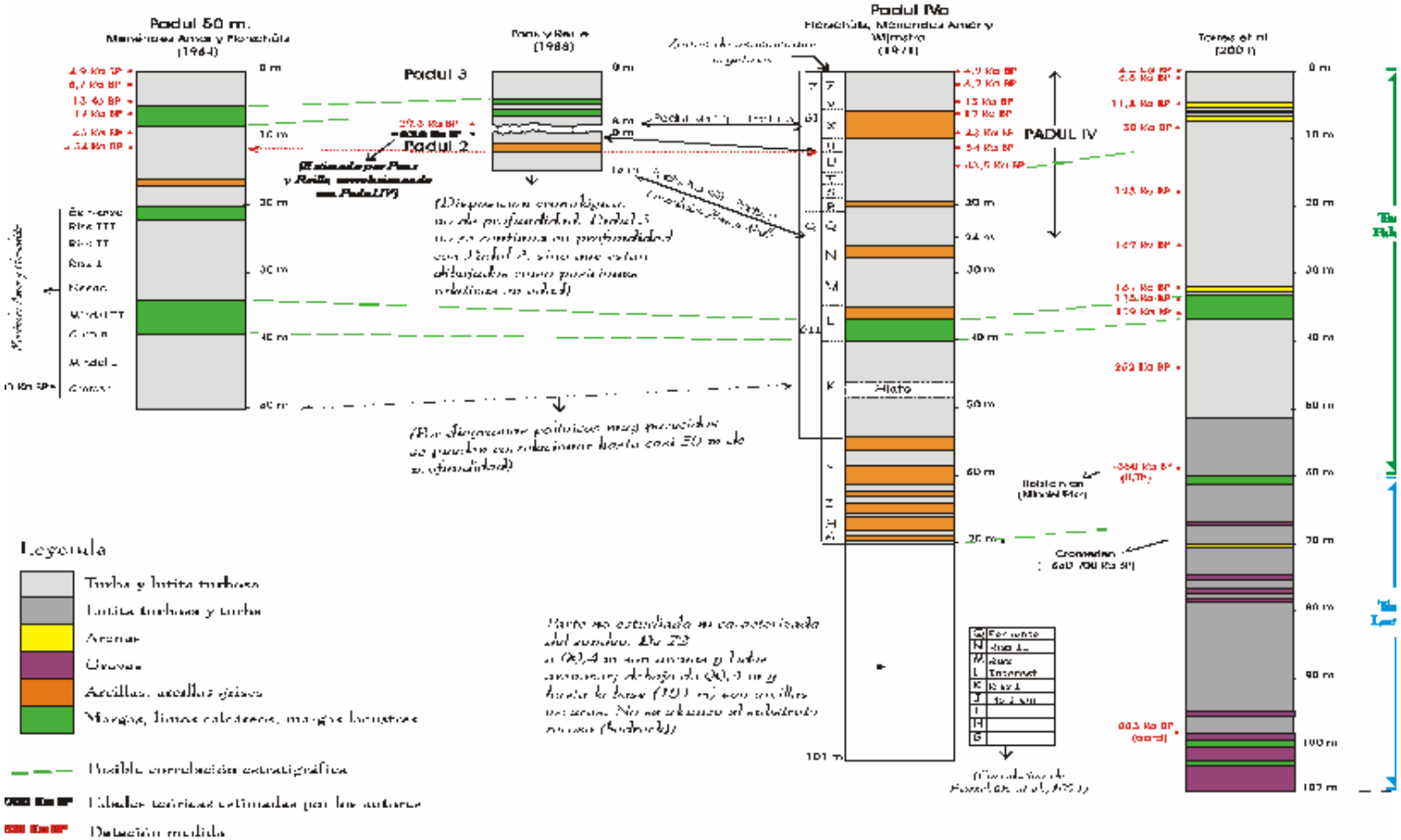

Figure A3. Synthesis of main pollen studies from Padul peat bog with the datations carried out by the different authors. Proposed chronostratigraphic correlations.

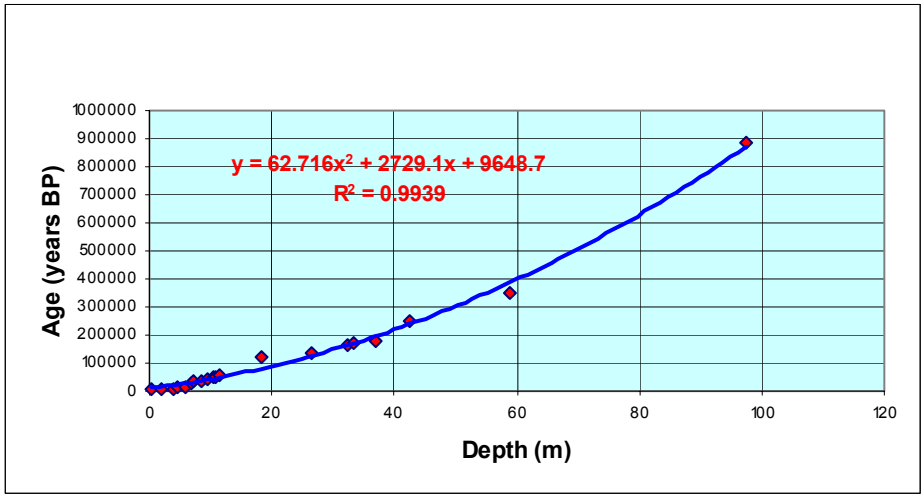

Figure A4. Age-Depth curve calculated from the analysed Padul peat bog records according to the available datations and proposed geochronological correlations between different boreholes.

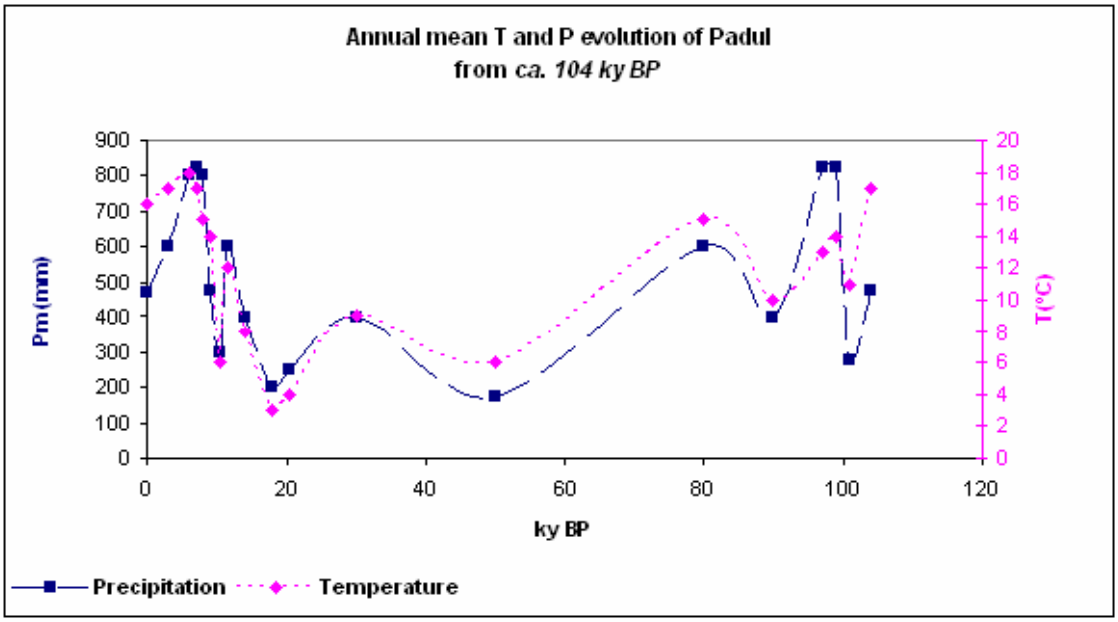

Figure A6. Proposed ombrothermic evolution from *ca.* 104 ky BP according Pons and Reille pollen diagram.

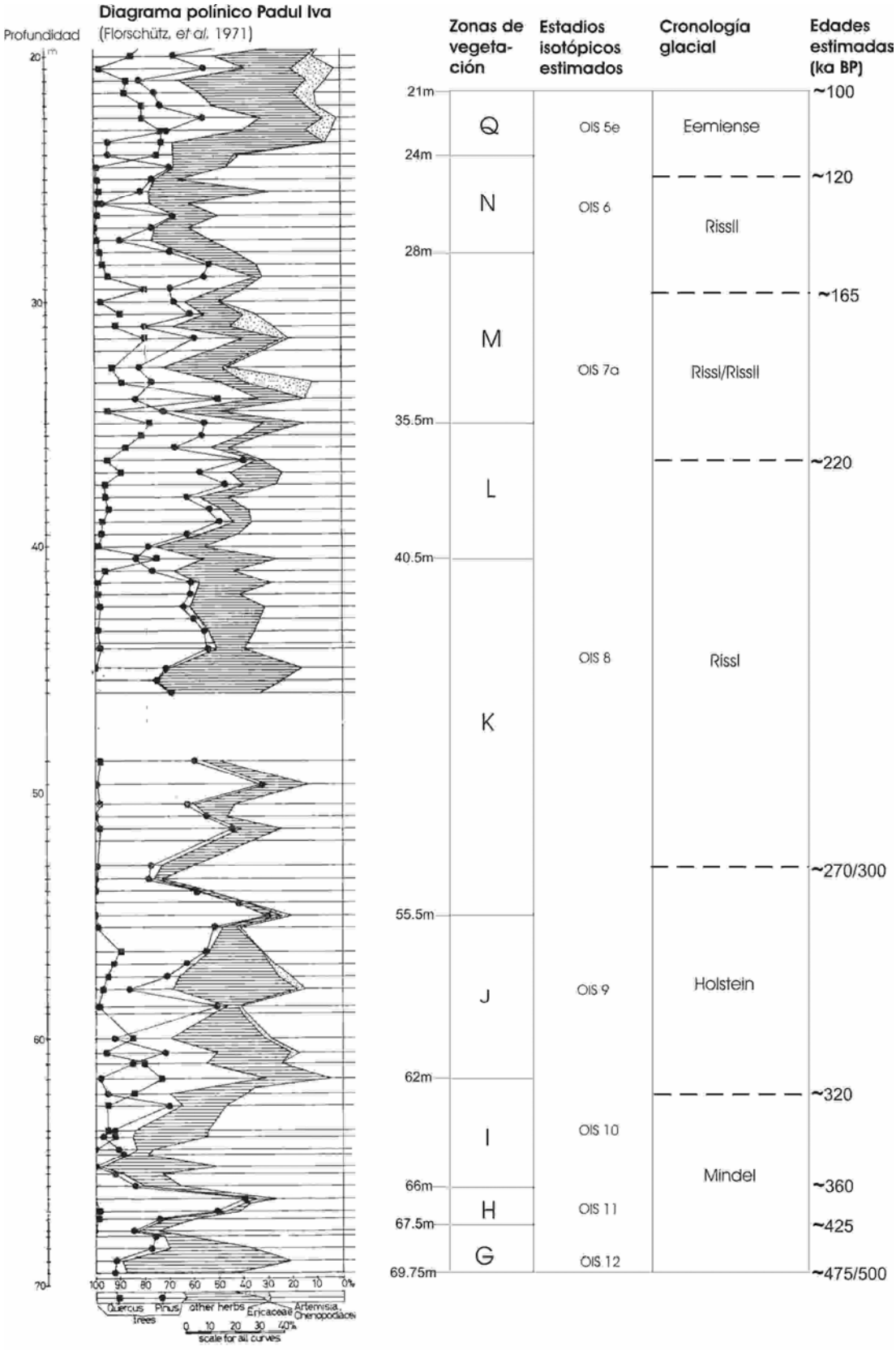

Figure A5. Proposed chronostratigraphic assignment for the lower part of 'Padul IVa' record: vegetal zonation, oxygen isotopic stages (OIS) and Glacial Chronology. Estimated ages.

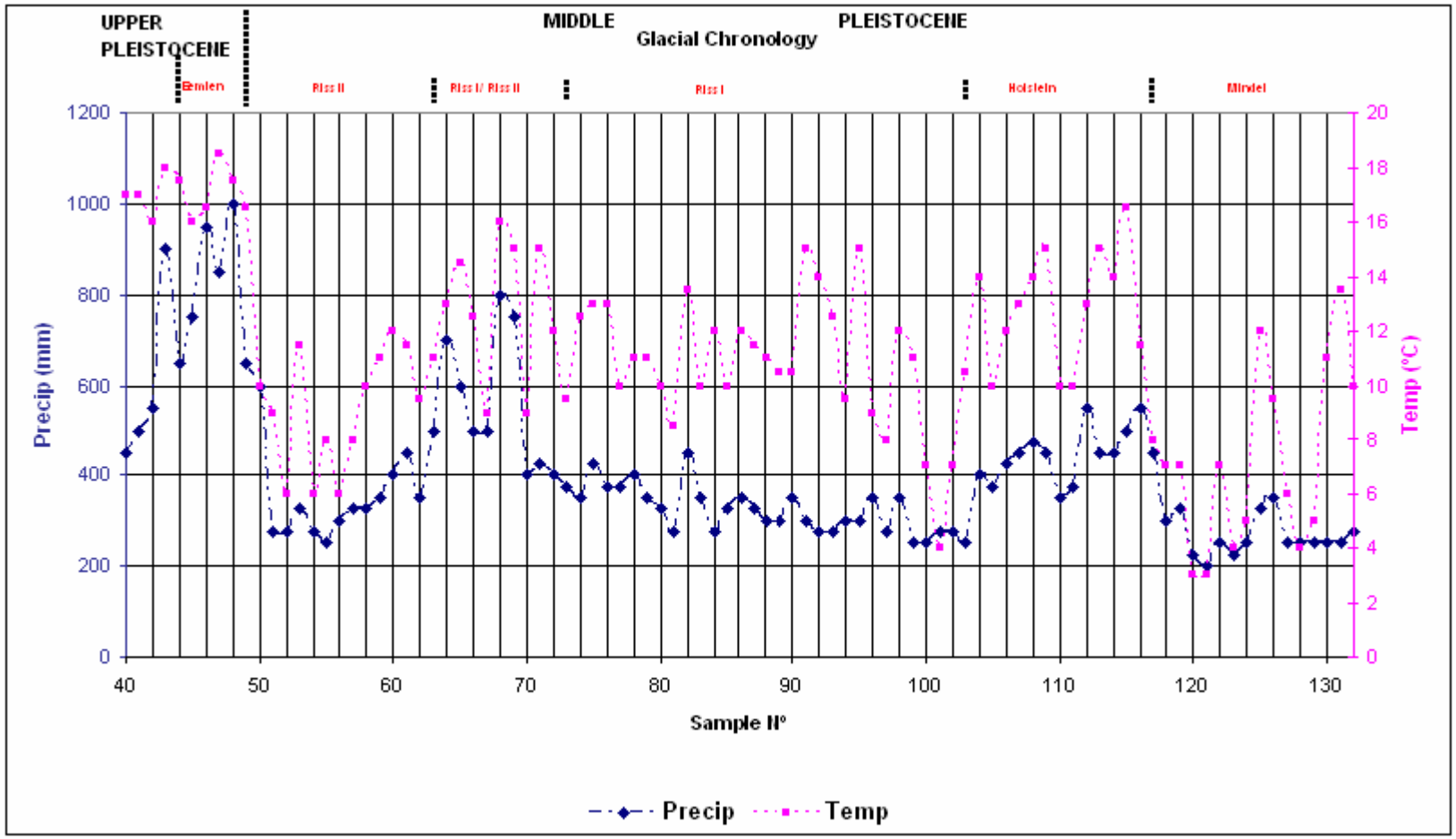

Figure A7. Ombrothermic evolution between *ca.* 500 ky BP and *ca.* 100 ky BP according the lower part samples of 'Padul IVa' pollen record.

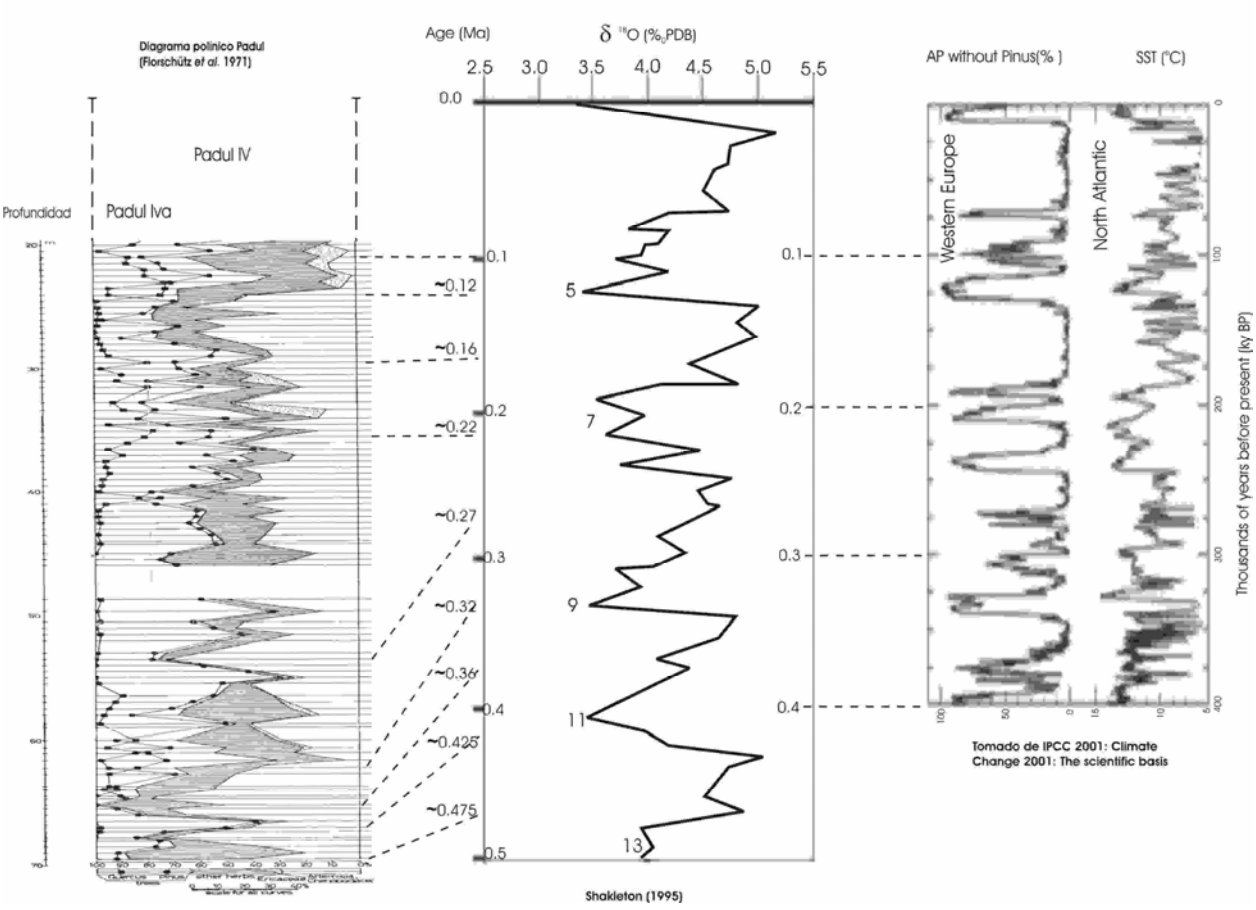

Figure A8. Correspondence between the lower part of the studied 'Padul IVa' pollen record and: temperature global curve from $\delta^{18}O$ (Shackleton, 1995), western Europe arborean pollen (AP) *Pinus* excluded, and the surface temperature of North Atlantic.

Table A2. Palaeoclimatic synthesis of Padul area carried out according to the pollen diagram from Pons and Reille (1988), between *ca.* 104 ky BP and the present time.

Calendar Age (ka BP)	OIS	Name used in this report	Mean annual Temperature Tm (ºC) (1)	Mean annual Precipitation Pm (mm) (2)	Climate Class			Comments
					Köppen	Walter	Rivas Martínez	
0-5.4	1	Subboreal	13-17 to 17-19	<600-1000	Csa	ZB IV	Mesomediterranean to thermomediterranean, dry to subhumid	More uncertainty and climatic variability, with marked pluvial fluctuations and drier tendency (Font Tullot, 1988). Sligtly deterioration of climatic conditions.
5.4-6.3	1	Atlantic	17-19	600-1000	Csa	ZB IV	Thermomediterranean,subhumid	Thermal Optimum. Warm climate and relatively stable period (Zubakov & Borzenkova, 1990)
6.3-7.9	1	Boreal/Atlantic	-	-	Csa	ZB IV	Mesomediterranean, subhumid	Maximum of deciduous *Quercus* curve (Pons & Reille,1988). Warm climate and relatively stable period (Zubakov & Borzenkova, 1990).
7.9-8.2	1	Boreal	13-17 to 17-19	600-1000	Csa	ZB IV	Mesomediterranean to Thermomediterranean, subhumid	*Quercus suber* abundant and persistent (Pons & Reille,1988).
8.2-10.3	1	Preboreal/Boreal	13-17	350-600	Csb	ZB IV	Mesomediterranean, dry	*Quercus ilex* and *Pistacia* recovery. Sclerophyllous mediterranean forest (Pons & Reille,1988).
10.3 or 10.0-11 or 10.7	1or2	Younger Dryas	4-8	<350	BSk	ZB VII	Oromediterranean, arid to semiarid	Rapid climatic deterioration. Arid but as cold as the Oldest Dryas (Pons & Reille,1988).
11.0 or 10.7-13.3 or 12	2	Bölling-Alleröd Interstadial late-glacial	8-13 to 13-17	200-600 to 600-1000	Csb	ZB IV	Supramediterranean to mesomediterranean, semiarid or dry to subhumid	Specific climatic amelioration toward 13 Ka BP (at 10 ka BP for the rest of Europe). Vegetation recovery, especially oak forests, *Quercus ilex* and deciduous *Quercus* (Pons & Reille,1988). Both will dominate the arboreal stratum to the present time.
13.3 or 12.8-15.2	2	Oldest Dryas	4-8 to 8-13	<450	BSk	ZE VI/VII	Oromediterranean to supramediterranean, dry to semiarid	Thermoclime could evolve from oromediterranean at the beginning to supramediterranean under dry to semiarid ombroclime and semidesertic bioclime with *Artemisia* predominant (Pons & Reille,1988).
15.2-19.8	2	Final Würm	<4	350 to <200	BSk-FT	ZE VIII/IX ZE VI/VII	Cryoromediterranean, dry	Last Glacial Maximum toward 18 ka BP. Steppe and semidesert conditions alternate. Minimum average temperature of coldest month, below –7ºC. Sea level descended 100-120m.. Forest-tundra in central highlands.
19.8-23.6	2	Middle/ Würm Final Würm	4-8 or <4	350 to <200	BSk	ZB VIIa	Oromediterranean or cryoromediterranean, arid	Cold and arid, semidesert. Around 19.8 ka BP becomes more like semidesert (Pons & Reille,1988).
24-38	3	Middle Würm	8-13 to 4-8	600-200	BSk	ZE VI/VII	Supramediterranean to oromediterranean, semiarid to dry	Sligtly arid environmental conditions. Poorly marked climatic episodes due to varied climatic gradations. Little climatic fluctuation.
>38	3		-	-	BWk	ZB VII (r III)	-	No data at Padul for this period. Palynology indicates very arid vegetation (Pons & Reille,1988).
<63.5	4	Eowürm	4-8	<200	BWk	ZB VII (r III)	Oromediterranean, arid	Cold and extremely arid episode.
>63.5-84	5a	St. Germain II	13-17	>200 to 650-1000	Csa	ZB IV	Mesomediterranean	General thermal recovery, although it includes the early part of the regression to the colder and arid OIS 4 period with an increment of steppic species (Pons & Reille,1988).
84-96	5b	Mélisey II	8-13	<450	BSk	ZE VI/VII	Supramediterranean, dry	Less arboreal pollen in steppic and semidesertic species interest (Pons & Reille,1988).
96-104	5c	St. Germain Ic	13-17	650-1000	Csb	ZB IV	Mesomediterranean, subhumid	Predominant mesohydrophyllous vegetation (Pons & Reille,1988).
	5c	St. Germain Ib	13-17	650-1000	Csb	ZB IV	Mesomediterranean, subhumid	Substitution of *Erica arborea* by *Quercus ilex* (Pons & Reille,1988).
	5c	St. Germain Ia	8-13	200-350	BSk	ZE VI/VII	Supramediterranean, semiarid	Slight climatic deterioration. More abundance of steppic species (Pons & Reille,1988).
	5c	-	17-19	350-650	Csa	ZB IV	Thermomediterranean, dry	Thermophyllous but no arid vegetation (Pons & Reille,1988).

(1) Actual mean annual temperature and precipitation (2) in Padul are 16.1 ºC and 409 mm respectively (1955-2001 period. Instituto Nacional de Meteorología).

Table A3. Ombrothermic characterisation, climate class and bioclimatic levels assignment of 'Padul IVa' pollen record samples.

Zona	*Edad aprox*	Muestra	Prof (m)	Precipitac	Incert Prec	Temperat	Incert Temp	Köppen	Rivas-Martínez	OIS	*Periodo*
R		**40**	19	**450**	350-550	**17**	15-20	***Csa***	Meso-Termomediterráneo Seco		
R		**41**	19.5	**500**	400-600	**17**	15-20	***Csa***	Mesomediterráneo Seco		
R		**42**	20	**550**	450-650	**16**	14-18	***Csa***	Mesomediterr. Seco (Subhúmedo)		
R		**43**	20.5	**900**	750-1050	**18**	16-20	***Csa***	Termomediterráneo Subhúmedo		
Q		**44**	21	**650**	500-800	**17.5**	16-20	***Csa***	Termomediterráneo Subhúmedo		
Q		**45**	21.5	**750**	600-900	**16**	14-18	***Csa***	Mesomediterráneo Subhúmedo		
Q		**46**	22	**950**	800-1100	**16.5**	15-19	***Csa***	Mesomedit. Subhúmedo-Húmedo	5e	*Eemiense*
Q		**47**	22.5	**850**	700-1000	**18.5**	17-21	***Csa***	Termomediterráneo Subhúmedo	5e	*Eemiense*
Q		**48**	23	**1000**	800-1200	**17.5**	16-20	***Csa***	Termomed. Subhúmedo-Húmedo		
Q	*ca. 120 ka BP*	**49**	23.5	**650**	500-800	**16.5**	15-19	***Csa***	Mesomedtirráneo Subhúmedo		
N		**50**	24	**600**	500-700	**10**	8 a 12	***Csb***	Supramedit. Seco-Subhúmedo		
N		**51**	24.5	**275**	200-350	**9**	7 a 11	***BSk***	Supramediterráneo Semiárido		
N		**52**	25	**275**	200-350	**6**	4 a 8	***BSk***	Oromediterráneo Semiárido	6	*Riss II*
N		**53**	25.5	**325**	250-400	**11.5**	10 a 14	***BSk***	Supramediterráneo Semiárido	6	*Riss II*
N		**54**	26	**275**	200-350	**6**	4 a 8	***BSk***	Oromediterráneo Semiárido	6	*Riss II*
N		**55**	26.5	**250**	175-325	**8**	6 a 10	***BSk***	Oro-Supramediterráneo Semiárido	6	*Riss II*
N		**56**	27	**300**	225-375	**6**	4 a 8	***BSk***	Oromediterráneo Semiárido	6	*Riss II*
N		**57**	27.5	**325**	250-400	**8**	6 a 10	***BSk***	Oro-Supramed. Semiárido (seco)		*Riss II*
N		**58**	28	**325**	250-400	**10**	8 a 12	***BSk***	Supramediterráneo Semiárido		*Riss II*
M		**59**	28.5	**350**	275-425	**11**	9 a 13	***BSk***	Supramedit. Semiárido a Seco		*Riss II*
M		**60**	29	**400**	300-500	**12**	10 a 14	***BSk***	Supramediterráneo Seco		
M		**61**	29.5	**450**	350-550	**11.5**	10 a 14	***Csb***	Supramediterráneo Seco		
M	*ca. 170 ka BP*	**62**	30	**350**	275-425	**9.5**	8 a 13	***BSk***	Supramedit. Semiárido a Seco	7a	*Ris I-Riss II*
M		**63**	30.5	**500**	400-600	**11**	9 a 13	***Csb***	Supramediterráneo Seco	7a	*Ris I-Riss II*
M	*ca. 180 ka BP*	**64**	31	**700**	550-850	**13**	11 a 15	***Csb***	Supra-Mesomedit. Subhúmedo	7a	*Ris I-Riss II*
M		**65**	31.5	**600**	500-700	**14.5**	13-17	***Csa***	Mesomedit. Subhúmedo-Seco	7a	*Ris I-Riss II*
M		**66**	32	**500**	400-600	**12.5**	11 a 15	***Csb***	Supramediterráneo Seco	7a	*Ris I-Riss II*
M		**67**	32.7	**500**	400-600	**9**	7 a 11	***Csb***	Supramediterráneo Seco	7a	*Ris I-Riss II*
M		**68**	33.3	**800**	650-950	**16**	14-18	***Csa***	Mesomediterráneo Subhúmedo		
M		**69**	34	**750**	600-900	**15**	13-17	***Csa***	Mesomediterráneo Subhúmedo		
M		**70**	34.5	**400**	300-500	**9**	7 a 11	***BSk***	Supramediterráneo Seco		
M		**71**	35	**425**	325-525	**15**	13-17	***Csa***	Mesomediterráneo Seco		
L		**72**	35.5	**400**	300-500	**12**	10 a 14	***BSk***	Supramediterráneo Seco		
L		**73**	36	**375**	300-450	**9.5**	7 a 12	***BSk***	Supramediterráneo Seco		
L	*ca. 220 ka BP*	**74**	36.5	**350**	275-425	**12.5**	11 a 15	***BSk***	Supramedit. Semiárido-Seco		
L		**75**	37	**425**	325-525	**13**	11 a 15	***Csb***	Supra-Mesomediterráneo Seco		
L		**76**	37.5	**375**	300-450	**13**	11 a 15	***BSk***	Supra-Mesomedit. Seco-Semiárido		
L		**77**	38	**375**	300-450	**10**	8 a 12	***BSk***	Supramedit. Seco-Semiárido		*Riss I*
L		**78**	38.5	**400**	300-500	**11**	9 a 13	***BSk***	Supramedit. Seco-Semiárido		*Riss I*
L		**79**	39	**350**	275-425	**11**	9 a 13	***BSk***	Supramedit. Semiárido-Seco	8	*Riss I*
L		**80**	39.5	**325**	250-400	**10**	8 a 12	***BSk***	Supramedit. Semiárido	8	*Riss I*
L		**81**	40	**275**	200-350	**8.5**	7 a 11	***BSk***	Supramedit. Semiárido	8	*Riss I*
K		**82**	40.5	**450**	350-550	**13.5**	12 a 16	***Csa***	Mesomediterráneo Seco	8	*Riss I*
K		**83**	41	**350**	275-425	**10**	8 a 12	***BSk***	Supramedit. Semiárido-Seco	8	*Riss I*
K		**84**	41.5	**275**	200-350	**12**	10 a 14	***BSk***	Supramediterráneo Semiárido	8	*Riss I*
K		**85**	42	**325**	250-400	**10**	8 a 12	***BSk***	Supramediterráneo Semiárido	8	*Riss I*

Zona	*Edad aprox*	Muestra	Prof(m)	Precipitac	Incert Prec	Temperat	Incert Temp	Köppen	Rivas-Martínez	OIS	*Periodo*
K		86	42.5	350	275-425	12	10 a 14	*BSk*	Supramedit. Semiárido-Seco		*Riss I*
K		87	43	325	250-400	11.5	10 a 14	*BSk*	Supramediterráneo Semiárido		*Riss I*
K		88	43.5	300	225-375	11	9 a 13	*BSk*	Supramediterráneo Semiárido		*Riss I*
K		89	44	300	225-375	10.5	9 a 13	*BSk*	Supramediterráneo Semiárido		
K		90	44.25	350	275-425	10.5	9 a 13	*BSk*	Supramedit. Semiárido-Seco		
K		91	45	300	225-375	15	13-17	*BSk*	Mesomediterráneo Semiárido		
K		92	45.5	275	200-350	14	12 a 16	*BSk*	Mesomediterráneo Semiárido		
K		93	46	275	200-350	12.5	10 a 14	*BSk*	Supramediterráneo Semiárido		
K		94	48.65	300	225-375	9.5	8 a 13	*BSk*	Supramediterráneo Semiárido		
K		95	49.65	300	225-375	15	14-16	*BSk*	Mesomediterráneo Semiárido		
K		96	50.5	350	275-425	9	6 a 12	*BSk*	Supramedit. Semiárido-Seco		
K		97	51	275	200-350	8	6 a 10	*BSk*	Supra-Oromediterr. Semiárido		
K		98	51.5	350	275-425	12	9 a 14	*BSk*	Supramedit. Semiárido-Seco		
K		99	52	250	175-325	11	7 a 13	*BSk*	Supramediterráneo Semiárido		
K		100	53	250	175-325	7	4 a 10	*BSk*	Oromediterráneo Semiárido		
K	*ca. 270 ka BP*	101	53.5	275	200-350	4	2 a 6	*BSk*	Oro-Criorromediterráneo Semiárido		
K		102	54	275	200-350	7	4 a 10	*BSk*	Oromediterráneo Semiárido		
K		103	54.5	250	175-325	10.5	8 a 12	*BSk*	Supramediterráneo Semiárido		
J		104	55	400	300-500	14	12 a 16	*BSk*	Mesomedit. Seco-Semiárido		*Holstein*
J		105	55.5	375	300-450	10	8 a 12	*BSk*	Supramedit. Seco-Semiárido		*Holstein*
J		106	56.5	425	325-525	12	10 a 14	*Csb*	Supramediterráneo Seco		*Holstein*
J		107	57	450	350-550	13	11 a 15	*Csb*	Meso-Supramediterráneo Seco	9	*Holstein*
J		108	57.5	475	375-575	14	12 a 16	*Csa*	Mesomediterráneo Seco	9	*Holstein*
J		109	58	450	350-550	15	13-17	*Csa*	Mesomediterráneo Seco	9	*Holstein*
J		110	58.75	350	275-425	10	8 a 12	*BSk*	Supramedit. Semiárido-Seco	9	*Holstein*
J		111	59	375	300-450	10	8 a 12	*BSk*	Supramedit. Seco-Semiárido	9	*Holstein*
J		112	60	550	450-650	13	12 a 16	*Csb*	Meso-Supramed. Seco (Subhúm)	9	*Holstein*
J		113	60.5	450	350-550	15	13 a 17	*Csa*	Mesomediterráneo Seco	9	*Holstein*
J		114	61	450	350-550	14	12 a 17	*Csa*	Mesomediterráneo Seco	9	*Holstein*
J		115	61.7	500	400-600	16.5	14-18	*Csa*	Mesomediterráneo Seco	9	*Holstein*
I	*ca. 320 ka BP*	116	62.2	550	450-650	11.5	9 a 14	*Csb*	Supramedit. Seco (Subhúmedo)		
I		117	62.75	450	350-550	8	6 a 10	*Csb*	Supra-Oromediterráneo Seco		
I		118	63.75	300	225-375	7	5 a 9	*BSk*	Oromediterráneo Semiárido		
I		119	64	325	250-400	7	5 a 9	*BSk*	Oromediterráneo Semiárido (Seco)	10	*Mindel*
I		120	64.5	225	175-275	3	1 a 5	*BWk-BSk*	Criorromediterr. Árido-Semiárido	10	*Mindel*
I		121	64.75	200	150-250	3	1 a 5	*BWk*	Criorromediterr. Árido a Semiárido	10	*Mindel*
I	*ca. 350 ka BP*	122	65.2	250	175-325	7	5 a 9	*BSk*	Oromediterr. Semiárido-Árido	10	*Mindel*
I		123	65.5	225	175-275	4	2 a 6	*BWk-BSk*	Oromediterráneo Árido-Semiárido	10	*Mindel*
H		124	66	250	175-325	5	3 a 7	*BSk*	Oromediterráneo Semiárido-Árido	10	*Mindel*
H		125	66.5	325	250-400	12	9 a 15	*BSk*	Mesomediterráneo Semiárido	11	*Mindel*
H		126	67	350	275-425	9.5	6 a 12	*BSk*	Supramedit. Semiárido-Seco	11	*Mindel*
H	*ca. 425 ka BP*	127	67.25	250	175-325	6	4 a 8	*BSk*	Oromediterráneo Semiárido-Árido		*Mindel*
G		128	67.75	250	175-325	4	2 a 6	*BSk*	Oromediterráneo Semiárido-Árido	12	*Mindel*
G		129	68	250	175-325	5	3 a 7	*BSk*	Oromediterráneo Semiárido-Árido	12	*Mindel*
G		130	68.5	250	175-325	11	9 a 13	*BSk*	Supramedit. Semiárido-Árido		*Mindel*
G		131	69	250	175-325	13.5	11 a 15	*BSk*	Mesomedit. Semiárido-Árido		*Mindel*
G	*ca. 475-500ka BP*	132	69.5	275	200-350	10	8 a 12	*BSk*	Supramediterráneo Semiárido		*Mindel*

Appendix B: Secondary Calcite in a Shallow Recharge-to-Discharge Fresh Groundwater System

Adrian Bath and David Noy

B1 Introduction

The chemical evolution of groundwaters and the deposition of secondary minerals along flow paths from recharge to discharge through fractured hard rocks is interesting because it has the potential to be influenced by direct impacts of climate, both physical (temperature, precipitation, permafrost, erosion, glaciation, water table fluctuations) and chemical (pCO_2, pH, redox, soil-derived organics, microorganisms). The conceptual model of groundwater flow and geochemical evolution is illustrated in Figure B1, in which the composition of waters evolve from 'immature' compositions that are not equilibrated with rock minerals and thus being modified by weathering reactions through to 'mature' waters that are equilibrated with primary and secondary minerals.

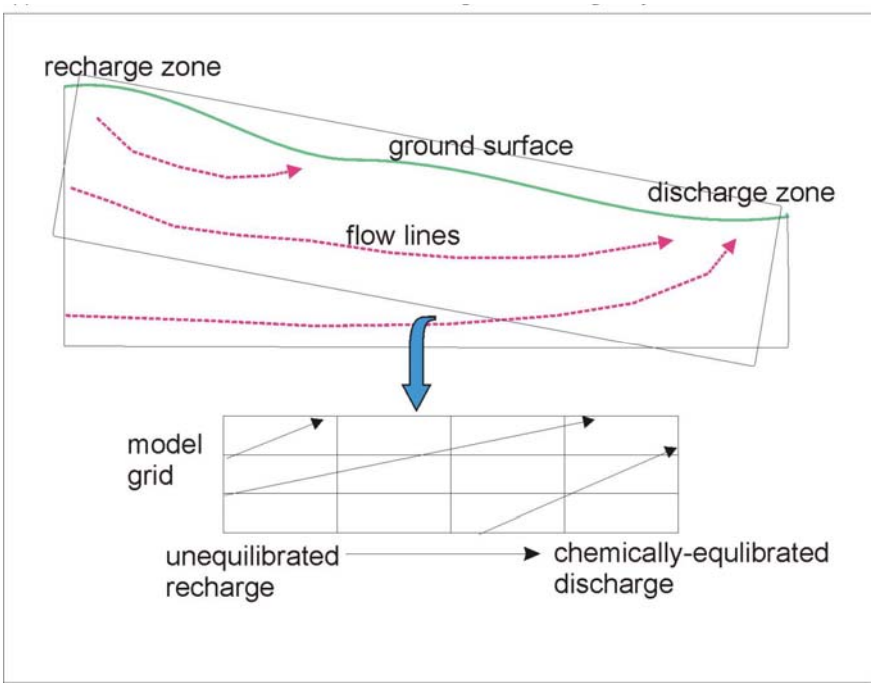

Figure B1. Conceptual model for progressive approach to geochemical equilibration along the flow lines of groundwater from recharge to discharge in a shallow groundwater system exemplified in this study by data from the Altnabreac site.

The sequence of secondary minerals being precipitated reflects the geochemistry of the source primary minerals and the coupled hydrogeochemical evolution of pH and alkalinity in groundwater. Secondary calcite precipitates along the flow path basically in response to rising Ca^{2+} and increasing pH and HCO_3^-. Earlier calcite may also be a source of these ions, as it dissolves in recharge water with relatively high pH and high pCO_2, and therefore secondary calcite may be a product of remobilisation of earlier (or primary) carbonate.

It has not been possible to identify a shallow 'recharge-to-discharge' groundwater system in the UK where mineral and groundwater data might be obtained to test this model of secondary calcite mineralisation (Milodowski and Bath, 2002). Therefore, in the absence of new data, spatial evolution of groundwater composition in a recharge-to-discharge shallow groundwater system has been simulated with data from Altnabreac in northern Scotland. This site is located on fairly low-lying fractured crystalline rocks and an investigation in the 1980's produced hydrochemical and hydrogeological data, but there are no data for secondary fracture-filling minerals.

The aim of the modelling has been to study possible reaction paths of hydrochemical evolution, compare these with observed groundwater composition in the down-gradient part of the flow system, and to deduce from the model where precipitation of secondary calcite might be occurring in this type of groundwater system. This relates to studies in WP2 in terms of supporting the hypothesis that secondary calcite may be precipitated in shallow groundwater systems below the most shallow weathering zone where only mineral dissolution reactions occur. The geochemistry and isotopic composition of secondary calcite deposited in those conditions might contain information about shallow hydrological, soil and climatic conditions in the past.

This type of shallow hydrogeological and geochemical system is comparable with the Melechov groundwater system in the Bohemian Massif (water-rock interaction in a tectonically younger host rock) which is being studied by Czech partners in WP2, and the Ratones groundwater system (water-rock reaction under a semi-arid climate) that is being studied by Spanish partners.

B2 The Groundwater System at Altnabreac

Hydrochemical and hydrogeological data sets from earlier investigations in the fractured crystalline rock at Altnabreac in northern Scotland have been used to construct the model (Glendining, 1980; Holmes et al., 1981; Kay and Bath, 1982). Two flow paths from high ground (i.e. the recharge zone) to lower ground discharge zones have been selected for modelling (Figure B2). Flow path C-A goes northwards through Strath Halladale granite and presumably discharges wholly or partially to Sleach water, about 1 km further north-east of A. Flow path C-B goes south-eastwards through the granite and then into Moine metasediments and presumably discharges into the Thurso River about 1.3 km south of B. Hydraulic testing over intervals in the boreholes gave the hydraulic conductivities shown in Table B1.

Table B1. Hydraulic test data from the A boreholes at Altnabreac.

Borehole	Interval, m	Hydraulic conductivity, m/s
A1A	30-50	10^{-6}
	50-100	$3x10^{-8}$
	100-250	10^{-9} to 10^{-7} (av. 10^{-8})
	250-300	10^{-10}
A1B	40-60	10^{-1} to 10^{-6} (av. 10^{-8})
	60-130	10^{-8} to 10^{-6} (av. $6x10^{-8}$)
	130-230	$4x10^{-9}$ to 10^{-10} (av. $6x10^{-10}$)
A1C	70-170	10^{-6}
	170-290	10^{-12} to 10^{-8} (av. $2x10^{-10}$)
Av A bhs	excluding faulted zones	$7x10^{-10}$
	all measurements	$6.7x10^{-9}$

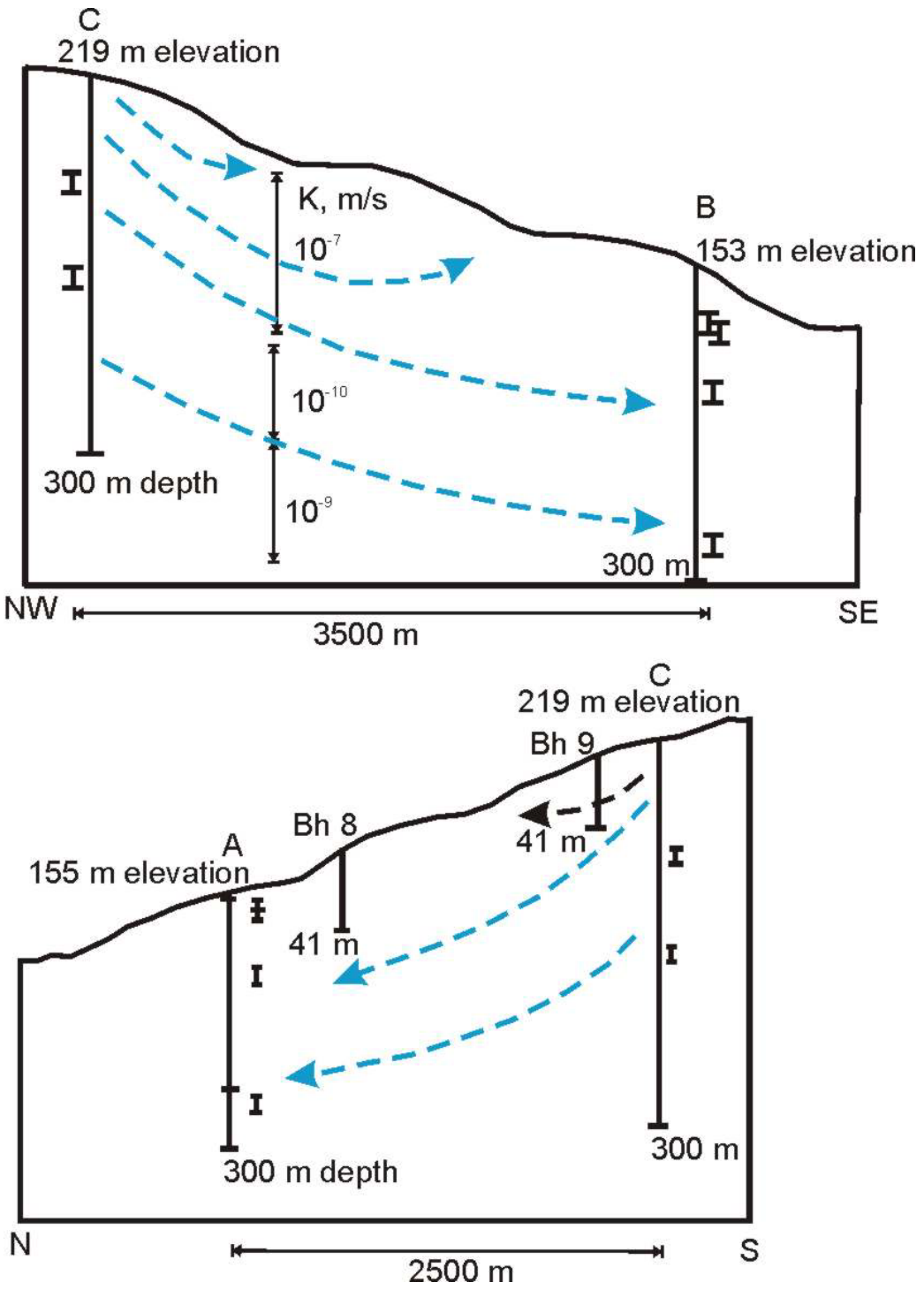

Figure B2. Two 2D sections through the Altnabreac area, Scotland, showing the flow paths along which hydrogeochemical evolution and precipitation of secondary calcite has been simulated.

B3 Geochemical Modelling

Initially, geochemical modelling with PHREEQC (Parkhurst and Appelo, 1999) was carried out to evaluate the mineral equilibria. The main findings from the geochemical modelling are:

- Shallow groundwater at C/96 is undersaturated with respect to calcite and log pCO_2 is +0.63 (i.e. high as expected); pyrite is strongly oversaturated but FeS(ppt) is close to equilibrium.

- Deeper groundwater at B/281 is oversaturated with calcite and log pCO_2 is -1.07; FeS(ppt) is at equilibrium (but note that redox data may not be reliable).
- Deeper groundwater at A/223 is oversaturated with calcite and log pCO_2 is -0.54; FeS(ppt) is just oversaturated.
- Inverse modelling indicates that the geochemical evolutions from shallow to deep groundwaters involve dissolution of plagioclase (albite or oligoclase) and of calcite, lowering of pCO_2 (presumably due to silicate weathering), and precipitation of SiO_2, Fe-ox, ?pyrite/FeS.

Then inverse modelling with PHREEQC was used to find the most plausible set of water-rock reactions that would account for the evolution of groundwater compositions between recharge and discharge. The inverse simulations were carried out for the following pairs of upgradient-downgradient groundwaters:

- Inverse model of groundwater evolution from the upper parts of borehole C (96 m depth) or the shallow borehole 9 to the deeper part of borehole A (223 m depth).
- Inverse model of groundwater evolution from the upper part of borehole C (96 m depth) to the deeper part of borehole B (281 m depth).

With these basic geochemical insights, the PRECIP program (Noy, 1998) was then used to carry out a simulation of hydrogeochemical evolution coupled with realistic groundwater flow and dispersion. Six model runs were carried out.

B3.1 REACTION OF PRIMARY MINERALS AND PRECIPITATION OF CALCITE AND OTHER SECONDARY MINERALS ALONG A CLOSED SYSTEM FLOW PATH

Model 1: Secondary calcite + kaolinite, chlorite, muscovite/ illite

The initial model for this series assumes a simple granite starting composition as indicated in Table B2 and a groundwater composition based upon the sample CPT96 as indicated in Table B3. In Table B2 a 10% biotite component is represented by equal amounts of its end members annite and phlogopite. As indicated in Table B4, a limited set of potential secondary minerals was selected, with chlorite being represented by end members clinochlore and daphnite. Flow and transport parameters used in the model are listed in Table B5.

Table B2. Rock composition

Mineral	Mole/m^3	%vol
Quartz	12782.1	29
Anorthite	1984.3	20
Albite	1995.0	20
K-feldspar	1837.1	20
Annite	324.0	5
Phlogopite	334.1	5
Porosity		1

Table B3. Groundwater composition for C/96

Species	mMole/dm^3
$AlOH^{2+}$	1.14e-6
Ca^{2+}	0.417
Cl^{-}	0.6208
Fe^{2+}	9.812e-2
H^{+}	1.252e-3
HCO_3^{-}	1.858
K^{+}	2.893
Mg^{2+}	0.3401
Na^{+}	0.6504
SiO_2	5.593e-2
pH	5.93

Table B4. Potential secondary minerals

Calcite	Dolomite
Clinochlore	Kaolinite
Daphnite	Muscovite

Table B5. Flow and transport parameters

Flow path length	200 m
Darcy flow rate, q	1.0e-9 m/s
Groundwater velocity, v	1.0e-7 m/s (= 3.2 m/yr)
Dispersivity	1 m
Diffusion coefficient	3.6e-10 m^2/s

Figure B3 shows the pH profile and secondary mineral distribution after a simulated time of 65 yr. The PRECIP calculation had to be stopped at that point due to numerical difficulties. A similar simulation using $CORE^{2D}$ (Samper et al., 2000) showed very similar results and indicates that the pH at 200 m eventually rises to a value close to 12. Thus this model confirms that mineral alteration reactions in granite may be expected to lead to saturation and subsequent precipitation of carbonates. The distance along the path that this occurs depends upon the details of the kinetics of the process, and in particular the reactive surface areas, and in this case it occurs within about 50 m. However, the simulation also indicates the alteration reactions lead to a net consumption of H^+ ions and cause the pH to rise to levels that are not normally seen in natural granite groundwaters. It would seem likely that in such natural systems that some minerals, although thermodynamically favoured, are in fact kinetically inhibited from precipitating and that alternative phases should be considered. The remaining models explore various possibilities.

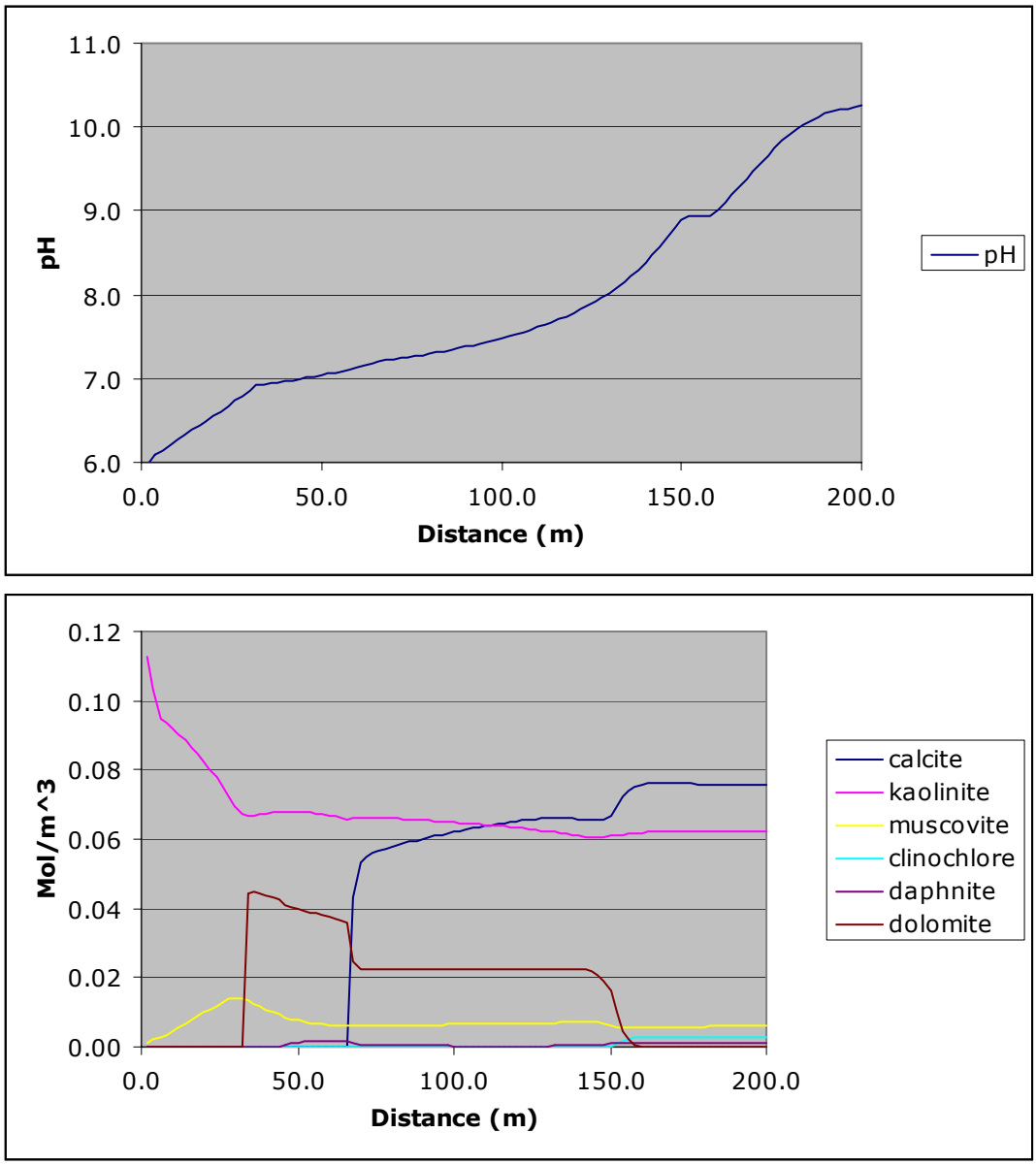

Figure B3. Evolution of pH (B3a) and amounts of secondary minerals (B3b) from modelling the Altnabreac recharge-discharge system: Model 1 at t = 65 yr. Base case in which calcite-undersaturated shallow upland recharge water reacts with granite along a flow path of 200 m length with properties in Table B5. No secondary minerals were suppressed. Calcite is precipitated about 65 m along the flow line. Note that pH rises to >10 in this simulation which does not compare with observed pH values.

Model 2: Secondary calcite + montmorillonite, chlorite, muscovite/ illite

For the first variation, kaolinite precipitation was suppressed and Na/Ca-montmorillonites were included as potential secondary minerals. Figure B4 shows that this model generates very similar results to model 1.

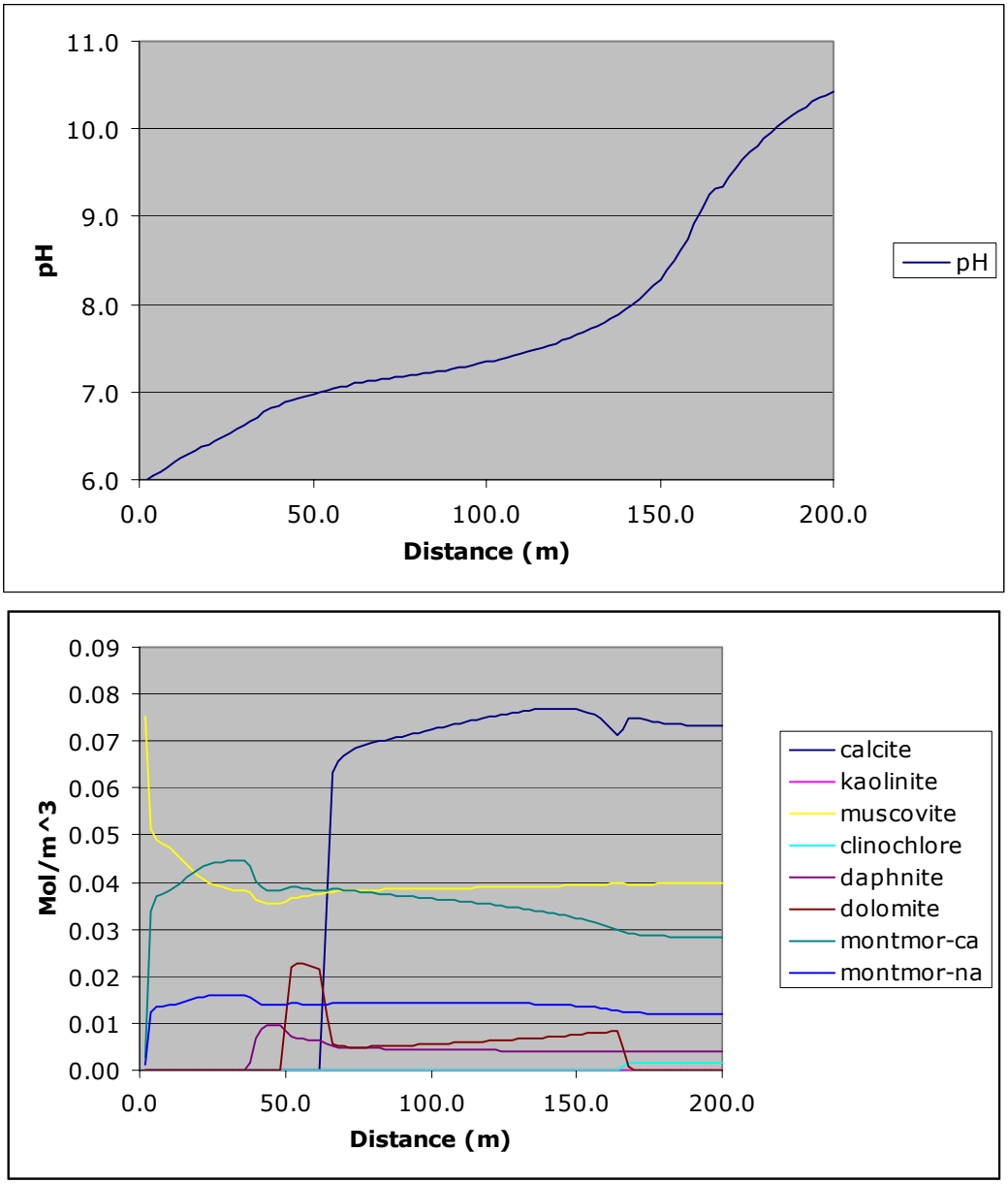

Figure B4. Evolution of pH (B4a) and amounts of secondary minerals (B4b) from modelling the Altnabreac recharge-discharge system: Model 2 at t = 65 yr. Base case as in Model 1 (Figure B3) except that kaolinite formation has been suppressed. Calcite is precipitated about 60 m along the flow line, and secondary muscovite and chlorite are more abundant. Note that pH again rises to >10.

Model 3: Secondary calcite + montmorillonite, chlorite

As for model 2 but with muscovite precipitation also suppressed. Figure B5 shows that the maximum pH on the profile has been reduced to about 8, although it will be noted that the pH is rising at the end of the profile and it is likely that high pH will still be obtained with this model at greater distances.

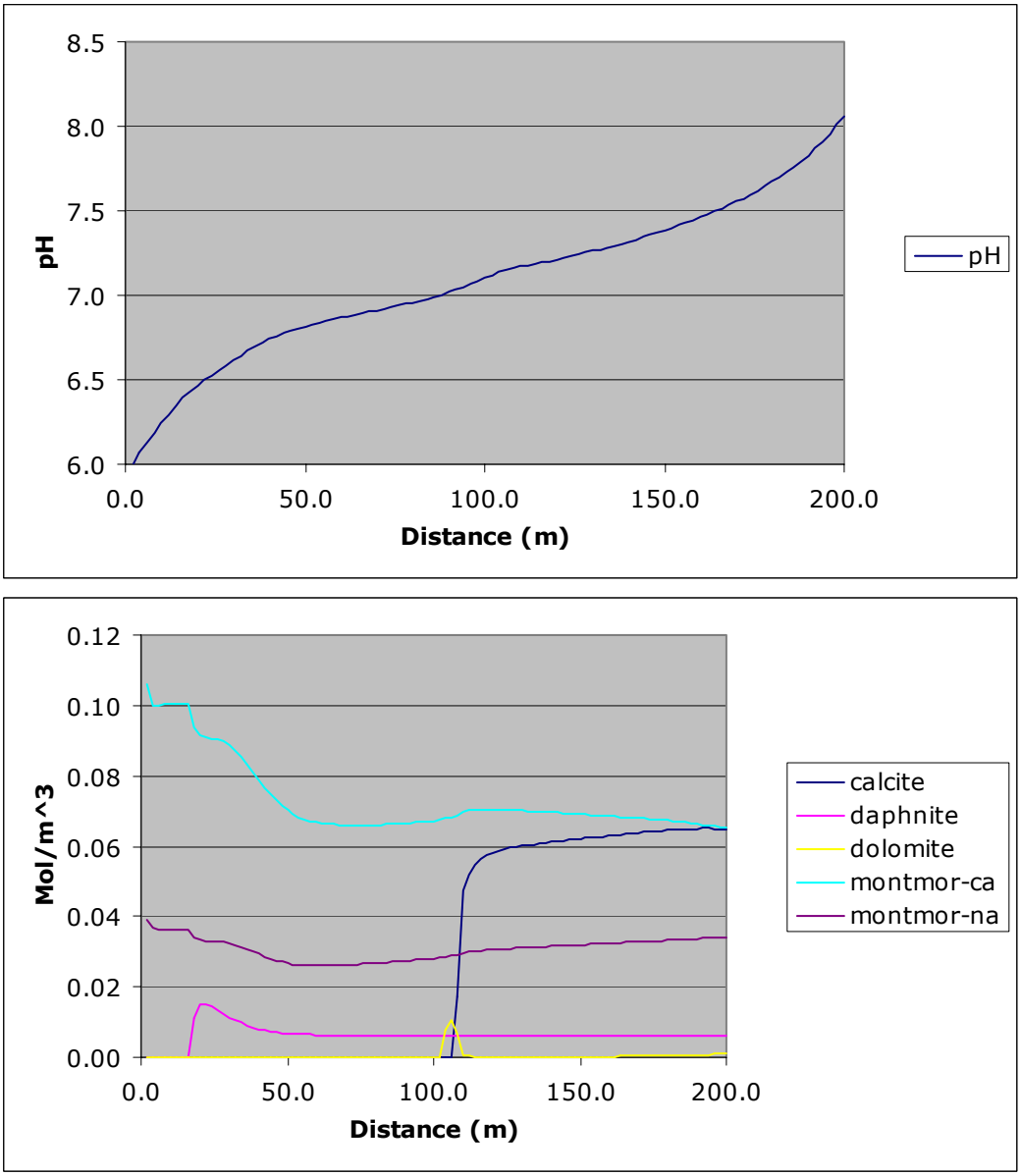

Figure B5. Evolution of pH (B5a) and amounts of secondary minerals (B5b) from modelling the Altnabreac recharge-discharge system: Model 3 at t = 100 yr. Base case as in Model 1 (Figure B3) except that kaolinite and muscovite formation has been suppressed. pH rises less dramatically to around 8, so that calcite is precipitated about 100 m along the flow line. Secondary montmorillonite is abundant.

Model 4: Secondary calcite + montmorillonite + goethite

As in model 3 but with 'biotite' and 'chlorite' phases as suggested by Guimera et al (1999) replacing the respective separate end members. Thermodynamic data for these phases had to be estimated from data for the end members. In addition, goethite and K/Mg-montmorillonites were added to the set of potential secondary minerals. The flow path length for this model was extended to 500 m and the simulation continued to 1000 yr to investigate whether 'steady-state' water chemistry would be achieved. Figure B6 shows that this model does extend the range of the near neutral pH groundwater, but the rising pH towards the end of the profile is still present.

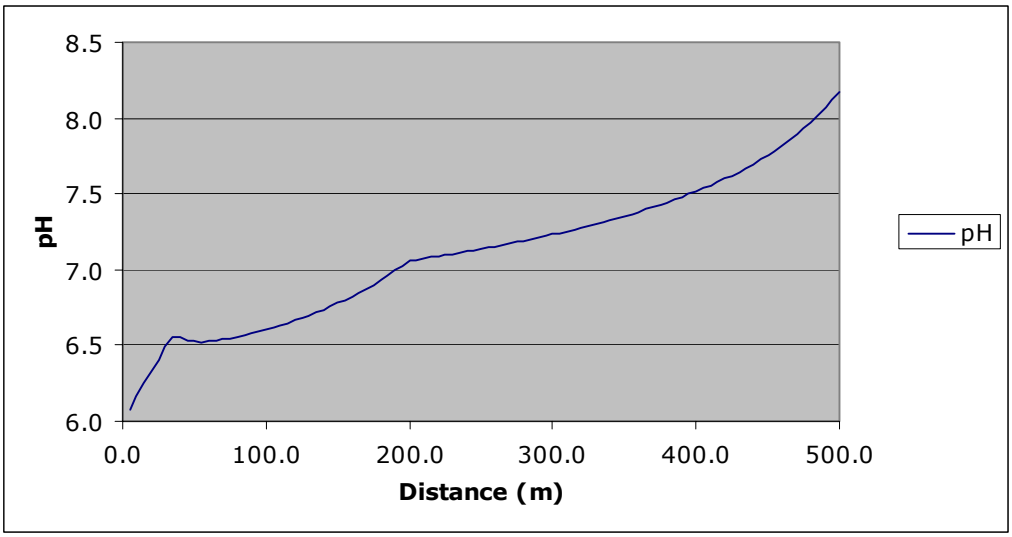

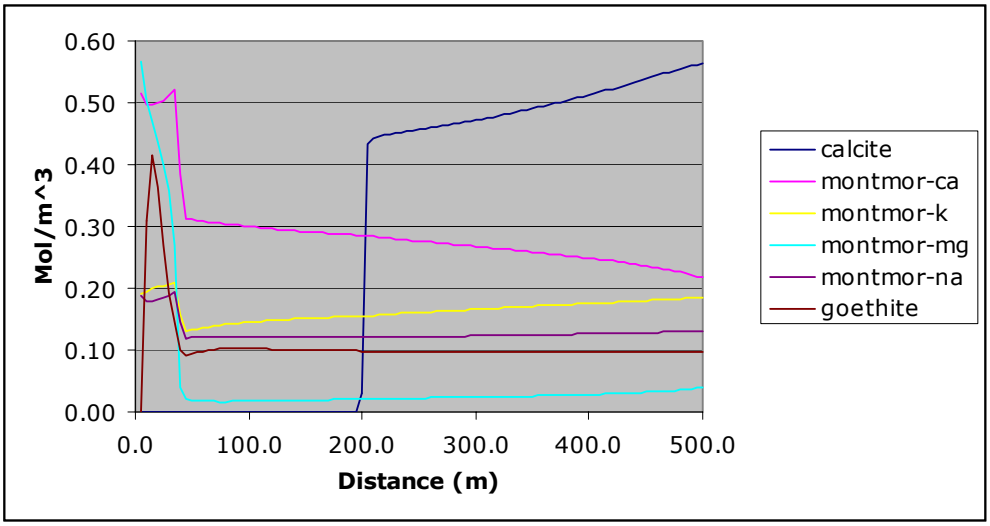

Figure B6. Evolution of pH (B6a) and amounts of secondary minerals (B6b) from modelling the Altnabreac recharge-discharge system: Model 4 at t = 1000 yr and path length = 500 m. Estimated thermodynamics data for solid solution 'biotite' and 'chlorite' as suggested by Guimera et al (1999) have been used in the model rather than the end member phases used in the Base Case. Goethite and K/Mg-montmorillonite are allowed to precipitate as secondary minerals. Calcite is precipitated about 200 m along the flow line.

Model 5: Slower reaction kinetics and longer path length

This model is exactly as model 4 except that the dissolution and precipitation rates for all minerals were reduced by an order of magnitude. The length of the model profile was extended to 5km and the simulation was run to 10 ky. This shows how adjusting the kinetic rates (or equivalently the surface areas) leads to a scaling of the length and time scales (Figure B7). A schematic diagram that summarises the secondary mineral assemblages that would form in fractures along the flow path is shown in Figure B8.

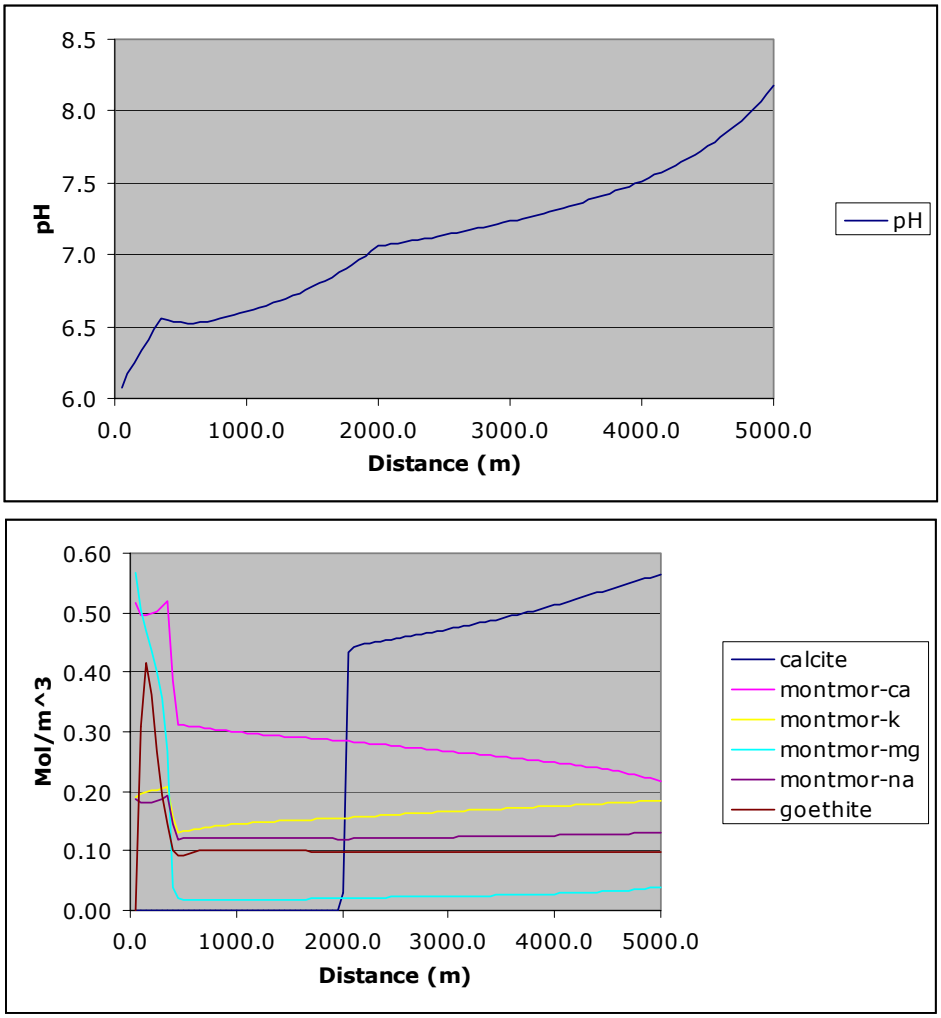

Figure B7. Evolution of pH (B7a) and amounts of secondary minerals (B7b) from modelling the Altnabreac recharge-discharge system: Model 5. Same minerals as Model 4, but parameters scaled to more realistic values: dissolution/precipitation rates x 0.1, path length = 5 km and t = 10,000 yr.

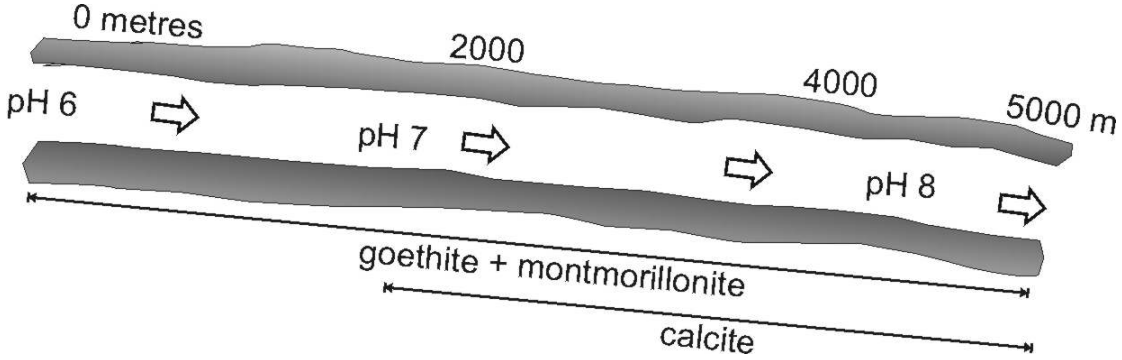

Figure B8. Schematic diagram of the secondary mineral assemblages that would form along the flow path of Model 5 (Figure B7).

B3.2 WATER-ROCK REACTION AND PRECIPITATION OF SECONDARY MINERALS IN AN OPEN SYSTEM WITH RESPECT TO CO_2

Model 6: Open system buffering of minimum pCO_2 with secondary calcite + montmorillonite, chlorite, muscovite/illite

This model shows an entirely different approach to controlling pH. Model 6 is as model 2 but with CO_2(g) added to the 'minerals' list with its activity product set to prevent CO_2 partial pressure from falling below 0.024. By using PRECIP's facility to separately specify dissolution and precipitation rates it is possible to prevent the CO_2 from 'precipitating' where the partial pressure is higher (near the start of the flowpath) by setting the precipitation rate to a very low value. Figure B9 shows that this is very effective at holding the pH close to neutral, although there remains a gradual rise with distance beyond the point at which CO_2 consumption starts to occur. If CO_2 were to be continually added at higher pCO_2, the pH would fall and further dissolution of primary minerals and precipitation of secondary calcite (and other minerals) would presumably be indicated by modelling. A schematic diagram of the open system processes and the secondary minerals along the flow path is shown in Figure B10.

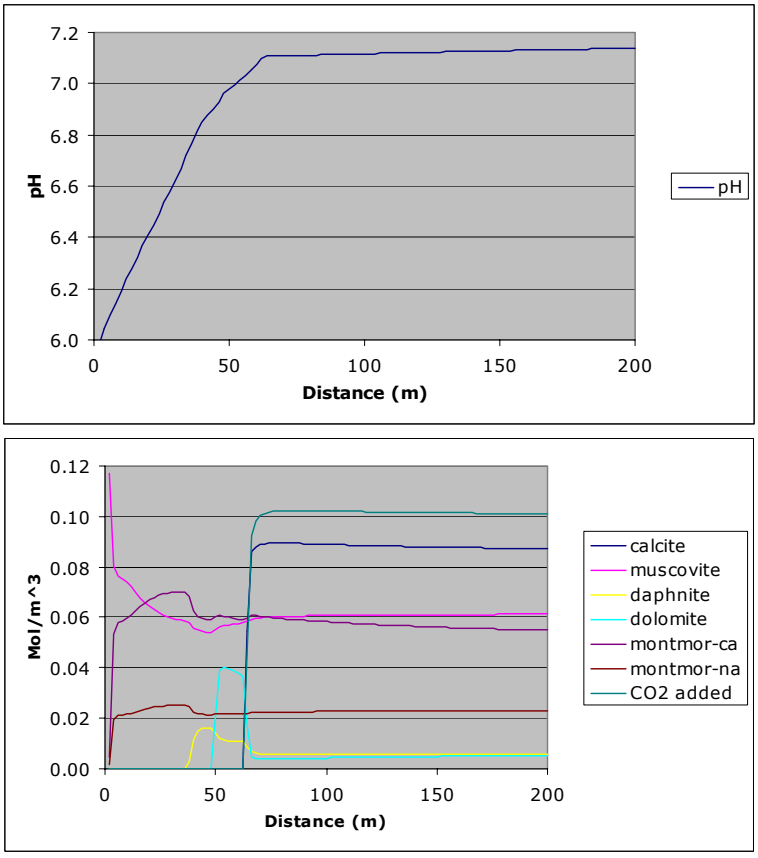

Figure B9. Evolution of pH (B9a) and amounts of secondary minerals (B9b) from modelling the Altnabreac recharge-discharge system: Model 6 at t = 100 yr. Same as Model 2 (Figure B4) except that pCO_2 is open system and is not allowed to fall below 0.024 atm ($10^{-1.6}$) and consequently pH is buffered at around 7.1-7.2. Calcite is precipitated transiently about 60 m along the flow line.

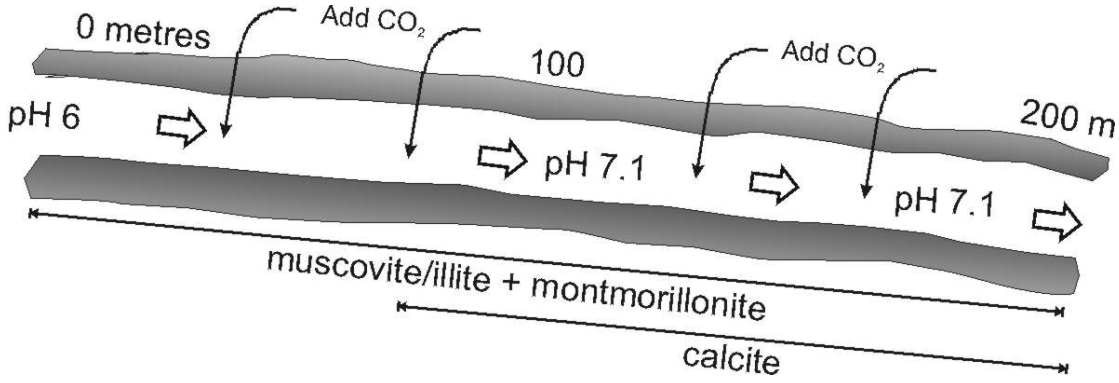

Figure B10. Schematic diagram of the open system processes and the secondary minerals along the flow path of Model 6 (Figure B9).

B3.3 SUMMARY OF MODELLING OF SECONDARY CALCITE IN A SHALLOW GROUNDWATER SYSTEM

The interim findings from the modelling of water-rock reaction and secondary calcite precipitation in a shallow recharge-discharge groundwater system in typical fractured rock are summarised as:

- Secondary calcite precipitates at an intermediate stage of the hydrochemical evolution of a shallow groundwater that is reacting with typical granitic rock minerals. Ca derives from alteration of Ca-containing primary minerals such as anorthite, and CO_3 derives from HCO_3 alkalinity of infiltration water.
- Other secondary minerals ('water-rock alteration' or 'weathering' products) that might form before and/or after calcite include kaolinite, chlorite, illite/muscovite, montmorillonite. Which of these actually forms might depend on ratios of the alkaline and alkaline earth elements coming from weathering of primary minerals and on nucleation kinetics of these secondary phases.
- If the model assumes a closed system with respect to inorganic carbon sources (i.e. CO_2 in soil zone of the recharge area), the pH of modelled water rises to unrealistically high values. An open (or semi-open) system that is buffered by external pCO_2 is a more realistic modelling approach.

B4 References

Glendining, S. (1980) A preliminary account of the hydrogeology of Altnabreac, Caithness. Rep. Inst. Geol. Sci. ENPU 80-6, Institute of Geological Sciences, Environmental Pollution Unit, Harwell, UK.

Guimerà, J., Duro, L., Jordana, S. and Bruno, J. (1999) Effects of ice melting and redox front migration in fractured rocks of low permeability. Technical Report TR-99-19. SKB Stockholm.

Holmes, D.C. (1981) Hydraulic testing of deep boreholes at Altnabreac: Development of the testing system and initial results. Rep. Inst. Geol. Sci. ENPU 82-12, Institute of Geological Sciences, Environmental Pollution Unit, Harwell, UK.

Kay, R.L.F. and Bath, A.H. (1982) Groundwater geochemical studies at the Altnabreac research site. Rep. Inst. Geol. Sci. ENPU 82-12, Institute of Geological Sciences, Environmental Pollution Unit, Harwell, UK.

Metcalfe, R. and Moore, Y.A. (1997) The possible geochemical and mineralogical consequences of Quaternary climate change: A theoretical scoping study. Technical Report WE/97/25C. Fluid Processes Group, British Geological Survey, Keyworth.

Milodowski, A.E. and Bath, A.H. (2002) Review of Secondary Mineralisation in Fractured Rocks in the UK. Report for Nirex.

Noy, D.J. (1998) User Guide to PRECIP. a Program for Coupled Flow and Reactive Solute Transport. Brit. Geol. Surv. Tech. Rep. WE/98/13. British Geological Survey, Keyworth, UK.

Parkhurst, D.L. and Appelo, C.A.J. (1999) User's guide to PHREEQC (version 2) – a computer program for speciation, batch-reaction, one-dimensional transport, and inverse geochemical calculations. Water-Resources Investigations Report 99-4259. U.S. Geological Survey, Denver.
Samper, J., Juncosa, R., Delgado, J. and Montenegro, L. (2000) CORE^{2D}. A code for non-isothermal water flow and reactive solute transport. Users manual version 2. Publicación técnica 6/2000

Appendix C: Mathematical Modelling of Groundwater Flow in Fractured Rocks at Melechov Massif

Václav Frydrych, Michal Havlík, Jiří Mls and Jan Šilar

C1 Introduction

The Melechov granite massif in the vicinity of Ledeč and Sázavou and Světlá and Sázavou has been chosen for PADAMOT project in the Czech republic. In order to achieve a basic understanding of the groundwater flow conditions in western part of this granite massif, a hydrogeological survey and following numerical modelling of the hydrogeological situation has been done.

Groundwater Vistas modelling software was used to perform spatial model of groundwater flow. The main objectives of the groundwater flow simulation were the determination of the spatial hydraulic potential distribution, velocity flow and travel time.

C2 Characteristics of Melechov Massif

Melechov granite massif is situated in central part of Czech Republic (Figure C1) exactly 5-20 km north of Humpolec and 15-20 km west of Havlíčkův Brod. Studied area with extent of 90 km^2 covers western part of Melechov granite massif and surrounding Moldanubic mantle.

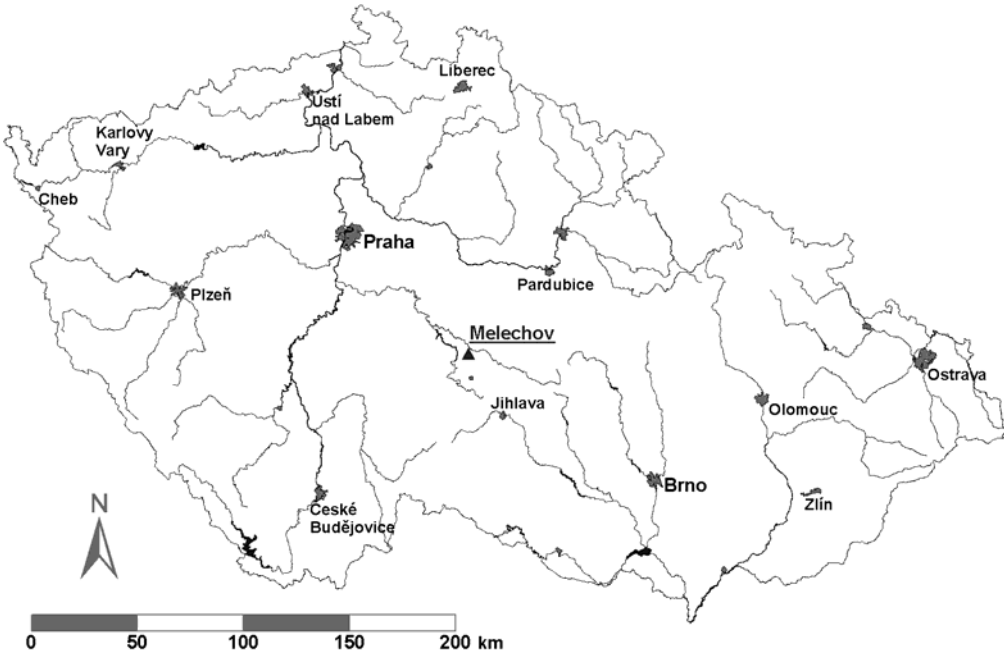

Figure C1. Melechov massif position

Limits of study area approximately constitute Sázava river at north, Pstružný stream at east, Želivka river and Švihov reservoir at west and join of villages Kejžlice, Kaliště and Hojanovice to the south.

Annual precipitation in study area ranges from 650 to 700 mm per year. Altitude of uplands formed by Melechov granite massif vary from 350 to 710 m above see level. The highest part of the massif is formed by the Melechov hill (708.9 m a. s. l.) after which the massif was named. Fairly dense river network covers Melechov massif. Most of surface water stream into Sázava river, in western part of massif into Želivka river (water reservoir Švihov).

Melechov massif belongs to Moldanubic zone of the Bohemian massif and is formed by several petrographic types of Variscan aged granite, which is surrounded by metamorphic rocks (mostly paragneiss) in western part (Figure C2). Granites of massif are relatively homogeneous, their differentiation can be only based on structure, texture and chemical compounds.

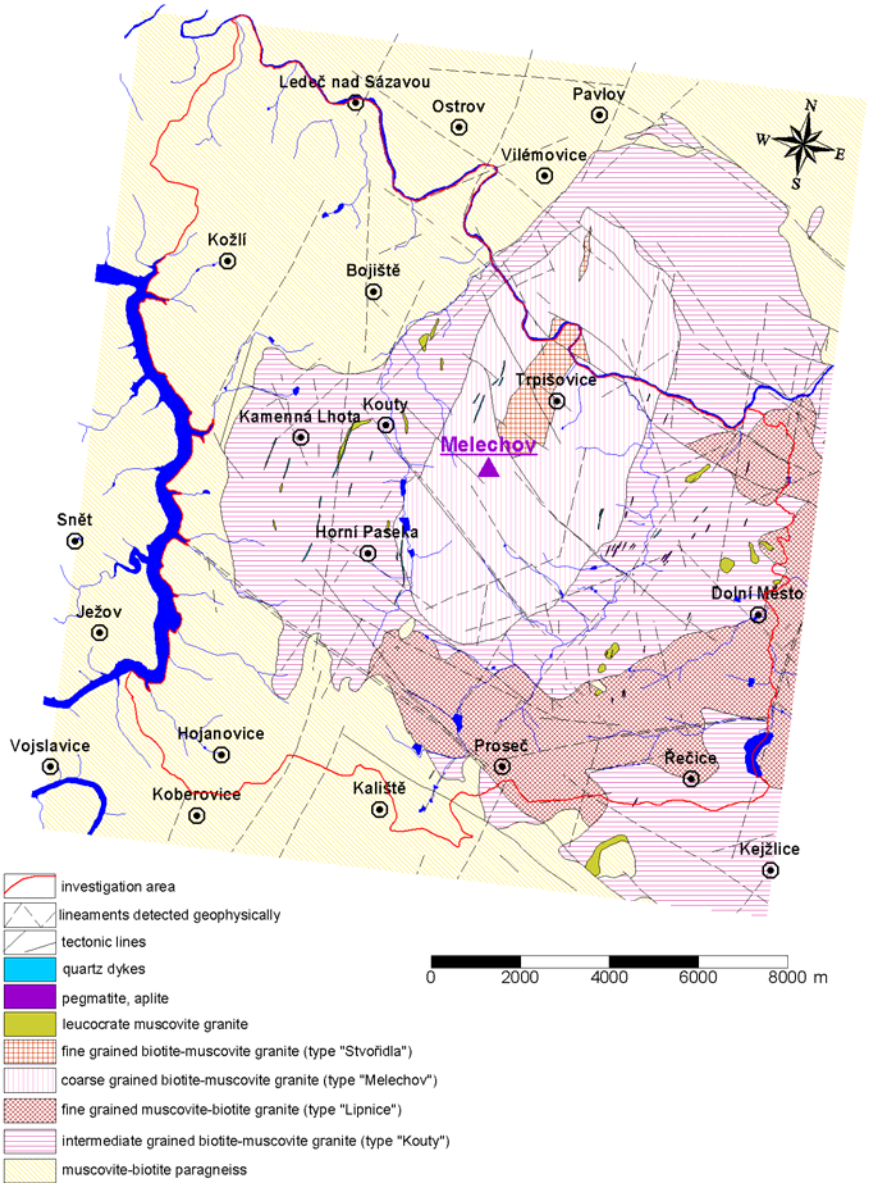

Figure C2. Geology of area of interest.

The deep structure of massif is known only from geophysics investigation. According to gravimetry measurement and computation (Šrámek and Sedlák 2001), Melechov granites constitute subvertical cylindrical body reaching depths more than 12 km. Granites general fall into depth is under angle 25-30° NE.

Two main systems of fracture at Melechov massif exist, older fracture system of NNE-SSW direction with inclination into centre of massif body and younger subvertical system WNW-ESE direction (Mlčoch 1994, Mlčoch et al. 2000). Especially, there is a good relation among geological boundaries and rivers courses with younger fracture system direction in some part of massif.

According to hydrogeological classification study area belongs to hydrogeological massif. Groundwater flow is mostly related to fracture porosity, which is represented by fracture occurrence and connectivity of single fractures. Only in the most upper part of massif (soil mantle) mixed porous and fracture porosity can by found. Thickness of mixed zone can reach depth maximally 30 m, according to rocks erosion intensity, topographic position of site, etc.

Values of hydraulic conductivity determined on pumping tests vary from $4.26 \cdot 10^{-5}$ $m \cdot s^{-1}$ to $1.18 \cdot 10^{-6}$ $m \cdot s^{-1}$ (Rukavičková,2001). These values represent only shallow part of massif (depth max. 30 m), deeper values are not known because of missing deep boreholes. Magnitude of hydraulic conductivity is related to thickness of soil mantle, topographic position and of course on fracture occurrence, and do not depend on geology.

C3 Conceptual model

Conceptual model construction is basic step to mathematical modelling. Conceptual model represents summary of geological and hydrogeological knowledge about interesting area and their mathematical idealization into numerical model. Conceptual model of groundwater and surface water flow, their interaction at study area is described in chapters below.

C3.1 FLOW CONCEPT

Precipitations, throughout interesting area, infiltrate into soil mantle of granite and metamorphic rocks composed of sandy material with clay admixture. Shallow aquifer of 10-30 m thickness with higher hydraulic conductivity is consisted of soil mantle together with quaternary sediments. Due to indented morphology, main part of infiltrated water flow only in shallow aquifer and is drained at proximate drainage basin. Minor part of water flows into deeper fracture aquifer of 300 m thickness maximally. As well as in shallow aquifer, main part of fracture aquifer groundwater is drained at proximate drainage basin. Residual volume of fracture aquifer water flows along fracture into deep fracture system.

C3.2 MODELLING AREA EXTENT

Model area covers central part of Melechov granite massif and paragneiss surrounding. Extent of interesting area is 13.8 km in north-south and 11.5 km in east-west direction (Figure C3). It makes area of 92 km^2.

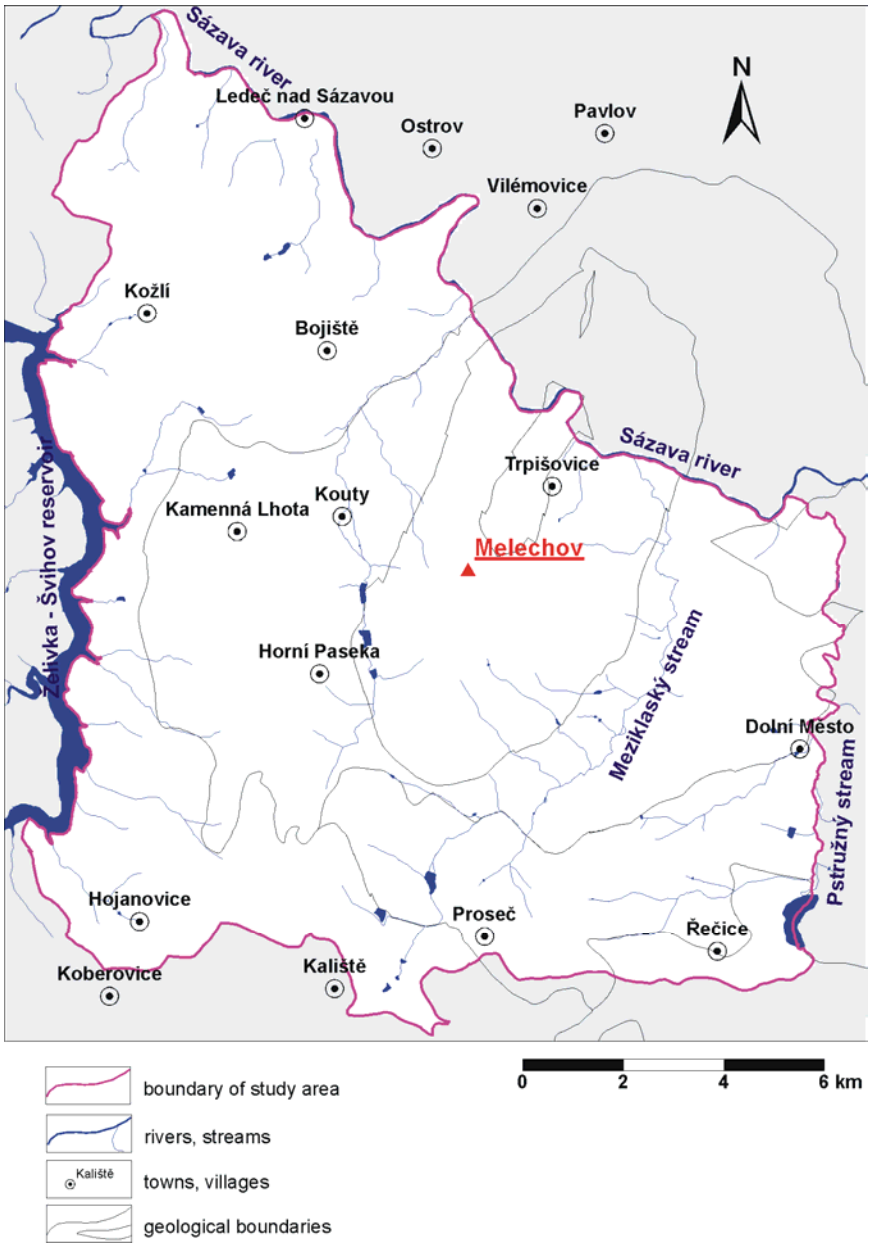

Figure C3. Modelling area extent

C3.3 BOUNDARY CONDITIONS

Top of modelled area is delimited by surface morphology. Through this limit, constant flow rate boundary (Neumann's boundary condition) representing rainfall infiltration is assessed. Bottom of model block reaches depth 1500 meters below sea level. This limit is no flow boundary considered. Starting value $.4.3 \cdot 10^{-9}$ $m \cdot s^{-1}$ (136 mm/year) of infiltration has been assessed. This value makes 20% of average annual precipitation.

Northern limit of model makes up Sázava river, Želivka river and Švihov reservoir western limits. There are assessed these watercourses like constant head boundary (Dirichlet's boundary condition) in model. Southern and north-western limits of modelled area watershed divide constitute (Figure C3). In this limits zero flow rates are assessed (Neumann's boundary condition).

Pstružný stream at eastern limit of model area and main watercourses within model area are set up in form of mixed boundary conditions assessed (Newton's boundary condition).

C3.4 HYDRAULIC CHARACTERISTIC OF ROCKS AND MODEL LAYERS

How was described above, Melechov is formed by several petrographic types of granite surrounded by metamorphic rocks. Granites of massif are relatively homogeneous. Their differentiation can be only based on structure, texture and chemical compounds. Groundwater flow is mostly related to fracture porosity, which is represented by fracture occurrence and connectivity of single fractures. Only in the most upper part of massif (soil mantle) mixed porous and fracture porosity can by found.

Due to possibility simulate decrease of hydraulic conductivity into depth, model was divided into 14 layers in vertical direction. Values of hydraulic conductivity represent only shallow part of massif and vary from $4.26 \cdot 10^{-5}$ m·s^{-1} to $1.18 \cdot 10^{-6}$ m·s^{-1}. Values of deeper massif part are not known. Owing to this ignorance, exponentially decrease of hydraulic conductivity into the depth according to equation [1] was assumed (Gustafson and Liedholm, 1989).

$$K(z) = K_0 \cdot 10^{-\frac{Z}{C}} \qquad [1]$$

where K(z) … the hydraulic permeability in depth Z(m)

K_0 ….. starting value of the hydraulic permeability close to the land surface

C(m) .. coefficient defining the rate of decreasing (for example, if C is set 1000 then K_0 is one order of magnitude smaller after each 1000 depth meters)

In top view, five hydraulic categories, based on geology, were determined– granite type Melechov, Kouty, Lipnice, Stvořidla and surrounding paragneiss. According to hydrogeological survey, first model layer starting values of hydraulic conductivity in particular categories has been assigned (Table C1). Hydraulic conductivity values of lower layers were determined according to equation [2] and first model layer conductivity, with value 500 m of coefficient C.

Table C1. Input values of hydraulic conductivity in first model layer

	moldanubic paragneiss	granite, type Kouty	granite, type Melechov	granite, type Lipnice	granite, type Stvořidla
hydraulic conductivity [m/s]	3.00×10^{-5}	4.26×10^{-5}	3.88×10^{-5}	3.70×10^{-5}	3.77×10^{-5}

C4 Numerical model

The main objectives of the groundwater flow simulation were the determination of the spatial hydraulic potential distribution, velocity flow and travel time. Two steps numerical simulations were used for estimation of hydrogeological and hydraulic conditions within study area. At first, numerical model and calibration according to known hydraulics parameters were accomplished. Consecutively, velocity flow and travel time at different depths and hydraulic conditions were simulated.

C4.1 MODELLING TOOLS

Groundwater Vistas (GWV) modelling package by J. and D. Rumbaugh, Environmental Simulation, Inc. was used. Flow solver MODFLOW (McDonald, Harbaugh, 1988), which is a part of GWV package, was used for groundwater flow and groundwater travel time modelling.

Well known MODFLOW solver uses finite difference method for flow governing equation solving.

$$\frac{\partial}{\partial x}\left(k_{xx}\frac{\partial h}{\partial x}\right)+\frac{\partial}{\partial y}\left(k_{yy}\frac{\partial h}{\partial y}\right)+\frac{\partial}{\partial z}\left(k_{zz}\frac{\partial h}{\partial z}\right)-W=S_s\frac{\partial h}{\partial t} \qquad [2]$$

where k_{xx}, k_{yy} a k_{zz}… hydraulic conductivity along *x, y* and *z* axis, parallel with main tensors of permeability (L/t),

h … piezometric head (L),

W … infiltration and evapotranspiration (1/t),

S_s … specific value of material storativity (1/L),

t … time (T)

Equation [2] describes three dimensional groundwater flows in heterogeneous and anisotropic environment. Equation, together with boundary and initial conditions represents numerical expression of transient groundwater movement in environment.

C4.2 RELATION BETWEEN CONCEPTUAL AND MATHEMATICAL MODEL

Mathematical model is analogy of conceptual model described above. Space delimitation of mathematical model, boundary condition selection and hydraulic parameters setting is in accordance with conceptual model. Due to higher model stability one change was made. Newton's boundary condition at Pstružný stream had been modified into constant head boundary (Dirichlet's).

C4.3 MODEL GEOMETRY

Model mesh was composed from 276 rows and 230 columns with uniform cell extent of 50 m. Total model extents represent area of 158 km^2, but approximately 92 km^2 is really simulated. Inactive cells were set in residual area (greyed area in Figure C3). In areal view, model contains 37,162 active and 26,318 inactive cells.

In vertical direction model was divided into 14 layers (Figure C4). First layer had uniform thickness 50 meters, next 5 layers uniform thickness 100 m. Average thickness of 8 remaining layers vary from 75 in layer no.7 to 250 meters in last layer no. 14. Total number of model active cells is 520,268.

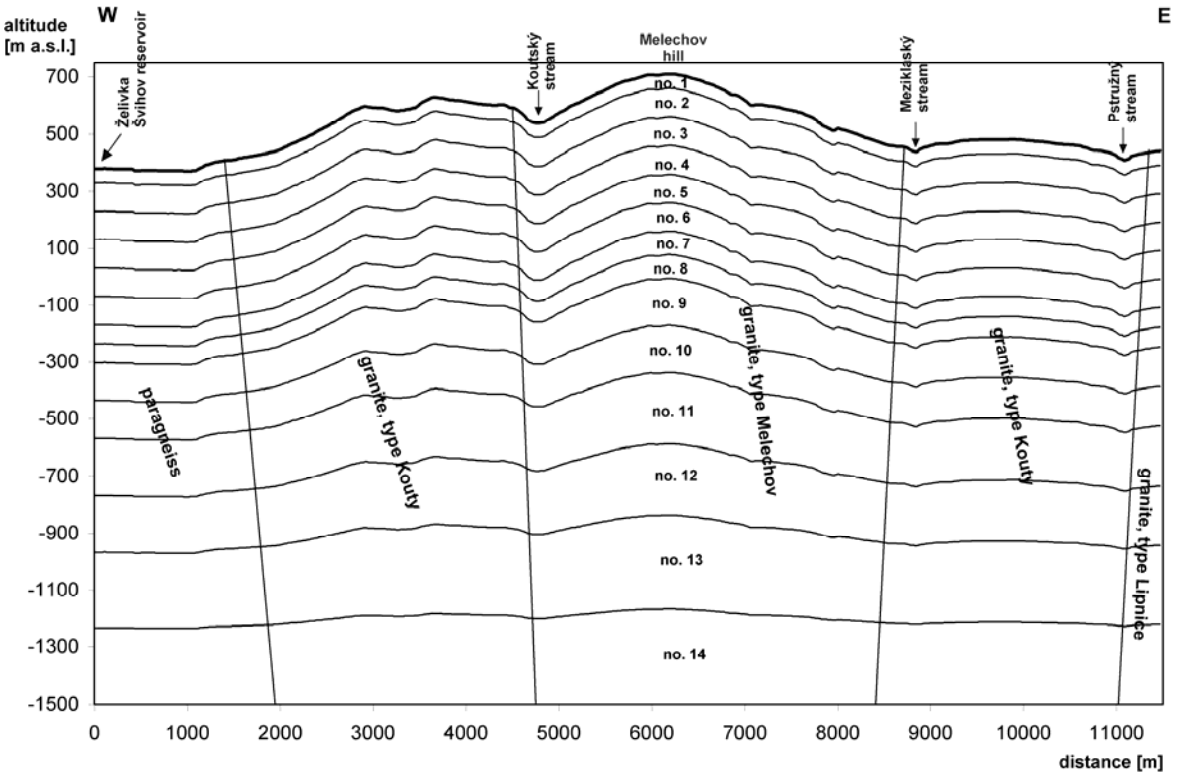

Figure C4. W-E model layers cross-section

C4.4 INITIAL PARAMETERS AND BOUNDARY CONDITIONS

Recharge

Average year precipitations at vicinity of Melechov massif vary from 650 to 700 mm/year. Amount of precipitation infiltration was estimated at 20%. So, starting value of recharge rate was set to $4.3 \cdot 10^{-9}$ m·s^{-1}.

Hydraulic conductivity

How was described above, in top view five hydraulic categories, based on geology, were determined. It was all granite types (Melechov, Kouty, Lipnice, Stvořidla) and surrounding paragneiss. Starting values of their hydraulic conductivity in the first model layer show Table C2, spatial distribution is shown in Figure C5. According to equation [1] decrease of hydraulic conductivity into the depth was assumed. Hydraulic conductivity values of deeper model layers are discussed further.

Boundary condition

Boundary conditions were described enough above. Space distribution of these conditions is shown in Figure C6.

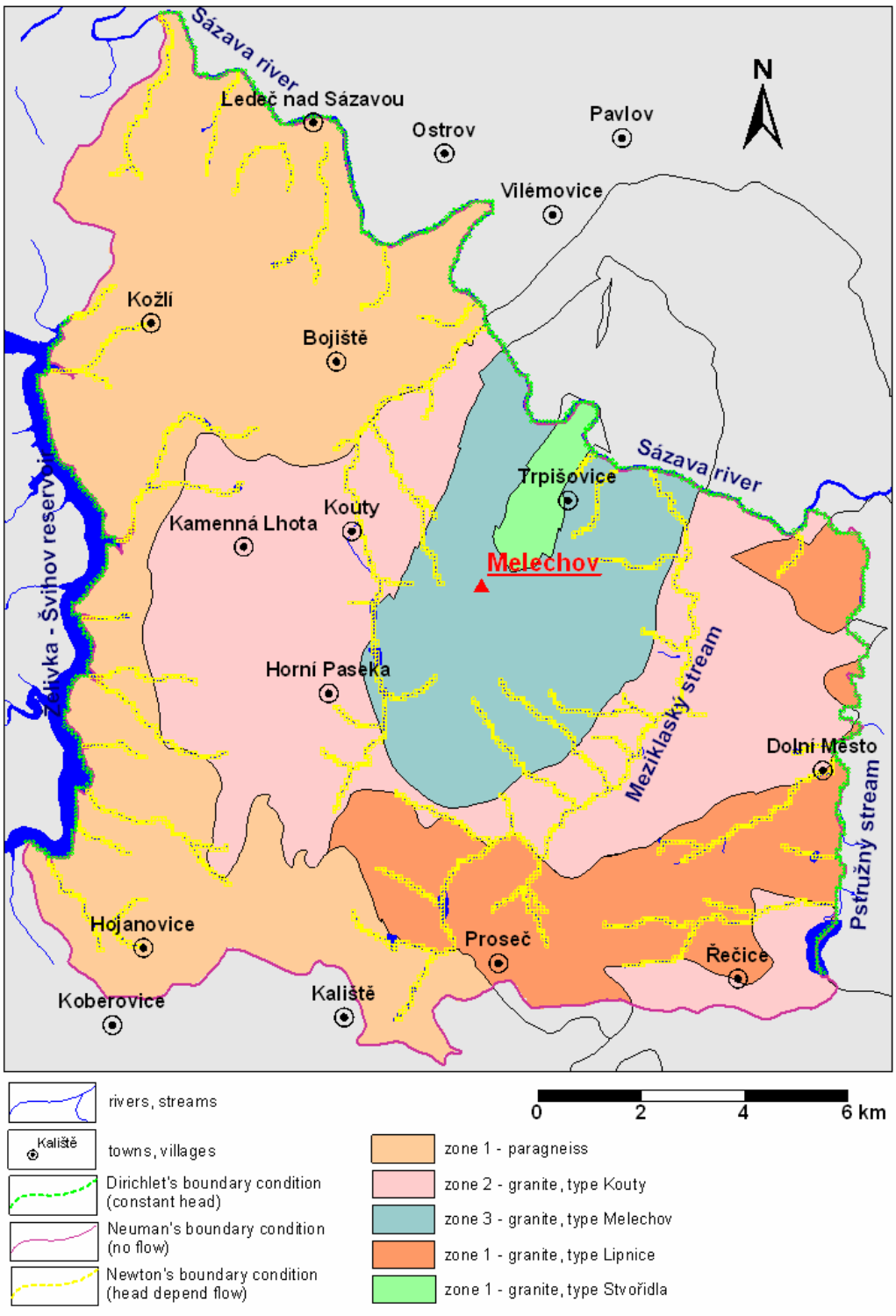

Figure C6. Model parameters and boundary condition distribution

C4.5 MODEL CALIBRATION

The main objectives of the model calibration are to accomplish spitting image of natural conditions at study area. So, calibration means minimization of difference between model results and known hydraulics values due to initial hydraulics parameters modification.

In this case, only recharge rate and hydraulic conductivity modification were used for model calibration. Model accuracy was compared with water level table at selected wells and

significant springs flow rate. Together with these values accuracy of rivers flow rate was observed.

Model calibration results and concluding hydraulics parameters are described and commented below.

Hydraulic conductivity

Modification of all hydraulics categories was used for model calibration. Resulting values of hydraulic conductivities in shallow part of Melechov massif are approximately 10xs lower than values determined on pumping tests. Reason for these differences is in thickness of the first model layer. While thickness of the first layer is 50 m, pumping test characterize only top part of massif to the depths of 30 m max.

Deeper values of hydraulic conductivity were assumed according to equation [1]. During model calibration, better model results were achieved using value 400 m of coefficient ***C*** instead original value 500 m. Table C3 show final values of hydraulic conductivity and their space distribution.

Table C3. Distribution of hydraulic conductivity

layer no.	average depth [m]	paragneiss	granite, type kouty [$m \cdot s^{-1}$]	granite, type melechov [$m \cdot s^{-1}$]	granite, type lipnice [$m \cdot s^{-1}$]	granite, type stvořidla [$m \cdot s^{-1}$]
1	25	2.70E-06	4.30E-06	3.90E-06	3.70E-06	3.60E-06
2	100	1.75E-06	2.79E-06	2.53E-06	2.40E-06	2.34E-06
3	200	9.86E-07	1.57E-06	1.42E-06	1.35E-06	1.31E-06
4	300	5.54E-07	8.83E-07	8.01E-07	7.60E-07	7.39E-07
5	400	3.12E-07	4.97E-07	4.50E-07	4.27E-07	4.16E-07
6	500	1.75E-07	2.79E-07	2.53E-07	2.40E-07	2.34E-07
7	590	9.04E-08	1.44E-07	1.31E-07	1.24E-07	1.21E-07
8	710	4.53E-08	7.22E-08	6.55E-08	6.21E-08	6.04E-08
9	820	2.41E-08	3.83E-08	3.48E-08	3.30E-08	3.21E-08
10	940	1.21E-08	1.92E-08	1.74E-08	1.65E-08	1.61E-08
11	1050	6.40E-09	1.02E-08	9.25E-09	8.77E-09	8.54E-09
12	1170	3.21E-09	5.11E-09	4.64E-09	4.40E-09	4.28E-09
13	1280	1.70E-09	2.71E-09	2.46E-09	2.33E-09	2.27E-09
14	1400	8.54E-10	1.36E-09	1.23E-09	1.17E-09	1.14E-09

Recharge

There was used initial model value $4.3 \cdot 10^{-9}$ $m \cdot s^{-1}$ of recharge rate in model. During model calibration this value was changed to $5.4 \cdot 10^{-9}$ $m \cdot s^{-1}$. This value represents 25% of total average annual precipitation. A little bit higher value can be acceptable due to sandy character of granite rocks weathering.

C5 Model Results

C5.1 HYDRAULIC HEAD DISTRIBUTION

Some of the model results are included as an example in Figures C7 to C11 showing spatial distribution of hydraulic head and water flow directions in selected layers and cross-sections.

Model results show significant drainage function of Sázava river and Švihov reservoir. Other watercourses drainage function is affected mainly in low located flat parts of massif. In this case Meziklaský stream drainage function is significant. In contrast with flat parts, drainage of watercourses situated in indented high located parts is reduced. Owning to surface slope, main shallow groundwater flow head directly to lower part of massif, where is drained. This is case of watercourses situated at west and north-west part of Melechov Massif. Into the depth, drainage function of watercourses decrease and impact of regional watershed contour formed by Melechov massif increase.

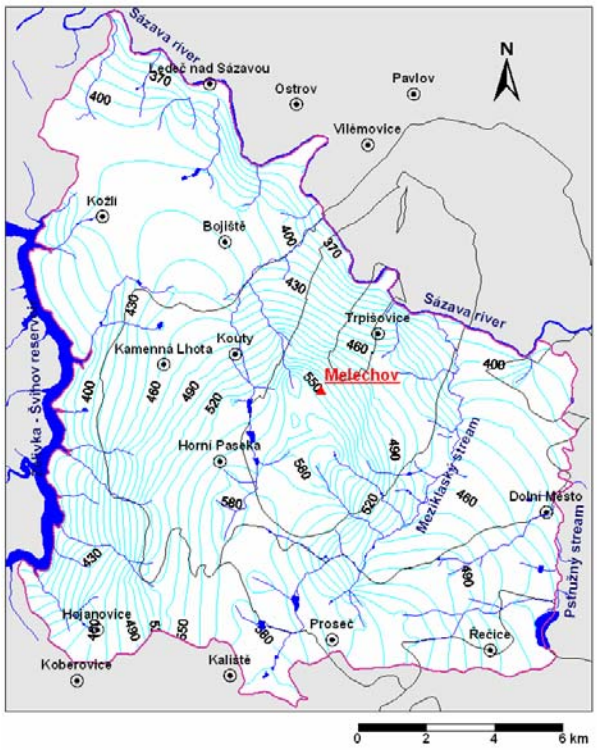

Figure C7. Contour lines of hydraulic head in first layer

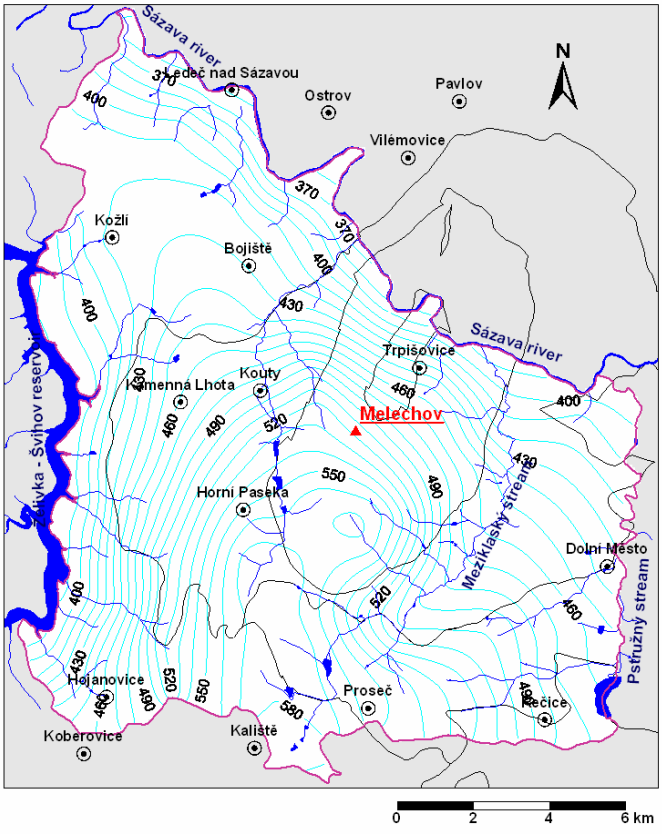

Figure C8. Contour lines of hydraulic head in fourth layer.

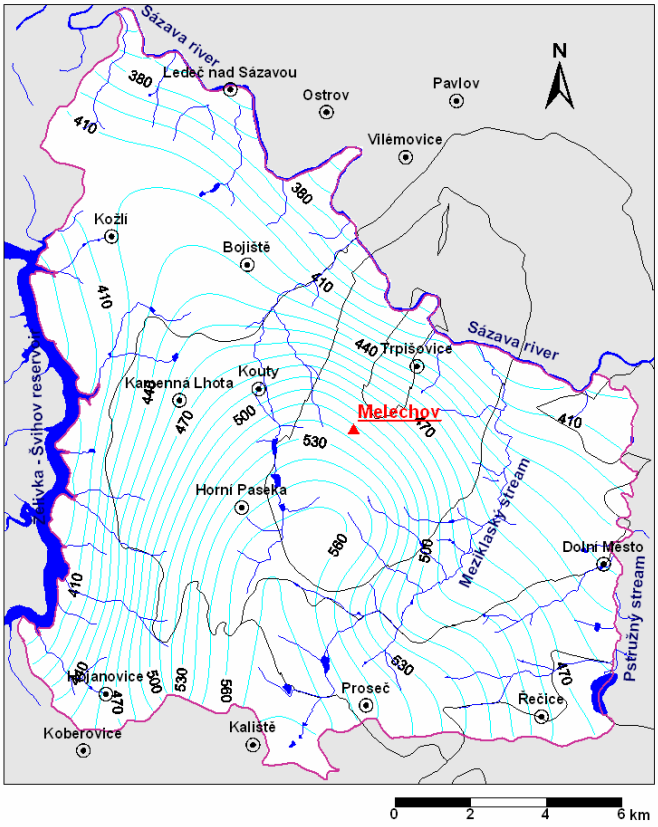

Figure C9. Contour lines of hydraulic head in tenth layer.

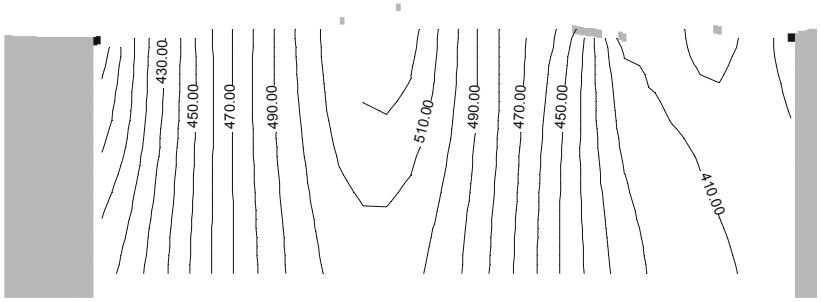

Figure C10. Contour lines of hydraulic head in W-E cross-section.

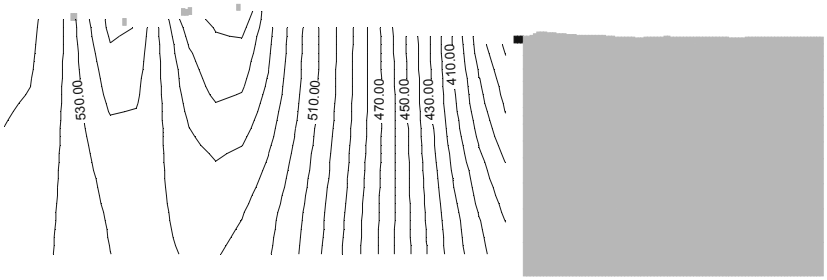

Figure C11. Contour lines of hydraulic head in N-S cross-section.

C5.2 FLOW VELOCITIES AND TRAVEL TIME

In case of flow velocities simulation and travel time a specific simplification was accepted. Fracture flow character of massif hard rocks has been replaced by porosity due to potential of used software. Owning to extent of simulated area, degree of massif exploration and objectives of model simulation is this simplification acceptable. Error magnitude caused by simplification depends on total amount of fracture, their depth progress and sediment filling, connection among fracture, etc. Because of massif exploration, knowledge about above written fracture characteristics are at low level.

Computation of velocity flow and travel time was performed for 3 eventualities, which include different level of massif fracturing. In model, level of fracturing has been simulated by means of vertical hydraulic conductivity and porosity changes. Resulting flow velocities and travel time for various levels fracturing of Melechov massif are shown in Table C4. Extreme values of fracturing (low and high in Table C4) present 10-20% changes against average values of vertical hydraulic conductivity and porosity of rocks.

Table C4. Flow velocities and travel time

depth level [m]	Average flow velocity [m·s^{-1}]			Travel time for distance of 1000 m [year]		
	low fracturing	average fracturing	high fracturing	low fracturing	average fracturing	high fracturing
0 – 100	2.40E-06	3.00E-06	3.60E-06	13	10	9
100 – 200	4.24E-07	5.30E-07	6.36E-07	75	60	50
200 – 500	5.44E-08	6.80E-08	8.16E-08	580	470	390
500 – 1000	4.64E-09	5.80E-09	6.96E-09	6800	5500	4600
1000 – 1800	3.28E-10	4.10E-10	4.92E-10	97000	77500	65000

C6 References

Gustafson G., Liedholm, (1989): Groundwater Flow Calculation on a Regional Scale at The Swedish Hard Rock Laboratory. SKB Progress Report 25-88-17, Stockholm.

McDonald, M.G. and A.W. Harbaugh (1988): A Modular Three-Dimensional Finite-Difference Ground-Water Flow Model, Techniques of Water-Resources Investigations of the U.S. Geological Survey Book 6, Ch. A1: 576 p.

Mlčoch, B., (1994): Zpráva o detailním geologickém mapování 1:10,000 lokality Dolní Město. MS ČGÚ. Praha.

Mlčoch, B., et al. (2000): Vysvětlivky k aktualizované účelové geologické mapě melechovského masívu 1:10 000

Mlčoch, B., et al. (2000): Aktualizovaná účelová geologická mapa melechovského masivu v měřítku 1: 10 000. SÚRAO. Praha.

Rumbaugh J. O., Rumbaugh D. B. (1998): Guide to Using Groundwater Vistas, Version 2, Environmental Simulations, Inc. Herndon, Virginia

Rukavičková, L., (2001): Účelová hydrogeologická mapa melechovského masivu (zpráva o hydrogeologickém výzkumu). ČGÚ, Praha. MS SÚRAO. Praha

Šrámek, J., Sedlák, K., (2001): Regionální sv.-jz. tíhový profil na lokalitě melechovský masiv. Geofyzika Brno a ČGÚ Praha